

Submitted to ApJ Supplement

# Ultra-luminous X-ray Sources in nearby galaxies from ROSAT HRI observations I. data analysis

Ji-Feng Liu and Joel N. Bregman

*Astronomy Department, University of Michigan, MI 48109*

## ABSTRACT

X-ray observations have revealed in other galaxies a class of extra-nuclear X-ray point sources with X-ray luminosities of  $10^{39}\text{--}10^{41}$  erg/sec, exceeding the Eddington luminosity for stellar mass X-ray binaries. These ultra-luminous X-ray sources (ULXs) may be powered by intermediate mass black hole of a few thousand  $M_\odot$  or stellar mass black holes with special radiation processes. In this paper, we present a survey of ULXs in 313 nearby galaxies with  $D_{25}>1'$  within 40 Mpc with 467 ROSAT HRI archival observations. The HRI observations are reduced with uniform procedures, refined by simulations that help define the point source detection algorithm employed in this survey. A sample of 562 extragalactic X-ray point sources with  $L_X = 10^{38}\text{--}10^{43}$  erg/sec is extracted from 173 survey galaxies, including 106 ULX candidates within the  $D_{25}$  isophotes of 63 galaxies and 110 ULX candidates between  $1\text{--}2\times D_{25}$  of 64 galaxies, from which a clean sample of 109 ULXs is constructed to minimize the contamination from foreground or background objects. The strong connection between ULXs and star formation is confirmed based on the striking preference of ULXs to occur in late-type galaxies, especially in star forming regions such as spiral arms. ULXs are variable on time scales over days to years, and exhibit a variety of long term variability patterns. The identifications of ULXs in the clean sample show some ULXs identified as supernovae (remnants), HII regions/nebulae, or young massive stars in star forming regions, and a few other ULXs identified as old globular clusters. In a subsequent paper, the statistic properties of the survey will be studied to calculate the occurrence frequencies and luminosity functions for ULXs in different types of galaxies to shed light on the nature of these enigmatic sources.

*Subject headings:* catalogs – galaxies: general – X-rays: binaries – X-rays: galaxies

## 1. INTRODUCTION

Ultra-luminous X-ray sources (ULXs) are extra-nuclear sources with luminosities in the range of  $10^{39} - 10^{41}$  erg/sec in other galaxies, and have been observed by ROSAT, ASCA, recently by XMM-Newton and Chandra Observatory in large numbers. As compared to the cases of the X-ray binaries in our Galaxy, which are powered by accretion onto neutron stars or stellar mass black holes and have luminosities of  $10^{33} - 10^{38}$  erg/sec, the luminosities of ULXs require accreting compact objects of masses  $10^3 - 10^4 M_{\odot}$  if they emit at  $10^{-2}$  of the Eddington luminosity, typical of Galactic X-ray binaries. While the required masses could be much larger if they emit at much less than  $10^{-2}$  of the Eddington luminosity, as in the cases of some low luminosity active galactic nuclei (AGN), the masses cannot be much greater than  $10^5 M_{\odot}$  for these extra-nuclear sources to survive the dynamic friction over a few Gigayears (Colbert 1999). Such intermediate mass compact objects can only be black holes, and if they exist, are the missing links between stellar mass black holes and super-massive black holes in the nuclei of galaxies.

While the explanation with intermediate mass black holes is simple, intriguing and astrophysically interesting, such black holes are not predicted by ordinary stellar evolution theories. It is suggested that black holes of a few hundred  $M_{\odot}$  can form from the death of Pop III stars, and more massive ones might form from multiple stellar interactions in some dense clusters, hencing manifest as ultra-luminous X-ray sources (Portegies Zwart et al. 2002). Alternatively, these X-ray sources could be stellar mass black holes or neutron stars whose apparent super-Eddington luminosities are due to some special processes. One suggestion is that radiation pressure-dominated accretion disks with photon-bubble instabilities are able to emit truly super-Eddington luminosities (Begelman 2002). Another suggestion is that beaming effects can produce the observed luminosities of ULXs (King et al. 2001).

The leading goals in ULX studies are to determine the masses of the primary, to understand how and where they form, and to find out how they emit at such high luminosities. In the last few years many efforts have been made to address these questions, and important clues have been revealed. However, these studies mainly focus on some well-known objects and galaxies (e.g., M81 X-9, NGC5204 X-1, Antenna galaxy, Cartwheel galaxy) except for a few works (e.g., Colbert & Ptak, 2002, hereafter CP2002; Swartz et al. 2004; Ptak & Colbert 2004), and now it is time to define a complete sample of ULXs to study the properties of the phenomenon and test critical ideas. One resource to rely on for this purpose is the data archive of the ROSAT High Resolution Imager (HRI), which includes 5403 observations in the ten years from June 1990 to February 1999. The HRI is a multichannel plate detector of  $38' \times 38'$  square field of view, large enough to contain all individual nearby galaxies other than LMC, SMC, M31, and M33 in our Local Group. Its spatial resolution is suitable for

extra-galactic point source studies, with on-axis  $\text{FWHM} < 5''$  and a pixel scale of  $0.''5/\text{pixel}$ , adequate to resolve point sources in most cases. Also, the archival observations have reasonable sky coverage for survey purposes. For example, the 5393 pointed HRI observations used in the First ROSAT HRI Source Catalog (1RXH; ROSAT scientific team, 2000) covers about 2% of the sky.

The large database of ROSAT HRI observations has not been thoroughly exploited for complete samples of ULXs in nearby galaxies. Roberts & Warwick (2000; hereafter RW2000) have used the HRI archive to study the X-ray properties of nearby galaxies, and detected in 83 galaxies 187 discrete X-ray sources of all luminosity ranges, among which 27 non-nuclear sources have  $L_X > 10^{39}$  erg/sec and can be taken as ULXs. They used the nearby galaxy sample by Ho, Filippenko & Sargent (1995), which was constructed to search for dwarf Seyfert nuclei in nearby galaxies and contains 486 bright northern galaxies. Many nearby galaxies with HRI observations are not included in this sample, and the HRI archive is far from being fully utilized for surveying ULX. Recently Colbert & Ptak (2002) made an effort to analyze the HRI observations to search for ULXs in a sample of 9999 galaxies in the Third Reference Catalog of galaxies (RC3; de Vaucouleurs et al. 1991) with  $cz < 5000 \text{ km/sec}$ . They found 87 ULXs in 54 galaxies, with 37 in early-type galaxies. However, many ULXs in the CP2002 catalog are projected far from the host galaxies, and may be false ULXs from foreground stars or background AGN/QSOs. For example, Irwin et al. (2004) pointed out that the radial distribution of ULXs in early-type galaxies in the CP2002 catalog is consistent with a random distribution, thus these ULXs are probably not physically associated with these early-type galaxies.

Here we present our study of ULXs in nearby galaxies with the wealth of HRI archive. To fully utilize the HRI archive, we choose all observations associated with any RC3 galaxies within 40 Mpc with isophotal diameters  $> 1 \text{ arcminute}$ . The RC3 galaxy sample, the selected HRI observations and the survey galaxies are described in section 2. In our analysis a wavelet algorithm is used for point source detection, and in section 3 we discuss its performance on HRI images through simulations. In section 4, we describe the analysis procedures applied on the data, including the point source detection, the variability tests, astrometric corrections, associations with galaxies and computation of luminosities. These efforts lead to a catalog of 562 extragalactic X-ray sources above  $3\sigma$  detection within  $2 \times D_{25}$  of 173 out of the 313 survey galaxies, including 106 ULX candidates within the  $D_{25}$  isophotes of 63 galaxies and 110 ULX candidates between  $1-2 \times D_{25}$  of 64 galaxies. The identifications of these sources are given in section 5. As a final product, we construct a clean sample of ULXs to include ULXs within, and a few outside the  $D_{25}$  isophotes, with identified foreground stars and background QSOs excluded. The comments and finding charts are given for these ULXs in section 6. In section 7 we summarize the procedures and preliminary results of the survey.

In a subsequent paper, we will study the occurrence rates and luminosity functions for ULXs in different types of galaxies.

## 2. ROSAT HRI survey of nearby galaxies

To search for the ultra-luminous X-ray sources in the nearby galaxies from the ROSAT HRI archival observations, we cross correlated a nearby galaxy sample with the list of HRI archival observations to select observations with nearby galaxies within their field of views. Here we describe the nearby galaxy sample, the selected HRI observations, and the survey galaxy sample.

The nearby galaxy sample is extracted from RC3, one of the most complete catalog for nearby galaxies having apparent diameters larger than 1 arcminute at the  $D_{25}$  isophotal level, total B-band magnitudes  $B_T$  brighter than 15.5, and redshifts not in excess of 15,000 km/sec. Distances to galaxies are collected from the literature, including the HST Key Project (designated as KP; Freedman et al. 2002), the surface brightness fluctuation method (SBF; Tonry et al. 2001), the nearby galaxy flow model by Tully (1992; T92), and the Nearby Galaxy Catalog (T88; Tully 1988). Distances are also computed using the Hubble relation  $v = H_0 D$  with  $H_0 = 75$  km/s/Mpc. The NED service provides the recessional velocity  $v$  for most galaxies, and distances computed from them are designated as NED. Another source of  $v$  is RC3, and the distances computed are designated as V3K, since we use the velocities corrected to the rest frame defined by the 3K cosmic microwave background. When multiple distance measurements are available we use the best distance measurement, which is KP, followed by SBF, T92, T88, NED, and V3K.

The positions of the galaxies are taken from RC3. NED also gives galaxy positions that are consistent with RC3 to a few arcseconds for most galaxies. In the rare occasions when the positions from the two sources differ by  $>1'$ , we verify the positions by overlaying the isophotal ellipses on the optical images from the Digital Sky Survey (DSS). The  $D_{25}$  isophotes, the elliptical contour best corresponding to the 25 mag/arcsec<sup>2</sup> blue isophote, are also taken from RC3. The  $D_{25}$  isophote is a quantitative description of the domain of a galaxy, though the galaxies can extend beyond  $D_{25}$  in some cases but usually within  $2 \times D_{25}$  as seen from DSS images.

For our ULX study, we choose galaxies with isophotal diameters  $>1$  arcminute, for which RC3 is reasonably complete for bright nearby galaxies. Given HRI position uncertainties typically below 10'', this choice of galaxy size leaves space for extra-nuclear sources to be distinguished from nuclear ones. For a short HRI observation of 10 kiloseconds, the count

threshold for  $3\sigma$  detection for on-axis point sources is  $\sim 12$  photons based on the simulations in section 3, and for the X-ray spectrum used in section 4 this corresponds to a flux level of  $\sim 8 \times 10^{-14}$  erg/sec/cm $^2$ , which in turn corresponds to a luminosity of  $\sim 10^{39}$  erg/sec for sources in galaxies at 10 Mpc. Sources with extremely high luminosities, e.g.,  $L_X > 10^{40}$  erg/sec, are usually very revealing about the nature of ULXs, and can still be detected in galaxies at larger distances. Here we choose to survey galaxies within 40 Mpc, with the hope of detecting these extreme ultra-luminous X-ray sources from the large number of galaxies between 10 Mpc and 40 Mpc. Galaxies in our Local Group usually have large projected areas and have severe contamination problems from foreground stars, we thus exclude them from our study here. Our above selection criteria lead to a sample of 4434 RC3 galaxies.

A complete list of ROSAT HRI observations was extracted from the MPE ROSAT site<sup>1</sup>. The list of HRI observations with exposures  $> 1000$  seconds was cross correlated with the above RC3 galaxy list with a correlation radius of  $15'$ . Galaxies only partly observed by the HRI are excluded from our survey for their incompleteness and large off-axis angles. Also excluded are galaxies behind the Galactic plane or the Magellanic Clouds for their dense foreground stellar fields to reduce the confusion problems for identifying X-ray sources. In total, our survey includes 467 observations for 313 galaxies. These observations were downloaded from the MPE ftp site<sup>2</sup> and processed with the uniform procedures described in section 4.

In the HRI galaxy sample, 313 galaxies were surveyed by 467 HRI observations, about 7.1% of the RC3 galaxy sample. This fraction is comparable to that in the work of Ptak & Colbert (2004), in which 766 ( $\sim 8\%$ ) of the 9452 RC3 galaxies with  $cz < 5000$  km/sec are surveyed by HRI observations. In Table 1 the survey galaxies are listed with galactic positions, sizes, the Galactic HI column densities, the distances, the galaxy types, the B-band, the IRAS 60 $\mu$ m and FIR luminosities. This HRI galaxy sample is compared to the RC3 galaxy sample to reveal possible preferences in the survey galaxies. The blue luminosity distribution of the survey galaxies resembles that of the RC3 galaxy sample to a large extent, as shown in Figure 1, except for a slight over-sampling of very bright galaxies. This over-sampling is related to the fact that the galaxies surveyed by the HRI tend to be larger and closer ones, as demonstrated in Figure 2 and Figure 3. The morphological type distributions of the galaxies are compared between these two samples, and an over-abundance of ellipticals, and over-abundances of lenticulars and S0/a-Sc early spirals to a lesser extent, are found in the HRI galaxy sample with respect to the RC3 galaxy sample as shown in Figure 4. In

---

<sup>1</sup><http://wave.xray.mpe.mpg.de/rosat/>

<sup>2</sup><ftp://ftp.xray.mpe.mpg.de/rosat/archive/>

contrast, there is an under-abundance of dwarf spirals and irregulars in the survey sample, reflecting a bias in selecting the HRI targets that is against the dwarf spirals and irregulars. To summarize, the HRI survey galaxy sample is representative for the galaxies within 40 Mpc, although there are preferences for galaxies that are larger, closer, optically or X-ray brighter.

### 3. simulations of the detection method

A point source detection method suitable for the HRI images is needed to study the X-ray point sources in HRI observations. Two packages for two detection algorithms are widely used in the X-ray astronomy community. One is celldetect, which uses the sliding cell method to check for local maxima and detect unresolved sources. This was the method adopted by 1RXH. Another popular package is wavdetect, which employs a wavelet method to detect point sources. For our purpose of detecting X-ray point sources in the HRI images, it is more effective to use wavdetect rather than celldetect, since celldetect does not treat diffuse emission well, and tends to split diffuse emission into multiple point sources. For example, celldetect reports 67 point sources for the 10 kilo-second HRI observation RH600463A02 of an elliptical galaxy NGC 4406, while there is really only one nuclear source plus diffuse X-ray emission, as correctly reported by wavdetect.

The wavdetect package was developed for use with the Chandra Observatory data, and can also be used with other X-ray instruments, including the ROSAT HRI. However, when using wavdetect with HRI images, we need to address the questions about the false detection rate, the count (rate) threshold for  $3\sigma$  detection, and the correction factor between the detected counts and the true counts. Here we study these questions by running wavdetect on simulated HRI images.

For this study, the HRI images are simulated with the task QPSIM in the PROS package. The PSF shape is chosen to be ROSHRI, the in-flight PSF for the HRI detector. The background rate is set to a constant of 5 count/second, which is typical for HRI observations and equivalent to  $2.5 \times 10^{-7}$  count/second/pixel. Artificial sources are evenly spaced on the images, with off-axis angles ( $\theta$ ) ranging from 0 to  $20'$ . An exposure time of  $T$  seconds and a source count are assigned to all artificial sources on one image. For our simulations, we use a series of source counts from 3 to  $10^4$ , and  $T$  from  $10^3$  to  $10^6$  seconds. The central 4098 pixels ( $\sim 34'$  for a pixel scale of  $0''.5/\text{pixel}$ ) of the simulated HRI images are binned by a factor of four to get a 1024x1024 image to run wavdetect on. During the wavdetect runs, the parameter of significance threshold (`sigtthresh`) is set to `1e-6` for the 1024x1024 images, which would cause about one out of the total `1e6` pixels be erroneously identified

with a source.

### 3.1. The Scale Set for HRI Images

The result of a wavdetect run depends on the scale set used in search of point sources. The scales chosen should include the range of source sizes across the image, since a source cannot be found by scales much larger or smaller than the source size. For ROSAT HRI images, the source size changes with the off-axis angle. One estimate of the source size is  $R_{50}$ , the radius encircling 50% of the total source count, which can be expressed in a closed form as<sup>3</sup>  $R_{50} = 1.175[\sigma_{HRI}^2 + \sigma_{aspect}^2 + (\sigma_{mirror} + a\theta^b)^2]^{0.5} \text{arcsec}$ , with  $\sigma_{HRI} = 0''.74$ ,  $\sigma_{aspect} = 1''.0$ ,  $\sigma_{mirror} = 1''.3$ ,  $a = 0.0205$ , and  $b = 2.349$ . This radius changes from an on-axis  $2''.1$  to  $23''.0$  at an off-axis angle of  $18'$ . Note that the source size is supposed to enclose (almost) all source counts, and should be larger than  $R_{50}$  by a factor of a few. Here five sets of scales (in binned pixels), i.e., (1 2 4 8), (2 4 8 16), (3 6 12), (4 8 16), and (5 10 20), are tried to determine the best scale set for HRI images.

One indicator for choosing the best scale set is the false detection rate. A source detected  $>25''$  away from any artificial sources is defined as a false source. Our simulations show that there are fewer false detections for larger scales. In Figure 5 we show the false detection percentages for five scale sets. While none of the five scale sets give false detections above  $6\sigma$ , the first three scale sets give many more false detections below  $6\sigma$  than the last two. The total numbers of detected sources from the same HRI images also depend on the scale sets, with smaller scale sets detecting fewer sources. This trend, shown in Figure 6, arises because smaller scales are sensitive to smaller source regions and tend to miss more source counts, leading to a lower detection significance or even a non-detection. These results make the last two scale sets favorable over the first three of smaller scales. Here we choose (4 8 16) as the best scale set to use in following simulations and data analysis. While the scale set (5 10 20) is also favorable, we choose (4 8 16) since scales of  $2^N$  are computationally convenient for the wavelet algorithm. For the chosen scale set, the false detection rate is about 2% for sources with  $3\text{--}4\sigma$ , 0.4% for sources with  $4\text{--}5\sigma$ , and there is no false detections above  $5\sigma$  (Figure 5). The false detection rate is  $>10\%$  for detections below  $3\sigma$ , which are discarded in our analysis of the HRI observations.

---

<sup>3</sup>[http://hea-www.harvard.edu/rosat/rsdc\\_www/HRI\\_CAL\\_REPORT/node12.html](http://hea-www.harvard.edu/rosat/rsdc_www/HRI_CAL_REPORT/node12.html)

### 3.2. Count Thresholds

An important quantity to determine for an observation is the count threshold for  $3\sigma$  detection. Completely different from the parameter of significance threshold in wavdetect, this quantity could mean the count level at which a source will be detected in a 99.7% chance, or the count level at which a source will be detected with a significance of  $3\sigma$ , i.e., with a source count equal to 3 times the background error. Though related, these two count levels are not always the same, and in our analysis we use the latter since it is easier to calculate both theoretically and through simulations. By comparing the thresholds from simulations with the theoretical thresholds as a function of the source size and the background rate, one would be able to study how the source size changes across the images, with which the count thresholds across the image of an observation can be computed given its background rate.

The count threshold can be computed theoretically given the background level and the source region. As adopted by the wavdetect package, the Gehrels error  $\sigma_G$  of the background count enclosed in a source region with an area of  $S$  pixels is  $\sigma_G = 1 + \sqrt{0.75 + dTS}$  for a uniform background rate of  $d$  count/second/pixel and an exposure of  $T$  seconds. The source count threshold for the  $3\sigma$  detection is then

$$3\sigma = 3 \times (1 + \sqrt{0.75 + dTS}) \quad (1)$$

At large off-axis angles the source region deviates from a circle and is usually described as an ellipse due to the elongation of the PSF. However, for the purpose of computing the background count, only the total area of the source region matters for a uniform background rate. The background rates in most of the observations in our HRI survey are reasonably uniform across the HRI images, because the background vignetting is mild for the central  $34' \times 34'$  square field of view of the HRI detector, and observations with foreground diffuse emission from the Galactic plane, LMC and SMC are excluded from our survey. Thus, for the purpose of calculating the area, the source region can be approximated as a circle with radius in unit of  $R_{50}$  as  $R = nR_{50}$ , and the source area  $S = \pi R^2 = \pi(nR_{50})^2$ . Here  $n$  should be  $> 1$ , and its exact value may vary for different off-axis angles.

The count threshold can also be obtained by simulation runs on images of artificial sources spanning a large range of count levels. In our simulations, when the artificial source counts change from the smallest 3 counts to more and more counts, the sources change from being missed, to being detected with  $1\sigma$ , to  $2\sigma$ , to  $3\sigma$ , to a few hundred  $\sigma$ . In Figure 7 we show how this count threshold is determined with a series of count values for certain off-axis angles and background levels. These sources are sorted in ascending order of counts and connected in the count– $\sigma$  plane, the point where the  $3\sigma$  line crosses this connecting line marks the count value for  $3\sigma$  detection. For artificial sources with the same counts that have

different detection  $\sigma$ , two methods are available to sort these sources, one in ascending order of detection  $\sigma$  and another in descending order of detection  $\sigma$ . Since the two methods may lead to different results, both methods are tried and their average is used as the method-independent count value of  $3\sigma$  detection. The situation can be rather complex, in which there are more than one crossing, i.e., detections above  $3\sigma$  and detections below  $3\sigma$  or non-detections alternate in a range of count values due to the complexity of the implementation of the detection algorithm. In this situation, the simulated count threshold is taken as the average of count values from all crossings.

The count thresholds are obtained from the simulations for a grid of off-axis angles and background levels to determine the dependencies on these two parameters. For a fixed off-axis angle  $\theta$ , the simulated count thresholds change with the background level the same way as thresholds computed for a fixed source region, shown in Figure 8, and consistent with the expectation that the source region is fixed for a fixed off-axis angle. With the source region approximated as a circle and its area computed as  $S = \pi(nR_{50})^2$ , the value of  $n$  can be obtained by fitting the simulated count thresholds to the count thresholds computed using equation (1) for that off-axis angle with a least square method. For example, for the off-axis angle of  $10'.23$  in Figure 8, the best fit  $n$  is 2.6, and the equivalent source radius is  $2.6R_{50}(\theta = 10'.23) = 20''.8$ . The fitted  $n$  shows a dependency on off-axis angle  $\theta$  that can be fitted to a 4-th polynomial,  $n(\theta) = 7.46 + 0.1184\theta - 0.1949\theta^2 + 0.01813\theta^3 - 0.00046\theta^4$ . With this analytical form, the equivalent radius, thus the area, of the source region can be computed for any off-axis angle, as shown in Figure 9. The equivalent source radius does not change much within  $10'$ , outside which the source radius increases rapidly with the off-axis angle. Note that the change can be attributed to mostly the change of point source sizes and partly the change of the effective area as described by the vignetting function. Equipped with the source area, the count thresholds can be computed with equation (1) given the background rate and the exposure time. In Figure 10, the count rate thresholds for  $3\sigma$  detection, or the observation sensitivity, for a few typical exposures are calculated and plotted. Thus computed thresholds are consistent with the simulated ones to within 20%.

### 3.3. Correction Factors

The detected source counts are usually not the true source counts due to a number of reasons, e.g., the mismatching between the source region sizes and the wavelet scales used by wavdetect, vignetting and other nonuniformities of the detector. To correct the detected counts to the true counts, one must apply a correction factor ( $C$ ), which we define as  $C = \frac{\text{detected counts}}{\text{true counts}}$ . Our simulations here, with known true source count, detection significance

and detected source count for each source, provide us a chance to study the correction factor that can be applied to real data.

The simulations reveal strong dependencies of the correction factor on the off-axis angle and the detection significance. The dependency of the correction factor upon the detection significance for a fixed off-axis angle is shown in Figure 11. For sources with high detection significance, the factor is close to unity and is approximately constant. It begins to decrease below a certain significance and drops to a few tenth at  $< 3\sigma$ . The details of this dependency vary with the off-axis angle  $\theta$ . For sources on the edge of the image, the factor begins to drop at  $\sim 100\sigma$ , and drops to  $\sim 0.2$  at  $< 3\sigma$ . For sources at smaller off-axis angles, the factor begins to drop at smaller significances, and drops to higher values. In contrast, there is no significant drop in the factor for on-axis sources.

For a fixed off-axis angle  $\theta$  and a fixed detection significance  $\sigma$ , sources show slightly different correction factors in the simulations. An average correction factor  $C(\theta, \sigma)$  can be computed from these simulated sources, with its error representing the dispersion of the simulated factors. Based on the simulations, average correction factors are computed for a grid of off-axis angles and detection significances. For a source with any combination of  $\theta$  and  $\sigma$ , the correction factor  $C(\theta, \sigma)$  can be interpolated from this grid, and applied to the detected count to obtain the true count. The interpolated correction factors, plotted as a function of off-axis angles for  $\sigma = 3, 10$ , and  $100$  in Figure 12, are approximately constant within  $10'$ , and decrease outward with the off-axis angle. This decrease means more source photons are missed by the used wavelet scales at larger off-axis angles, which can be attributed to the increase of point source sizes and the vignetting function with the off-axis angle.

The interpolated correction factors are tested by applying them to compute “corrected” counts from detected counts and comparing to the true counts of the simulated sources. The results are shown in Figure 12. For sources with a high detection significance, the detected counts can be corrected to within a few percents of the true counts. For example, the detected counts for 67% ( $1\sigma$ ) of the simulated sources can be corrected to within 1% of their true counts for detection  $\sigma \geq 150$ , i.e., the ( $1\sigma$ ) fractional error of the corrected counts is 1%. This error is 1.2% for sources with  $\sigma = 100$ , 2.7% for  $\sigma = 50$ , and 7% for  $\sigma = 20$ . The error is considerably larger for sources with lower  $\sigma$ , e.g., 12% for  $\sigma = 10$ , 20% for  $\sigma = 5$ , and up to 30% for  $\sigma = 3$ . For sources with  $\sigma < 3$ , the corrected counts are significantly lower than their true counts. This systematic inaccuracy is caused by the small number of low  $\sigma$  sources in the simulation, and will not affect the applicability of the interpolated correction factors on our HRI data, since we only work on sources above  $3\sigma$ .

#### 4. Data Analysis of HRI observations

The selected HRI observations are processed to extract point sources with uniform procedures in light of the simulations in section 3. Each HRI observation is binned by a factor of 4 into a 1024x1024 image, on which wavdetect is run with the scale set (4 8 16), i.e., (8" 16" 32"). The source list from wavdetect includes the position, detection significance  $\sigma$  and the detected net count for each source.

The off-axis angle  $\theta$  is computed for a source from its position on the image, and  $C(\theta, \sigma)$  is computed based on the simulations to correct the detected count to the true count. The corrected count rate, computed as the corrected count divided by the exposure time, is converted to flux with the conversion factor computed with PIMMS<sup>4</sup> by assuming a power-law spectrum between 0.3–8 KeV with a photon index of 1.7, with the Galactic HI column density derived from the HI map by Dickey & Lockman (1990). Such a spectrum, also used by CP2002, was adopted to enable comparison with recent Chandra observations. For each source, a Kolmogorov-Smirnov test is also run to check for the variability during the observation.

For each observation, efforts have been made to improve the source positions by cross correlating X-ray sources with sources in optical, radio or infrared. Sources are also cross correlated to galaxy isophotal ellipses to determine whether they are associated with galaxies, and if they are, their luminosities are calculated.

In the following subsections we describe the data analysis procedures, which result in a catalog of point sources in other galaxies (Table 2), and a list of individual observations for ULXs (Table 3).

##### 4.1. Variability During An Observation

The temporal variations of an X-ray source can be visualized by its light curve. In our study, the background-subtracted light curves are constructed for bright sources. The event list for an X-ray source is extracted from the  $3\sigma$  elliptical source region as taken from wavdetect results, which contains 95% of the source count for an assumed 2-D Gaussian distribution. In Figure 13 we show the light curve for a ULX in the Circinus galaxy, in comparison to the scaled background. For this observation, multiple observation intervals (OBIs) of total  $\sim 13$  hours scatter over a  $\sim 22$  day period, and only a few days with

---

<sup>4</sup><http://heasarc.gsfc.nasa.gov/Tools/w3pimms.html>

significant exposure time are plotted. The light curve shows clear variations over these days. However, some temporal features are missing from the light curves of HRI sources due to the discontinuous observation scheme. The ULX in Figure 13 is an X-ray eclipsing source with a period of 7.5 hours as revealed by Chandra observations (Bauer et al. 2001), yet the periodicity is not obvious in the HRI light curve due to the wide separations between OBIs.

The variability can be described quantitatively with the Kolmogorov-Smirnov test. The Kolmogorov-Smirnov test is a widely used nonparametric method to test whether two distributions differ significantly, and here it is used to test the null hypothesis that the source is constant during an observation. A source can be viewed as constant if the null hypothesis probability (listed in Table 3) is of the order of 1. A source can be viewed as variable if the probability is much smaller, for example,  $\leq 0.1$ . To be conservative, we define a source as variable if the null hypothesis probability is  $< 0.01$ , i.e., the source is variable with a significance of  $> 99\%$ . The timescale for this variability is the duration of the observation, which ranges from a few hours to a few months. In Figure 14, we plot for the above mentioned ULX the cumulative probability curves of the Kolmogorov-Smirnov tests. The null hypothesis probability is 11% for the ULX to be constant over the 22 day observation for this source, and the probability for it to be variable is 89%. We caution here that even if the source is constant by a high probability during OBIs, the source could be variable during the wide separations between OBIs.

#### 4.2. Astrometric Corrections

The positional accuracy of an X-ray source is important in our study for determining whether the source is associated with a galaxy and whether it is a nuclear source, and for identifying the source in other wavelengths. For sources from HRI observations, the positions usually have an uncertainty of  $\sim 4''$  attributable to the smearing and elongation of HRI PSF due to residual errors in the aspect solutions associated with the ROSAT wobble or the reacquisition of the guide star (Morse, 1994). The detected positions may offset from the true positions by up to  $\sim 10''$  in rare occasions of very bad aspect solutions.

The astrometric solution for an observation can be improved if some X-ray sources can be identified with objects whose positions have been accurately catalogued. In our study, the X-ray sources are cross correlated with the two micron all sky survey (2MASS; Cutri et al. 2003) and the Faint Images of the Radio Sky at Twenty centimeters (FIRST) survey catalog (Becker et al. 2003) to identify optical and radio counterparts. The correlation procedure works iteratively by re-correlating after adjusting the source positions based on the identified sources in the previous correlation, until the number of identified sources and

the adjusted positions stabilize. The identifications are visually checked after the iterative procedure stabilizes. This process was carried out for 416 observations, and the distribution of the offsets  $\alpha$  between the HRI and catalogued positions for all identified sources is plotted in Figure 15. Assuming a 2-D normal distribution of the HRI positions relative to the catalogued positions,  $P(\alpha) = \frac{1}{2\pi\sigma^2} \exp(-\frac{\alpha^2}{2\sigma^2})$ , a least square fit to the plotted distribution results in  $\sigma = 3''.62 \pm 0''.02$ . This is consistent with what was found by Morse (1994).

With the identified sources registered to their accurate positions, the positions of unidentified sources are corrected using their positions relative to the identified ones on the X-ray image. Such corrections are carried out when there are X-ray sources identified with objects within  $5''$  of their uncorrected positions to reduce the misidentifications. This process removes the possible large offsets induced by aspect solution errors. The position error after correction is mainly attributable to statistical errors of centroiding and plate scale variations. In Table 2 the number of identified sources used to correct the position is listed for each source. A number  $\gg 0$  indicates the source position error is less than  $4''$ . In the rare occasions when this number is zero, the position error could be up to  $10''$ . Note that the identification based merely on positional coincidence may be insecure, and the astrometric correction based on the identifications may be in error. Extra cautions should be exercised when there are only one such identification for an observation, especially when this identification is for the ULX in the obaservation.

After the above astrometric corrections, multiple observations for the same galaxies are aligned to identify the same source in different observations. The position of a source, as listed in Table 2, is computed from averaging the positions in these observations. If a source is not detected but within the field of view of an observation, the  $3\sigma$  upper limit at its supposed position is computed based on the simulations and listed in Table 3.

### 4.3. Sources Associated with Galaxies

One question for studying the ULXs in other galaxies is to determine whether an X-ray source is associated with a galaxy, and further whether it is an extra-nuclear source. Once a source is known to be associated with a galaxy, its luminosity can be calculated from its flux using the distance of the galaxy it is associated with.

The association of a source with a galaxy is determined by means of the blue  $D_{25}$  isophote in our study. The separation  $\alpha$  between the galaxy center and the source is computed and compared to the elliptical radius  $R_{25}$  of the  $D_{25}$  isophotal ellipse along the great arc connecting the galaxy center and the source. This elliptical radius  $R_{25}$  has a minimum value

of the length of the semi-minor axis when the source is along the minor axis, and has a maximum value of the length of the semi-major axis when the source is along the major axis. A source with  $\alpha < R_{25}$ , i.e., within the  $D_{25}$  isophote, is considered as associated with the galaxy. Visual inspections of the DSS images show that the  $D_{25}$  isophotes are a good delimiter of the optical domain of the galaxies, though galactic features extend apparently beyond  $D_{25}$ , but within  $2 \times D_{25}$  of some galaxies. For example, in NGC1313 there are dusty star forming regions between  $1 - 2 \times D_{25}$ , and in NGC1316 there are dust loops and strips between  $1 - 2 \times D_{25}$ . To not miss any ULXs, a source with  $R_{25} < \alpha < 2 \times R_{25}$  is tentatively associated with the galaxy. In follow-up studies for the statistical properties, sources within the  $D_{25}$  isophote and sources between  $1 - 2 \times D_{25}$  are treated differently.

Nuclear X-ray sources powered by accretion onto central supermassive black holes of galaxies should be excluded from the class of ULXs. In this work the source positions after astrometric corrections are better than  $5''$ , and the positions of optical nuclei are better than a few arcseconds for most galaxies. An offset limit of  $10''$  is thus chosen to tentatively identify nuclear and non-nuclear sources. The identification is verified by examining the X-ray positions on DSS images, to account for possible large errors in the positions of optical nuclei. A nuclear source is labeled as ‘N’ in Table 2. We note that RW2000 used  $25''$  to identify nuclear sources based on the positions without astrometric corrections. This will miss ULXs near the nuclear region. For example, the ULX in NGC 5204 is  $\sim 17''$  from the nucleus, and was classified as nuclear source in RW2000.

## 5. A Catalog of Extragalactic X-ray sources

Data analysis of the 467 HRI observations in our survey as described in section 4 leads to 562 X-ray sources with detection significance above  $3\sigma$  within  $2 \times D_{25}$  of 173 out of the 313 survey galaxies. These include 371 sources within the  $D_{25}$  isophotes in 155 galaxies, and 191 sources between  $1-2 \times D_{25}$  in 88 galaxies.

These extragalactic sources are listed in Table 2 by the host galaxy and the source number within the galaxy in the order of the nuclear offsets. The positions are corrected with the help of  $N_c$  (col 6) X-ray sources identified with objects that have accurate cataloged positions in the same field, and are generally reliable to better than  $5''$  for  $N_C > 0$ . The position of a source with respect to its host galaxy is described by the nuclear offsets in arcseconds and in unit of the elliptical radius  $R_{25}$ . For each source, also listed are the maximum detection significance, the maximum luminosity, and number of observations during which the source was variable by a probability  $> 99\%$ . Inspection of the source environments shows that some sources are located in dusty regions such as dust rings/loops/patches/strips/lanes or spiral

arms that usually harbor star-forming activities and young massive stars. Sources in such dusty environments are flagged as ‘D’ in the table. Particularly, those on spiral arms are flagged as ‘S’, and those on dust rings are flagged as ‘R’.

Efforts have been made to identify the sources in other wavelengths by cross correlating with the databases of SIMBAD, NED and VizieR. While based primarily on positional coincidence, some identifications are strengthened by the rarity and strong X-ray emission power of the objects. The X-ray sources are identified to a variety of objects. Some sources are identified with objects not physically associated with the host galaxy, such as background QSO/AGNs, or bright foreground stars (denoted as ‘\*’, prefixed with their spectral type if available). Some sources are identified with objects within the host galaxy, such as supernovae (remnants), globular clusters (GC), young massive stars, or nuclei of the host galaxies. These identifications are given in Table 2 enclosed by parenthesis. Many sources are identified with objects for which the current limited knowledge can not dictate whether they are foreground stars, objects in the galaxies, or background QSO/AGNs. These include faint point sources from optical catalogs such as the USNO-B1 catalog (Monet et al. 2003), which are denoted as ‘P’ in Table 2, or point sources from radio catalogs such as the FIRST survey catalog, which are denoted as ‘Pr’. The sources are denoted as ‘mP’ when there are multiple faint objects close to the X-ray position. Usually magnitudes for these point sources are quoted from the catalogs<sup>5</sup> to illustrate their optical/infrared brightness. Visual inspections of the optical images reveal some sources positionally coincident with faint fuzzy non-pointlike features, and they are denoted as ‘Z/mZ’. These P/Pr/Z sources make promising targets for future identification programs with better positional accuracies and spatial resolutions with instruments such as Chandra and HST to better understand their nature.

Here we define ULX candidates as those with  $L_X > 10^{39}$  erg/sec in at least one observation, and with X-ray positions offset from optical galactic nuclei by  $> 10''$ . Note that for a few X-ray nuclear sources the nuclear offset listed in Table 2 are larger than  $10''$  due to the inaccuracy of optical nuclear positions in RC3. ULXs are grouped by their nuclear offsets. ULXs within the  $D_{25}$  isophote are defined as ‘1ULX’, and those between  $1-2 \times R_{25}$  defined as ‘2ULX’. The most extreme ULXs which show  $L_X > 10^{40}$  erg/sec are defined as ‘EULX’. If a source is above  $10^{39}$  erg/sec in the observations with the deepest sensitivity for the host galaxies, it is defined as ‘ULXd’. In our survey there are 216 ULXs found in 95 galaxies, with 106 ‘1ULX’ (of which 14 are ‘EULX’) in the  $D_{25}$  isophotes of 63 galaxies, and 110 ‘2ULX’ (of which 19 are ‘EULX’) between  $1-2 \times R_{25}$  of 64 galaxies.

---

<sup>5</sup>The B1/B2 magnitudes are taken from USNO-B1; the J/H/K/B/V magnitudes are from 2MASS; the BT/VT magnitudes are from the Tycho-2 catalog (Hog et al. 2000).

The individual observations for the 216 ULX candidates from Table 2 are listed in Table 3. For an individual observation of a ULX candidate, we list the observation date, the exposure time, the duration of the observation, the detection  $\sigma$ , the correction factor  $C(\theta, \sigma)$ , the corrected count and its percentage error, the flux, the luminosity, and the probability of being constant during the observation from Kolmogorov-Smirnov tests. If a source is not detected in an observation, we list the upper limits computed from the count thresholds for  $3\sigma$  detection based on the simulations. The information in this table can be used for long term variability studies, possibly along with recent observations from instruments on the Chandra and XMM-Newton observatories.

## 6. A Clean Sample of ULXs

The ULX sample defined in the above section is based on the proximity of the sources to the host galaxies, and is subject to contamination from background or foreground objects, as demonstrated by the identifications of some ULXs to background QSO/AGNs or foreground stars. To form a basis for future studies on ULXs' environments and optical identifications, here we construct a clean sample of ULXs to minimize contamination. For this clean sample, we exclude identified QSOs and foreground stars. Since the ULX candidates between  $1-2 \times D_{25}$  of host galaxies are outside the optical domain of most galaxies and less likely to associate with the galaxies, they are also excluded from the clean sample, except for a few which show apparent connections to the host galaxies by means of dust loops/strips or spiral arms. In total, this clean sample includes 109 ULXs within 61 galaxies, for which the names are given as ‘UName’ in Table 2, and the finding charts are shown in Figures 16–75. In the following we comments on the host galaxies, the environments, possible identifications and variabilities for these ULXs. The IXO number for a ULX is given if it is listed in CP2002.

### 6.1. NGC253

This Sc spiral galaxy (at a distance of 3.0 Mpc) is a prototype starburst galaxy. ULX1 is on the outer edge of the galaxy. During seven years, the source was detected once at  $2.4 \pm 0.1 \times 10^{39}$  erg/sec, and it was below  $0.3 \times 10^{39}$  erg/sec in the other five observations.

## 6.2. NGC891

NGC891 is an edge-on Sb galaxy at a distance of 8.36 Mpc. ULX1 is close to but not the nucleus and on the edge of the dust lane. ULX2 is on the dust lane and is identified as SN1986J. ULX3 (IXO 3) is on the tip of the dust lane, and showed a steady luminosity increase from  $1.4 \times 10^{39}$  to  $2.4 \times 10^{39}$  erg/sec in three years.

## 6.3. NGC1042

ULX1 (IXO 4 in CP2002) is on the tip of the spiral arm of this face-on Scd spiral galaxy, for which the distance is 8.4 Mpc.

## 6.4. NGC1068

NGC1068 at a distance of 14.4 Mpc is a Sb spiral galaxy with an outer ring. The luminosities of ULX1 changed from below  $1.5 \times 10^{39}$  erg/sec to  $\sim 4 \times 10^{39}$  erg/sec between four observations over five years. ULX2 is positioned on the outer ring, and showed variability during an 18 day observation.

## 6.5. NGC1073

NGC1073 (at a distance of 15.2 Mpc) is a barred Sc spiral galaxy. ULX1 (IXO 5) is close to a star forming knot on the spiral arm, and its luminosities increased by more than 50% between two observations separated by half a year.

## 6.6. NGC1291

ULX1 (IXO 6) is located on the outer ring-like spiral arm of this barred S0/a spiral galaxy, for which the distance is 8.6 Mpc.

### 6.7. NGC1313

Three ULXs are associated with the barred Sd galaxy NGC1313 (at a distance of 3.7 Mpc), which shows scattered star-forming regions outside its  $D_{25}$  isophote. ULX1 (IXO 7) is close to but definitely not the nucleus, and it exhibits extremely high luminosities with  $L_X > 10^{40}$  erg/s. During six years of observations, its luminosities vary by more than 50% and showed a dramatic decrease from  $10^{40}$  to  $\sim 4 \times 10^{39}$  erg/sec in less than a month. Pakull & Mirioni (2002; hereafter PM2002) found a  $H_\alpha$  nebula around this ULX. ULX2 is identified as SN1978K in a star forming region outside the  $D_{25}$  isophote. ULX3 (IXO 8) is in another star forming region outside the  $D_{25}$  isophote. During the observations, it has shown variations of  $> 50\%$ . It has been identified with a R=21.6 mag stellar-like object (Zampieri et al. 2003) within a bubble nebula (PM2002). Both ULX1 and ULX3 are variable on time scales of a few tens of days.

### 6.8. NGC1316

This peculiar S0 (lenticular) radio galaxy at a distance of 21.48 Mpc is a member of the Fornax cluster, and shows pronounced dusty patches/loops/shells outside its  $D_{25}$  isophote, reminiscent of recent merger events and possibly star forming activities. ULX1 (IXO 11) and ULX2 (IXO 10) are within the isophote. ULX2 is close to a faint point source with  $B2^6 = 20.24$  mag and  $R2^7 = 19.90$  mag. Assuming  $V \sim 20$ , the X-ray-to-optical ratio  $\log(f_x/F_v) = \log f_x(0.3 - 3.5\text{KeV}) + V/2.5 + 5.37 \sim -0.2$ , and indicates it might be a background AGN (Stocke et al. 1991). However, due to the large uncertainties in the optical magnitudes (up to 0.5 mag) and the X-ray spectral shape, this could be a red old cluster with  $M_{B2} \sim -10$  mag in NGC1316, or a M dwarf in our Galaxy. Five ULXs are on the dusty features outside the  $D_{25}$  isophote. ULX3 is IXO 12 in CP2002. ULX4 is close to a faint point source with  $B2 = 20.25$  mag and  $R2 = 19.52$  mag. ULX6 (IXO 13) is close to a faint point source with  $B2 = 21.56$  mag and  $R2 = 19.93$  mag. Multiple faint optical objects are found around ULX7.

---

<sup>6</sup>The blue photographic magnitude from the J plate used in the second Palomar sky survey.

<sup>7</sup>The red photographic magnitude from the F plate in the second Palomar sky survey.

### 6.9. NGC1365

NGC1365 is a two armed Sb galaxy with a giant bar. ULX1 is on the edge of the bar. Its luminosity dropped from  $7 \times 10^{39}$  to below  $3 \times 10^{39}$  erg/sec in one year. Two ULXs are outside the  $D_{25}$  isophote but lie on the extension of a spiral arm. ULX2 (IXO 16) is close to a faint point source with  $B_2 = 18.73$  and  $R_2 = 19.32$ . This could be a very young massive star cluster ( $M_{B_2} \sim -12$  mag) in NGC1365, or a background QSO. The luminosity of ULX3 (IXO 15) dropped from  $6 \times 10^{39}$  to below  $3 \times 10^{39}$  erg/sec in one year.

### 6.10. NGC1380

NGC1380 is a lenticular galaxy at a distance of 7.2 Mpc. ULX1 is on the edge of the galaxy.

### 6.11. NGC1399

This peculiar E1 elliptical is the central and brightest galaxy in the Fornax cluster, and is known to have globular clusters four times more abundant than a typical elliptical and 15 times more abundant than a typical spiral. ULX1 (IXO 18) and ULX2 (IXO 17) are identified with globular clusters from Chandra and WFPC2 observations (Angelini et al. 2001). ULX1 showed a change in luminosities from  $\sim 8 \times 10^{39}$  to below  $2 \times 10^{39}$  erg/sec in less than a year. ULX3 is located around some faint fuzzy features.

### 6.12. NGC1427A

This magellanic irregular galaxy is an asymmetric barred galaxy with many small knots at a distance of 16.9 Mpc in the Fornax I cluster. ULX1 (IXO 21) is located on the dusty bar.

### 6.13. PGC13826

PGC13826 (IC342) is a face-on Scd spiral at a distance of 3.9 Mpc with a very bright nucleus and weak surface brightness spiral arms. Three ULXs are all on spiral arms. ULX1 is close to but not the second nuclear source. ULX2 was highly variable during the two day

HRI observation. ULX3 (IXO 22) is coincident with a tooth-shaped nebula (PM2002), and is quite variable and showed spectral state transitions reminiscent of black hole candidates during ASCA observations (Kobuta et al. 2001).

#### 6.14. NGC1553

ULX1 and ULX2 are within the  $D_{25}$  isophote in this lenticular galaxy at a distance of 18.54 Mpc.

#### 6.15. NGC1559

ULX1 and ULX2 are both nearby knots on the dusty spiral arms of this Scd spiral galaxy at a distance of 13.6 Mpc.

#### 6.16. NGC1566

This face-on barred Sbc spiral galaxy (at a distance of 13.4 Mpc) shows clear spiral patterns. ULX1 (IXO 24) and ULX2 are on the thin spiral arms, and ULX3 is on the edge of a spiral arm. During five years of observations, all three ULXs showed variations in luminosity by more than 50%. ULX3 showed variability during a five day observation.

#### 6.17. NGC1672

ULX1 and ULX2 (IXO 26 and 27) are on the spiral arms of this barred Sb spiral galaxy at a distance of 14.5 Mpc.

#### 6.18. NGC1792

NGC1792 is a Sbc spiral galaxy at a distance of 10.1 Mpc. ULX1 and ULX2 (IXO 28) are both close to knots on the spiral arms. Between two observations in two years, ULX1 showed a change in luminosity from below  $0.7 \times 10^{39}$  to  $3 \times 10^{39}$  erg/s.

### 6.19. NGC2276

This Sc spiral galaxy at a distance of 36.8 Mpc shows unusual asymmetric spiral patterns perhaps because of a tidal encounter with its E3 companion NGC2300. There are many bright knots on the spiral arms, some of them are known to be recent supernovae. ULX1 is an extreme ULX on the spiral arm and close to a bright knot. Its luminosity increased from  $24 \pm 4 \times 10^{39}$  to  $34 \pm 8 \times 10^{39}$  erg/sec in half a year.

### 6.20. NGC2403

NGC2403 is a Sc galaxy with open spiral arms at a distance of 3.133 Mpc. ULX1 is on the amorphous spiral arms.

### 6.21. PGC23324

PGC23324 (Holmberg II) is a magellanic irregular galaxy at a distance of 4.5 Mpc with numerous HII regions and blue stellar complexes. ULX1 (IXO 31) is an extreme ULX with  $L_X = 28.4 \times 10^{39}$  erg/s. It is located in an HII complex that shows strong He II  $\lambda 4686$  that requires ionizing X-ray emission of  $\sim 1 \times 10^{40}$  erg/sec, thus arguing against beaming of the X-ray emission (PM2002). This region also exhibits flat spectrum radio emission indicative of a supernova remnant (Tongue & Westpfahl 1995).

### 6.22. NGC2775

This nearly face-on ring Sab spiral galaxy (at a distance of 17.0 Mpc) shows multiple arms of fine structure. ULX1 is on the outer edge of the galaxy and close to a faint object with B2 = 21.58 mag and R2 = 20.15 mag.

### 6.23. NGC2782

This ringed Sa spiral galaxy (at a distance of 37.3 Mpc) is a starburst galaxy with tidal plumes/tails. ULX1 is an extreme ULX with  $L_X \approx 2 \times 10^{40}$  erg/sec, and is located on the dusty plume near the disk.

### 6.24. NGC2903

This barred Sbc spiral is a starburst galaxy at a distance of 7.4 Mpc. ULX1 is on the edge of a spiral arm.

### 6.25. NGC3031

NGC3031 (M81) is an Sc spiral galaxy at a distance of 3.42 Mpc. ULX1 and ULX2 are both on a thin spiral arm. ULX1 is identified with SN1993J. ULX2 is identified as a black hole binary system with a O8V secondary based on Chandra and HST/WFPC2 observations (Liu et al. 2003).

### 6.26. PGC28757

PGC28757 (Holmberg IX) is a dwarf irregular companion to M81 with a low surface brightness and very blue color, suggesting this is a young galaxy just condensing out of the HI tidal material. The ULX (IXO 34) is outside the  $D_{25}$  isophote, and surrounded by a barrel shaped  $H_{\alpha}$  emission nebula (PM2002); this source is M81-X9 (Fabbiano et al. 1989). It is an extreme ULX with luminosities varying between  $5\text{--}13 \times 10^{39}$  erg/sec during six years of observations. Its luminosity once dropped from  $13 \times 10^{39}$  to  $5 \times 10^{39}$  erg/sec between two observations in half a year. La Perola et al. (2001) showed that the X-ray emission is highly variable over 20 years with spectral changes reminiscent of black hole candidates.

### 6.27. NGC3310

This nearly face-on Sbc spiral galaxy at a distance of 18.7 Mpc shows spiral arms with sporadic star forming knots. ULX1 and ULX2 (IXO 38) are both around knots on spiral arms.

### 6.28. NGC3623

NGC3623 (M65) is an Sa spiral galaxy at a distance of 12.3 Mpc with a pronounced dust arm in its silhouette against the disk. ULX1 is positioned on the dust arm.

### 6.29. NGC3627

NGC3627 (M66) is an Sb spiral galaxy at a distance of 8.75 Mpc with great quantity of dust throughout the disk. ULX1 is on the outer edge of a spiral arm and close to a very faint feature on the DSS image.

### 6.30. NGC3628

NGC3628 is an edge-on Sb spiral galaxy at the distance of 10.6 Mpc with a starburst nucleus, and distorted dust lanes due to its interaction with other Leo Triplet galaxies NGC3627 and NGC3623. ULX1 is located on the tip of the dust lane where distortions occur due to tidal interactions. Note that the aspect solution of the HRI observation for this galaxy was offset by up to 15".

### 6.31. NGC4088

This asymmetric Sbc spiral galaxy at a distance of 17.0 Mpc shows distorted massive knotty arms with many HII regions. ULX1 (IXO 42) is located at a bright knot on the spiral arm, and is coincident with a radio point source from the FIRST survey catalog.

### 6.32. NGC4136

NGC4136 is a face-on Sc spiral galaxy at a distance of 9.7 Mpc. ULX1 is located on a spiral arm and surrounded by several knots of emission.

### 6.33. NGC4151

This almost face-on ringed Sab galaxy (at a distance of 20.3 Mpc) hosts a prototype Seyfert 1.5 AGN, and its low surface brightness spiral arms extend slightly beyond the isophote. ULX1 (IXO 44) is within the  $D_{25}$  isophote and close to a faint point source with  $B1^8 = 19.70$  mag and  $R1^9 = 19.40$  mag. Three ULXs are on the spiral arms outside the

---

<sup>8</sup>The blue photographic magnitude from the O plate in the first Palomar sky survey.

<sup>9</sup>The red photographic magnitude from the E plate used in the first Palomar sky survey.

$D_{25}$  isophote. Multiple faint features are around ULX4 on the DSS image. ULX4 showed a luminosity drop from  $\sim 10 \times 10^{39}$  to below  $1 \times 10^{39}$  erg/sec between two observations separated by two years.

#### 6.34. NGC4190

This peculiar magellanic irregular galaxy at a distance of 2.8 Mpc show a moderately high surface brightness indicative of a high recent star-formation rate. ULX1 is located  $\sim 10''$  east of the optical nucleus.

#### 6.35. NGC4254

NGC4254 (M99) is a face-on Sc grand design spiral galaxy at a distance of 16.8 Mpc in the Virgo cluster. ULX1 is located on a thin spiral arm, while ULX2 (IXO 46) is an extreme ULX with  $L_X \approx 15 \times 10^{39}$  erg/sec which is located  $\sim 10''$  north of a foreground star.

#### 6.36. NGC4258

NGC4258 (M106) is a large barred Sbc spiral galaxy at the distance of 7.727 Mpc which hosts a weak Seyfert 2 nucleus. ULX1 is on the edge of a spiral arm, and ULX2 is on a thin spiral arm. The luminosities of both ULX1 and ULX2 changed from below  $0.3 \times 10^{39}$  to  $\sim 1.6 \times 10^{39}$  erg/sec in 500 days. ULX1 showed variability during an 20 day observation.

#### 6.37. NGC4303

NGC4303 (M61) is a face-on Sc spiral galaxy with a Seyfert 2 nucleus at a distance of 15.2 Mpc in the Virgo cluster. ULX1 is located on a thin knotty spiral arm.

#### 6.38. NGC4321

NGC4321 (M100) is a grand-design Sbc spiral galaxy at a distance of 14.13 Mpc. ULX1 is identified with SN1979C. ULX2 is on the tenuous tip of a spiral arm.

### 6.39. NGC4395

This is a magellanic spiral galaxy at a distance of 3.6 Mpc hosting a Seyfert 1 nucleus. ULX1 (IXO 53) is located on a knotty spiral arm.

### 6.40. NGC4485 and NGC4490

The magellanic irregular NGC4485 (at a distance of 9.3 Mpc) and the Sd spiral NGC4490 (at a distance of 7.8 Mpc) are interacting, and their morphologies are distorted. There are three ULXs in NGC4490, all located on irregular dusty regions. Within the isophote of NGC4485 is NGC4485-ULX1 (IXO 62), located on a dust lane. Its luminosity decreased steadily from  $4 \times 10^{39}$  to  $1.5 \times 10^{39}$  erg/sec between three observations separated by 600 days.

### 6.41. NGC4501

NGC4501 (M88) is a Sb spiral galaxy at a distance of 16.8 Mpc. ULX1 is an extreme ULX with  $L_X \approx 15 \times 10^{39}$  erg/s. This ULX is located on a spiral arm, and showed a luminosity drop from  $15 \times 10^{39}$  to  $8 \times 10^{39}$  erg/sec between two observations separated by half a year.

### 6.42. NGC4559

This Scd spiral galaxy, at a distance of 5.8 Mpc, hosts two ULXs, NGC4559-ULX1 and ULX2. ULX1 (IXO 66) is  $10''$  east of the optical nucleus, while ULX2 (IXO 65) is coincident with some blue fuzzy objects on the extension of a spiral arm.

### 6.43. NGC4565

NGC4565 is an edge-on Sb spiral galaxy at a distance of 17.46 Mpc. ULX1 (IXO 67) is an extreme ULX with  $L_X \approx 25 \times 10^{39}$  erg/s. It has been identified to a globular cluster in the halo of NGC4565 with Chandra and HST/WFPC2 observations (Wu et al. 2002).

#### 6.44. NGC4594

NGC4594 is a nearly edge-on Sa spiral galaxy with pronounced dust lanes at a distance of 9.77 Mpc. ULX1 and ULX2 are both on the dust lane.

#### 6.45. NGC4631

NGC4631 is an edge-on Sd galaxy at a distance of 6.9 Mpc. ULX1 (IXO 68) is located on the dust lanes.

#### 6.46. NGC4656 and NGC4657

The magellanic spiral NGC4656 at a distance of 7.2 Mpc is interacting with its companion NGC4657 to its north-east. ULX1 is on the tenuous tip of the tidal tail, and is coincident with a very faint object in the DSS image.

#### 6.47. NGC4697

This E6 elliptical galaxy at a distance of 11.75 Mpc has an appreciable globular cluster population. ULX1 is on the outer edge of the galaxy and coincident with a faint object with  $B_1 = 18.81$  mag,  $R_1 = 19.15$  mag,  $B_2 = 19.39$  mag, and  $R_2 = 19.04$  mag. It showed a luminosity drop from  $3.4 \times 10^{39}$  to below  $0.4 \times 10^{39}$  erg/sec between two observations over one year.

#### 6.48. NGC4861

This magellanic spiral galaxy at a distance of 17.8 Mpc has no regular structure but appears to be a strand of HII regions, with a huge HII complex or OB association as the bright spot at the south end. ULX1 (IXO 73) is on the strand of HII regions, and ULX2 (IXO 72) is coincident with the OB association. ULX1 is an extreme ULX, and its luminosity increased from  $\sim 10 \times 10^{39}$  to  $30 \times 10^{39}$  erg/sec between two observations in half a year.

#### 6.49. NGC5055

This Sbc spiral galaxy at a distance of 8.5 Mpc show flocculent spiral arms in the DSS image. ULX1 is close to but not the nucleus. ULX2 and ULX3 are on the spiral arms. ULX4 (IXO 74) is on the outer edge of the galaxy. ULX4 showed a luminosity drop from  $9 \times 10^{39}$  to  $5 \times 10^{39}$  erg/sec between two observations separated by three years.

#### 6.50. NGC5128

NGC5128 (Centarus A) is a peculiar lenticular galaxy at a distance of 4.21 Mpc with a warped lane of gas and dust. It is also a bright radio galaxy with an X-ray jet. ULX1 (IXO 76) is located on the edge of the bulge. This ULX showed luminosities  $\sim 8 \times 10^{39}$  erg/sec in five observations in a ten day time window, but it was below  $0.2 \times 10^{39}$  erg/sec in the other three observations over eight years.

#### 6.51. NGC5194

NGC5194 (M51) is a grand-design Sbc galaxy at a distance of 7.7 Mpc which is interacting with its companion NGC5195. Six ULXs are associated with the galaxy, with ULX6 on the outer edge of a spiral arm, and all the other five right on the thin knotty spiral arms. ULX1 (IXO 79), ULX2 and ULX3 (IXO 80) are near bright knots on the DSS image that are probably young star clusters. All ULXs have exhibited variations by more than 50% during six years of observations. ULX3 showed a luminosity drop from  $4 \times 10^{39}$  to below  $0.7 \times 10^{39}$  erg/sec in the observations. This source appears to have two-hour periodic variations in a recent Chandra observation (Liu et al. 2003). ULX4 is IXO 78 in CP2002. ULX5 (IXO 81) showed variability during a six day observation.

#### 6.52. NGC5204

NGC5204 is a magellanic irregular galaxy at a distance of 4.3 Mpc. ULX1 (IXO 77) is positioned  $\sim 17''$  east of the optical nucleus. It showed high variability within a one day observation. This ULX has been identified with a B0Ib supergiant presumably as a secondary in a black hole X-ray binary from Chandra and HST observations (Liu et al. 2004).

### 6.53. NGC5236

NGC5236 (M83) is a starburst barred Sc spiral galaxy at a distance of 4.7 Mpc with very luminous spiral arms. ULX1 (IXO 82) is located on the edge of a spiral arm, and its luminosity showed an increase from  $1.5 \times 10^{39}$  to  $2.5 \times 10^{39}$  erg/sec between two observations separated by 600 days.

### 6.54. NGC5457

NGC5457 (M101) is a face-on prototype Sc spiral galaxy at a distance of 6.855 Mpc. ULX1 is coincident with an object with  $B = 17.80$  mag and  $R = 15.00$  mag, and showed variability within a two day observation. ULX2 and ULX3 (IXO 83) are both on spiral arms, both showed variability within a 26 day observation, and the luminosities of both varied by more than 50% during the four observations in five years.

### 6.55. NGC5774

NGC5774 is a face-on Sd spiral with bright blue knots in the arms at a distance of 26.8 Mpc. ULX1 (IXO 84) is close to knotty features on a chain of knots across the disk.

### 6.56. NGC6946

NGC6946 is a Scd spiral at a distance of 5.5 Mpc with recent star formation throughout the spiral arm structure and a mild starburst at the center. ULX1 (IXO 85) and ULX2 are on knotty spiral arms. ULX1 showed a steady luminosity decrease from  $1.8 \times 10^{39}$  to below  $0.7 \times 10^{39}$  erg/sec in 800 days. ULX3 is on the edge of a spiral arm and coincident with a cocoon shaped supernova remnant (Dunne et al. 2001). Its extreme luminosity  $L_X = 11 \times 10^{39}$  erg/sec either comes from the colliding SNR or from accretion onto a newborn black hole (Roberts & Colbert, 2003).

### 6.57. NGC7314

This Sbc spiral, at a distance of 12.6 Mpc, has a Seyfert 1.9 nucleus and HII regions all over its spiral arms. ULX1 (IXO 86) is on the outer edge of the galaxy.

### 6.58. NGC7590

This Sbc spiral at a distance of 17.3 Mpc has a Seyfert 2 nucleus and very bright spiral arms in the inner part. ULX1 (IXO 87) is close to knotty features on the spiral arm. Its luminosity showed a drop from  $6.5 \times 10^{39}$  to  $3.4 \times 10^{39}$  erg/sec in a year.

### 6.59. NGC7714

This Sc spiral at a distance of 36.9 Mpc is interacting with its dwarf irregular companion NGC7715. ULX1 is an extreme ULX with  $L_X \sim 40 \times 10^{39}$  erg/sec, and is located on the tenuous plume on the outer edge of a spiral arm in NGC7714.

### 6.60. NGC7742

This Sb spiral at a distance of 22.2 Mpc has an extremely bright nucleus and many poorly resolved knotty arms. ULX1 is on the outer edge of the galaxy.

## 7. Summary

In this paper, we report our archival ROSAT HRI survey of extragalactic X-ray point sources and ultraluminous X-ray sources in a sample of 313 nearby galaxies with  $D_{25} > 1'$  within 40 Mpc.

The survey was carried out with well defined data reduction procedures. To detect point sources from HRI observations we utilize the wavdetect package, an implementation of a wavelet algorithm, for which simulations were run to better understand its characteristics such as the count thresholds for  $3\sigma$  detection and correction factors. For sources detected above  $3\sigma$  from the HRI observations in our survey, we compute their count rate and fluxes, and test whether they are variable during the observations with Kolmogorov-Smirnov tests. The X-ray positions were corrected by registering X-ray sources to the accurate positions of their counterparts in other wavelengths, and the positional accuracy is better than  $5''$  for most X-ray sources. X-ray Sources within  $2 \times D_{25}$  of a galaxy are considered associated with the galaxy and their luminosities are computed by placing them at the distance for the galaxy. The uniform data reduction procedures lead to 562 extragalactic X-ray sources in 173 nearby galaxies spanning a luminosity range of  $10^{38} - 10^{43}$  erg/sec, with 371 sources within the  $D_{25}$  isophotes in 155 galaxies, and 191 sources between  $1-2 \times D_{25}$  in 88 galaxies.

In our survey we define those extra-nuclear sources with  $L_X > 10^{39}$  erg/sec as ULX candidates. This leads to a sample of 216 ULX candidates, which includes a sample of 106 ULXs within the  $D_{25}$  isophotes in 63 galaxies (1ULX), and a sample of 116 ULXs between  $1-2 \times D_{25}$  in 64 galaxies (2ULX). Thus defined ULX candidates are possibly not in the host galaxies, and ten (16) in the 1ULX (2ULX) sample are already identified as background QSOs or foreground stars. To minimize such contaminations, we constructed a clean sample of 109 ULXs in 61 galaxies by excluding those identified stars and QSOs, and excluding most of the 2ULX sample since they are more likely contaminating sources due to their large separations from the galaxies. This clean sample forms a good basis for studies on ULX's environments and identifications.

A few conclusions can be drawn from examinations of the clean sample. ULXs are preferentially found in late-type galaxies. for example, 49 out of 181 spiral galaxies in our survey host 89 ULXs, while 4 out of 93 early-type galaxies host 7 ULXs if we exclude the 8 ULXs in two peculiar lenticular galaxies NGC1316 and NGC5128. There is also a strong tendency for ULXs to occur in dusty regions of star formation, with 84 of the 109 ULXs in the clean sample in such regions. Specifically, 51 ULXs occur on thin dusty spiral arms. Also note that the seven ULXs in NGC1316 are associated with dust loops/shells/patches reminiscent of star forming activities. The above statistics reveals a strong connection between the ULX phenomenon and star formation, as reported by previous authors.

Some ULXs have demonstrated great variability over a range of time scales from days to up to 10 years. Fifteen out of 109 ULXs in the clean sample have shown variability during at least one observation lasting from days to months. These ULXs are all located in star forming regions in late-type galaxies. For ULXs with more than one HRI observations, a variety of temporal behaviors have been exhibited. These include sudden bursts with small duty cycles (e.g., NGC5128-ULX1), steady increases (e.g., NGC891-ULX3), steady decreases (e.g., NGC6946-ULX1), or occasional sharp drops from almost constant high luminosity (e.g., NGC1313-ULX1).

ULXs show a very diverse nature seen from the identifications for the clean sample. Five ULXs are identified as recent supernovae (remnants). Many ULXs on knotty spiral arms in the DSS images are clearly identified with HII regions/nebulae in recent observations with better resolutions (PM2002). There are two confirmed cases in which the ULXs are identified with very young massive stars: NGC3031-ULX2 with an O8V star (Liu et al. 2003); and NGC5204-ULX1 with a B0Ib star (Liu et al. 2004). These identifications are consistent with the strong link between ULXs and star formation. However, there are also ULXs identified with old globular clusters lacking recent star formation. For example, NGC4565-ULX1 is identified with a halo globular cluster, and two ULXs are identified with globular clusters in

the elliptical galaxy NGC1399. These ULXs in the globular clusters may have been formed differently from those in star forming regions.

While many qualitative properties have been revealed from studying the clean sample of ULXs, the quantitative properties such as the occurrence rates of ULXs derived from the clean sample are not strictly accurate because the clean sample is not a complete sample in the statistical sense, and the contamination, though small, is not known. In a subsequent paper, statistical properties, such as the occurrence frequencies and luminosity functions, of ULXs in different types of galaxies will be studied quantitatively with the contamination carefully calculated and subtracted, in comparison to statistical studies of ULXs in 766 nearby galaxies with  $cz < 5000$  km/sec in HRI observations by Ptak & Colbert (2004) and of ULXs in 82 nearby galaxies in Chandra observations by Swartz et al. (2004).

We are grateful to the NED, VizieR services. We would like to thank Dan Harris, Samantha Stevenson, Renato Dupke, James Irwin, Ed Lloyd-Davies and Eric Miller for helpful discussions. We thank the referee for his constructive suggestions. We gratefully acknowledge support for this work from NASA under grants HST-GO-09073.

## REFERENCES

- Angelini, L., Loewenstein, M., and Mushotzky, F., 2001, ApJ, 557, L35
- Bauer, F.E., Brandt, W.N., Sambruna, R.M., Chartas, G., Garmire, G.P., Kaspi, S., and Netzer, H., 2001, AJ, 122, 182
- Becker, R., Helfand, D., White R., Gregg M., and Laurent-Muehleisen S., 1997, ApJ, 475, 479, version2003 (the FIRST survey catalog)
- Begelman, M.C., 2002, ApJ, 568, L97
- Colbert, E. J. M. and Mushotzky, R. F. 1999, ApJ, 519, 89
- Colbert, E. and Ptak, A. 2002, ApJS, 143, 25 (CP2002)
- Cutri, R., et al. 2003 (2MASS)
- Dickey, J, and Lockman, F., 1990, ARA&A, 28, 215
- Dunne, B., Points, S., and Chu, Y., 2001, AJ, 119, 1172

- Freedman, W., Madore, B., Gibson, B., Ferrarese, L., Kelson, D. et al., 2001, ApJ, 553, 47  
(KP)
- Fabbiano, G., Gioia, I., and Trinchieri, G., 1989, ARA&A, 27, 87
- Hasinger, G., Burg, R., Giacconi, R., Hartner, G., Schmidt, M., Trumper, J. and Zamorani, G. . 1993, A&A, 275,1
- Ho, L., Filippenko, A., and Sargent, W., 1995, ApJS, 98, 477
- Hog, E., Fabricius, C., Makarov, V.V., Urban, S., Corbin T., et al. 2000, A&A 355, L27  
(Tycho-2)
- Irwin, J., Bregman, J., and Athey, A., 2004, ApJL, 60, 143
- King, A. R., Davies, M. B., Ward, M. J., Fabbiano, G. and Elvis, M. 2001, ApJ, 552, L109
- Kobuta, A., Mizuno, T., Makishima, K., et al. 2001, ApJ, 547, L119
- La Perola, V., Peres, G., et al. 2001, ApJ, 556, 47
- Liu, J., Bregman, J., and Seitzer, P., 2002, ApJL, 580, 31
- Liu, J., Bregman, J., and Irwin, J., 2002, ApJL, 581, 93
- Liu, J., Bregman, J., and Seitzer, P., 2004, ApJ, 602, 249
- Monet D.G., Levine S.E., Casian B., et al. 2003, AJ, 125, 984 (USNO-B1.0)
- Morse J., 1994, PASP, 106, 675
- Pakull, M., and Mirioni, L., 2002, astro-ph/0202488 (PM2002)
- Portegies Zwart, S., 2004, AAS203, 102.03, and private discussions
- Ptak, A., and Colbert, E., 2004, astro-ph/0401525
- Roberts, T. P. and Warwick, R. S. 2000, MNRAS, 315, 98 (RW2000)
- Roberts, T., and Colbert, E., 2003, MNRAS, 341, L49
- ROSAT Scientific Team, ROSAT NEWS No. 71, The ROSAT Consortium (2000)
- Stocke, J., Morris, S., et al. 1991, ApJS, 76, 813
- Swartz, D., Ghosh, K., Tennant, A., and Wu, K., 2004, astro-ph/0405498

Tongue, T., and Westpfahl, D., 1995, AJ, 109, 2462

Tonry J.L., Dressler A., Blakeslee J.P., Ajhar E.A., Fletcher A.B., et al., 2001, ApJ, 546, 681 (SBF)

TULLY R.B, 1988, *Nearby Galaxies Catalogue*, Cambridge University Press. (T88)

Tully R.B., Shaya E.J., Pierce M.J., 1992, ApJS, 80, 479 (T92)

Zampieri, L, Mucciarelli, P., et al., 2004, ApJ, 603, 523

Table 1. Properties of surveyed galaxies

galaxy	GLON <sup>a</sup> (deg)	GLAT <sup>b</sup> (deg)	D25 <sup>c</sup> ( $\prime$ )	d25 <sup>d</sup> ( $\prime$ )	nH <sup>e</sup> (cm $^{-2}$ )	Distance <sup>f</sup> (Mpc)	Morphol. <sup>g</sup> Type	Hubble <sup>h</sup> T	$L_B$ <sup>i</sup> ( $L_\odot$ )	$f_{\nu}$ (60 $\mu m$ ) <sup>j</sup> (Jy)	$M_{FIR}$ <sup>k</sup> (mag)	Starburst <sup>l</sup>
NGC247	113.95	-83.56	21.4	6.9	1.55E20	2.8[T92]	SAB(s)d	7	1.6E09	7.8e-01	-16.7	...
NGC253	97.36	-87.96	27.5	6.8	1.42E20	3.0[T92]	SAB(s)c	5	6.8E09	7.6e+02	-21.8	Sbrst
NGC300	299.20	-79.42	21.9	15.5	3.23E20	2.023[KP]	SA(s)d	7	2E09	<6.8e+00	-17.1	...
NGC404	127.03	-27.01	3.5	3.5	5.31E20	3.27[SBF]	SA(s)o-	-3	5.9E08	2.3e+00	-15.4	...
NGC520	138.70	-58.06	4.5	1.8	3.27E20	27.8[T88]	peculiar	99	1.9E10	3.2e+01	-22.8	...
NGC613	229.07	-80.30	5.5	4.2	1.63E20	26.7[T92]	SB(rs)bc	4	5.6E10	2.0e+01	-22.4	...
NGC720	173.02	-70.36	4.7	2.4	1.54E20	27.67[SBF]	E5	-5	4.1E09	<2.2e-01	<-17.3	...
NGC891	140.38	-17.42	13.5	2.5	7.64E20	8.36[SBF]	SA(s)b	3	6.3E09	3.4e+01	-21.3	HII
NGC1042	182.08	-58.17	4.7	3.6	3.12E20	8.4[T92]	SAB(rs)cd	6	2.1E09	1.2e+00	-17.3	...
NGC1047	181.70	-57.96	1.3	0.6	3.07E20	17.9[NED]	S0+	-0.5	...	<1.5e-02	<-13.4	...
NGC1052	182.02	-57.93	3.0	2.1	3.07E20	19.41[SBF]	E4	-5	1.5E10	9.4e-01	-18.1	...
NGC1068	172.10	-51.94	7.1	6.0	3.53E20	14.4[T88]	SA(rs)b	3	4.3E10	1.9e+02	-23.2	...
NGC1073	170.91	-50.73	4.9	4.5	4.23E20	15.2[T88]	SB(rs)c	5	8.3E09	1.1e+00	-18.5	...
NGC1097	226.91	-64.68	9.3	6.3	1.85E20	16.8[T92]	SB(s)b	3	4.5E10	4.6e+01	-22.3	...
NGC1291	247.52	-57.05	9.8	8.1	2.12E20	8.6[T88]	SB(s)o/a	0	1.9E10	1.7e+00	-17.8	...
NGC1313	283.36	-44.64	9.1	6.9	3.89E20	3.7[T88]	SB(s)d	7	2.8E09	1.0e+01	-18.8	HII
NGC1316	240.16	-56.69	12.0	8.5	1.89E20	21.48[SBF]	SAB(s)o/o	-2	1.2E11	3.1e+00	-19.9	...
NGC1317	239.97	-56.69	2.8	2.4	1.91E20	16.9[T88]	SAB(r)a	1	8E09	3.6e+00	-19.6	...
NGC1332	212.18	-54.37	4.7	1.4	2.23E20	22.91[SBF]	S(s)o-	-3	2.4E10	5.2e-01	-18.3	...
NGC1365	237.95	-54.60	11.2	6.2	1.39E20	17.38[KP]	SB(s)b	3	3.8E10	7.8e+01	-23.0	...
NGC1369	238.10	-53.96	1.5	1.4	1.40E20	18.9[NED]	SB(rs)o/a	0	1.8E09	<4.3e-02	<-14.7	...
NGC1380	235.93	-54.06	4.8	2.3	1.31E20	17.62[SBF]	SA0	-2	1.7E10	1.1e+00	-18.4	...
NGC1380A	235.52	-53.99	2.4	0.7	1.29E20	15.85[SBF]	S0o	-2	1.8E09	<3.4e-02	<-14.0	...
NGC1382	236.29	-53.92	1.5	1.3	1.31E20	22.59[SBF]	SAB(s)o-	-2.7	2.5E09	<4.0e-02	<-15.0	...
NGC1386	237.66	-53.97	3.4	1.3	1.37E20	16.52[SBF]	SB(s)o/+	-0.6	5.3E09	5.9e+00	-19.8	...
NGC1395	216.21	-52.12	5.9	4.5	1.99E20	24.10[SBF]	E2	-5	3.9E10	<5.2e-01	<-17.9	...
NGC1398	221.53	-52.79	7.1	5.4	9.46E19	22.2[T92]	SB(r)ab	2	4.8E10	9.3e-01	-19.5	...
NGC1399	236.71	-53.64	6.9	6.5	1.34E20	19.95[SBF]	E1	-5	4.9E10	<8.9e-01	<-18.1	...
NGC1404	236.95	-53.56	3.3	3.0	1.36E20	20.99[SBF]	E1	-5	2.6E10	<2.0e-01	<-16.6	...
NGC1427A	236.99	-53.29	2.3	1.5	1.36E20	16.9[T88]	IB(s)m	10	1.9E09	2.1e-01	<-15.0	...
NGC1433	255.69	-51.20	6.5	5.9	1.44E20	11.6[T88]	SB(r)ab	2	1E10	3.3e+00	-19.0	...
NGC1481	214.00	-47.81	1.0	0.7	3.73E20	23.1[NED]	SA0-	-3.3	1.4E09	3.6e-01	<-13.9	...
NGC1482	214.12	-47.80	2.5	1.4	3.69E20	19.6[T88]	SA0+	-0.8	3.3E09	3.2e+01	-22.0	HII
NGC1531	233.13	-46.60	1.3	0.9	1.68E20	13.0[T88]	S0-	-3.2	1.4E09	<2.5e-02	<-13.3	...
NGC1532	233.17	-46.58	12.6	3.3	1.68E20	16.8[T92]	SB(s)b	2.7	1.5E10	<8.3e-01	-19.7	...
NGC1549	265.41	-43.80	4.9	4.1	1.46E20	19.68[SBF]	E0	-5	3.3E10	1.3e-01	<-17.2	...
NGC1553	265.63	-43.69	4.5	2.8	1.50E20	18.54[SBF]	SA(r)o/o	-2	4.2E10	5.2e-01	-17.4	...
NGC1559	274.51	-41.20	3.5	2.0	2.65E20	13.6[T92]	SAB(s)cd	6	9.2E09	2.4e+01	<-15.2	...
NGC1566	264.31	-43.39	8.3	6.6	1.34E20	13.4[T88]	SAB(s)bc	4	2.5E10	1.3e+01	-20.6	...
NGC1574	266.89	-42.58	3.4	3.1	1.64E20	19.86[SBF]	SA(s)o-	-2.7	1.4E10	3.1e-01	<-16.5	...
NGC1640	218.87	-37.22	2.6	2.0	2.99E20	19.1[T88]	SB(r)b	3	5.8E09	1.1e+00	-18.7	...
NGC1672	268.79	-38.99	6.6	5.5	2.28E20	14.5[T88]	SB(s)b	3	1.6E10	3.5e+01	-21.6	...
NGC1705	261.08	-38.74	1.9	1.4	4.19E20	6.0[T88]	SA0-	-3	4.2E08	1.1e+00	-15.7	HII
NGC1792	241.69	-36.45	5.2	2.6	2.58E20	10.1[T92]	SA(rs)bc	4	7.4E09	2.5e+01	-20.6	...
NGC2146	135.66	24.90	6.0	3.4	7.30E20	17.2[T88]	SB(s)ab	2	1.8E10	1.4e+02	-23.3	...
NGC2273	154.97	23.31	3.2	2.5	6.97E20	28.4[T88]	SB(r)a	0.5	1.4E10	6.3e+00	-21.1	...
NGC2276	127.67	27.71	2.8	2.7	5.32E20	36.8[T88]	SAB(rs)c	5	2.6E10	1.2e+01	-22.5	...
NGC2300	127.71	27.81	2.8	2.0	5.27E20	31.0[T88]	SA0o	-2	2.4E10	<1.2e-01	<-16.8	...
NGC2366	146.42	28.54	8.1	3.3	4.08E20	2.7[T92]	IB(s)m	10	3.2E08	<5.4e-01	-15.2	...
NGC2403	150.57	29.19	21.9	12.3	4.13E20	3.133[KP]	SAB(s)cd	6	3.4E09	1.8e+01	-18.8	HII
NGC2442	281.30	-21.50	5.5	4.9	1.18E21	17.1[T88]	SAB(s)bc	3.7	1.7E10	5.3e+00	<-17.2	...
NGC2715	134.73	33.32	4.9	1.7	1.94E20	20.4[T88]	SAB(rs)c	5	1.2E10	1.7e+00	-19.7	...
NGC2775	223.27	33.99	4.3	3.3	4.07E20	17.0[T88]	SA(r)ab	2	1.6E10	1.7e+00	<-16.5	...
NGC2782	182.15	43.68	3.5	2.6	1.76E20	37.3[T88]	SAB(rs)a	1	3.4E10	8.5e+00	-22.0	Sbrst
NGC2853	182.05	45.44	1.7	0.9	1.60E20	28.2[T88]	SB0	-2	2.4E09	2.6e-01	<-15.2	...
NGC2903	208.71	44.54	12.6	6.0	3.14E20	7.4[T92]	SAB(rs)bc	4	1.2E10	2.8e+01	-20.7	HII
NGC2974	239.51	35.01	3.5	2.0	3.72E20	21.48[SBF]	E4	-5	1.2E10	4.8e-01	-18.0	...
NGC2992	249.71	28.78	3.5	1.1	5.26E20	30.5[T88]	Sa	1	1.3E10	6.9e+00	-21.4	...
NGC2993	249.76	28.77	1.3	0.9	5.27E20	30.5[T88]	Sa	1	7.9E09	1.0e+01	-21.7	HII
NGC3031	142.09	40.90	26.9	14.1	4.16E20	3.42[KP]	SA(s)ab	2	1.2E10	7.0e+00	-19.1	...
NGC3034	141.40	40.57	11.2	4.3	3.98E20	5.2[T88]	I0	90	8.3E09	1.2e+03	-23.0	Sbrst
NGC3049	227.57	44.72	2.2	1.4	3.03E20	19.9[NED]	SB(rs)ab	2	3.7E09	2.7e+00	-19.4	Sbrst
NGC3073	157.99	48.25	1.3	1.2	8.22E19	33.73[SBF]	SAB0-	-2.5	6E09	<3.1e-02	<-15.6	...
NGC3079	157.81	48.36	7.9	1.4	7.89E19	17.3[T92]	SB(s)c	7	1.3E10	4.3e+01	-22.2	...
NGC3115	247.78	36.78	7.2	2.5	4.32E20	9.68[SBF]	S0-	-3	2.2E10	2.1e-01	<-15.5	...

Table 1—Continued

galaxy	GLON <sup>a</sup> (deg)	GLAT <sup>b</sup> (deg)	D25 <sup>c</sup> ( $\prime$ )	d25 <sup>d</sup> ( $\prime$ )	nH <sup>e</sup> (cm $^{-2}$ )	Distance <sup>f</sup> (Mpc)	Morphol. <sup>g</sup> Type	Hubble <sup>h</sup> T	$L_B^i$ ( $L_\odot$ )	$f_{\nu}(60\mu m)^j$ (Jy)	$M_{FIR}^k$ (mag)	Starburst <sup>l</sup>
NGC3185	213.22	54.70	2.3	1.6	2.12E20	21.3[T88]	SB(r)a	1	5.6E09	1.6e+00	-19.1	...
NGC3187	212.93	54.79	3.0	1.3	2.12E20	26.1[T88]	SB(s)c	5	5.5E09	9.1e-01	-19.1	HII
NGC3190	213.03	54.85	4.4	1.5	2.12E20	22.4[T88]	SA(s)a	1	1.4E10	3.5e+00	-20.2	...
NGC3193	212.97	54.93	3.0	2.7	2.12E20	34.04[SBF]	E2	-5	2.6E10	<1.6e-01	<-17.4	...
NGC3226	216.93	55.44	3.2	2.8	2.14E20	23.55[SBF]	E2	-5	7.9E09	<1.8e-01	<-16.7	...
NGC3227	217.00	55.45	5.4	3.6	2.15E20	20.6[T88]	SAB(s)a	1	1.5E10	8.0e+00	-20.8	...
NGC3252	134.80	40.05	2.0	0.6	4.09E20	20.8[T88]	SBd	6.7	1.5E09	9.4e-01	-18.5	...
NGC3294	184.62	59.84	3.5	1.8	1.65E20	26.7[T88]	SA(s)c	5	2.4E10	6.1e+00	-21.2	...
NGC3310	156.61	54.06	3.1	2.4	1.13E20	18.7[T88]	SAB(r)bc	4	2.1E10	3.3e+01	-21.9	HII
NGC3370	225.35	59.67	3.2	1.8	2.64E20	23.4[T88]	SA(s)c	5	1E10	3.6e+00	-20.3	...
NGC3377	231.18	58.31	5.2	3.0	2.86E20	11.22[SBF]	E5	-5	7.9E09	<3.2e-01	<-15.7	...
NGC3377A	230.96	58.29	2.2	2.1	2.87E20	5.1[T88]	SAB(s)m	9	1.5E08	<9.6e-02	<-12.7	...
NGC3379	233.49	57.63	5.4	4.8	2.75E20	10.57[SBF]	E1	-5	1.3E10	<5.2e-01	<-16.1	...
NGC3384	233.52	57.75	5.5	2.5	2.73E20	11.59[SBF]	SB(s)o-	-3	1.2E10	<2.8e-01	<-15.6	...
NGC3389	233.72	57.74	2.8	1.4	2.72E20	22.5[T88]	SA(s)c	5	9.2E09	<7.5e-02	<-15.7	...
NGC3395	192.93	63.14	2.1	1.2	1.98E20	27.4[T88]	SAB(rs)cd	6	1.2E10	8.2e+00	<-15.7	...
NGC3396	192.90	63.16	3.1	1.2	1.98E20	21.8[T92]	IBm	10	6.5E09	8.2e+00	<-15.6	...
NGC3398	152.01	54.36	1.3	0.6	7.84E19	38.2[NED]	Sa	1	1.7E09	8.2e-01	<-15.1	...
NGC3440	149.55	53.50	2.1	0.5	5.78E19	25.4[NED]	SBb	3	2.5E09	5.5e-01	-18.4	...
NGC3486	202.07	65.49	7.1	5.2	1.91E20	12.3[T92]	SAB(r)c	5	1.1E10	4.6e+00	<-16.8	...
NGC3513	273.08	33.31	2.8	2.2	5.58E20	14.7[T92]	SB(rs)c	5	4.9E09	2.6e+00	-19.0	...
NGC3516	133.24	42.40	1.7	1.4	3.05E20	38.9[T88]	SB(s)o	-2	2.9E10	1.7e+00	-20.3	...
NGC3622	135.77	47.55	1.2	0.5	1.28E20	17.5[NED]	S	...	1.2E09	1.1e+00	-18.3	...
NGC3623	241.33	64.22	9.8	2.9	2.16E20	12.3[T92]	SAB(rs)a	1	2.4E10	2.1e+00	-19.1	...
NGC3627	241.95	64.42	9.1	4.2	2.43E20	8.75[KP]	SAB(s)b	3	1.8E10	3.4e+01	-21.1	...
NGC3628	240.85	64.78	14.8	3.0	2.22E20	10.6[T92]	SB	3	1.2E10	4.8e+01	-21.4	...
NGC3642	142.55	54.53	5.4	4.5	8.05E19	27.5[T88]	SA(r)bc	4	2.9E10	1.5e+00	-19.8	...
NGC3658	175.38	68.45	1.6	1.5	2.06E20	27.3[NED]	SA(r)o	-2.3	6.1E09	<4.8e-02	<-15.6	...
NGC3665	174.71	68.49	2.5	2.0	2.06E20	32.4[T88]	SA(s)o	-2	3.4E10	2.0e+00	-20.5	...
NGC3738	144.56	59.32	2.5	1.9	1.08E20	4.3[T88]	Im	10	5.5E08	2.0e+00	-15.8	HII
NGC3972	138.85	60.06	3.9	1.1	1.20E20	17.0[T88]	SA(s)bc	4	3.5E09	1.0e+00	-18.4	...
NGC3982	138.83	60.27	2.3	2.0	1.22E20	17.0[T88]	SAB(r)b	3	8.6E09	6.9e+00	-20.2	...
NGC3990	138.25	60.04	1.4	0.8	1.21E20	10.28[SBF]	S0-	-3	6E08	<2.3e-02	<-12.7	...
NGC3998	138.17	60.06	2.7	2.2	1.22E20	14.13[SBF]	SA(r)o	-2	8.6E09	4.4e-01	<-15.2	...
NGC4036	132.98	54.25	4.3	1.7	1.89E20	24.6[T88]	S0-	-3	2.4E10	5.4e-01	<-16.6	...
NGC4041	132.70	54.05	2.7	2.5	1.97E20	22.7[T88]	SA(rs)bc	4	1.6E10	1.4e+01	-21.6	...
NGC4051	148.88	70.08	5.2	3.9	1.32E20	17.0[T88]	SAB(rs)bc	4	1.3E10	8.3e+00	-20.5	...
NGC4085	140.59	65.17	2.8	0.8	2.00E20	17.0[T88]	SAB(s)c	5	3.1E09	5.5e+00	-20.1	...
NGC4088	140.33	65.01	5.8	2.2	2.00E20	17.0[T88]	SAB(rs)bc	4	1.6E10	1.7e+01	<-16.4	...
NGC4105	291.46	32.11	2.7	2.0	4.99E20	26.55[SBF]	E3	-5	2.4E10	2.3e-01	<-16.4	...
NGC4106	291.48	32.11	1.6	1.3	4.98E20	30.6[T88]	SB(s)o+	-1	2.1E10	2.3e-01	<-15.7	...
NGC4136	193.63	80.34	4.0	3.7	1.62E20	9.7[T88]	SAB(r)c	5	3.1E09	1.3e+00	-17.4	HII
NGC4138	147.29	71.40	2.6	1.7	1.36E20	13.80[SBF]	SA(r)o+	-1	4.3E09	<8.8e-02	<-14.8	...
NGC4144	143.17	69.01	6.0	1.3	1.28E20	5.7[T92]	SAB(s)cd	6	7.2E08	1.4e+00	-16.2	HII
NGC4150	190.45	80.47	2.3	1.6	1.62E20	13.74[SBF]	SA(r)o	-2	3E09	1.2e+00	-17.8	...
NGC4151	155.07	75.06	6.3	4.5	1.98E20	20.3[T88]	SAB(rs)ab	2	2.8E10	<5.6e-01	<-17.6	...
NGC4156	154.75	75.04	1.4	1.1	1.99E20	15.5[T88]	SB(rs)b	3	8.6E08	<3.2e-02	<-13.9	...
NGC4190	160.62	77.59	1.7	1.5	1.54E20	2.8[T88]	Im	10	6.1E07	3.7e-01	<-10.7	...
NGC4203	173.03	80.08	3.4	3.2	1.19E20	15.14[SBF]	SAB0-	-3	8.5E09	6.4e-01	-17.6	...
NGC4214	160.25	78.07	8.5	6.6	1.49E20	3.5[T88]	IAB(s)m	10	1.6E09	1.4e+01	-17.5	HII
NGC4235	279.17	68.47	4.2	0.9	1.53E20	35.1[T88]	SA(s)a	1	1.8E10	3.2e-01	-18.4	...
NGC4236	127.41	47.36	21.9	7.2	1.76E20	2.2[T88]	SB(s)dm	8	5.4E08	<3.2e+00	-15.2	...
NGC4242	140.77	70.31	5.0	3.8	1.18E20	7.5[T88]	SAB(s)dm	8	2.1E09	<3.8e-01	<-15.1	...
NGC4244	154.56	77.16	16.6	1.9	1.67E20	4.2[T92]	SA(s)cd	6	1.7E09	4.5e-01	-16.9	HII
NGC4248	138.71	68.68	3.0	1.1	1.20E20	7.3[T88]	I0	90	3E08	<6.6e-02	<-13.1	...
NGC4254	270.42	75.19	5.4	4.7	2.72E20	16.8[T88]	SA(s)c	5	3.7E10	2.3e+01	-22.2	...
NGC4257	281.72	67.26	1.3	0.4	1.55E20	36.7[NED]	Sab	2	2.3E09	<9.1e-03	<-14.4	...
NGC4258	138.32	68.84	18.6	7.2	1.16E20	7.727[KP]	SAB(s)bc	4	1.8E10	<2.7e+00	-20.0	...
NGC4261	281.80	67.37	4.1	3.6	1.55E20	31.62[SBF]	E2	-5	4.4E10	<3.0e-01	<-17.9	...
NGC4269	281.91	67.59	1.1	0.8	1.54E20	27.7[NED]	SO+	-1	3.1E09	<1.8e-02	<-14.6	...
NGC4278	193.79	82.77	4.1	3.8	1.77E20	16.07[SBF]	E1	-5	1.5E10	5.7e-01	-17.5	...
NGC4283	193.44	82.81	1.5	1.5	1.77E20	15.70[SBF]	E0	-5	2.5E09	<4.5e-02	<-14.3	...
NGC4286	193.02	82.88	1.6	1.0	1.79E20	8.6[NED]	SA(r)o/a	0	2.6E08	<3.2e-02	<-12.6	...
NGC4291	125.55	41.60	1.9	1.6	2.96E20	26.18[SBF]	E	-5	1.3E10	<6.0e-02	<-15.8	...
NGC4292	283.90	66.35	1.7	1.1	1.66E20	30.1[NED]	SB(r)o	-1.7	5E09	<3.8e-02	<-15.6	...

Table 1—Continued

galaxy	GLON <sup>a</sup> (deg)	GLAT <sup>b</sup> (deg)	D25 <sup>c</sup> ( $\prime$ )	d25 <sup>d</sup> ( $\prime$ )	nH <sup>e</sup> (cm $^{-2}$ )	Distance <sup>f</sup> (Mpc)	Morphol. <sup>g</sup> Type	Hubble <sup>h</sup> T	$L_B^i$ ( $L_\odot$ )	$f_\nu(60\mu m)^j$ (Jy)	$M_{FIR}^k$ (mag)	Starburst <sup>l</sup>
NGC4298	272.36	75.67	3.2	1.8	2.68E20	16.8[T88]	SA(rs)c	5	6.1E09	4.2e+00	-19.6	...
NGC4302	272.51	75.69	5.5	1.0	2.69E20	16.8[T88]	Sc	5	3.8E09	<1.1e-01	-20.0	...
NGC4303	284.37	66.27	6.5	5.8	1.67E20	15.2[T88]	SAB(rs)bc	4	2.9E10	2.4e+01	-21.8	HII
NGC4303A	284.62	66.40	1.5	1.3	1.67E20	17.0[NED]	SAB(s)cd	5.5	1.6E09	5.5e-01	-17.4	...
NGC4319	125.44	41.66	3.0	2.3	2.91E20	28.2[T88]	SB(r)ab	2	9.3E09	4.0e-01	<-16.8	...
NGC4321	271.14	76.90	7.4	6.3	2.39E20	14.13[KP]	SAB(s)bc	4	2.4E10	1.8e+01	-21.5	HII
NGC4328	271.53	76.95	1.3	1.2	2.39E20	6.4[NED]	SA0-	-3	1.2E08	<3.3e-02	<-12.0	...
NGC4374	278.20	74.48	6.5	5.6	2.60E20	18.37[SBF]	E1	-5	4E10	5.1e-01	<-17.7	...
NGC4387	278.84	74.47	1.8	1.1	2.60E20	21.38[SBF]	E	-5	4.3E09	<3.9e-02	<-14.9	...
NGC4388	279.12	74.34	5.6	1.3	2.60E20	16.8[T88]	SA(s)b	3	7.8E09	1.1e+01	-20.6	...
NGC4395	162.08	81.54	13.2	11.0	1.35E20	3.6[T88]	SA(s)m	9	8.5E08	2.1e+00	-16.5	...
NGC4402	278.79	74.79	3.9	1.1	2.65E20	3.1[NED]	Sb	3	1.1E08	5.8e+00	-16.5	...
NGC4406	279.08	74.64	8.9	5.8	2.62E20	17.14[SBF]	E3	-5	4.8E10	<1.0e+00	<-17.9	...
NGC4411A	283.86	70.82	2.0	1.9	1.68E20	16.8[T88]	SB(rs)c	5	1.7E09	<7.9e-02	-16.9	...
NGC4411B	284.07	70.85	2.5	2.5	1.68E20	16.8[T88]	SAB(s)cd	6	3E09	4.2e-01	-17.3	...
NGC4413	279.82	74.35	2.3	1.5	2.61E20	16.8[T88]	SB(rs)ab	2	2.8E09	1.0e+00	-18.3	...
NGC4435	280.18	74.89	2.8	2.0	2.66E20	16.8[T88]	SB(s)o0	-2	9.2E09	2.1e+00	-18.8	HII
NGC4438	280.34	74.83	8.5	3.2	2.66E20	16.8[T88]	SA(s)o/a	0	2.1E10	4.1e+00	-19.7	...
NGC4449	136.85	72.40	6.2	4.4	1.37E20	3.0[T88]	IBm	10	1.2E09	<5.4e-01	<-13.4	HII
NGC4464	286.50	70.32	1.1	0.8	1.66E20	16.8[T88]	S	...	1.4E09	<1.8e-02	<-13.5	...
NGC4467	286.73	70.17	1.2	0.9	1.66E20	16.8[T88]	E2	-5	8E08	<2.2e-02	<-13.7	...
NGC4470	286.95	70.01	1.3	0.9	1.65E20	31.2[NED]	Sa	1	7.8E09	1.9e+00	-20.1	HII
NGC4472	286.92	70.19	10.2	8.3	1.66E20	16.29[SBF]	E2	-5	7.8E10	<1.7e+00	<-18.4	...
NGC4476	283.09	74.39	1.7	1.2	2.54E20	17.22[SBF]	SA(r)o-	-3	2.9E09	5.9e-01	-17.7	...
NGC4478	283.38	74.39	1.9	1.6	2.53E20	18.11[SBF]	E2	-5	6.8E09	<6.2e-02	<-15.0	...
NGC4485	137.98	74.81	2.3	1.6	1.78E20	9.3[T88]	IB(s)m	10	1.4E09	<7.5e-02	<-13.7	HII
NGC4486	283.78	74.49	8.3	6.6	2.54E20	16.07[SBF]	E0+	-4	5.5E10	4.3e-01	<-17.9	...
NGC4490	138.00	74.87	6.3	3.1	1.78E20	7.8[T88]	SB(s)d	7	6.9E09	4.0e+01	<-15.2	...
NGC4501	282.33	76.51	6.9	3.7	2.48E20	16.8[T88]	SA(rs)b	3	3.3E10	1.4e+01	-21.5	...
NGC4523	283.12	77.36	2.0	1.9	2.33E20	16.8[T88]	SAB(s)m	8.5	1.2E09	3.4e-01	-17.3	...
NGC4526	290.16	70.14	7.2	2.4	1.65E20	16.90[SBF]	SAB(s)o0	-2	3E10	5.9e+00	-20.1	...
NGC4527	292.60	65.18	6.2	2.1	1.87E20	13.5[T88]	SAB(s)bc	4	7.7E09	2.6e+01	-21.2	HII
NGC4533	292.85	64.86	2.1	0.4	1.82E20	23.4[NED]	SAd	7.1	1.5E09	<1.7e-02	<-14.2	...
NGC4536	292.95	64.73	7.6	3.2	1.82E20	14.32[KP]	SAB(rs)bc	4	1.3E10	3.0e+01	-21.2	HII
NGC4539	278.55	80.27	3.3	1.4	2.15E20	18.6[NED]	SB(s)a	0.5	3.3E09	<9.0e-02	<-15.5	...
NGC4540	283.68	77.80	1.9	1.5	2.29E20	16.8[T88]	SAB(rs)cd	6	4.4E09	1.4e+00	-18.7	...
NGC4545	126.09	53.50	2.5	1.5	1.76E20	28.9[T92]	SB(s)cd	5.5	8.2E09	1.0e+00	-19.4	...
NGC4552	287.93	74.97	5.1	4.7	2.57E20	15.35[SBF]	E0	-5	1.9E10	<4.8e-01	<-16.8	HII
NGC4559	198.35	86.47	10.7	4.4	1.49E20	5.8[T92]	SAB(rs)cd	6	3.9E09	5.3e+00	-18.4	HII
NGC4562	231.85	86.23	2.5	0.8	1.34E20	9.7[T88]	SB(s)dm	8	3.6E08	<3.9e-02	<-13.1	...
NGC4565	230.73	86.44	15.8	2.1	1.30E20	17.46[SBF]	SA(s)b	3	4.3E10	6.0e+00	-21.1	...
NGC4569	288.47	75.62	9.5	4.4	2.49E20	16.8[T88]	SAB(rs)ab	2	3.2E10	7.2e+00	-20.7	...
NGC4586	294.64	66.98	4.0	1.3	1.88E20	17.5[T88]	SA(s)a	1	4.5E09	5.5e-01	-17.6	...
NGC4593	297.48	57.40	3.9	2.9	2.31E20	39.5[T88]	SB(rs)b	3	5.2E10	2.8e+00	-21.0	...
NGC4594	298.46	51.15	8.7	3.5	3.77E20	9.77[SBF]	SA(s)a	1	5.5E10	3.2e+00	-19.0	...
NGC4605	125.33	55.47	5.8	2.2	1.43E20	4.0[T88]	SB(s)c	5	1.1E09	1.2e+01	-17.7	HII
NGC4627	142.96	84.18	2.6	1.8	1.27E20	7.2[NED]	E4	-5	5.4E08	<9.2e-02	<-13.4	...
NGC4631	142.82	84.22	15.5	2.7	1.27E20	6.9[T88]	SB(s)d	7	1E10	5.2e+01	-21.0	...
NGC4636	297.75	65.47	6.0	4.7	1.81E20	14.66[SBF]	E0	-5	1.9E10	<5.6e-01	<-16.9	...
NGC4638	295.14	74.18	2.2	1.4	2.17E20	21.68[SBF]	S0-	-3	1.1E10	<6.2e-02	<-15.4	...
NGC4639	294.30	75.99	2.8	1.9	2.35E20	20.8[KP]	SAB(rs)bc	4	9.6E09	1.4e+00	-19.3	...
NGC4647	295.75	74.34	2.9	2.3	2.20E20	16.8[T88]	SAB(rs)c	5	6.5E09	5.0e+00	-20.1	...
NGC4649	295.88	74.31	7.4	6.0	2.20E20	16.83[SBF]	E2	-5	6E10	<9.0e-01	<-17.7	...
NGC4651	293.07	79.12	4.0	2.6	1.99E20	16.8[T88]	SA(rs)c	5	1.3E10	5.2e+00	-20.1	...
NGC4656	140.32	84.70	15.1	3.0	1.23E20	7.2[T88]	SB(s)m	9	4.8E09	2.2e+00	-18.1	...
NGC4666	299.54	62.37	4.6	1.3	1.74E20	14.1[T88]	SABc	5	6.3E09	2.6e+01	<-15.2	...
NGC4668	299.75	62.30	1.4	0.8	1.74E20	21.6[NED]	SB(s)d	7	3E09	7.2e-01	-18.3	...
NGC4697	301.63	57.06	7.2	4.7	2.12E20	11.75[SBF]	E6	-5	1.9E10	<6.8e-01	<-16.7	...
NGC4736	123.36	76.01	11.2	9.1	1.44E20	5.20[SBF]	SA(r)ab	2	1.4E10	5.6e+01	-20.0	...
NGC4757	303.50	52.56	1.5	0.4	3.46E20	11.3[NED]	S0	-2	...	<1.1e-02	<-12.1	...
NGC4758	304.53	78.72	3.1	0.7	1.96E20	16.2[T88]	Im	10	1.2E09	9.2e-01	-18.2	...
NGC4772	304.14	65.04	3.4	1.7	1.79E20	16.3[T88]	SA(s)a	1	4.4E09	<1.2e-01	<-15.4	...
NGC4826	315.71	84.42	10.0	5.4	2.57E20	7.48[SBF]	SA(rs)ab	2	2E10	3.7e+01	-20.2	...
NGC4861	111.52	82.10	4.0	1.5	1.19E20	17.8[T88]	SB(s)m	9	4.7E09	1.8e+00	<-15.7	Sbrst
NGC4904	308.15	62.75	2.2	1.4	1.55E20	15.6[NED]	SB(s)cd	6	2.9E09	2.5e+00	-19.0	Sbrst

Table 1—Continued

galaxy	GLON <sup>a</sup> (deg)	GLAT <sup>b</sup> (deg)	D25 <sup>c</sup> ( $\prime$ )	d25 <sup>d</sup> ( $\prime$ )	nH <sup>e</sup> (cm $^{-2}$ )	Distance <sup>f</sup> (Mpc)	Morphol. <sup>g</sup> Type	Hubble <sup>h</sup> T	$L_B$ <sup>i</sup> ( $L_\odot$ )	$f_\nu(60\mu m)$ <sup>j</sup> (Jy)	$M_{FIR}$ <sup>k</sup> (mag)	Starburst <sup>l</sup>
NGC5005	101.61	79.25	5.8	2.8	1.08E20	21.3[T88]	SAB(rs)bc	4	3.1E10	1.9e+01	-22.0	...
NGC5033	98.05	79.45	10.7	5.0	9.96E19	15.2[T92]	SA(s)c	5	2.1E10	1.3e+01	-21.1	...
NGC5035	311.02	46.01	1.4	1.1	4.99E20	29.1[NED]	SAB(r)o+	-1	...	3.7e-01	<-15.3	...
NGC5037	311.05	45.91	2.2	0.7	5.10E20	29.0[T88]	SA(s)a	1	6.9E09	7.1e-01	-19.3	...
NGC5044	311.23	46.10	3.0	3.0	4.93E20	31.19[SBF]	E0	-5	2.8E10	<1.8e-01	<-17.3	...
NGC5049	311.43	46.07	1.9	0.6	4.98E20	39.3[T88]	S0	-2	...	<2.2e-02	<-15.5	...
NGC5055	106.01	74.28	12.6	7.2	1.32E20	8.5[T92]	SA(rs)bc	4	1.7E10	2.8e+01	-20.9	HII
NGC5076	313.52	49.55	1.3	0.7	3.23E20	39.9[NED]	SB(rs)o+	-1	...	<1.9e-02	<-15.4	...
NGC5079	313.57	49.59	1.6	1.0	3.19E20	38.3[NED]	SB(rs)bc	3.5	...	2.4e+00	-20.9	...
NGC5088	313.87	49.68	2.6	0.8	3.09E20	24.5[T88]	SAB(s)bc	3.7	4.9E09	1.8e+00	-19.5	...
NGC5089	61.41	83.07	1.7	0.9	1.12E20	35.1[T88]	S	...	4.7E09	6.8e-01	-19.2	...
NGC5117	44.43	82.93	2.2	1.0	1.18E20	38.3[T88]	SBcd	6	6.2E09	3.2e-01	<-16.3	...
NGC5128	309.52	19.42	25.7	19.9	8.62E20	4.21[SBF]	S0	-2	2.3E10	1.7e+02	-20.9	...
NGC5194	104.85	68.56	11.2	6.9	1.57E20	7.7[T88]	SA(s)bc	4	2.1E10	3.2e+01	-21.6	HII
NGC5195	104.89	68.48	5.8	4.6	1.56E20	7.66[SBF]	I0	90	5E09	1.0e+01	<-15.4	...
NGC5204	113.50	58.01	5.0	3.0	1.39E20	4.3[T92]	SA(s)m	9	6.2E08	2.4e+00	-16.1	HII
NGC5236	314.58	31.97	12.9	11.5	3.82E20	4.7[T88]	SAB(s)c	5	1.6E10	1.0e+02	-21.4	Sbrst
NGC5238	107.40	64.19	1.7	1.4	1.10E20	4.9[T88]	SAB(s)dm	8	1E08	<4.9e-02	<-11.9	...
NGC5273	74.35	76.25	2.8	2.5	9.40E19	16.52[SBF]	SA(s)o0	-2	4.8E09	<1.4e-01	<-15.7	...
NGC5322	110.28	55.49	5.9	3.9	1.81E20	31.19[SBF]	E3	-5	6E10	4.1e-01	<-18.3	...
NGC5350	82.84	71.59	3.2	2.3	9.79E19	37.8[T88]	SB(r)b	3	2.7E10	2.2e+00	-21.0	Sbrst
NGC5353	82.61	71.63	2.2	1.1	9.76E19	37.8[T88]	S0	-2	3.2E10	3.0e-01	<-16.3	...
NGC5354	82.66	71.62	1.4	1.3	9.77E19	34.3[NED]	S0	-2	1.8E10	<3.8e-02	<-15.8	...
NGC5355	82.62	71.55	1.2	0.7	9.86E19	31.3[NED]	S0	-2	3.9E09	<1.7e-02	<-14.8	...
NGC5358	82.37	71.56	1.1	0.3	9.87E19	32.0[NED]	S0/a	0	2.1E09	<7.4e-03	<-13.9	...
NGC5371	82.17	71.19	4.4	3.5	1.03E20	37.8[T88]	SAB(rs)bc	4	6.4E10	2.6e+00	-21.4	...
NGC5457	102.04	59.77	28.8	26.9	1.16E20	6.855[KP]	SAB(rs)cd	6	4.6E10	3.9e+00	-21.1	...
NGC5506	339.15	53.81	2.8	0.9	3.81E20	28.7[T88]	Sa	1	6.4E09	8.8e+00	-21.3	...
NGC5507	339.23	53.85	1.7	0.9	3.84E20	34.3[T88]	SAB(r)o0	-2.3	7.4E09	<3.2e-02	<-15.7	...
NGC5774	359.41	52.49	3.0	2.5	3.46E20	26.8[T88]	SAB(rs)d	7	8.4E09	5.6e-01	-19.1	...
NGC5775	359.43	52.42	4.2	1.0	3.48E20	26.7[T88]	SBc	5	1.2E10	1.5e+01	-22.2	...
NGC5813	359.18	49.85	4.2	3.0	4.21E20	32.21[SBF]	E1	-5	3.2E10	<2.5e-01	<-17.8	...
NGC5839	.20	49.01	1.3	1.2	4.28E20	22.59[SBF]	SAB(rs)o0	-2	2.8E09	<3.0e-02	<-14.7	...
NGC5846	.43	48.80	4.1	3.8	4.26E20	24.89[SBF]	E0	-5	3.2E10	<3.1e-01	<-17.4	HII
NGC5850	.52	48.64	4.3	3.7	4.26E20	28.5[T88]	SB(r)b	3	1.9E10	7.3e-01	-19.5	...
NGC5951	23.52	50.45	3.5	0.8	3.33E20	20.4[T92]	SBc	5.3	2.9E09	6.0e-01	-18.2	...
NGC5953	23.92	50.35	1.6	1.3	3.27E20	33.0[T88]	SAA	1	...	1.0e+01	-22.0	...
NGC5954	23.94	50.34	1.3	0.6	3.26E20	32.1[T88]	SAB(rs)cd	6	...	1.0e+01	<-14.7	...
NGC6217	111.32	33.36	3.0	2.5	4.04E20	23.9[T88]	SB(rs)bc	4	1.3E10	1.0e+01	-21.4	...
NGC6434	102.97	31.43	2.3	1.0	3.73E20	33.1[NED]	SBbc	4	8.8E09	1.8e+00	-20.2	HII
NGC6503	100.57	30.64	7.1	2.4	4.09E20	6.1[T88]	SA(s)cd	6	2.2E09	7.2e+00	-18.3	HII
NGC6654	103.97	27.84	2.6	2.1	5.42E20	29.5[T88]	SB(s)o/a	0	1.2E10	4.0e-01	<-16.7	...
NGC6764	81.50	18.23	2.3	1.3	6.07E20	25.9[T92]	SB(s)bc	3.5	6E09	6.5e+00	-21.0	...
NGC6946	95.72	11.67	11.5	9.8	2.11E21	5.5[T88]	SAB(rs)cd	6	6.5E09	5.2e+01	-21.1	HII
NGC7172	15.13	-53.06	2.5	1.4	1.65E20	33.9[T88]	Sa	1.4	1.4E10	6.0e+00	-21.5	...
NGC7173	14.96	-53.08	1.2	0.9	1.64E20	31.33[SBF]	E+	-4.1	2.2E10	<2.1e-02	<-15.0	...
NGC7174	14.93	-53.09	2.3	1.2	1.64E20	35.5[T88]	Sab	1.8	2.4E10	3.5e+00	-21.1	...
NGC7176	14.93	-53.10	1.0	0.8	1.64E20	32.3[T88]	E	-4.6	2.3E10	3.5e+00	<-14.8	...
NGC7213	349.59	-52.58	3.1	2.8	2.04E20	22.0[T88]	SA(s)a	1	1.9E10	2.6e+00	-19.9	...
NGC7217	86.51	-19.71	3.9	3.2	1.06E21	16.0[T88]	SA(r)ab	2	1.3E10	4.8e+00	-20.0	...
NGC7314	27.13	-59.74	4.6	2.1	1.46E20	12.9[T92]	SAB(rs)bc	4	5.7E09	3.4e+00	-19.2	...
NGC7322	87.39	-29.67	4.1	1.1	4.57E20	23.01[SBF]	S0	-2	1.2E10	<9.1e-02	<-15.9	...
NGC7339	87.46	-29.73	3.0	0.7	4.57E20	19.3[T88]	SAB(s)bc	4	3.4E09	<4.5e-02	<-14.8	...
NGC7463	88.04	-39.35	2.9	0.7	6.04E20	33.5[T88]	SABb	3	8.1E09	<3.9e-02	<-15.8	...
NGC7465	88.07	-39.39	1.2	0.8	6.03E20	27.2[T88]	SB(s)o0	-1.5	5.4E09	2.7e+00	-20.3	...
NGC7507	23.44	-68.04	2.8	2.7	2.47E20	25.00[SBF]	E0	-5	2.1E10	<1.5e-01	<-16.6	...
NGC7552	348.15	-65.24	3.4	2.7	1.85E20	19.5[T88]	SB(s)ab	2	1.7E10	7.3e+01	-22.9	HII
NGC7582	348.08	-65.70	5.0	2.1	1.93E20	17.6[T88]	SB(s)ab	2	1.5E10	4.8e+01	-22.2	...
NGC7590	348.23	-65.85	2.7	1.0	1.96E20	17.3[T88]	SA(rs)bc	4	6.1E09	7.4e+00	-20.4	...
NGC7599	348.09	-65.91	4.4	1.3	1.98E20	20.2[T88]	SA(s)c	5	1.1E10	6.1e+00	-20.6	...
NGC7714	88.22	-55.57	1.9	1.4	4.86E20	36.9[T88]	SB(s)b	3	1.4E10	1.1e+01	-22.1	HII
NGC7715	88.27	-55.58	2.6	0.5	4.86E20	36.3[T88]	Im	10	3.3E09	<2.6e-02	<-15.6	...
NGC7742	97.43	-48.75	1.7	1.7	5.14E20	22.2[T88]	SA(r)b	3	8E09	3.0e+00	-19.9	HII
PGC4013	131.57	-61.53	1.1	0.9	3.13E20	8.9[NED]	S	...	1.3E08	<2.1e-02	<-12.3	...
PGC5208	138.72	-57.99	1.2	0.9	3.30E20	28.7[NED]	Im	10	...	<2.2e-02	<-14.9	...

Table 1—Continued

galaxy	GLON <sup>a</sup> (deg)	GLAT <sup>b</sup> (deg)	D25 <sup>c</sup> ( $\prime$ )	d25 <sup>d</sup> ( $\prime$ )	nH <sup>e</sup> (cm $^{-2}$ )	Distance <sup>f</sup> (Mpc)	Morphol. <sup>g</sup> Type	Hubble <sup>h</sup> T	$L_B^i$ ( $L_\odot$ )	$f_{\nu}(60\mu m)^j$ (Jy)	$M_{FIR}^k$ (mag)	Starburst <sup>l</sup>
PGC12827	212.16	-54.42	2.3	0.7	2.23E20	28.3[NED]	S	...	8E08	<3.3e-02	<-15.3	...
PGC13381	215.95	-52.26	1.3	0.6	2.02E20	17.9[NED]	S0	...	4.7E08	<1.6e-02	<-13.5	...
PGC13449	236.58	-53.49	1.3	1.0	1.30E20	11.0[NED]	SAB(s)o0	-2	...	<2.7e-02	<-13.0	...
PGC13452	237.17	-53.46	1.1	1.1	1.40E20	12.0[NED]	E0	-5	...	<2.4e-02	<-13.1	...
PGC13826	138.17	10.58	21.4	20.9	3.02E21	3.9[T88]	SAB(rs)cd	6	5.4E09	8.6e+01	-21.0	HII
PGC14656	233.10	-46.47	1.1	0.6	1.73E20	16.8[NED]	SAB(s)o0	-2	6.2E08	<1.4e-02	<-13.2	...
PGC14664	233.38	-46.44	1.7	1.1	1.72E20	11.7[NED]	IB(s)m	10	2.7E08	<3.9e-02	<-13.5	...
PGC15455	256.76	-42.55	2.6	0.4	1.71E20	21.5[T88]	Sb	3	3.2E09	1.4e+00	-19.1	...
PGC16790	242.20	-35.94	3.5	2.7	2.96E20	11.1[T88]	SB(s)dm	8	1.1E09	2.3e-01	<-15.2	...
PGC20844	143.69	28.08	1.8	1.1	3.76E20	38.8[V3K]	Scd	6	1.3E10	8.0e-01	-20.0	...
PGC21406	281.13	-21.37	1.6	1.5	1.19E21	19.4[NED]	IBm	10	...	<4.8e-02	<-14.9	...
PGC21457	281.30	-21.33	1.9	1.0	1.17E21	20.4[NED]	SB(s)o/a	-0.5	2.6E09	<4.0e-02	<-14.8	...
PGC23324	144.28	32.69	7.9	6.3	3.42E20	4.5[T88]	Im	10	1.4E09	<1.0e+00	-15.4	...
PGC23852	207.51	29.32	1.5	0.9	3.79E20	27.7[NED]	SB(s)cd	6	2.7E09	3.0e-01	<-14.9	...
PGC26068	181.09	43.81	1.7	1.4	1.80E20	33.3[NED]	SAB(s)d	7	2.3E09	<4.6e-02	<-16.0	...
PGC28757	141.98	41.06	2.5	2.0	4.07E20	3.42[KP]	Im	10	...	<1.0e-01	<-11.9	...
PGC29584	158.67	49.93	1.4	0.9	7.53E19	14.7[NED]	S	...	...	<2.6e-02	<-13.6	...
PGC30819	140.20	43.60	13.2	5.4	2.37E20	3.5[T92]	SAB(s)m	9	9E08	<1.4e+00	-16.0	...
PGC31586	269.55	26.99	2.6	1.8	5.08E20	30.2[NED]	E4+	-4	1.1E10	<9.4e-02	<-16.6	...
PGC32390	193.39	63.07	1.3	0.9	2.01E20	21.8[NED]	SB(s)m	9.3	9.7E08	3.4e-01	<-14.3	...
PGC32604	151.76	54.33	1.3	1.1	7.80E19	15.9[NED]	Scd	6	4.3E08	<2.8e-02	<-13.8	...
PGC35286	127.84	37.33	1.4	0.8	3.83E20	1.4[T88]	peculiar	99	4.8E06	3.8e-01	<-8.4	...
PGC35450	181.07	70.67	1.5	0.6	2.13E20	29.6[NED]	Im	10	...	<1.7e-02	<-14.7	...
PGC35684	151.91	63.28	1.2	0.7	1.54E20	4.0[T88]	Im	10	6.4E07	<1.6e-02	<-10.3	...
PGC37532	138.38	59.83	1.4	0.4	1.17E20	18.1[NED]	Sdm	8	4.3E08	<1.2e-02	<-13.2	...
PGC37580	288.51	33.65	1.1	0.9	6.21E20	23.8[NED]	SB(r)dm	7.9	1.2E09	<2.0e-02	<-14.4	...
PGC37951	132.68	53.85	1.6	0.5	2.00E20	21.2[T88]	Im	10	1.1E09	2.5e-01	<-13.9	...
PGC38811	154.65	75.15	1.0	0.9	1.97E20	13.3[NED]	SBm	9	...	<1.9e-02	<-13.0	...
PGC40045	270.47	76.79	1.1	0.8	2.42E20	17.3[NED]	I	...	...	<1.9e-02	<-13.6	...
PGC41054	281.29	74.82	1.3	0.4	2.64E20	6.3[NED]	SO+	-1	6.6E07	<1.1e-02	<-10.8	...
PGC41258	287.14	70.14	1.1	0.9	1.65E20	3.7[NED]	Im	10	2.5E07	<2.0e-02	<-10.3	...
PGC41763	283.00	77.55	1.5	1.1	2.31E20	31.1[NED]	SB(rs)c	4.7	3.5E09	3.8e-01	<-15.5	...
PGC42081	288.28	75.71	2.2	1.1	2.48E20	16.8[T88]	IBm	10	1.3E09	6.1e-01	-17.6	...
PGC45561	117.40	62.87	1.6	0.6	1.57E20	33.0[NED]	SB	...	3.6E09	3.6e-01	<-14.9	...
PGC46093	106.40	74.36	1.6	0.6	1.32E20	5.2[NED]	Im	10	...	<1.8e-02	<-11.0	...
PGC53683	359.57	49.78	1.4	0.5	4.22E20	16.6[NED]	SB(rs)dm	8	6.1E08	2.5e-01	<-13.2	...
PGC55095	67.94	55.22	1.6	0.5	1.98E20	37.1[T88]	IBm	10	...	<1.5e-02	<-15.0	...
PGC58052	96.22	39.82	1.4	0.7	2.62E20	36.8[NED]	Sdm	8	2.1E09	<2.0e-02	<-15.3	...
PGC59551	104.03	33.74	1.8	0.3	4.02E20	14.4[NED]	Sb	3	8E08	1.1e+00	-18.0	HII
PGC67352	10.04	-50.17	1.4	1.4	2.04E20	33.3[T88]	SB0-	-3	8.2E09	<4.0e-02	<-15.8	...
PGC67707	344.49	-49.43	1.5	0.9	2.17E20	36.0[NED]	IBm	10	1.2E09	<2.6e-02	<-15.5	...
PGC67910	14.94	-53.22	1.2	0.4	1.63E20	30.9[NED]	S	...	1.8E09	<9.1e-03	<-14.1	...
PGC68498	352.26	-54.53	1.3	1.0	2.24E20	22.5[T88]	IB(s)m	10	8.6E08	<2.6e-02	<-14.5	...
PGC68618	350.32	-54.84	8.5	3.9	1.80E20	11.1[T88]	SB(rs)cd	6	4.3E09	3.3e-01	-17.6	...
PGC69404	60.93	-51.99	2.6	0.9	4.01E20	38.9[NED]	SAB(s)dm	7.6	...	<4.6e-02	<-16.3	...
PGC70070	5.19	-64.04	4.1	0.8	1.19E20	20.5[T88]	SB(rs)cd	5.5	2.7E09	<6.4e-02	<-15.3	...
PGC70081	4.48	-64.03	2.5	0.5	1.18E20	25.9[NED]	Sab	2.3	4.4E09	5.1e-01	-18.7	...
PGC70090	4.67	-64.11	5.2	3.8	1.18E20	29.24[SBF]	E3	-5	6E10	4.2e-01	<-18.1	...
PGC70110	5.58	-64.31	1.8	0.8	2.12E20	26.9[T88]	SAB(rs)0	-1.8	5.9E09	<2.9e-02	<-15.0	...
PGC70117	5.94	-64.39	3.2	0.6	1.23E20	25.7[NED]	SB(r)cd	5.7	6.5E09	3.1e+00	-20.4	HII
PGC70285	88.05	-39.26	1.4	0.3	6.07E20	27.0[NED]	Im	10	...	<8.0e-03	<-13.6	...
PGC71120	87.53	-48.51	1.2	1.1	5.04E20	37.5[NED]	Sm	9	...	<2.6e-02	<-15.6	...

<sup>a</sup>Galactic longitude of the galaxy.

<sup>b</sup>Galactic latitude of the galaxy.

<sup>c</sup>The major axis of the D<sub>25</sub> isophotal ellipsis.

<sup>d</sup>The minor axis of the D<sub>25</sub> isophotal ellipsis.

<sup>e</sup>The Galactic HI column density, taken from the dust map by Dickey & Lockman (1990).

<sup>f</sup>Enclosed in brackets are the references for the distances, with KP for the Key Project (Freedman et al. 2002), SBF for the surface brightness fluctuation method (Tonry et al. 2001), T92 for the nearby galaxy flow model by Tully (1992), T88 for the Nearby Galaxy Catalog (Tully 1988). Distances computed from recessional velocities taken from the NED service (RC3) are labelled as NED(V3K).

<sup>g</sup>The morphological type is taken from RC3. In the type code S stands for spiral, E for elliptical, S0 for lenticular, I for irregular; (r) for inner

ring, (s) for S-shaped, (rs) for mixed; B for barred, A for non-barred, AB for mixed; Im for magellanic irregular, I0 for non-magellanic irregular; the trailing -/o/+ for early/intermediate/late stage; etc. The detailed explanations can be found in the RC3 catalogue (p. 15, Vol. I).

<sup>h</sup>The Hubble type T of galaxies is taken from RC3.

<sup>i</sup>The blue luminosity calculated from the apparent blue magnitude taken from RC3. The luminosity is expressed in unit of solar luminosity assuming a absolute blue magnitude of 5.47 for the Sun.

<sup>j</sup>The flux density at 60 $\mu$ m taken from the IRAS point source catalog (IPAC, 1986), with some nearby galaxies from Rice et al. (1988). When the galaxy is below detection, the 3 $\sigma$  upper limit is calculated by adopting noise levels of 8.5 mJy/arcmin<sup>2</sup> for 60  $\mu$ m (Rice et al. 1988).

<sup>k</sup>The absolute FIR magnitude, computed from the flux densities at 60 $\mu$ m and 100 $\mu$ m as prescribed in RC3. A prefixed '<' means the magnitude is computed from the upper limits of the flux densities.

<sup>l</sup>This flag indicates the galaxy is a HII/starburst galaxy with high star formation rate.

Table 2. X-ray sources in surveyed galaxies

Galaxy	Name	R.A. (hh:mm:ss)	Decl. (dd:mm:ss)	$N_c^a$	r <sup>b</sup> ( $\prime$ )	r/R25 <sup>c</sup>	$\sigma_{Max}^d$	$L/10^{39e}$ (erg/s)	$N_v^f$	Env <sup>g</sup>	ID <sup>h</sup>	ULX <sup>i</sup>	UName <sup>j</sup>
NGC247	X1	00:47:10.30	-20:47:10.7	0	95.4	0.16	5.9	0.133					
NGC247	X2	00:47:04.00	-20:47:45.7	1	143.8	0.42	32.4	0.853		D			
NGC247	X3	00:46:51.78	-20:43:27.2	1	271.1	1.10	17.9	0.427			QSO PHL6625		
NGC247	X4	00:47:27.57	-20:47:24.6	1	285.2	1.23	12.3	0.265			P B2/18.83		
NGC247	X5	00:47:03.69	-20:40:15.5	0	330.1	0.54	3.7	0.0628			mZ		
NGC247	X6	00:46:47.98	-20:38:36.9	1	511.8	1.37	5.3	0.095					
NGC247	X7	00:47:03.31	-20:36:57.1	1	526.4	0.83	9.3	0.243		D			
NGC253	X1	00:47:33.55	-25:17:24.4	1	8.9	0.04	15.4	1.74			(NGC253)	N	
NGC253	X2	00:47:32.97	-25:17:50.2	0	32.3	0.12	23.5	0.823					
NGC253	X3	00:47:29.69	-25:17:03.4	0	48.5	0.20	4.0	0.157					
NGC253	X4	00:47:34.87	-25:15:11.0	0	129.3	0.44	11.0	0.3					
NGC253	X5	00:47:24.93	-25:19:47.0	0	185.6	0.33	3.5	0.063					
NGC253	X6	00:47:42.58	-25:15:00.4	0	188.3	0.27	13.6	0.322					
NGC253	X7	00:47:17.37	-25:18:12.7	1	220.3	0.50	12.3	0.451					
NGC253	X8	00:47:18.10	-25:19:13.6	0	234.0	0.33	5.1	0.131					
NGC253	X9	00:47:22.43	-25:20:51.8	1	258.1	0.49	12.6	0.631					
NGC253	X10	00:47:10.68	-25:20:55.1	0	373.5	0.46	13.0	0.419					
NGC253	X11	00:47:09.27	-25:14:01.5	0	378.4	1.75	4.3	0.0786					
NGC253	X12	00:47:05.29	-25:19:44.0	0	404.4	0.74	5.6	0.122					
NGC253	X13	00:47:09.08	-25:21:25.0	0	408.7	0.50	10.3	0.203					
NGC253	X14	00:47:22.89	-25:10:52.2	0	409.9	1.93	6.6	0.149			P B1/19.42		
NGC253	X15	00:47:31.49	-25:09:58.2	0	440.3	1.80	3.4	0.0652					
NGC253	X16	00:47:10.86	-25:23:33.9	0	481.9	0.79	3.5	0.0589			P		
NGC253	X17	00:47:50.55	-25:08:39.0	0	570.5	1.43	4.3	0.11			P B2/21.06		
NGC253	X18	00:48:00.26	-25:09:51.8	1	578.7	0.92	5.8	0.21			QSO J0047.9-2509		
NGC253	X19	00:46:47.16	-25:21:51.6	0	680.3	1.15	6.8	0.159			mP		
NGC253	X20	00:48:19.99	-25:10:09.8	0	767.0	0.96	38.6	2.37				1ULX	ULX1
NGC253	X21	00:48:29.81	-25:08:40.1	0	927.6	1.17	3.3	0.194					
NGC300	X1	00:54:40.33	-37:40:46.0	1	160.3	0.25	4.2	0.0535		S			
NGC300	X2	00:55:10.07	-37:42:16.2	1	208.7	0.32	24.2	0.367	1	S			
NGC300	X4	00:55:11.18	-37:48:41.1	1	507.8	0.95	9.5	0.157		D			
NGC300	X5	00:54:44.86	-37:51:07.1	1	619.3	1.32	4.2	0.0511					
NGC300	X6	00:55:41.74	-37:35:33.5	1	655.0	1.26	5.1	0.0855			P B2/20.34		
NGC300	X7	00:55:26.82	-37:31:26.2	1	692.6	1.47	17.4	0.314	1	G5*			
NGC300	X8	00:54:14.18	-37:29:45.2	1	820.4	1.43	7.0	0.122					
NGC300	X9	00:56:01.65	-37:32:47.9	1	943.0	1.83	4.2	0.151					
NGC404	X1	01:09:27.01	35:43:04.2	2	0.2	0.00	4.7	0.178			(NGC404)	N	
NGC613	X1	01:34:18.17	-29:25:06.1	2	12.0	0.07	20.6	76.8			(NGC613)	N	
NGC720	X1	01:53:00.48	-13:44:18.7	1	2.5	0.03	25.3	73.2			(NGC720)	N	
NGC720	X2	01:53:03.50	-13:46:54.6	1	160.1	1.37	9.3	12.7			2EULXd		
NGC720	X3	01:52:49.38	-13:42:17.4	1	202.6	1.53	4.5	5.86			2ULXd		
NGC891	X1	02:22:31.39	42:20:30.3	8	25.9	0.16	11.4	1.53		D		1ULXd	ULX1
NGC891	X2	02:22:31.27	42:19:58.8	8	53.2	0.13	27.0	3.77			(SN1986J)	1ULXd	ULX2
NGC891	X3	02:22:30.42	42:19:14.5	8	98.1	0.26	3.8	0.367		D			
NGC891	X4	02:22:24.31	42:21:40.0	8	110.5	1.45	5.7	0.633					
NGC891	X5	02:22:26.31	42:18:32.4	8	155.1	0.46	4.6	0.496		D			
NGC891	X6	02:22:32.47	42:26:24.2	8	336.3	1.91	9.8	1.27			P B2/21.32	2ULXd	
NGC891	X7	02:22:45.55	42:25:57.8	8	339.1	0.85	11.9	2.28		D		1ULXd	ULX3
NGC891	X8	02:22:07.97	42:11:45.4	8	610.1	1.67	3.8	0.354			P B/17.00		
NGC1042	X1	02:40:25.51	-08:24:30.5	2	94.3	0.68	17.1	4.27		S		1ULXd	ULX1
NGC1042	X2	02:40:21.97	-08:21:40.0	2	263.7	1.89	4.3	0.789			P B1/20.68		
NGC1052	X1	02:41:04.98	-08:15:20.2	2	2.2	0.04	21.4	32.8			(NGC1052)	N	
NGC1068	X1	02:42:40.88	-00:00:45.3	3	10.6	0.05	635.3	1330			(NGC1068)	N	
NGC1068	X2	02:42:37.65	-00:01:21.0	2	50.6	0.24	8.6	4.26			1ULXd	ULX1	
NGC1068	X3	02:42:42.64	-00:03:28.2	3	164.4	0.91	4.5	2.59	1	R		1ULXd	ULX2
NGC1068	X4	02:42:44.56	-00:06:35.0	3	353.1	1.95	44.1	25.9	1		* V/12.505	2EULXd	
NGC1068	X5	02:43:00.59	-00:04:03.4	2	362.9	1.90	4.7	1.46					
NGC1068	X7	02:43:06.59	00:01:31.0	2	419.6	1.98	4.4	1.27					
NGC1073	X1	02:43:39.69	01:21:06.9	2	89.8	0.61	5.8	3.16			QSO 0241+0111	1ULXd	
NGC1073	X2	02:43:38.48	01:24:10.2	2	98.5	0.69	4.0	3.63		S		1ULXd	ULX1
NGC1073	X3	02:43:33.53	01:22:18.2	2	104.5	0.77	3.3	1.61			QSO N1073U1	1ULXd	
NGC1073	X4	02:43:33.49	01:21:33.9	2	120.8	0.86	13.9	8.4			QSO N1073U2	1ULXd	
NGC1073	X6	02:43:46.70	01:25:10.5	2	181.1	1.24	4.2	2.91			P B/17.30	2ULXd	
NGC1097	X1	02:46:18.96	-30:16:30.2	2	9.2	0.04	50.3	134	1		(NGC1097)	N	
NGC1291	X1	03:17:17.99	-41:06:22.4	0	7.1	0.03	13.5	7			(NGC1291)	N	

Table 2—Continued

Galaxy	Name	R.A. (hh:mm:ss)	Decl. (dd:mm:ss)	$N_c^a$	$r^b$ ( $\prime\prime$ )	$r/R25^c$	$\sigma_{Max}^d$	$L/10^{39}e$ (erg/s)	$N_v^f$	Env <sup>g</sup>	ID <sup>h</sup>	ULX <sup>i</sup>	UName <sup>j</sup>
NGC1291	X2	03:17:13.54	-41:10:32.5	0	248.8	0.85	10.9	3.03		R		1ULXd	ULX1
NGC1291	X3	03:17:45.95	-41:01:26.5	0	440.2	1.67	5.1	1.62				2ULXd	
NGC1313	X1	03:18:18.46	-66:30:00.2	1	20.0	0.09	8.0	0.417		D			
NGC1313	X2	03:18:19.80	-66:29:09.6	1	48.8	0.20	139.3	10.8	7	D		1EULXd	ULX1
NGC1313	X3	03:18:20.59	-66:30:34.1	0	52.7	0.21	16.6	0.789					
NGC1313	X4	03:18:04.65	-66:30:09.3	1	67.4	0.32	4.6	0.177					
NGC1313	X5	03:18:18.64	-66:32:28.9	1	159.1	0.58	4.1	0.126					
NGC1313	X6	03:17:38.23	-66:33:03.4	1	294.3	1.28	59.0	3.12				(SN1978K)	2ULXd
NGC1313	X7	03:18:22.00	-66:36:04.3	1	375.2	1.38	54.1	3.98	3	D		(P R/21.56)	2ULXd
NGC1313	X8	03:17:16.21	-66:26:37.6	1	404.3	1.85	4.1	0.168					ULX3
NGC1316	X1	03:22:41.71	-37:12:30.4	2	2.8	0.01	44.2	110				( NGC1316)	N
NGC1316	X3	03:22:51.40	-37:09:47.1	2	199.0	0.57	5.4	4.45				1ULXd	ULX1
NGC1316	X4	03:22:40.44	-37:16:41.8	2	254.2	0.87	7.4	9.69				P B2/20.24	1ULXd
NGC1316	X5	03:22:57.45	-37:15:56.0	2	281.3	1.10	4.7	4.53		D		2ULXd	ULX3
NGC1316	X6	03:22:15.49	-37:16:59.5	2	413.5	1.15	3.5	3.05		D		P B2/20.25	2ULXd
NGC1316	X7	03:22:39.13	-37:20:04.5	2	457.4	1.57	3.5	2.76		D		2ULXd	ULX4
NGC1316	X8	03:23:14.33	-37:16:54.5	2	473.0	1.82	4.3	3.55		D		P B2/21.56	2ULXd
NGC1316	X9	03:23:28.86	-37:10:10.9	2	581.2	1.76	4.6	4.11		D	mP	2ULXd	ULX7
NGC1317	X1	03:22:44.41	-37:06:12.6	2	4.3	0.05	9.7	7.99				N	
NGC1332	X1	03:26:17.24	-21:20:07.2	1	2.0	0.02	17.5	59.6				(NGC1332)	N
NGC1365	X1	03:33:36.56	-36:08:22.7	2	5.6	0.02	30.0	67.4				(NGC1365)	N
NGC1365	X2	03:33:34.60	-36:09:35.0	1	81.6	0.26	5.9	7.29		D		1ULX	ULX1
NGC1365	X3	03:33:12.85	-36:11:50.4	2	358.1	1.22	6.2	5.98				P B2/18.73	2ULXd
NGC1365	X4	03:33:11.63	-36:11:32.7	1	360.2	1.27	5.7	6.31				2ULX	ULX3
NGC1365	X5	03:34:07.88	-36:03:57.2	2	459.6	1.60	9.1	9.32				2ULXd	
NGC1386	X1	03:36:46.20	-35:59:57.3	1	2.5	0.06	14.7	27.1				(NGC1386)	N
NGC1380	X1	03:36:27.23	-34:58:32.7	4	4.1	0.06	20.0	19.3				( NGC1380)	N
NGC1380	X2	03:36:25.21	-34:59:19.8	4	51.2	0.40	3.0	1.43		D		1ULXd	ULX1
NGC1395	X1	03:38:29.66	-23:01:37.4	2	2.7	0.02	11.7	31.4				(NGC1395)	N
NGC1395	X2	03:38:17.64	-23:02:30.5	2	172.6	1.27	3.9	4.8				P B1/20.04	2ULXd
NGC1395	X3	03:38:31.19	-23:05:03.3	2	204.5	1.16	3.5	4.51				2ULXd	
NGC1395	X4	03:38:11.29	-23:00:38.3	2	260.2	1.92	4.1	6.13			Z	2ULXd	
NGC1395	X5	03:38:29.55	-23:07:04.8	2	324.8	1.84	4.2	6.45			Z	2ULX	
NGC1398	X1	03:38:51.71	-26:20:09.3	2	2.2	0.01	9.2	15.4				(NGC1398)	N
NGC1398	X2	03:39:09.37	-26:20:12.9	2	236.2	1.12	4.6	5.51				2ULXd	
NGC1398	X3	03:39:11.94	-26:19:57.5	2	271.0	1.30	4.9	5.91				2ULXd	
NGC1399	X1	03:38:28.97	-35:27:01.1	4	3.2	0.02	109.7	257				(NGC1399)	N
NGC1399	X2	03:38:32.96	-35:27:05.2	3	48.9	0.25	10.6	7.69				(GC)	1ULXd
NGC1399	X3	03:38:31.99	-35:26:02.4	4	66.4	0.33	8.5	5.87				(GC)	1ULXd
NGC1399	X4	03:38:25.53	-35:25:19.6	1	107.1	0.52	3.9	2.35			mZ	1ULX	
NGC1399	X5	03:38:31.86	-35:30:58.1	4	242.6	1.17	4.7	1.96				2ULXd	
NGC1399	X6	03:38:25.53	-35:22:40.9	1	260.6	1.26	3.1	1.32				2ULX	
NGC1399	X7	03:38:48.99	-35:28:36.4	3	263.3	1.35	3.3	1.51				2ULXd	
NGC1399	X8	03:38:51.61	-35:26:41.9	4	276.8	1.43	14.1	9.03	1		Z	2ULXd	
NGC1399	X9	03:38:41.42	-35:31:34.7	4	315.6	1.55	44.3	42.3	1		P B2/20.11	2EULXd	
NGC1399	X10	03:38:31.71	-35:33:43.3	1	406.7	1.96	3.4	1.5				2ULX	
NGC1404	X1	03:38:52.07	-35:35:39.8	4	5.9	0.06	108.0	288				(NGC1404)	N
NGC1404	X2	03:38:43.66	-35:33:48.3	4	145.7	1.55	5.7	3.65			P B2/18.72	2ULXd	
NGC1427A	X1	03:40:12.20	-35:37:34.7	4	36.8	0.69	8.6	8.81		D		1ULX	ULX1
NGC1433	X1	03:42:01.49	-47:13:18.9	1	2.7	0.01	5.0	2.33				(NGC1433)	N
PGC13826	X1	03:46:48.82	68:05:49.5	3	6.7	0.01	17.9	2.57				(PGC13826)	N
PGC13826	X2	03:46:57.17	68:06:22.4	3	56.1	0.09	10.6	1.21		S		1ULXd	ULX1
PGC13826	X3	03:46:45.54	68:09:51.7	3	247.7	0.39	13.7	1.49	1	S		1ULXd	ULX2
PGC13826	X4	03:46:06.31	68:07:07.2	3	256.3	0.41	6.2	0.641					
PGC13826	X6	03:45:55.17	68:04:58.6	3	308.7	0.49	21.5	2.77		S		(HII)	1ULXd
PGC13826	X7	03:46:15.70	68:11:19.7	3	384.8	0.60	7.2	0.723					ULX3
PGC13826	X8	03:45:41.40	68:02:42.2	3	424.1	0.67	3.0	0.252					
PGC13826	X9	03:48:06.58	68:04:55.4	3	433.1	0.69	4.5	0.467					
PGC13826	X10	03:47:17.97	67:51:11.7	3	887.7	1.39	9.7	2.23				* BT/12.152	2ULXd
NGC1482	X1	03:54:38.95	-20:30:14.6	1	8.5	0.18	9.3	32.3				(NGC1482)	N
NGC1532	X1	04:12:05.86	-32:52:18.4	2	10.6	0.03	3.9	1.88				(NGC1532)	N
NGC1549	X1	04:15:45.87	-55:35:29.6	2	6.7	0.05	13.2	13				( NGC1549)	N
NGC1549	X2	04:15:16.86	-55:34:55.7	2	242.0	1.77	4.3	3.01				* J/12.857	2ULX
NGC1553	X1	04:16:11.07	-55:46:49.2	2	5.9	0.07	20.1	20.7				( NGC1553)	N
NGC1553	X2	04:16:03.51	-55:46:54.1	2	58.2	0.64	5.1	2.6				1ULXd	ULX1

Table 2—Continued

Galaxy	Name	R.A. (hh:mm:ss)	Decl. (dd:mm:ss)	$N_c^a$	$r^b$ ( $\prime\prime$ )	$r/R25^c$	$\sigma_{Max}^d$	$L/10^{39}e$ (erg/s)	$N_v^f$	Env <sup>g</sup>	ID <sup>h</sup>	ULX <sup>i</sup>	UName <sup>j</sup>
NGC1553	X3	04:16:08.19	-55:48:16.4	2	87.5	0.85	3.0	1.39				1ULX	ULX2
NGC1559	X1	04:17:42.27	-62:46:40.7	2	40.7	0.40	5.8	3.73	D			1ULXd	ULX1
NGC1559	X2	04:17:30.39	-62:47:24.7	2	52.3	0.51	5.8	2.97	D			1ULXd	ULX2
NGC1559	X3	04:17:28.00	-62:48:20.1	2	99.7	1.10	6.0	2.89		Z		2ULXd	
NGC1566	X1	04:20:00.41	-54:56:16.7	1	1.3	0.01	454.1	371	1	(NGC1566)	N		
NGC1566	X2	04:19:56.11	-54:56:38.3	1	42.2	0.17	12.6	4.96	S			1ULXd	ULX1
NGC1566	X3	04:19:56.73	-54:55:23.0	1	63.5	0.32	7.4	3.43	S			1ULXd	ULX2
NGC1566	X4	04:20:10.12	-54:56:42.1	1	87.1	0.40	9.6	3.6	1	S		1ULXd	ULX3
NGC1566	X5	04:20:16.22	-54:59:51.9	1	253.6	1.28	4.5	1.17	D	mZ		2ULXd	
NGC1574	X1	04:21:58.69	-56:58:29.4	2	4.7	0.05	16.1	25.8		(NGC1547)	N		
NGC1672	X1	04:45:41.98	-59:14:53.3	1	4.1	0.02	25.8	18.6		(NGC1672)	N		
NGC1672	X2	04:45:34.11	-59:14:44.2	1	63.4	0.38	7.5	3.76	S			1ULXd	ULX1
NGC1672	X3	04:45:52.87	-59:14:59.1	1	81.8	0.49	8.2	3.53	S			1ULXd	ULX2
NGC1672	X4	04:46:22.77	-59:15:25.5	1	312.4	1.88	3.8	1.56		P B2/20.70	2ULX		
NGC1672	X5	04:45:28.64	-59:09:35.3	1	338.1	1.71	4.7	2		P B2/21.97	2ULXd		
NGC1705	X1	04:54:19.32	-53:20:44.8	1	78.3	1.39	3.9	0.441					
NGC1792	X1	05:05:15.83	-37:58:29.7	2	19.3	0.23	5.0	3.04	S			1ULX	ULX1
NGC1792	X2	05:05:11.01	-37:58:44.6	1	48.4	0.48	6.4	1.53	S			1ULXd	ULX2
NGC2146	X1	06:18:40.48	78:21:32.1	1	13.1	0.11	12.7	46.2		(NGC2146)	N		
NGC2273	X1	06:50:08.57	60:50:44.9	1	0.2	0.00	8.2	17.6		(NGC2273)	N		
NGC2273	X2	06:50:12.76	60:48:36.7	1	131.9	1.71	10.4	23.6		Z		2EULXd	
NGC2273	X3	06:50:22.68	60:53:00.4	1	170.0	1.78	5.9	10.9		Z		2EULXd	
NGC2276	X1	07:26:49.45	85:45:48.3	1	38.2	0.47	7.9	33.8	S			1EULXd	ULX1
NGC2276	X2	07:25:22.75	85:44:18.2	1	137.0	1.65	9.7	27.5		F8*		2EULXd	
NGC2300	X1	07:32:22.84	85:42:26.3	1	6.8	0.09	28.8	144		(NGC2300)	N		
NGC2366	X1	07:28:51.67	69:07:26.0	0	326.3	1.77	6.6	0.131					
NGC2366	X2	07:29:30.58	69:19:38.8	0	449.9	1.85	5.6	0.111		P B2/19.68			
NGC2403	X1	07:36:56.05	65:35:38.6	1	21.7	0.04	10.7	0.38	D				
NGC2403	X2	07:36:25.95	65:35:38.9	1	178.0	0.38	32.5	1.4	S			1ULXd	ULX1
NGC2403	X3	07:37:02.83	65:39:35.5	1	223.6	0.57	10.0	0.326	S				
NGC2403	X5	07:35:09.17	65:40:25.3	1	704.5	1.14	44.3	2.29		G0*	2ULXd		
NGC2403	X6	07:35:38.68	65:52:09.4	1	1078.0	1.98	7.8	0.585	1				
NGC2442	X1	07:36:23.51	-69:31:51.7	1	2.6	0.02	6.1	5.93		(NGC2442)	N		
NGC2442	X2	07:37:05.67	-69:32:06.5	1	219.7	1.49	4.8	3.72				2ULXd	
PGC23324	X1	08:19:29.90	70:42:18.6	0	122.8	0.65	123.5	28.4	1	D	(HII)	1EULXd	ULX1
NGC2775	X1	09:10:20.63	07:02:17.3	3	2.6	0.02	3.5	1.97		(NGC2775)	N		
NGC2775	X3	09:10:14.17	07:02:49.7	3	99.1	0.90	3.7	1.83		P B2/21.58	1ULXd	ULX1	
NGC2775	X4	09:10:32.29	07:03:44.5	3	195.2	1.97	5.9	2.97		* B1/14.07	2ULXd		
NGC2775	X5	09:10:27.08	06:59:09.5	3	213.3	1.67	7.9	5.65		P B2/21.28	2ULXd		
NGC2775	X6	09:10:19.90	07:06:00.4	3	221.6	1.82	4.9	2.42				2ULXd	
NGC2782	X1	09:14:05.01	40:06:51.4	1	5.6	0.07	17.0	98.5		(NGC2782)	N		
NGC2782	X2	09:14:03.93	40:07:41.6	1	52.8	0.53	5.8	19.4	D			1EULXd	ULX1
NGC2903	X1	09:32:09.95	21:30:05.4	0	4.8	0.02	15.8	5.26		(NGC2903)	N		
NGC2903	X2	09:32:02.04	21:31:19.2	0	131.8	0.70	4.7	1.5	S			1ULX	ULX1
NGC2974	X1	09:42:33.27	-03:41:56.7	2	2.3	0.03	21.1	31.7		(NGC2974)	N		
NGC2992	X1	09:45:41.95	-14:19:34.8	1	4.7	0.08	87.2	429		(NGC2992)	N		
NGC2993	X1	09:45:48.27	-14:22:05.1	1	3.5	0.10	14.4	51.1		(NGC2993)	N		
NGC3031	X1	09:55:33.38	69:03:54.3	4	5.8	0.01	411.5	74.4	8	(NGC3031)	N		
NGC3031	X2	09:55:42.15	69:03:35.1	4	52.7	0.09	8.5	0.472					
NGC3031	X3	09:55:36.29	69:02:38.5	1	82.9	0.11	5.0	0.209					
NGC3031	X4	09:55:22.13	69:05:11.2	4	93.7	0.13	4.9	0.209					
NGC3031	X5	09:55:50.05	69:05:32.6	4	128.2	0.29	8.1	0.445					
NGC3031	X6	09:55:09.59	69:04:08.8	3	128.4	0.28	13.1	0.504					
NGC3031	X7	09:55:10.43	69:05:01.7	4	138.1	0.25	8.0	0.31					
NGC3031	X8	09:55:24.74	69:01:11.8	4	174.7	0.31	44.2	2.61		(SN1993J)	1ULX	ULX1	
NGC3031	X9	09:55:33.08	69:00:31.4	4	208.6	0.31	64.7	3.37	S	(O8*)	1ULX	ULX2	
NGC3031	X10	09:54:51.25	69:02:51.3	2	236.7	0.56	9.0	0.427					
NGC3031	X11	09:56:09.25	69:01:03.7	4	260.5	0.39	6.5	0.227					
NGC3031	X12	09:55:00.06	69:07:45.5	4	287.8	0.39	5.9	0.226					
NGC3031	X13	09:55:12.84	69:08:27.7	2	289.6	0.36	4.8	0.18					
NGC3031	X14	09:56:26.67	69:05:11.1	4	293.5	0.69	3.2	0.114					
NGC3031	X15	09:55:49.64	68:58:33.0	4	338.3	0.43	4.6	0.288	S				
NGC3031	X17	09:55:24.33	69:09:59.9	4	363.2	0.49	17.8	0.682					
NGC3031	X18	09:56:36.81	69:00:27.8	4	400.6	0.68	4.6	0.154					
NGC3031	X19	09:56:14.29	68:57:20.8	4	455.5	0.57	9.4	0.348	1				

Table 2—Continued

Galaxy	Name	R.A. (hh:mm:ss)	Decl. (dd:mm:ss)	$N_c^a$	r <sup>b</sup> ( $\prime\prime$ )	r/R25 <sup>c</sup>	$\sigma_{Max}^d$	$L/10^{39}e$ (erg/s)	$N_v^f$	Env <sup>g</sup>	ID <sup>h</sup>	ULX <sup>i</sup>	UName <sup>j</sup>
NGC3031	X20	09:55:01.81	68:56:18.9	4	491.6	0.91	6.1	0.229					
NGC3031	X21	09:54:45.40	68:56:55.8	4	496.8	1.02	5.8	0.208					
NGC3031	X22	09:53:56.71	69:03:56.0	2	518.8	1.16	3.5	0.0946					
NGC3031	X23	09:56:09.60	69:12:49.0	2	563.0	1.04	3.2	0.115					
NGC3031	X24	09:57:01.74	68:54:57.1	4	721.1	1.00	7.3	0.314					
NGC3031	X25	09:58:02.47	68:57:08.6	4	900.0	1.61	7.6	0.444					
NGC3034	X1	09:55:52.79	69:40:37.0	2	21.1	0.13	74.7	61.7		( NGC3034)		N	
NGC3034	X2	09:56:00.98	69:41:06.5	2	37.6	0.12	4.5	0.516					
NGC3034	X3	09:55:52.07	69:42:02.4	2	66.2	0.50	6.5	0.957					
NGC3034	X5	09:55:26.84	69:39:24.5	2	169.1	0.53	3.0	0.155					
NGC3034	X7	09:55:14.99	69:36:09.5	2	352.3	1.64	3.7	0.164					
NGC3034	X8	09:57:32.60	69:46:01.2	2	596.0	1.83	4.4	0.214					
PGC28757	X1	09:57:36.72	69:02:23.1	1	33.5	0.51	3.0	0.0804					
PGC28757	X2	09:57:54.05	69:03:47.3	4	753.4	1.67	131.8	13.4	1	D		2EULX	ULX1
NGC3079	X1	10:01:59.27	55:40:49.0	2	10.9	0.24	17.2	19.4		(NGC3079)		N	
NGC3115	X1	10:05:14.51	-07:43:08.7	0	6.3	0.08	3.8	4.88		(NGC3115)		N	
NGC3190	X1	10:18:05.35	21:50:00.5	3	5.1	0.05	7.7	8.79		(NGC3190)		N	
NGC3226	X1	10:23:26.94	19:53:56.5	1	6.7	0.08	11.5	18		(NGC3226)		N	
NGC3226	X3	10:23:25.74	19:56:17.6	1	144.5	1.56	5.1	5.46		P B1/18.84		2ULXd	
NGC3227	X1	10:23:30.51	19:51:54.0	1	15.2	0.12	166.2	489	2	(NGC3227)		N	
PGC30819	X1	10:28:42.94	68:28:17.1	3	227.9	0.73	8.0	0.385					
PGC30819	X2	10:29:24.60	68:25:50.8	3	346.4	1.35	3.4	0.136					
PGC30819	X3	10:29:32.44	68:30:13.7	2	497.4	1.26	4.5	0.166					
PGC30819	X4	10:27:21.97	68:18:43.2	3	503.3	1.34	5.6	0.282					
NGC3294	X1	10:36:12.26	37:18:48.2	2	60.7	1.08	3.5	9.41				2ULXd	
PGC31586	X1	10:37:47.38	-27:05:09.0	3	14.6	0.19	4.9	12.3		(PGC31586)		N	
PGC31586	X2	10:37:39.69	-27:05:24.6	3	111.0	1.98	26.9	84.3	1	Pr		2ULXd	
NGC3310	X1	10:38:45.71	53:30:10.6	2	4.3	0.06	57.3	83.1		(NGC3310)		N	
NGC3310	X2	10:38:46.25	53:30:43.2	1	35.2	0.38	10.2	5.41	S			1ULXd	ULX1
NGC3310	X3	10:38:42.86	53:31:06.6	1	65.4	0.75	8.9	6.04	S			1ULXd	ULX2
NGC3377	X1	10:47:42.58	13:59:10.5	1	16.6	0.11	4.7	1.5		(NGC3377)		N	
NGC3379	X1	10:47:49.80	12:34:58.3	1	1.9	0.01	14.1	6.35	1	(NGC3379)		N	
NGC3396	X2	10:49:47.96	33:00:30.2	2	123.1	1.85	10.2	15.9		?* B2/17.33		2EULXd	
PGC32390	X1	10:49:24.90	32:46:25.9	2	10.6	0.32	4.1	6.79		(PGC32390)		N	
NGC3516	X1	11:06:47.47	72:34:07.1	1	4.9	0.09	395.9	5140	1	(NGC3516)		N	
NGC3623	X1	11:18:55.79	13:05:38.2	3	7.9	0.09	8.6	3.03		(NGC3623)		N	
NGC3623	X2	11:18:54.41	13:05:33.6	3	45.5	0.52	6.3	1.75	S			1ULXd	ULX1
NGC3623	X3	11:18:52.39	13:03:35.2	3	127.1	0.75	4.5	1.07		* B/12.163		1ULXd	
NGC3627	X1	11:20:14.44	12:59:31.3	1	8.5	0.06	5.9	2.21		(NGC3627)		N	
NGC3627	X2	11:20:20.88	12:58:48.2	1	95.1	0.67	6.3	2.06	S	P		1ULXd	ULX1
NGC3627	X3	11:20:22.04	12:52:49.4	1	412.6	1.56	6.9	2.55		mZ		2ULXd	
NGC3628	X1	11:20:15.43	13:35:19.8	0	12.8	0.06	28.3	11.9	D	(NGC3628)		N	
NGC3628	X2	11:20:37.17	13:34:32.0	1	308.3	0.75	7.9	2.9	D			1ULXd	ULX1
NGC3628	X3	11:20:39.76	13:36:26.6	0	348.1	1.79	3.9	1.22		QSO J1120.6+1336		2ULXd	
NGC3628	X4	11:20:41.49	13:35:57.9	0	369.1	1.60	3.4	0.986		QSO WEE52			
NGC3642	X1	11:22:17.88	59:04:28.3	1	7.0	0.05	5.1	11.4		(NGC3642)		N	
NGC3642	X2	11:22:40.36	59:02:37.1	1	205.7	1.31	3.6	7.9		P B1/19.60		2ULXd	
NGC3665	X1	11:24:43.38	38:45:42.9	1	4.3	0.06	9.1	33.5		(NGC3665)		N	
PGC35286	X1	11:28:03.12	78:59:56.5	0	57.2	1.36	37.3	0.386		Z			
NGC3738	X1	11:35:45.42	54:33:15.4	1	117.1	1.57	7.4	0.371		(NGC3982)		N	
NGC3982	X1	11:56:28.21	55:07:29.8	1	1.2	0.02	4.5	5.13		(NGC3998)		N	
NGC3998	X1	11:57:55.92	55:27:13.5	0	6.0	0.09	186.9	259				2ULXd	
NGC3998	X2	11:57:49.69	55:28:30.2	0	95.4	1.18	4.3	2.88					
NGC4036	X1	12:01:26.89	61:53:38.1	3	4.1	0.06	4.7	15.7		(NGC4036)		N	
NGC4041	X1	12:02:12.13	62:08:15.3	3	5.7	0.07	13.0	21.5		(NGC4041)		N	
NGC4051	X1	12:03:09.46	44:31:54.3	0	2.0	0.01	626.1	2770	2	(NGC4051)		N	
NGC4088	X1	12:05:32.02	50:32:48.8	2	36.4	0.52	4.9	5.86	S	Pr		1ULXd	ULX1
NGC4105	X1	12:06:40.29	-29:45:40.8	2	5.5	0.08	9.4	13.4		(NGC4105)		N	
NGC4105	X2	12:06:40.97	-29:48:03.0	2	141.1	1.89	6.9	6.34		* V/11.03		2ULXd	
NGC4106	X1	12:06:45.67	-29:46:04.7	2	12.7	0.26	5.5	6.63		(NGC4106)		N	
NGC4136	X1	12:09:22.50	29:55:53.8	0	59.6	0.53	3.5	3.96	S			1ULXd	ULX1
NGC4144	X1	12:10:09.94	46:27:10.6	1	110.0	0.67	4.2	0.507	D				
NGC4150	X1	12:10:34.69	30:23:57.9	1	17.4	0.28	41.0	40.3		* J/16.049			
NGC4151	X1	12:10:32.57	39:24:20.9	4	8.6	0.05	720.4	1330	1	(NGC4151)		N	
NGC4151	X2	12:10:22.45	39:23:14.6	4	142.7	0.76	4.8	1.84		P B1/19.70		1ULXd	ULX1

Table 2—Continued

Galaxy	Name	R.A. (hh:mm:ss)	Decl. (dd:mm:ss)	$N_c^a$	$r^b$ ( $\prime\prime$ )	$r/R25^c$	$\sigma_{Max}^d$	$L/10^{39}e$ (erg/s)	$N_v^f$	Env <sup>g</sup>	ID <sup>h</sup>	ULX <sup>i</sup>	UName <sup>j</sup>
NGC4151	X3	12:10:47.48	39:23:10.7	4	184.8	1.32	5.4	2.13	S			2ULXd	ULX2
NGC4151	X4	12:10:21.81	39:21:53.1	4	202.0	1.08	4.4	1.62	S			2ULXd	ULX3
NGC4151	X5	12:10:17.76	39:21:24.5	3	254.7	1.36	5.9	9.84	S			2ULX	ULX4
NGC4151	X6	12:10:07.90	39:23:10.6	4	301.1	1.73	9.0	3.86		P B1/18.49 (NGC4156)		2ULXd	
NGC4156	X1	12:10:49.63	39:28:23.5	4	0.9	0.03	13.3	4.32				N	
PGC38811	X1	12:11:13.71	39:24:33.3	4	41.0	1.42	4.9	0.872					
NGC4190	X1	12:13:45.41	36:37:55.2	1	9.8	0.21	52.1	2.31	D			1ULXd	ULX1
NGC4203	X1	12:15:04.97	33:11:51.3	1	4.5	0.05	122.4	109		(NGC4203)		N	
NGC4203	X2	12:15:09.23	33:09:55.4	1	127.5	1.28	98.7	78.7		QSO Ton1480		2EULXd	
NGC4203	X3	12:15:15.67	33:10:11.9	1	164.9	1.72	4.9	2.3		P B2/20.09		2ULXd	
NGC4214	X1	12:15:38.06	36:19:17.6	1	27.6	0.12	11.4	0.223					
NGC4214	X2	12:15:59.10	36:22:26.8	1	290.2	1.36	7.1	0.138		P B2/19.76			
NGC4214	X3	12:15:43.01	36:26:28.5	1	411.7	1.62	5.4	0.109		Z			
NGC4235	X1	12:17:10.06	07:11:30.2	1	17.3	0.44	198.6	1270	1	(NGC4235)		N	
NGC4236	X1	12:17:29.73	69:15:16.8	1	797.8	1.22	11.5	0.466	1	K5*			
NGC4242	X1	12:17:46.79	45:36:57.8	2	175.6	1.51	5.7	3.03		P		2ULXd	
NGC4242	X2	12:17:21.57	45:34:46.1	2	179.4	1.20	5.3	3.16		P B1/18.68		2ULXd	
NGC4242	X3	12:17:42.71	45:39:28.6	2	183.0	1.27	3.7	2.15		P B1/18.67		2ULXd	
NGC4244	X1	12:17:48.64	37:50:22.0	1	248.9	1.19	3.2	0.239					
NGC4254	X1	12:18:52.13	14:24:52.3	1	42.3	0.30	4.6	4.71	S			1ULXd	ULX1
NGC4254	X2	12:18:56.34	14:24:18.1	1	112.1	0.78	15.6	15.3	S			1EULXd	ULX2
NGC4254	X3	12:18:34.12	14:23:55.1	1	233.3	1.64	3.9	2.78				2ULXd	
NGC4258	X1	12:19:05.06	47:18:30.7	3	74.3	0.33	7.7	1.63	1	S		1ULX	ULX1
NGC4258	X2	12:18:54.70	47:16:48.9	3	93.0	0.35	3.7	1.59	S			1ULX	ULX2
NGC4258	X3	12:18:57.67	47:15:58.1	3	137.9	0.39	5.7	0.701	S				
NGC4258	X4	12:18:43.79	47:17:21.4	3	153.6	0.70	3.5	0.408					
NGC4258	X5	12:18:56.10	47:21:18.9	3	183.8	0.46	5.0	0.674					
NGC4258	X6	12:18:46.18	47:14:16.8	1	267.3	1.06	4.2	0.572					
NGC4258	X7	12:18:45.42	47:24:11.6	3	377.6	0.74	5.4	0.701					
NGC4258	X8	12:18:47.85	47:25:24.1	3	440.1	0.95	4.5	0.585					
NGC4258	X9	12:19:22.98	47:09:33.8	3	581.3	1.05	14.6	2.38		mP		2ULXd	
NGC4258	X10	12:18:16.31	47:27:10.2	3	681.1	1.29	4.5	0.438					
NGC4258	X11	12:19:09.39	47:05:27.5	1	777.4	1.84	4.4	0.759		QSO 12166+4722			
NGC4258	X12	12:18:28.04	47:30:18.1	3	783.2	1.46	4.7	0.537					
NGC4261	X1	12:19:22.96	05:49:30.0	1	6.5	0.05	37.1	229		(NGC4261)		N	
NGC4278	X1	12:20:06.94	29:16:51.9	1	6.0	0.05	24.1	42.8		(NGC4278)		N	
NGC4291	X1	12:20:20.41	75:22:09.6	3	14.2	0.27	11.1	57.3		(NGC4291)		N	
NGC4319	X1	12:21:44.53	75:18:35.9	3	52.1	0.60	385.9	2210	1	QSO MARK205		1EULXd	
NGC4319	X2	12:22:06.80	75:19:03.2	3	90.5	1.22	4.2	13.3		P B1/20.89		2EULXd	
NGC4292	X1	12:21:14.49	04:36:51.9	2	70.9	1.62	6.8	25.5		G0*		2EULXd	
NGC4303	X1	12:21:55.00	04:28:25.6	2	7.1	0.04	11.1	8.51		(NGC4303)		N	
NGC4303	X2	12:21:58.41	04:28:14.3	1	55.7	0.32	3.6	2.46	S			1ULX	ULX1
NGC4303	X4	12:21:37.55	04:29:07.8	2	260.9	1.50	3.5	1.6				2ULXd	
NGC4303	X5	12:22:03.76	04:34:07.0	1	372.5	1.95	4.2	4.85				2ULX	
NGC4321	X1	12:22:54.60	15:49:19.7	3	9.2	0.04	25.7	17.2		(NGC4321)		N	
NGC4321	X2	12:22:58.49	15:47:51.8	3	102.8	0.52	4.7	1.57	S	(SN1979C)		1ULXd	ULX1
NGC4321	X3	12:22:48.01	15:51:56.9	3	185.6	0.95	4.0	1.44	S			1ULXd	ULX2
NGC4321	X4	12:23:08.47	15:51:22.9	1	225.9	1.06	3.2	1.6				2ULX	
NGC4321	X6	12:22:42.80	15:44:00.5	3	368.8	1.66	6.2	2.23		P B1/20.31		2ULXd	
NGC4321	X7	12:22:48.23	15:43:05.8	3	390.4	1.78	4.3	1.29		Z		2ULXd	
NGC4374	X1	12:25:04.07	12:53:16.0	2	5.4	0.03	48.3	137		(NGC4374)		N	
NGC4374	X2	12:25:12.13	12:51:55.7	2	146.5	0.76	16.7	19.4		QSO		1EULXd	
NGC4374	X3	12:25:15.52	12:56:05.6	2	242.8	1.44	8.8	7.33				2ULXd	
NGC4374	X4	12:25:18.49	12:49:03.0	2	332.1	1.72	3.9	5.43		P B2/20.23		2ULXd	
NGC4374	X5	12:24:40.79	12:54:16.2	2	340.5	1.85	4.6	3.49				2ULXd	
NGC4388	X1	12:25:47.12	12:39:37.6	2	4.8	0.11	12.0	23		(NGC4388)		N	
NGC4406	X1	12:26:11.85	12:56:53.8	2	4.9	0.03	13.3	43	1	(NGC4406)		N	
NGC4395	X1	12:26:01.52	33:31:34.7	1	161.8	0.43	32.1	1.73	D			1ULXd	ULX1
NGC4395	X2	12:25:32.31	33:25:34.0	1	484.7	1.42	7.1	0.308					
NGC4395	X3	12:25:49.58	33:41:05.3	1	499.3	1.34	6.0	0.288					
NGC4395	X4	12:26:28.92	33:36:30.7	1	536.9	1.63	5.3	0.23					
NGC4435	X1	12:27:40.45	13:04:48.1	2	2.2	0.04	7.1	6.67		(NGC4435)		N	
NGC4438	X1	12:27:45.53	13:00:30.5	3	5.5	0.04	19.3	25.7		(NGC4438)		N	
NGC4438	X2	12:27:57.22	13:02:32.6	3	207.2	1.27	16.6	16.4		P B2/19.54		2EULXd	
NGC4449	X1	12:28:09.36	44:05:52.0	3	25.0	0.19	4.7	0.107					

Table 2—Continued

Galaxy	Name	R.A. (hh:mm:ss)	Decl. (dd:mm:ss)	$N_c^a$	$r^b$ ( $\prime\prime$ )	$r/R25^c$	$\sigma_{Max}^d$	$L/10^{39}e$ (erg/s)	$N_v^f$	Env <sup>g</sup>	ID <sup>h</sup>	ULX <sup>i</sup>	UName <sup>j</sup>
NGC4449	X2	12:28:09.28	44:05:09.2	3	38.3	0.21	14.7	0.492					
NGC4449	X3	12:28:12.76	44:06:22.5	3	44.9	0.27	12.4	0.301					
NGC4449	X4	12:28:11.07	44:06:45.3	3	65.5	0.44	14.2	0.45					
NGC4449	X5	12:28:17.74	44:06:34.9	3	87.5	0.48	9.9	0.289					
NGC4449	X6	12:28:10.63	44:03:36.4	3	123.9	0.80	11.3	0.247					
NGC4449	X7	12:28:01.81	44:08:04.5	3	177.7	1.35	4.6	0.103					
NGC4449	X8	12:27:47.56	44:02:06.0	3	334.4	1.82	4.6	0.093					
NGC4472	X1	12:29:46.92	08:00:06.1	0	10.3	0.04	63.9	181			(NGC4472)	N	
NGC4472	X2	12:30:06.35	08:02:05.3	0	321.2	1.29	4.5	2.91				2ULXd	
NGC4472	X3	12:29:39.73	07:53:30.6	0	400.3	1.43	18.0	13			P B2/20.98	2EULXd	
NGC4472	X4	12:29:27.63	08:06:40.5	0	490.5	1.61	7.4	4.9			mP B2/19.96	2ULXd	
NGC4472	X5	12:29:23.63	07:53:60.0	0	493.6	1.93	15.4	13.3			P B2/20.11	2EULXd	
NGC4472	X6	12:29:34.63	08:09:37.4	0	605.6	1.98	4.9	4.9				2ULXd	
NGC4476	X1	12:29:58.11	12:21:48.1	1	55.8	1.26	4.6	4.31		Z		2ULX	
NGC4486	X1	12:30:49.34	12:23:39.5	2	16.3	0.07	159.5	1740	1		(NGC4486)	N	
NGC4486	X2	12:30:41.99	12:17:59.1	1	343.9	1.42	3.1	3.13				2ULX	
NGC4485	X1	12:30:30.34	41:41:41.0	2	25.1	0.39	9.2	3.87		D		1ULXd	ULX1
NGC4490	X1	12:30:36.47	41:38:39.8	2	17.0	0.15	15.3	3.42			(NGC4490)	N	
NGC4490	X2	12:30:32.45	41:39:16.3	2	71.5	0.41	9.3	1.39		D		1ULXd	ULX1
NGC4490	X3	12:30:43.17	41:38:13.7	2	73.1	0.50	7.6	1.57		D		1ULXd	ULX2
NGC4490	X4	12:30:30.42	41:39:06.4	2	82.7	0.44	7.2	1.32		D		1ULXd	ULX3
NGC4501	X1	12:32:00.71	14:24:41.6	2	38.9	0.20	5.9	14.7		S		1EULXd	ULX1
NGC4523	X1	12:33:52.93	15:11:44.8	2	118.6	1.98	5.2	4.84				2ULXd	
PGC41763	X1	12:33:51.98	15:21:48.6	2	77.0	1.90	8.4	19.2			mP	2EULXd	
NGC4526	X1	12:34:02.65	07:42:04.3	1	5.0	0.03	5.0	7.16			(NGC4526)	N	
NGC4536	X1	12:34:27.11	02:11:15.6	0	4.6	0.02	4.0	5.76			(NGC4536)	N	
NGC4536	X2	12:34:33.81	02:13:07.6	0	150.1	1.54	7.2	10.5		Z		2EULXd	
NGC4552	X1	12:35:39.60	12:33:23.7	0	4.6	0.03	45.7	82.6			(NGC4552)	N	
NGC4552	X2	12:35:29.42	12:31:05.9	0	207.0	1.42	3.9	2.67				2ULX	
NGC4559	X1	12:35:58.63	27:57:39.0	1	11.3	0.08	43.3	3.16		D		1ULXd	ULX1
NGC4559	X2	12:35:58.07	27:58:07.1	1	31.3	0.16	10.2	0.46					
NGC4559	X3	12:36:03.23	27:58:03.7	1	77.2	0.58	5.5	0.314					
NGC4559	X4	12:35:56.57	27:59:22.4	1	107.7	0.43	5.2	0.207		S			
NGC4559	X5	12:35:51.58	27:56:01.7	1	125.2	0.91	66.9	5.05			mP	1ULXd	ULX2
NGC4559	X6	12:35:56.29	27:55:30.2	1	127.4	0.69	4.9	0.216					
NGC4559	X7	12:35:40.91	27:58:28.0	1	229.8	1.37	3.7	0.158					
NGC4559	X8	12:36:14.41	27:55:43.3	1	247.3	1.21	4.2	0.178					
NGC4559	X9	12:35:33.57	28:00:08.5	1	355.4	1.79	8.6	0.464					
NGC4559	X10	12:36:19.00	27:48:16.2	1	626.4	1.96	5.0	0.258					
NGC4565	X1	12:36:20.79	25:59:14.2	1	9.5	0.13	6.8	12.1			(NGC4565)	N	
NGC4565	X2	12:36:17.45	25:58:53.1	1	44.1	0.61	12.6	25.2			(GC)	1EULXd	ULX1
NGC4565	X3	12:36:31.35	25:59:36.2	1	148.3	1.97	3.5	5.34			P B2/20.55	2ULXd	
NGC4569	X1	12:36:49.76	13:09:44.8	3	6.0	0.03	13.5	13.3			(NGC4569)	N	
NGC4569	X2	12:37:09.48	13:15:09.7	3	428.5	1.76	9.6	6.37			* J/11.028	2ULXd	
NGC4593	X1	12:39:39.47	-05:20:34.7	1	5.9	0.05	275.7	15600	1		(NGC4593)	N	
NGC4594	X1	12:39:59.55	-11:37:24.1	4	3.1	0.02	30.7	22	1		(NGC4594)	N	
NGC4594	X2	12:40:01.84	-11:37:22.8	4	35.8	0.14	10.8	5.83		D		1ULXd	ULX1
NGC4594	X3	12:39:48.69	-11:37:17.8	4	157.4	0.60	3.6	1.25		D		1ULXd	ULX2
NGC4594	X4	12:39:45.22	-11:38:54.7	4	228.0	1.18	14.2	5.84			G0*	2ULXd	
NGC4594	X5	12:40:22.64	-11:39:33.4	4	365.8	1.80	3.7	1.04				2ULXd	
NGC4627	X1	12:42:04.07	32:34:07.7	0	59.2	1.10	4.0	0.584			P B2/20.29		
NGC4631	X1	12:41:57.29	32:32:01.4	0	134.2	0.36	4.7	0.569		D			
NGC4631	X2	12:41:55.43	32:32:14.3	0	155.8	0.34	13.2	2.42		D	(HII)	1ULXd	ULX1
NGC4636	X1	12:42:49.73	02:41:13.0	3	4.1	0.03	42.6	148			(NGC4636)	N	
NGC4649	X1	12:43:39.81	11:33:12.1	0	15.8	0.08	65.4	229			(NGC4649)	N	
NGC4649	X2	12:43:36.27	11:30:07.9	0	180.1	0.99	7.3	10.3			P B1/17.84	1EULXd	
NGC4649	X3	12:44:09.05	11:33:35.9	0	424.1	1.96	13.1	12.1			P B1/19.79	2EULXd	
NGC4639	X1	12:42:52.38	13:15:26.8	1	4.6	0.08	26.2	113			(NGC4639)	N	
NGC4651	X1	12:43:42.69	16:23:35.2	2	4.9	0.06	4.6	3.45			(NGC4651)	N	
NGC4656	X1	12:43:41.11	32:04:58.0	0	385.2	0.85	10.5	1.39		D	Z	1ULXd	ULX1
NGC4666	X1	12:45:08.36	-00:27:37.6	2	9.7	0.20	3.4	2.08			(NGC4666)	N	
NGC4697	X1	12:48:35.87	-05:48:02.6	2	0.7	0.00	6.5	1.29	1		(NGC4697)	N	
NGC4697	X2	12:48:32.92	-05:47:42.4	2	48.7	0.29	3.2	0.517					
NGC4697	X3	12:48:39.58	-05:48:08.7	2	55.3	0.29	4.2	0.777					
NGC4697	X5	12:48:47.01	-05:48:49.3	0	172.4	0.97	3.1	3.33			P B1/18.81	1ULX	ULX1

Table 2—Continued

Galaxy	Name	R.A. (hh:mm:ss)	Decl. (dd:mm:ss)	$N_c^a$	$r^b$ (‘)	$r/R25^c$	$\sigma_{Max}^d$	$L/10^{39}^e$ (erg/s)	$N_v^f$	Env <sup>g</sup>	ID <sup>h</sup>	ULX <sup>i</sup>	UName <sup>j</sup>
NGC4697	X6	12:48:45.45	-05:45:37.6	2	202.9	1.05	3.5	0.638					
NGC4697	X7	12:48:47.92	-05:45:08.1	2	249.8	1.28	5.2	1.01				2ULXd	
NGC4697	X8	12:48:20.11	-05:51:55.3	2	331.6	1.70	3.2	0.422			P B1/20.29 (NGC4736)	N	
NGC4736	X1	12:50:53.02	41:07:17.2	1	9.7	0.03	136.4	13.3					
NGC4736	X2	12:50:47.24	41:05:15.0	1	135.5	0.49	5.2	0.121					
NGC4736	X3	12:50:44.25	41:04:59.3	1	168.1	0.60	4.8	0.121					
NGC4736	X4	12:50:59.90	41:10:59.7	1	240.5	0.88	6.2	0.386					
NGC4736	X5	12:50:52.19	41:02:55.2	1	255.2	0.93	5.0	0.106					
NGC4736	X6	12:50:23.24	41:07:53.0	1	345.8	1.03	8.4	0.275					
NGC4736	X7	12:51:03.77	41:00:11.6	1	433.9	1.52	5.9	0.142					
NGC4736	X8	12:50:27.55	41:13:19.4	1	472.3	1.53	4.8	0.119					
NGC4736	X9	12:50:58.56	40:59:08.7	1	484.6	1.73	6.3	0.132					
NGC4736	X10	12:51:11.45	41:15:14.9	1	525.1	1.91	5.6	0.241					
NGC4736	X11	12:50:34.66	41:15:27.5	1	541.4	1.85	4.7	0.0973					
NGC4736	X12	12:50:02.29	41:09:27.9	1	595.7	1.77	3.2	0.0717					
NGC4826	X1	12:56:43.54	21:40:56.3	1	13.7	0.08	11.8	4.49		(NGC4826)	N		
NGC4861	X1	12:59:02.00	34:51:12.0	1	34.3	0.30	25.1	31.4		D	1EULXd	ULX1	
NGC4861	X2	12:59:00.45	34:50:41.3	1	69.0	0.59	7.2	8.4			(HII)	1ULXd	ULX2
NGC5005	X1	13:10:56.16	37:03:25.2	0	3.8	0.04	26.6	58.3			(NGC5005)	N	
NGC5033	X1	13:13:27.56	36:35:36.5	0	5.5	0.04	54.1	135			(NGC5033)	N	
NGC5055	X1	13:15:49.30	42:01:45.5	2	20.5	0.09	7.3	2.2			(NGC5055)	N	
NGC5055	X2	13:15:46.71	42:01:58.4	2	29.9	0.10	7.5	1.96		S	1ULXd	ULX1	
NGC5055	X3	13:15:40.69	42:01:48.2	2	97.6	0.30	4.9	1.18		S	1ULXd	ULX2	
NGC5055	X4	13:15:47.13	42:00:25.1	2	103.8	0.48	4.5	1.05		S	1ULXd	ULX3	
NGC5055	X5	13:16:02.49	42:01:55.4	2	147.3	0.40	3.7	0.762		S			
NGC5055	X6	13:15:30.27	42:03:14.0	2	222.6	0.59	5.9	1.44		K0*	1ULXd	ULX4	
NGC5055	X7	13:15:19.43	42:03:03.2	2	337.6	0.90	28.2	9.36			1ULXd	ULX4	
NGC5055	X8	13:15:18.12	42:04:08.6	2	368.3	0.98	3.8	0.785			* J/9.457	2ULXd	
NGC5055	X9	13:15:08.51	42:01:13.9	2	457.4	1.37	4.2	1.02				2ULX	
NGC5055	X10	13:14:54.58	42:02:39.1	2	610.6	1.69	4.8	1.19					
NGC5128	X1	13:25:40.68	-43:01:18.8	6	129.5	0.21	3.0	0.0953					
NGC5128	X2	13:25:38.23	-43:03:09.5	6	164.3	0.27	3.3	0.115					
NGC5128	X3	13:25:40.83	-43:02:42.8	6	165.5	0.28	3.4	0.11					
NGC5128	X4	13:25:19.94	-43:03:15.8	3	168.2	0.22	39.0	9.27				1ULX	ULX1
NGC5128	X5	13:25:12.89	-43:01:13.9	6	177.2	0.27	3.1	0.103					
NGC5128	X7	13:25:07.59	-43:01:13.5	6	235.2	0.36	5.2	0.41					
NGC5128	X8	13:25:22.33	-42:57:15.5	6	236.2	0.37	6.0	0.742					
NGC5128	X9	13:25:06.31	-43:02:23.3	6	262.3	0.38	7.1	0.308					
NGC5128	X10	13:25:33.44	-43:05:26.4	6	270.8	0.41	3.3	0.105		F0*			
NGC5128	X12	13:25:54.60	-42:59:20.9	6	297.8	0.43	5.0	0.154					
NGC5128	X13	13:25:07.34	-43:04:07.9	6	302.8	0.40	45.6	2.68	1	* J/10.358	1ULXd		
NGC5128	X14	13:25:02.40	-43:02:42.6	6	309.2	0.44	10.4	0.485					
NGC5128	X16	13:25:58.84	-43:04:29.8	6	388.6	0.65	14.8	0.974					
NGC5128	X17	13:26:01.49	-43:05:28.0	6	445.7	0.74	12.0	0.808					
NGC5128	X18	13:24:57.08	-43:05:36.6	6	446.0	0.59	7.6	0.287					
NGC5128	X19	13:25:00.68	-43:06:43.7	6	463.0	0.60	11.1	0.481	1				
NGC5128	X20	13:25:35.40	-42:52:57.4	6	487.7	0.67	3.9	0.13					
NGC5128	X21	13:24:52.31	-43:05:43.2	3	491.8	0.66	3.8	0.793					
NGC5128	X22	13:25:49.32	-42:52:38.8	6	548.6	0.72	6.2	0.236					
NGC5128	X23	13:25:46.47	-43:09:42.6	6	556.6	0.87	4.5	0.155					
NGC5128	X24	13:25:41.96	-43:10:42.9	6	599.9	0.91	8.7	0.408					
NGC5128	X25	13:25:30.64	-43:11:15.8	6	616.1	0.89	4.6	0.15					
NGC5128	X26	13:24:57.97	-43:09:46.7	6	626.8	0.81	5.1	0.17					
NGC5128	X27	13:25:45.94	-43:11:01.8	6	629.8	0.97	6.8	0.347					
NGC5128	X28	13:26:26.18	-43:02:55.4	6	637.4	1.03	9.2	0.961	1				
NGC5128	X29	13:25:05.64	-43:11:09.4	6	660.9	0.87	3.9	0.131					
NGC5128	X30	13:24:32.66	-42:56:11.4	6	682.3	1.13	14.4	0.844					
NGC5128	X31	13:25:00.96	-43:12:00.1	6	728.0	0.95	4.7	0.195					
NGC5128	X32	13:26:12.65	-43:10:52.1	6	761.0	1.25	7.3	0.338					
NGC5128	X33	13:26:04.47	-42:47:03.2	6	923.1	1.21	6.5	1.01		* B2/14.11	2ULX		
NGC5128	X35	13:24:28.45	-42:46:01.4	6	1118.2	1.83	3.7	0.381					
NGC5128	X36	13:24:14.82	-43:14:15.6	2	1136.9	1.49	3.2	0.621					
NGC5128	X37	13:26:26.16	-43:17:15.6	3	1158.8	1.88	3.4	1.96			2ULX		
NGC5128	X38	13:26:56.81	-42:49:53.6	2	1172.3	1.58	3.7	1.97			2ULX		
NGC5194	X1	13:29:52.63	47:11:45.9	4	7.1	0.03	52.9	17.2		(NGC5194)	N		

Table 2—Continued

Galaxy	Name	R.A. (hh:mm:ss)	Decl. (dd:mm:ss)	$N_c^a$	$r^b$ (‘)	$r/R_{25}^c$	$\sigma_{Max}^d$	$L/10^{39}e$ (erg/s)	$N_v^f$	Env <sup>g</sup>	ID <sup>h</sup>	ULX <sup>i</sup>	UName <sup>j</sup>
NGC5194	X3	13:29:45.79	47:10:45.2	4	99.0	0.46	4.8	0.516		* J/12.261			
NGC5194	X4	13:29:43.18	47:11:36.6	4	103.8	0.49	5.8	1.65	S		1ULX	ULX1	
NGC5194	X5	13:29:47.60	47:09:43.7	2	137.2	0.54	4.7	1.12	S		1ULX	ULX2	
NGC5194	X6	13:30:01.08	47:13:45.4	4	141.7	0.59	18.0	3.95	S		1ULXd	ULX3	
NGC5194	X7	13:29:39.89	47:12:42.5	4	147.1	0.62	10.4	1.81	S		1ULXd	ULX4	
NGC5194	X8	13:30:07.71	47:11:07.1	4	152.5	0.67	23.4	3.65	1	S	1ULXd	ULX5	
NGC5194	X9	13:29:53.54	47:14:40.0	4	172.0	0.55	4.8	1.31	S		1ULX	ULX6	
NGC5194	X10	13:30:06.10	47:08:36.5	4	231.8	0.74	4.4	0.415					
NGC5194	X11	13:29:58.71	47:05:29.5	4	382.5	1.16	4.8	0.43					
NGC5194	X12	13:29:38.53	47:18:58.7	4	456.2	1.36	4.2	0.882		P B1/20.07 (NGC5195)			
NGC5195	X1	13:29:59.28	47:16:02.1	4	19.9	0.14	13.2	3.27					N
NGC5195	X2	13:30:06.23	47:15:45.3	4	84.5	0.54	5.5	0.488					
NGC5195	X4	13:30:29.11	47:16:11.2	4	309.7	1.82	4.3	0.417					
NGC5204	X1	13:29:38.75	58:25:07.5	1	18.8	0.20	54.0	5.15	1	(B0Ib*) (NGC5236)	1ULXd	ULX1	
NGC5236	X1	13:37:00.73	-29:51:56.5	3	9.4	0.03	46.3	7.13					N
NGC5236	X2	13:37:04.68	-29:51:21.7	3	71.0	0.20	7.8	0.644					
NGC5236	X3	13:37:01.42	-29:53:23.0	3	80.3	0.21	3.9	0.268					
NGC5236	X4	13:37:05.67	-29:53:06.6	3	93.8	0.26	4.6	0.281					
NGC5236	X6	13:36:59.85	-29:49:55.5	3	128.6	0.33	4.9	0.323					
NGC5236	X7	13:37:04.45	-29:54:05.3	3	132.7	0.35	6.7	0.451		S			
NGC5236	X8	13:36:49.30	-29:52:58.7	3	153.2	0.44	4.8	0.302					
NGC5236	X9	13:36:46.01	-29:52:01.9	3	185.9	0.54	3.4	0.217					
NGC5236	X11	13:37:20.12	-29:53:47.7	3	277.9	0.80	32.5	2.63	1	S		1ULXd	ULX1
NGC5236	X12	13:37:37.21	-29:48:21.0	3	529.6	1.51	4.7	0.265					
NGC5273	X1	13:42:08.18	35:39:14.4	0	3.6	0.05	5.5	4.72		(NGC5273)			N
NGC5322	X1	13:49:15.36	60:11:24.2	0	5.2	0.04	9.7	29.7		(NGC5322)			N
NGC5350	X1	13:53:21.94	40:21:52.2	0	5.8	0.06	5.0	21.4		(NGC5350)			N
NGC5353	X1	13:53:26.36	40:17:03.6	0	5.2	0.13	18.8	106		(NGC5353)			N
NGC5457	X1	14:03:12.66	54:20:54.9	4	1.4	0.00	8.2	0.466	1	(NGC5457)			N
NGC5457	X2	14:03:21.58	54:19:45.2	3	105.8	0.13	5.2	0.282	1	S			
NGC5457	X3	14:03:24.80	54:19:47.6	4	126.9	0.15	4.5	0.321	1	S			
NGC5457	X4	14:02:52.99	54:21:12.6	3	171.5	0.21	3.9	0.187					
NGC5457	X5	14:03:32.17	54:21:02.7	3	172.1	0.21	6.2	0.362					
NGC5457	X6	14:03:31.11	54:21:55.8	4	173.6	0.21	4.2	0.335					
NGC5457	X7	14:03:35.94	54:19:23.1	3	224.7	0.28	6.3	0.302	1	S			
NGC5457	X8	14:03:19.70	54:17:15.9	4	227.9	0.26	6.9	0.694		S			
NGC5457	X9	14:03:41.19	54:19:02.5	3	275.0	0.34	4.5	0.307		S			
NGC5457	X11	14:03:54.01	54:21:58.8	4	368.4	0.46	8.1	0.48	1	S			
NGC5457	X12	14:02:29.67	54:21:18.1	4	375.1	0.46	26.8	1.57	1	S	P B/17.80	1ULXd	ULX1
NGC5457	X13	14:03:50.83	54:24:14.2	4	389.7	0.47	3.8	0.178					
NGC5457	X14	14:03:16.03	54:27:28.4	4	394.6	0.46	3.9	0.309					
NGC5457	X15	14:03:03.93	54:27:35.8	4	407.8	0.47	21.8	1.54	1	S		1ULXd	ULX2
NGC5457	X16	14:02:46.82	54:26:53.8	4	423.1	0.50	4.5	0.398					
NGC5457	X17	14:02:28.43	54:16:24.0	4	471.4	0.57	14.0	0.891	1	S			
NGC5457	X18	14:02:21.90	54:17:56.9	4	477.1	0.59	6.3	0.374					
NGC5457	X19	14:02:28.53	54:26:31.8	4	510.8	0.61	6.3	0.541	1				
NGC5457	X20	14:02:14.21	54:21:57.2	2	513.3	0.63	4.1	0.173	1				
NGC5457	X21	14:04:22.14	54:19:21.8	4	616.1	0.76	12.6	1.25	2	* J/10.732			
NGC5457	X22	14:02:03.23	54:18:28.7	3	623.3	0.77	4.6	0.23					
NGC5457	X23	14:04:14.40	54:26:05.9	4	623.6	0.76	43.7	3.17	1	S		1ULXd	ULX3
NGC5457	X24	14:04:16.85	54:16:10.9	3	630.8	0.77	8.1	0.424	1				
NGC5457	X25	14:02:27.93	54:12:39.0	4	631.1	0.75	11.7	0.773	1				
NGC5457	X26	14:04:29.41	54:23:56.7	3	696.1	0.86	10.0	0.615	1				
NGC5457	X27	14:04:01.23	54:11:27.6	2	710.1	0.84	3.6	0.165	1				
NGC5457	X28	14:02:09.88	54:30:18.4	4	784.9	0.94	4.5	0.549					
NGC5457	X29	14:04:00.25	54:09:15.6	3	815.0	0.96	4.2	0.228					
NGC5457	X30	14:03:05.64	54:07:06.5	3	830.7	0.96	4.0	0.327					
NGC5457	X31	14:02:07.72	54:10:30.2	2	844.1	1.01	5.6	0.376	1				
NGC5457	X32	14:01:34.04	54:20:42.5	2	860.9	1.07	7.4	1.26					
NGC5457	X34	14:01:19.30	54:18:36.1	4	999.8	1.24	18.7	2.26	1		* J/10.453	2ULXd	
NGC5457	X35	14:03:03.93	54:04:14.7	3	1003.1	1.16	7.1	0.891	2				
NGC5457	X36	14:01:23.46	54:15:19.1	2	1011.8	1.24	4.3	0.529	1				
NGC5506	X1	14:13:14.83	-03:12:26.6	1	1.1	0.02	216.6	455	1	(NGC5506)	N		
NGC5774	X1	14:53:45.07	03:33:31.0	1	89.5	1.00	4.7	7.72		S		2ULXd	ULX1
NGC5774	X2	14:53:43.19	03:37:06.9	1	131.9	1.58	3.8	5.3					2ULXd

Table 2—Continued

Galaxy	Name	R.A. (hh:mm:ss)	Decl. (dd:mm:ss)	$N_c^a$	r <sup>b</sup> (‘“)	r/R25 <sup>c</sup>	$\sigma_{Max}^d$	$L/10^{39}^e$ (erg/s)	$N_v^f$	Env <sup>g</sup>	ID <sup>h</sup>	ULX <sup>i</sup>	UName <sup>j</sup>
NGC6434	X1	17:36:36.16	72:05:29.3	3	57.2	0.83	16.1	78.6			QSO J17366+7205 (NGC6500)	1EULXd	
NGC6500	X1	17:55:59.58	18:20:15.9	2	13.0	0.27	4.6	64.3				N	
NGC6503	X1	17:49:12.42	70:09:28.4	2	91.1	0.43	3.9	0.554		D			
NGC6654	X1	18:24:03.60	73:09:29.0	3	92.8	1.19	4.8	13.5			P	2EULXd	
NGC6654	X2	18:24:36.45	73:10:51.8	3	120.2	1.91	5.8	13.8			P	2EULXd	
NGC6764	X1	19:08:16.30	50:56:00.6	4	7.6	0.19	31.4	68.2			(NGC6764)	N	
NGC6946	X1	20:34:52.62	60:09:11.9	7	5.6	0.02	13.9	1.67			(NGC6946)	N	
NGC6946	X2	20:35:00.33	60:09:07.0	7	62.7	0.21	20.5	1.8	1	S		1ULXd	ULX1
NGC6946	X3	20:35:01.52	60:10:07.2	7	88.1	0.29	4.5	0.421					
NGC6946	X4	20:34:36.53	60:09:30.4	7	116.5	0.40	15.8	1.6		S		1ULXd	ULX2
NGC6946	X5	20:34:34.86	60:10:33.3	7	150.0	0.49	4.2	0.358					
NGC6946	X6	20:35:01.05	60:11:31.8	7	152.5	0.46	71.1	11		S	(SNR)	1EULXd	ULX3
NGC6946	X7	20:35:11.81	60:07:30.9	7	180.9	0.59	3.8	0.309					
NGC6946	X8	20:34:49.59	60:12:21.8	7	187.7	0.55	3.5	0.244					
NGC6946	X9	20:34:25.95	60:09:09.7	7	194.5	0.66	8.5	0.584					
NGC6946	X10	20:34:49.04	60:05:55.1	7	201.2	0.59	5.1	0.392			*	B/12.18	
NGC6946	X11	20:35:17.88	60:10:56.2	7	218.0	0.72	4.5	0.355					
NGC6946	X12	20:35:36.64	60:06:42.0	7	366.8	1.22	4.3	0.25					
NGC6946	X13	20:33:51.83	60:10:48.8	7	458.7	1.55	5.2	0.414					
NGC6946	X14	20:34:27.22	60:02:06.7	7	466.7	1.40	6.2	0.45					
NGC6946	X15	20:35:11.97	60:01:19.0	7	498.8	1.47	5.8	0.432					
NGC6946	X16	20:34:09.46	60:16:15.9	7	527.0	1.63	4.8	0.327					
NGC6946	X17	20:33:46.22	60:14:18.2	7	576.5	1.89	6.0	0.555					
NGC7172	X1	22:02:01.46	-31:52:08.5	1	2.3	0.05	7.8	21.8			(NGC7172)	N	
NGC7213	X1	22:09:16.24	-47:09:59.9	1	7.0	0.08	526.8	3080			(NGC7213)	N	
NGC7217	X1	22:07:52.59	31:21:38.3	1	5.9	0.05	5.6	12.5			(NGC7217)	N	
NGC7217	X2	22:07:36.99	31:21:15.4	1	195.8	1.69	3.3	4.67				2ULXd	
PGC68618	X1	22:20:37.01	-46:02:28.6	5	213.6	1.51	5.8	1.28			P B/18.40	2ULXd	
NGC7314	X1	22:35:46.21	-26:03:01.6	1	5.8	0.09	201.5	202	1		(NGC7314)	N	
NGC7314	X2	22:35:48.13	-26:01:28.2	1	99.8	0.82	5.6	2.34		S		1ULXd	ULX1
NGC7314	X4	22:35:41.51	-26:00:30.6	1	163.0	1.50	4.4	1.81				2ULXd	
NGC7314	X5	22:35:48.03	-25:58:33.9	1	270.8	1.98	11.3	5.21			P B1/20.44	2ULXd	
PGC70090	X1	22:57:10.32	-36:27:43.0	2	2.9	0.03	29.5	140			(PGC70090)	N	
NGC7465	X1	23:02:00.95	15:57:53.3	1	3.5	0.12	60.5	331	1		(NGC7465)	N	
NGC7552	X1	23:16:10.85	-42:35:05.6	2	4.6	0.05	19.7	80.8			(NGC7552)	N	
NGC7582	X1	23:18:23.40	-42:22:14.1	3	3.3	0.02	27.9	41.3			(NGC7582)	N	
NGC7582	X2	23:18:30.15	-42:20:35.9	1	121.6	1.74	7.9	7.81			P B2/20.23	2ULXd	
NGC7590	X1	23:18:56.48	-42:13:57.6	3	25.4	0.32	5.0	6.54				1ULX	ULX1
NGC7714	X1	23:36:14.12	02:09:18.1	1	8.6	0.20	20.2	91			(NGC7714)	N	
NGC7714	X2	23:36:15.75	02:09:28.5	1	18.9	0.41	13.7	41.8		D		1EULXd	ULX1
NGC7742	X1	23:44:15.34	10:46:07.2	1	10.2	0.20	4.7	14.8			(NGC7742)	N	
NGC7742	X2	23:44:17.47	10:45:51.0	1	25.3	0.48	3.4	7.39				1ULXd	ULX1

<sup>a</sup>The number of X-ray sources identified with objects in astrometric catalogs used to correct the X-ray positions.

<sup>b</sup>The nuclear offset in arcseconds.

<sup>c</sup>The nuclear offset in unit of elliptical radius  $R_{25}$

<sup>d</sup>The maximum detection significance among all observations.

<sup>e</sup>The maximum luminosity among all observations. The X-ray luminosities are computed using a power-law spectrum between 0.3–8 keV with a photon index of 1.7.

<sup>f</sup>The number of observations in which the probability for the Kolmogorov-Smirnov test of the source being constant is less than 0.01, i.e., the source is highly variable during the observation.

<sup>g</sup>The environments of the X-ray source. A flag 'D' indicates the source is in a dusty region usually associative of star forming activities. A flag 'S' means the source is associated with spiral arms.

<sup>h</sup>The identification of the X-ray source. Flag '\*' means the source is a bright foreground star, 'P'/'(Pr') means the source is positionally coincident with a point source in optical/IR/(Radio), 'mP' means the source is close to multiple such point sources and unique identification requires better positions, 'Z' means the source is close to faint fuzzy features on the optical image. The identification is enclosed with brackets when it is within the host galaxy.

<sup>i</sup>This indicates whether the source is a nuclear source (N) or a ULX candidate (ULX). Prefix '1' stands for ULXs within the  $D_{25}$  isophote of the galaxy, '2' for ULXs between  $1 - 2 \times D_{25}$ , and 'E' for ULXs with  $L_X > 10^{40}$  erg/s. Suffix 'd' stands for ULXs that are above  $10^{39}$  erg/s in the deepest observation for the galaxy.

<sup>j</sup>The ULX name in the clean ULX sample.

Table 3. Individual observations for ULX candidates

Name	Obs.Src <sup>a</sup>	Date <sup>b</sup> (MJD)	T <sup>c</sup> ksec	$\Delta D$ <sup>d</sup>	$\sigma$ <sup>e</sup>	$\theta$ <sup>f</sup> ( $'$ )	$C(\theta, \sigma)$ <sup>g</sup>	CorCnt <sup>h</sup> (count)	pErr <sup>i</sup> (%)	Flux <sup>j</sup> (cgs)	$L_X$ <sup>k</sup> ( $10^{39}$ erg/s)	$P_{KS}^{-1}$
NGC253-ULX1	rh600088a00.u	48599	3.1	1.2d	<3			<12.5		<2.64e-13	<0.285	
	rh600088a01.u+	48779	25.4	1.2d	<3			<30.2		<7.88e-14	<0.0851	
	rh600714n00.u	49720	10.9	4.1d	<3			<19.7		<1.19e-13	<0.129	
	rh600714a01.u	49882	19.7	23.9d	<3			<23.0		<7.72e-14	<0.0834	
	rh601111n00.1	50802	17.3	6.9d	38.6	15.49	0.85	566.1	3.92	2.19e-12	2.37	0.42
	rh601111n00.u	50996	2.1	0.6h	<3			<16.5		<5.36e-13	<0.579	
NGC720-X2	rh600472n00.15+	49360	56.8	4.4d	9.3	2.61	0.95	116.3	13.56	1.38e-13	12.7	0.67
NGC720-X3	rh600472n00.17+	49360	56.8	4.4d	4.5	3.36	0.96	53.8	26.40	6.38e-14	5.86	0.52
NGC891-ULX1	rh600690n00.10+	49744	97.2	8.7d	11.4	0.68	0.94	178.5	11.13	1.82e-13	1.53	0.034
	rh500501n00.6	50663	41.5	4.0d	5.5	0.69	0.98	45.0	23.31	1.07e-13	0.897	
	rh500539n00.u	50867	5.0	5.4h	<3			<11.3		<2.22e-13	<1.86	
NGC891-ULX2	rh600690n00.11+	49744	97.2	8.7d	27.0	1.15	0.89	440.0	5.69	4.49e-13	3.77	0.99
	rh500501n00.7	50663	41.5	4.0d	12.4	0.17	0.93	128.1	10.36	3.05e-13	2.56	0.54
	rh500539n00.u	50867	5.0	5.4h	<3			<11.3		<2.22e-13	<1.86	
NGC891-X6	rh600690n00.9+	49744	97.2	8.7d	9.8	5.40	0.95	147.7	13.06	1.51e-13	1.27	0.19
	rh500501n00.5	50663	41.5	4.0d	7.1	6.53	0.99	57.6	17.76	1.37e-13	1.15	0.036
	rh500539n00.u	50867	5.0	5.4h	<3			<11.2		<2.21e-13	<1.85	
NGC891-ULX3	rh600690n00.7+	49744	97.2	8.7d	11.9	5.41	0.94	168.3	10.71	1.72e-13	1.44	0.085
	rh500501n00.4	50663	41.5	4.0d	11.6	6.67	0.95	103.3	10.93	2.46e-13	2.06	0.91
	rh500539n00.2	50867	5.0	5.4h	3.5	6.70	1.00	13.8	26.06	2.72e-13	2.28	
NGC1042-ULX1	rh600469n00.2	49569	3.4	8.1d	5.6	8.95	1.02	19.7	23.10	4.61e-13	3.9	
	rh600469a01.2+	49911	21.9	16.9d	17.1	8.93	0.95	139.9	7.99	5.04e-13	4.27	0.71
NGC1068-ULX1	rh150020n00.u	48097	19.9	1.3d	<3			<15.6		<6.38e-14	<1.59	
	rh700347n00.u	49548	22.4	3.8d	<3			<16.6		<6.02e-14	<1.5	
	rh701352n00.u	49562	2.2	21.0h	<3			<7.6		<2.78e-13	<6.92	
	rh701352a01.10+	49914	71.4	17.9d	8.6	1.06	0.96	149.7	14.49	1.71e-13	4.26	0.55
NGC1068-ULX2	rh150020n00.u	48097	19.9	1.3d	<3			<15.3		<6.25e-14	<1.56	
	rh700347n00.5	49548	22.4	3.8d	4.0	2.85	0.95	28.6	26.41	1.04e-13	2.59	
	rh701352n00.u	49562	2.2	21.0h	<3			<7.5		<2.75e-13	<6.84	
	rh701352a01.8+	49914	71.4	17.9d	4.5	2.95	0.96	57.5	26.40	6.57e-14	1.63	0.00019
NGC1068-X4	rh150020n00.2	48097	19.9	1.3d	32.8	6.15	0.89	254.8	4.63	1.04e-12	25.9	3.9e-06
	rh700347n00.4	49548	22.4	3.8d	21.6	6.02	0.90	175.6	6.77	6.37e-13	15.9	0.77
	rh701352n00.1	49562	2.2	21.0h	8.1	6.09	0.97	24.6	15.45	9.03e-13	22.5	
	rh701352a01.7+	49914	71.4	17.9d	44.1	6.07	0.89	669.0	3.37	7.64e-13	19	0.66
NGC1068-X5	rh150020n00.u	48097	19.9	1.3d	<3			<15.5		<6.32e-14	<1.57	
	rh700347n00.u	49548	22.4	3.8d	<3			<16.4		<5.95e-14	<1.48	
	rh701352n00.u	49562	2.2	21.0h	<3			<7.6		<2.77e-13	<6.89	
	rh701352a01.5+	49914	71.4	17.9d	4.7	6.07	1.00	51.2	26.39	5.85e-14	1.46	0.098
NGC1068-X7	rh150020n00.u	48097	19.9	1.3d	<3			<15.7		<6.40e-14	<1.59	
	rh700347n00.u	49548	22.4	3.8d	<3			<16.6		<6.03e-14	<1.5	
	rh701352n00.u	49562	2.2	21.0h	<3			<7.6		<2.79e-13	<6.94	
	rh701352a01.4+	49914	71.4	17.9d	4.4	6.82	1.00	44.9	26.40	5.12e-14	1.27	
NGC1073-X1	rh600999n00.4+	50659	27.5	9.5d	5.8	1.69	0.96	36.8	22.10	1.14e-13	3.16	
	rh600999a01.1	50828	11.8	2.7d	3.7	1.72	0.95	15.6	26.35	1.12e-13	3.11	
NGC1073-ULX1	rh600999n00.5+	50659	27.5	9.5d	3.5	1.54	0.95	21.4	26.16	6.63e-14	1.84	
	rh600999a01.2	50828	11.8	2.7d	4.0	1.43	0.96	18.3	26.41	1.31e-13	3.63	
NGC1073-X3	rh600999n00.6+	50659	27.5	9.5d	3.3	1.86	0.94	18.7	25.80	5.80e-14	1.61	
	rh600999a01.u	50828	11.8	2.7d	<3			<12.8		<9.17e-14	<2.54	
NGC1073-X4	rh600999n00.7+	50659	27.5	9.5d	13.9	2.19	0.92	97.7	9.36	3.03e-13	8.4	
	rh600999a01.3	50828	11.8	2.7d	7.2	2.19	0.96	39.2	17.55	2.82e-13	7.82	
NGC1073-X6	rh600999n00.10+	50659	27.5	9.5d	4.2	2.82	0.95	33.8	26.41	1.05e-13	2.91	
	rh600999a01.u	50828	11.8	2.7d	<3			<12.6		<9.08e-14	<2.52	
NGC1291-ULX1	rh600828n00.3+	50085	14.7	9.3h	10.9	4.00	0.94	69.3	11.48	3.41e-13	3.03	0.1
NGC1291-X3	rh600828n00.1+	50085	14.7	9.3h	5.1	7.54	1.01	37.1	24.97	1.83e-13	1.62	
NGC1313-ULX1	rh400065n00.3	48730	5.4	36.0d	65.1	6.88	0.89	423.4	1.97	6.58e-12	10.8	1.4e-05
	rh600505n00.3	49527	22.4	22.9d	107.2	4.35	0.87	1327.8	1.21	4.94e-12	8.12	0.018
	rh500403n00.2	49749	13.4	10.7d	110.6	5.67	0.88	984.2	1.15	6.08e-12	9.99	0.00031
	rh500404n00.3	49750	27.1	8.9d	139.3	5.66	0.88	2063.4	1.06	6.32e-12	10.4	8.5e-06
	rh600505a01.3	49819	20.2	8.1d	122.8	4.37	0.87	1504.1	1.07	6.19e-12	10.2	1.2e-16
	rh500404a01.3	49846	18.9	72.6d	76.1	5.68	0.88	829.5	1.54	3.64e-12	5.98	3.5e-15
	rh500403a01.2+	49846	31.0	72.4d	76.3	5.68	0.88	1114.2	1.55	2.98e-12	4.9	1.1e-07
	rh500492n00.3	50722	22.8	6.9d	124.6	5.64	0.88	1738.2	1.05	6.33e-12	10.4	0.0015
	rh500550n00.2	50893	23.9	28.4d	68.4	5.67	0.88	807.5	1.81	2.80e-12	4.6	0.2
NGC1313-ULX2	rh400065n00.4	48730	5.4	36.0d	21.2	5.03	0.90	89.9	6.84	1.40e-12	2.3	0.72
	rh600505n00.5	49527	22.4	22.9d	47.0	2.10	0.88	427.0	3.03	1.59e-12	2.61	0.52

Table 3—Continued

Name	Obs.Src <sup>a</sup>	Date <sup>b</sup> (MJD)	T <sup>c</sup> ksec	$\Delta D^d$	$\sigma^e$	$\theta^f$ ( $'$ )	$C(\theta, \sigma)^g$	CorCnt <sup>h</sup> (count)	pErr <sup>i</sup> (%)	Flux <sup>j</sup> (cgs)	$L_X^{k}$ ( $10^{39}$ erg/s)	$P_{KS}^{l}$
	rh500403n00.3	49749	13.4	10.7d	37.9	0.10	0.88	307.8	4.07	1.90e-12	3.12	0.15
	rh500404n00.6	49750	27.1	8.9d	48.1	0.09	0.88	525.6	2.95	1.61e-12	2.64	0.81
	rh600505a01.5	49819	20.2	8.1d	52.3	2.13	0.88	423.1	2.75	1.74e-12	2.86	0.32
	rh500404a01.5	49846	18.9	72.6d	44.1	0.08	0.88	405.2	3.37	1.78e-12	2.92	0.31
	rh500403a01.6+	49846	31.0	72.4d	59.0	0.11	0.87	692.1	2.28	1.85e-12	3.04	0.41
	rh500492n00.5	50722	22.8	6.9d	47.0	0.10	0.88	388.1	3.03	1.41e-12	2.32	0.092
	rh500550n00.4	50893	23.9	28.4d	42.5	0.05	0.88	424.2	3.47	1.47e-12	2.41	0.98
NGC1313-ULX3	rh400065n00.2	48730	5.4	36.0d	24.7	0.31	0.89	114.5	6.13	1.78e-12	2.92	0.076
	rh600505n00.1	49527	22.4	22.9d	27.2	3.84	0.89	224.2	5.64	8.35e-13	1.37	0.79
	rh500403n00.1	49749	13.4	10.7d	51.1	5.39	0.88	392.6	2.75	2.42e-12	3.98	0.47
	rh500404n00.1	49750	27.1	8.9d	54.1	5.37	0.88	558.5	2.54	1.71e-12	2.81	0.00035
	rh600505a01.1	49819	20.2	8.1d	36.0	3.76	0.88	276.7	4.32	1.14e-12	1.87	0.39
	rh500404a01.2	49846	18.9	72.6d	36.0	5.38	0.89	332.1	4.32	1.46e-12	2.4	3.7e-07
	rh500403a01.1+	49846	31.0	72.4d	40.4	5.38	0.89	414.4	3.75	1.11e-12	1.82	0.035
	rh500492n00.2	50722	22.8	6.9d	53.9	5.36	0.88	432.8	2.57	1.58e-12	2.6	0.58
	rh500550n00.1	50893	23.9	28.4d	46.1	5.30	0.88	437.3	3.16	1.51e-12	2.48	1.2e-13
NGC1316-ULX1	rh600255n00.2	49367	11.0	3.6h	2.5	3.55	0.92	10.8	24.72	6.85e-14	3.79	
	rh600255a01.5+	49540	29.4	3.2d	5.4	3.52	0.97	33.5	23.84	8.04e-14	4.45	
NGC1316-ULX2	rh600255n00.5	49367	11.0	3.6h	4.8	4.14	0.97	27.4	26.06	1.75e-13	9.69	
	rh600255a01.8+	49540	29.4	3.2d	7.4	4.09	0.97	63.8	16.90	1.53e-13	8.47	0.66
NGC1316-ULX3	rh600255n00.u	49367	11.0	3.6h	<3			<13.8		<8.78e-14	<4.86	
	rh600255a01.4+	49540	29.4	3.2d	4.7	4.72	0.98	34.1	26.39	8.18e-14	4.53	
NGC1316-ULX4	rh600255n00.u	49367	11.0	3.6h	<3			<14.1		<8.98e-14	<4.97	
	rh600255a01.10+	49540	29.4	3.2d	3.5	6.66	0.99	22.9	26.05	5.50e-14	3.05	
NGC1316-ULX5	rh600255n00.u	49367	11.0	3.6h	<3			<14.3		<9.14e-14	<5.06	
	rh600255a01.9+	49540	29.4	3.2d	3.5	7.48	1.00	20.8	26.05	4.98e-14	2.76	
NGC1316-ULX6	rh600255n00.u	49367	11.0	3.6h	<3			<14.5		<9.26e-14	<5.13	
	rh600255a01.3+	49540	29.4	3.2d	4.3	7.96	1.01	26.8	26.40	6.42e-14	3.55	
NGC1316-ULX7	rh600255n00.u	49367	11.0	3.6h	<3			<16.1		<1.02e-13	<5.65	
	rh600255a01.2+	49540	29.4	3.2d	4.6	9.90	1.02	31.0	26.39	7.42e-14	4.11	
NGC1365-ULX1	rh701297n00.2	49554	9.8	14.7d	5.9	1.29	0.97	30.0	22.05	2.01e-13	7.29	
	rh701297a02.u+	49902	9.8	1.1d	<3			<11.5		<7.78e-14	<2.82	
NGC1365-ULX2	rh701297n00.3	49554	9.8	14.7d	6.2	5.86	0.99	24.5	20.68	1.65e-13	5.98	
	rh701297a02.4+	49902	9.8	1.1d	5.7	5.83	0.99	20.0	22.51	1.35e-13	4.89	
NGC1365-ULX3	rh701297n00.5	49554	9.8	14.7d	5.7	5.87	0.99	26.0	22.56	1.74e-13	6.31	
	rh701297a02.u+	49902	9.8	1.1d	<3			<11.4		<7.69e-14	<2.79	
NGC1365-X5	rh701297n00.u	49554	9.8	14.7d	<3			<12.5		<8.39e-14	<3.04	
	rh701297a02.2+	49902	9.8	1.1d	9.1	7.77	0.98	38.0	13.84	2.57e-13	9.32	
NGC1380-ULX1	rh600676n00.7+	49924	42.1	1.6d	3.0	0.57	0.98	24.8	25.51	3.83e-14	1.43	
NGC1395-X2	rh600492n00.u	49386	17.6	3.2d	<3			<14.9		<6.02e-14	<4.2	
	rh600492a01.4+	49553	19.9	34.8d	3.9	2.65	0.95	19.3	26.42	6.89e-14	4.8	
NGC1395-X3	rh600492n00.u	49386	17.6	3.2d	<3			<14.8		<5.99e-14	<4.17	
	rh600492a01.1+	49553	19.9	34.8d	3.5	3.32	0.94	18.1	26.10	6.47e-14	4.51	
NGC1395-X4	rh600492n00.u	49386	17.6	3.2d	<3			<14.8		<5.97e-14	<4.16	
	rh600492a01.5+	49553	19.9	34.8d	4.1	4.17	0.96	24.6	26.41	8.80e-14	6.13	
NGC1395-X5	rh600492n00.2	49386	17.6	3.2d	4.2	5.25	0.99	22.8	26.41	9.25e-14	6.45	
	rh600492a01.u+	49553	19.9	34.8d	<3			<15.3		<5.46e-14	<3.81	
NGC1398-X2	rh500518n00.5+	50650	17.2	37.5d	4.6	3.34	0.96	26.1	26.39	9.32e-14	5.51	
NGC1398-X3	rh500518n00.3+	50650	17.2	37.5d	4.9	3.89	0.97	28.0	25.79	9.99e-14	5.91	
NGC1399-ULX1	rh600256n00.u	49035	7.3	7.1h	<3			<12.2		<1.10e-13	<5.25	
	rh600220n00.u	49035	8.5	3.4d	<3			<13.0		<1.01e-13	<4.82	
	rh600831n00.14	50087	72.7	49.1d	8.2	0.38	0.96	148.8	15.26	1.34e-13	6.4	0.21
	rh600831a01.10+	50272	87.6	49.4d	10.6	0.35	0.94	215.5	11.87	1.61e-13	7.69	0.64
NGC1399-ULX2	rh600256n00.u	49035	7.3	7.1h	<3			<12.2		<1.10e-13	<5.25	
	rh600220n00.u	49035	8.5	3.4d	<3			<14.0		<1.08e-13	<5.16	
	rh600831n00.17	50087	72.7	49.1d	7.3	0.88	0.97	136.1	17.28	1.23e-13	5.87	0.84
	rh600831a01.11+	50272	87.6	49.4d	8.5	0.97	0.96	163.0	14.74	1.22e-13	5.83	0.4
	rh600940n00.12	50475	63.1	7.4d	6.8	10.34	1.00	109.0	18.53	1.13e-13	5.4	0.35
NGC1399-ULX3	rh600256n00.u	49035	7.3	7.1h	<3			<12.1		<1.09e-13	<5.21	
	rh600220n00.u	49035	8.5	3.4d	<3			<16.0		<1.24e-13	<5.92	
	rh600831n00.21	50087	72.7	49.1d	3.9	2.02	0.95	54.7	26.41	4.93e-14	2.35	0.83
	rh600831a01.u+	50272	87.6	49.4d	<3			<33.9		<2.53e-14	<1.21	
	rh600940n00.u	50475	63.1	7.4d	<3			<43.9		<4.58e-14	<2.19	
NGC1399-X5	rh600256n00.u	49035	7.3	7.1h	<3			<11.9		<1.07e-13	<5.11	

Table 3—Continued

Name	Obs.Src <sup>a</sup>	Date <sup>b</sup> (MJD)	T <sup>c</sup> ksec	$\Delta D^d$	$\sigma^e$	$\theta^f$ ( $'$ )	$C(\theta, \sigma)^g$	CorCnt <sup>h</sup> (count)	pErr <sup>i</sup> (%)	Flux <sup>j</sup> (cgs)	$L_X^{k}$ ( $10^{39}$ erg/s)	$P_{KS}^{l}$	
NGC1399-X6	rh600220n00.u	49035	8.5	3.4d	<3			<11.9		<9.22e-14	<4.4		
	rh600831n00.16	50087	72.7	49.1d	3.4	4.01	0.95	37.6	25.93	3.39e-14	1.62	0.48	
	rh600831a01.12+	50272	87.6	49.4d	4.7	4.01	0.97	54.8	26.39	4.10e-14	1.96	0.46	
	rh600940n00.11	50475	63.1	7.4d	3.1	6.25	0.99	33.9	25.52	3.54e-14	1.69	0.016	
NGC1399-X7	rh6002256n00.u	49035	7.3	7.1h	<3			<11.9		<1.07e-13	<5.11		
	rh600220n00.u	49035	8.5	3.4d	<3			<24.5		<1.90e-13	<9.07		
	rh600831n00.20	50087	72.7	49.1d	3.1	4.45	0.95	30.7	25.58	2.77e-14	1.32		
	rh600831a01.u+	50272	87.6	49.4d	<3			<33.3		<2.49e-14	<1.19		
	rh600940n00.u	50475	63.1	7.4d	<3			<71.2		<7.42e-14	<3.54		
NGC1399-X8	rh6002256n00.u	49035	7.3	7.1h	<3			<11.9		<1.07e-13	<5.11		
	rh600220n00.u	49035	8.5	3.4d	<3			<12.0		<9.32e-14	<4.45		
	rh600831n00.u	50087	72.7	49.1d	<3			<29.8		<2.69e-14	<1.28		
	rh600831a01.7+	50272	87.6	49.4d	3.3	3.96	0.94	42.4	25.81	3.17e-14	1.51	0.31	
	rh600940n00.u	50475	63.1	7.4d	<3			<30.7		<3.20e-14	<1.53		
NGC1399-X9	rh6002256n00.u	49035	7.3	7.1h	<3			<11.9		<1.07e-13	<5.11		
	rh600220n00.u	49035	8.5	3.4d	<3			<12.6		<9.81e-14	<4.69		
	rh600831n00.11	50087	72.7	49.1d	10.2	4.17	0.95	128.6	12.42	1.16e-13	5.54	0.0012	
	rh600831a01.6+	50272	87.6	49.4d	14.1	4.14	0.92	252.0	9.23	1.89e-13	9.03	0.019	
	rh600940n00.7	50475	63.1	7.4d	8.7	8.75	0.99	114.4	14.30	1.19e-13	5.68	0.24	
NGC1399-X10	rh6002256n00.2	49035	7.3	7.1h	16.1	5.03	0.92	82.6	8.34	7.45e-13	35.6	0.28	
	rh600220n00.3	49035	8.5	3.4d	20.5	4.52	0.90	114.1	6.96	8.85e-13	42.3	0.69	
	rh600831n00.13	50087	72.7	49.1d	21.3	5.02	0.90	339.3	6.83	3.06e-13	14.6	2.6e-05	
	rh600831a01.9+	50272	87.6	49.4d	44.3	5.07	0.88	786.4	3.35	5.88e-13	28.1	0.95	
	rh600940n00.9	50475	63.1	7.4d	21.4	4.52	0.90	271.8	6.81	2.83e-13	13.5	0.43	
NGC1404-X2	rh6002256n00.u	49035	7.3	7.1h	<3			<12.2		<1.10e-13	<5.25		
	rh600220n00.u	49035	8.5	3.4d	<3			<11.7		<9.10e-14	<4.35		
	rh600831n00.15	50087	72.7	49.1d	3.4	6.76	1.00	34.9	26.01	3.14e-14	1.5		
	rh600831a01.u+	50272	87.6	49.4d	<3			<34.3		<2.57e-14	<1.23		
	rh600940n00.u	50475	63.1	7.4d	<3			<29.8		<3.10e-14	<1.48		
NGC1427A-ULX1	rh600220n00.u	49035	8.5	3.4d	<3			<12.3		<1.11e-13	<5.87		
	rh600940n00.18	50475	63.1	7.4d	8.6	16.24	0.53	246.8	14.62	2.57e-13	8.81	0.27	
	PGC13826-ULX1	48300	19.0	1.9d	10.6	0.76	0.94	72.8	11.77	6.64e-13	1.21	0.91	
	PGC13826-ULX2	rh600022n00.5+	48300	19.0	1.9d	13.7	3.87	0.92	89.2	9.46	8.14e-13	1.49	1.3e-06
	PGC13826-ULX3	rh600022n00.8+	48300	19.0	1.9d	21.5	5.22	0.90	166.8	6.79	1.52e-12	2.77	0.63
NGC1549-X2	rh600022n00.10+	48300	19.0	1.9d	9.7	15.05	0.70	133.7	13.18	1.22e-12	2.23	0.83	
	rh600490n00.u	49365	3.5	1.1d	<3			<10.3		<1.97e-13	<9.16		
	rh600479n00.u+	49518	46.1	72.3d	<3			<49.4		<7.17e-14	<3.33		
	rh600490a01.16	49527	39.3	61.5d	4.3	8.92	1.02	38.0	26.40	6.47e-14	3.01		
	NGC1553-ULX1	rh600490n00.u	49365	3.5	1.1d	<3			<9.6		<1.84e-13	<7.59	
NGC1553-ULX2	rh600479n00.12+	49518	46.1	72.3d	5.1	0.84	0.98	43.5	24.89	6.31e-14	2.6	0.74	
	rh600490a01.u	49527	39.3	61.5d	<3			<20.1		<3.42e-14	<1.41		
	NGC1553-ULX2	rh600490n00.u	49365	3.5	1.1d	<3			<9.7		<1.86e-13	<7.67	
NGC1559-ULX1	rh600479n00.u+	49518	46.1	72.3d	<3			<21.2		<3.08e-14	<1.27		
	rh600490a01.6	49527	39.3	61.5d	3.0	6.54	0.99	19.8	25.47	3.37e-14	1.39		
	NGC1559-ULX1	rh600717n00.10+	49992	17.5	7.2d	5.8	1.03	0.97	38.6	22.14	1.68e-13	3.73	0.12
NGC1559-ULX2	rh600717n00.11+	49992	17.5	7.2d	5.8	0.61	0.98	30.7	22.31	1.34e-13	2.97		
	NGC1559-X3	rh600717n00.3+	49992	17.5	7.2d	6.0	1.30	0.97	30.0	21.38	1.30e-13	2.89	
	NGC1566-ULX1	rh700024n00.u	48631	9.3	21.3h	<3			<11.5		<8.13e-14	<1.75	
NGC1566-ULX2	rh701668n00.u	49988	2.1	0.7h	<3			<9.6		<3.00e-13	<6.46		
	rh600860n00.4	50320	15.0	17.6d	6.0	0.58	0.97	37.0	21.48	1.61e-13	3.47	0.5	
	rh600962n00.7+	50469	40.4	5.1d	12.6	0.62	0.93	141.7	10.14	2.30e-13	4.96	0.19	
	NGC1566-ULX3	rh700024n00.u	48631	9.3	21.3h	<3			<11.4		<8.10e-14	<1.75	
NGC1566-X5	rh701668n00.u	49988	2.1	0.7h	<3			<9.6		<2.99e-13	<6.44		
	rh600860n00.2	50320	15.0	17.6d	3.2	1.54	0.94	14.5	25.65	6.33e-14	1.36		
	rh600962n00.4+	50469	40.4	5.1d	9.6	1.45	0.95	103.2	13.26	1.67e-13	3.6	0.0083	
	NGC1566-X5	rh700024n00.u	48631	9.3	21.3h	<3			<11.2		<7.93e-14	<1.71	

Table 3—Continued

Name	Obs.Src <sup>a</sup>	Date <sup>b</sup> (MJD)	T <sup>c</sup> ksec	$\Delta D^d$	$\sigma^e$	$\theta^f$ ( $'$ )	$C(\theta, \sigma)^g$	CorCnt <sup>h</sup> (count)	pErr <sup>i</sup> (%)	Flux <sup>j</sup> (cgs)	$L_X^{k}$ ( $10^{39}$ erg/s)	$P_{KS}^{l}$
	rh701668n00.u	49988	2.1	0.7h	<3		<9.4		<2.93e-13		<6.31	
	rh600860n00.u	50320	15.0	17.6d	<3		<14.0		<6.11e-14		<1.32	
	rh600962n00.3+	50469	40.4	5.1d	4.5	4.14	0.97	33.5	26.40	5.43e-14	1.17	
NGC1672-ULX1	rh701022n00.5	48798	24.3	78.8d	4.8	1.18	0.97	29.2	26.06	8.82e-14	2.23	
	rh601011n00.5+	50476	34.6	33.6d	7.5	1.22	0.96	70.2	16.66	1.49e-13	3.76	0.98
NGC1672-ULX2	rh701022n00.3	48798	24.3	78.8d	7.0	1.30	0.96	44.8	18.02	1.36e-13	3.43	
	rh601011n00.2+	50476	34.6	33.6d	8.2	1.20	0.96	66.1	15.24	1.40e-13	3.53	0.85
NGC1672-X4	rh701022n00.1	48798	24.3	78.8d	3.8	5.12	0.98	20.4	26.42	6.18e-14	1.56	
	rh601011n00.u+	50476	34.6	33.6d	<3		<21.1		<4.47e-14		<1.13	
NGC1672-X5	rh701022n00.u	48798	24.3	78.8d	<3		<16.7		<5.07e-14		<1.28	
	rh601011n00.6+	50476	34.6	33.6d	4.7	5.80	1.00	37.3	26.39	7.91e-14	2	
NGC1792-ULX1	rh600433n00.u+	48878	25.9	15.6h	<3		<18.7		<5.46e-14		<0.668	
	rh600584n00.2	49607	7.8	3.8h	5.0	0.85	0.98	25.5	25.26	2.48e-13	3.04	
NGC1792-ULX2	rh600433n00.3+	48878	25.9	15.6h	6.4	0.18	0.97	42.8	19.95	1.25e-13	1.53	
	rh600584n00.u	49607	7.8	3.8h	<3		<12.4		<1.21e-13		<1.48	
NGC2273-X2	rh601000n00.4+	50531	34.2	7.9d	10.4	2.38	0.94	86.2	12.09	2.44e-13	23.6	0.18
	rh601000a01.u	50882	3.4	8.4h	<3		<8.8		<2.48e-13		<24	
NGC2273-X3	rh601000n00.2+	50531	34.2	7.9d	5.9	2.60	0.96	39.9	22.02	1.13e-13	10.9	
	rh601000a01.u	50882	3.4	8.4h	<3		<8.8		<2.48e-13		<24	
NGC2276-ULX1	rh600498n00.5+	49429	51.7	3.9d	7.9	0.46	0.96	83.8	15.83	1.46e-13	23.7	0.74
	rh600498a01.4	49593	21.5	1.3d	5.8	0.51	0.98	49.8	22.47	2.08e-13	33.8	0.86
NGC2276-X2	rh600498n00.6+	49429	51.7	3.9d	9.7	2.37	0.95	97.2	13.14	1.69e-13	27.5	0.17
	rh600498a01.3	49593	21.5	1.3d	3.9	2.37	0.95	27.2	26.41	1.14e-13	18.5	
NGC2403-ULX1	rh600767n00.4+	49978	26.2	4.1d	32.5	3.02	0.88	368.3	4.70	1.19e-12	1.4	0.36
NGC2403-X5	rh600767n00.6+	49978	26.2	4.1d	44.3	11.79	0.94	603.0	3.35	1.94e-12	2.29	0.055
NGC2442-X2	rh600953n00.3+	50770	40.4	23.6d	4.8	3.70	0.96	37.7	26.31	1.06e-13	3.72	
PGC23324-ULX1	rh600745n00.1+	49643	7.8	6.6d	123.5	0.31	0.87	1122.0	1.05	1.17e-11	28.4	0.0092
NGC2775-ULX1	rh500385n00.u	49832	10.8	22.9h	<3		<13.7		<1.07e-13		<3.71	
	rh600826n00.u	50046	3.1	2.3h	<3		<8.6		<2.36e-13		<8.18	
	rh600826a01.8+	50198	48.1	16.3d	3.7	1.91	0.94	30.0	26.38	5.27e-14	1.83	
NGC2775-X4	rh500385n00.1	49832	10.8	22.9h	2.8	3.85	0.93	13.2	25.18	1.03e-13		
	rh600826n00.u	50046	3.1	2.3h	<3		<8.6		<2.34e-13		<8.12	
	rh600826a01.4+	50198	48.1	16.3d	5.9	2.94	0.96	48.9	21.99	8.57e-14	2.97	
NGC2775-X5	rh500385n00.2	49832	10.8	22.9h	4.7	3.35	0.96	20.8	26.39	1.63e-13	5.65	
	rh600826n00.u	50046	3.1	2.3h	<3		<8.6		<2.34e-13		<8.12	
	rh600826a01.5+	50198	48.1	16.3d	7.9	3.51	0.96	74.1	15.78	1.30e-13	4.51	0.64
NGC2775-X6	rh500385n00.u	49832	10.8	22.9h	<3		<13.4		<1.05e-13		<3.64	
	rh600826n00.u	50046	3.1	2.3h	<3		<8.6		<2.34e-13		<8.12	
	rh600826a01.6+	50198	48.1	16.3d	4.9	3.63	0.97	39.8	25.78	6.98e-14	2.42	
NGC2782-ULX1	rh700462n00.3+	48731	21.5	1.5d	5.8	0.50	0.98	36.0	22.17	1.16e-13	19.4	
NGC2903-ULX1	rh600602n00.u+	49470	13.5	1.1d	<3		<13.8		<8.08e-14		<0.531	
	rh600602a01.2	49663	8.2	8.2h	4.7	2.12	0.96	23.8	26.39	2.29e-13	1.5	
NGC3031-ULX1	rh600247n00.u+	48919	26.3	3.7d	<3		<17.8		<5.73e-14		<0.0804	
	rh180015n00.u	49094	1.7	1.3h	<3		<7.6		<3.80e-13		<0.533	
	rh600247a01.12	49095	21.1	26.4d	44.2	3.08	0.88	463.5	3.36	1.86e-12	2.61	0.096
	rh600739n00.12	49644	19.9	2.1d	20.6	3.12	0.90	159.9	6.94	6.81e-13	0.956	0.64
	rh600740n00.7	49821	19.0	20.9d	18.7	3.09	0.90	172.1	7.40	7.68e-13	1.08	0.34
	rh600881n00.6	50003	14.8	12.8d	24.9	3.15	0.89	187.8	6.09	1.07e-12	1.5	0.31
	rh600882n00.6	50189	18.3	21.7d	25.9	3.09	0.89	220.0	6.01	1.02e-12	1.43	0.41
	rh600882a01.5	50384	5.1	13.2d	11.6	3.16	0.93	51.0	10.89	8.47e-13	1.19	
	rh601001n00.8	50537	19.2	2.5d	26.1	3.07	0.89	214.6	5.95	9.45e-13	1.33	0.72
	rh601002n00.7	50721	19.6	15.4d	24.5	3.15	0.89	202.6	6.18	8.77e-13	1.23	0.39
	rh601095n00.5	50898	12.4	17.7h	12.3	3.10	0.93	92.3	10.43	6.28e-13	0.881	0.69
NGC3031-ULX2	rh600247n00.7+	48919	26.3	3.7d	64.7	3.70	0.87	736.2	2.01	2.37e-12	3.33	0.42
	rh180015n00.u	49094	1.7	1.3h	<3		<7.6		<3.80e-13		<0.533	
	rh600247a01.10	49095	21.1	26.4d	58.4	3.65	0.87	562.4	2.30	2.26e-12	3.17	0.99
	rh600739n00.11	49644	19.9	2.1d	56.8	3.73	0.88	564.4	2.42	2.40e-12	3.37	0.56
	rh600740n00.5	49821	19.0	20.9d	48.1	3.67	0.88	508.8	2.95	2.27e-12	3.19	0.13
	rh600881n00.5	50003	14.8	12.8d	50.7	3.73	0.88	369.8	2.74	2.11e-12	2.96	0.51
	rh600882n00.5	50189	18.3	21.7d	48.1	3.65	0.88	430.1	2.95	1.99e-12	2.79	0.56
	rh600882a01.3	50384	5.1	13.2d	23.5	3.74	0.89	120.3	6.49	2.00e-12	2.81	0.033
	rh601001n00.7	50537	19.2	2.5d	55.9	3.63	0.88	511.4	2.44	2.25e-12	3.16	0.87
	rh601002n00.5	50721	19.6	15.4d	47.4	3.73	0.88	441.8	2.99	1.91e-12	2.68	0.026
	rh601095n00.4	50898	12.4	17.7h	24.9	3.66	0.89	203.7	6.09	1.39e-12	1.95	0.39
PGC28757-ULX1	rh600247n00.1+	48919	26.3	3.7d	81.6	12.59	0.93	1205.1	1.47	3.88e-12	5.45	0.035

Table 3—Continued

Name	Obs.Src <sup>a</sup>	Date <sup>b</sup> (MJD)	T <sup>c</sup> ksec	$\Delta D$ <sup>d</sup>	$\sigma$ <sup>e</sup>	$\theta$ <sup>f</sup> ( $'$ )	$C(\theta, \sigma)$ <sup>g</sup>	CorCnt <sup>h</sup> (count)	pErr <sup>i</sup> (%)	Flux <sup>j</sup> (cgs)	$L_X$ <sup>k</sup> ( $10^{39}$ erg/s)	$P_{KS}^{-1}$
	rh180015n00.u	49094	1.7	1.3h	<3			<12.3		<6.16e-13	<0.865	
	rh600247a01.1	49095	21.1	26.4d	97.4	12.55	0.93	1416.9	1.31	5.70e-12	8	0.00026
	rh600739n00.1	49644	19.9	2.1d	59.7	12.63	0.94	716.1	2.25	3.05e-12	4.28	0.37
	rh600740n00.1	49821	19.0	20.9d	80.1	12.56	0.93	1129.9	1.43	5.04e-12	7.07	0.13
	rh600881n00.1	50003	14.8	12.8d	69.1	12.59	0.93	717.1	1.77	4.10e-12	5.75	0.89
	rh600882n00.1	50189	18.3	21.7d	82.1	12.54	0.93	1172.0	1.46	5.42e-12	7.61	0.48
	rh600882a01.1	50384	5.1	13.2d	64.7	12.61	0.93	562.9	2.01	9.37e-12	13.2	0.68
	rh601001n00.1	50537	19.2	2.5d	131.8	12.57	0.93	2170.9	1.11	9.56e-12	13.4	0.41
	rh601002n00.1	50721	19.6	15.4d	60.8	12.57	0.94	789.5	2.21	3.42e-12	4.8	0.71
	rh601095n00.1	50898	12.4	17.7h	48.1	12.55	0.94	568.7	2.95	3.87e-12	5.43	0.065
NGC3226-X3	rh701299n00.5+	49478	30.0	5.6d	5.1	4.89	0.98	34.0	25.01	8.21e-14	5.46	
	rh701870n00.u	49869	7.5	1.7d	<3			<11.0		<1.07e-13	<7.12	
NGC3294-X1	rh500389n00.5+	49860	11.2	16.3h	3.5	1.39	0.95	18.0	26.15	1.10e-13	9.41	
PGC31586-X2	rh800741n00.4+	49866	32.4	15.7d	26.9	1.47	0.89	279.7	5.71	7.70e-13		0.0012
NGC3310-ULX1	rh600685n00.u	49680	4.1	6.6h	<3			<8.4		<1.31e-13	<5.5	
	rh600685a01.7+	49826	41.5	27.9d	10.2	0.75	0.95	84.4	12.49	1.29e-13	5.41	0.94
NGC3310-ULX2	rh600685m00.u	49680	4.1	6.6h	<3			<8.4		<1.31e-13	<5.5	
	rh600685a01.9+	49826	41.5	27.9d	8.9	1.18	0.95	94.2	14.04	1.44e-13	6.04	0.4
NGC3396-X2	rh600771n00.6+	49859	24.7	22.2h	10.2	1.67	0.94	96.2	12.37	2.78e-13	15.9	0.12
NGC3623-ULX1	rh600827n00.u	50249	4.3	1.1d	<3			<9.5		<1.60e-13	<2.9	
	rh600827a01.7+	50426	36.6	6.4d	6.3	0.85	0.97	48.7	20.41	9.66e-14	1.75	
NGC3623-X3	rh600827n00.u	50249	4.3	1.1d	<3			<9.4		<1.59e-13	<2.89	
	rh600827a01.9+	50426	36.6	6.4d	4.5	1.96	0.95	29.8	26.40	5.92e-14	1.07	
NGC3627-ULX1	rh600836a01.4+	50423	9.4	1.5d	6.3	1.80	0.96	28.1	20.36	2.24e-13	2.06	
NGC3627-X3	rh600836a01.3+	50423	9.4	1.5d	6.9	6.95	0.99	34.9	18.23	2.78e-13	2.55	
NGC3628-ULX1	rh700009n00.3+	48598	13.5	2.2d	7.9	4.99	0.97	39.8	15.87	2.15e-13	2.9	
	rh700009a01.1	49495	5.3	1.3d	3.3	5.19	0.97	12.7	25.85	1.77e-13	2.39	
NGC3628-X3	rh700009n00.2+	48598	13.5	2.2d	3.9	5.68	0.99	16.7	26.41	9.05e-14	1.22	
	rh700009a01.u	49495	5.3	1.3d	<3			<10.7		<1.48e-13	<2	
NGC3642-X2	rh701003n00.1+	48918	9.9	2.9d	3.6	3.51	0.95	14.4	26.21	8.71e-14	7.9	
NGC3998-X2	rh600430n00.3+	49121	13.5	29.2d	4.3	1.18	0.97	25.2	26.40	1.20e-13	2.88	
NGC4088-ULX1	rh500391n00.1+	49700	9.9	10.0h	4.9	0.43	0.98	23.5	25.91	1.69e-13	5.86	
NGC4105-X2	rh600975n00.6+	50618	81.1	8.1d	6.9	2.41	0.96	68.5	18.30	7.49e-14	6.34	0.7
NGC4136-ULX1	rh702734n00.1+	50259	2.0	0.8h	3.5	1.25	0.96	10.1	26.09	3.51e-13	3.96	
NGC4151-ULX1	rh700023n00.u	49124	9.2	7.1h	<3			<12.3		<9.59e-14	<4.74	
	rh701707n00.20+	49856	107.2	13.8d	4.8	2.53	0.96	56.0	26.26	3.72e-14	1.84	0.061
	rh701692n00.u	49870	1.5	0.7h	<3			<7.6		<3.62e-13	<17.9	
	rh701989n00.16	50254	102.4	3.9d	3.4	2.52	0.94	42.1	25.98	2.93e-14	1.45	0.23
NGC4151-ULX2	rh700023n00.u	49124	9.2	7.1h	<3			<12.3		<9.55e-14	<4.72	
	rh701707n00.9+	49856	107.2	13.8d	4.8	3.05	0.96	55.1	26.15	3.66e-14	1.81	0.65
	rh701692n00.u	49870	1.5	0.7h	<3			<7.6		<3.60e-13	<17.8	
NGC4151-ULX3	rh700023n00.u	49124	9.2	7.1h	<3			<12.3		<9.52e-14	<4.71	
	rh701707n00.21+	49856	107.2	13.8d	4.4	3.52	0.96	49.4	26.40	3.28e-14	1.62	
	rh701692n00.u	49870	1.5	0.7h	<3			<7.6		<3.60e-13	<17.8	
	rh701989n00.u	50254	102.4	3.9d	5.4	3.03	0.96	62.1	24.00	4.31e-14	2.13	0.92
NGC4151-ULX4	rh700023n00.4	49124	9.2	7.1h	5.4	4.42	0.98	25.6	24.01	1.99e-13	9.84	
	rh701707n00.u+	49856	107.2	13.8d	<3			<32.7		<2.17e-14	<1.07	
	rh701692n00.u	49870	1.5	0.7h	<3			<7.5		<3.60e-13	<17.8	
	rh701989n00.18	50254	102.4	3.9d	5.9	4.42	0.98	73.6	21.96	5.11e-14	2.53	0.43
NGC4151-X6	rh700023n00.u	49124	9.2	7.1h	<3			<12.3		<9.55e-14	<4.72	
	rh701707n00.27+	49856	107.2	13.8d	9.0	5.18	0.96	117.5	13.93	7.80e-14	3.86	0.024
	rh701692n00.u	49870	1.5	0.7h	<3			<7.6		<3.60e-13	<17.8	
	rh701989n00.22	50254	102.4	3.9d	4.0	5.05	0.98	53.9	26.41	3.75e-14	1.85	0.18
NGC4190-ULX1	rh600733n00.2	49860	3.4	8.8d	22.0	0.48	0.90	93.1	6.71	1.83e-12	1.72	0.65
	rh600968n00.2+	50773	10.7	3.8d	52.1	0.45	0.88	389.3	2.76	2.46e-12	2.31	0.049
NGC4203-X2	rh600221n00.4+	49150	25.2	2.2d	98.7	2.26	0.87	1128.4	1.28	2.86e-12	78.7	0.3
NGC4203-X3	rh600221n00.3+	49150	25.2	2.2d	4.9	2.89	0.96	32.9	25.91	8.35e-14	2.3	
NGC4242-X1	rh600943n00.1+	50767	2.4	14.5h	5.7	2.76	0.96	17.0	22.64	4.49e-13	3.03	
NGC4242-X2	rh600943n00.3+	50767	2.4	14.5h	5.3	2.90	0.96	17.7	24.07	4.68e-13	3.16	
NGC4242-X3	rh600943n00.2+	50767	2.4	14.5h	3.7	3.09	0.95	12.0	26.38	3.19e-13	2.15	
NGC4254-ULX1	rh600972n00.7+	50629	20.8	6.2d	4.6	0.50	0.98	37.7	26.39	1.39e-13	4.71	0.31
NGC4254-ULX2	rh600972n00.1+	50629	20.8	6.2d	15.6	1.66	0.92	122.6	8.55	4.52e-13	15.3	0.36
NGC4254-X3	rh600972n00.3+	50629	20.8	6.2d	3.9	4.19	0.96	22.3	26.42	8.22e-14	2.78	
NGC4258-ULX1	rh701008n00.u+	49122	27.3	1.6d	<3			<18.1		<4.21e-14	<0.302	

Table 3—Continued

Name	Obs.Src <sup>a</sup>	Date <sup>b</sup> (MJD)	T <sup>c</sup> ksec	$\Delta D^d$	$\sigma^e$	$\theta^f$ ( $'$ )	$C(\theta, \sigma)^g$	CorCnt <sup>h</sup> (count)	pErr <sup>i</sup> (%)	Flux <sup>j</sup> (cgs)	$L_X^{k}$ ( $10^{39}$ erg/s)	$P_{KS}^{l}$
NGC4258-ULX2	rh600599n00.u	49492	2.4	11.0h	<3			<9.0		<2.38e-13	<1.71	
	rh600598n00.u	49519	1.7	3.7h	<3			<7.7		<2.81e-13	<2.01	
	rh600599a01.16	49680	25.3	19.4d	7.7	8.62	1.00	89.9	16.28	2.27e-13	1.63	0.0013
	rh701008n00.u+	49122	27.3	1.6d	<3			<18.1		<4.21e-14	<0.302	
NGC4258-X9	rh600599n00.2	49492	2.4	11.0h	2.7	7.74	0.99	8.4	25.02	2.22e-13	1.59	
	rh600598n00.u	49519	1.7	3.7h	<3			<7.8		<2.85e-13	<2.04	
	rh600599a01.6	49680	25.3	19.4d	3.7	7.69	1.01	26.4	26.33	6.68e-14	0.479	
	rh701008n00.1+	49122	27.3	1.6d	14.6	9.53	0.96	142.7	8.99	3.32e-13	2.38	0.48
NGC4319-X1	rh600599n00.u	49492	2.4	11.0h	<3			<23.8		<6.28e-13	<4.5	
	rh600598n00.u	49519	1.7	3.7h	<3			<7.7		<2.82e-13	<2.02	
	rh600599a01.15	49680	25.3	19.4d	5.8	15.98	0.48	77.9	22.46	1.97e-13	1.41	0.84
	rh600441n00.4	48917	12.3	3.5d	297.4	0.59	0.87	3671.1	0.46	2.32e-11	2.21e+03	0.06
NGC4319-X2	rh600834n00.4+	50039	35.0	10.7d	385.9	6.68	0.88	9373.4	0.44	2.09e-11	1.99e+03	2.5e-08
	rh600441n00.2	48917	12.3	3.5d	3.9	1.64	0.95	21.9	26.42	1.39e-13	13.3	
	rh600834n00.2+	50039	35.0	10.7d	4.2	7.66	1.01	36.2	26.41	8.09e-14	7.72	0.42
	rh600854n00.6	50267	15.9	6.0d	6.8	13.41	0.82	54.6	18.38	2.35e-13	25.5	
NGC4292-X1	rh600854a01.9+	50608	27.3	14.2d	6.1	13.36	0.81	58.6	20.93	1.47e-13	16	
	rh600854a02.0	50819	5.6	13.2h	<3			<17.0		<2.10e-13	<22.8	
	rh600854n00.2	50267	15.9	6.0d	3.6	0.76	0.98	20.5	26.18	8.86e-14	2.46	
	rh600854a01.u+	50608	27.3	14.2d	<3			<18.6		<4.68e-14	<1.3	
NGC4303-X4	rh600854a02.u	50819	5.6	13.2h	<3			<9.8		<1.22e-13	<3.38	
	rh600854n00.u	50267	15.9	6.0d	<3			<14.4		<6.22e-14	<1.72	
	rh600854a01.6+	50608	27.3	14.2d	3.5	4.54	0.96	22.9	26.12	5.76e-14	1.6	
	rh600854a02.u	50819	5.6	13.2h	<3			<9.6		<1.19e-13	<3.3	
NGC4303-X5	rh600854n00.u	50267	15.9	6.0d	<3			<14.7		<6.33e-14	<1.75	
	rh600854a01.u+	50608	27.3	14.2d	<3			<18.5		<4.64e-14	<1.29	
	rh600854a02.2	50819	5.6	13.2h	4.2	6.32	1.00	14.2	26.41	1.75e-13	4.85	
	rh600731n00.3+	49873	42.4	23.2d	4.7	1.55	0.96	37.4	26.39	6.55e-14	1.57	
NGC4321-ULX1	rh500422n00.u	49899	8.9	5.6h	<3			<12.4		<1.03e-13	<2.47	
	rh500542n00.u	50801	24.8	16.4d	<3			<18.1		<5.42e-14	<1.3	
	rh600731n00.9+	49873	42.4	23.2d	4.0	3.25	0.95	34.3	26.41	6.00e-14	1.44	
	rh500422n00.u	49899	8.9	5.6h	<3			<12.1		<1.01e-13	<2.42	
NGC4321-ULX2	rh500542n00.u	50801	24.8	16.4d	<3			<17.8		<5.32e-14	<1.27	
	rh600731n00.u+	49873	42.4	23.2d	<3			<22.2		<3.88e-14	<0.93	
	rh500422n00.u	49899	8.9	5.6h	<3			<12.1		<1.01e-13	<2.42	
	rh500542n00.3	50801	24.8	16.4d	3.2	3.90	0.94	22.2	25.71	6.67e-14	1.6	
NGC4321-X6	rh600731n00.6+	49873	42.4	23.2d	6.2	5.95	0.99	43.5	20.82	7.62e-14	1.83	
	rh500422n00.u	49899	8.9	5.6h	<3			<12.2		<1.01e-13	<2.42	
	rh500542n00.7	50801	24.8	16.4d	4.5	5.95	1.00	31.1	26.40	9.32e-14	2.23	
	rh600731n00.5+	49873	42.4	23.2d	4.3	6.30	1.00	30.6	26.40	5.37e-14	1.29	
NGC4321-X7	rh500422n00.u	49899	8.9	5.6h	<3			<12.2		<1.01e-13	<2.42	
	rh500542n00.u	50801	24.8	16.4d	<3			<18.1		<5.42e-14	<1.3	
	rh600731n00.u+	49873	42.4	23.2d	<3			<22.2		<3.88e-14	<0.93	
	rh500422n00.u	49899	8.9	5.6h	<3			<12.1		<1.01e-13	<2.42	
NGC4374-X2	rh600463n00.u	48801	1.5	0.4h	<3			<17.7		<8.67e-13	<35.1	
	rh600463a02.u	49516	10.4	16.3d	<3			<40.7		<2.96e-13	<12	
	rh600493n00.5+	49699	26.2	7.3d	16.7	2.31	0.91	165.6	8.15	4.78e-13	19.4	
	rh600463a03.2	49882	8.4	8.2h	4.3	15.49	0.48	43.5	26.40	3.95e-13	16	
NGC4374-X3	rh600463n00.u	48801	1.5	0.4h	<3			<13.2		<6.45e-13	<26.1	
	rh600463a02.u	49516	10.4	16.3d	<3			<28.7		<2.09e-13	<8.46	
	rh600493n00.4+	49699	26.2	7.3d	8.8	3.70	0.96	62.8	14.22	1.81e-13	7.33	
	rh600463a03.u	49882	8.4	8.2h	<3			<26.3		<2.38e-13	<9.64	
NGC4374-X4	rh700192n00.4	48598	11.2	1.9d	6.2	15.13	0.60	60.0	20.53	4.06e-13	16.4	
	rh600463n00.u	48801	1.5	0.4h	<3			<17.7		<8.67e-13	<35.1	
	rh600463a02.u	49516	10.4	16.3d	<3			<40.7		<2.96e-13	<11.6	
	rh600493n00.2+	49699	26.2	7.3d	3.9	5.50	0.99	24.4	26.41	7.06e-14	2.86	
	rh600463a03.u	49882	8.4	8.2h	<3			<35.9		<3.25e-13	<13.2	
NGC4374-X5	rh600493n00.9+	49699	26.2	7.3d	4.6	5.93	1.00	29.9	26.39	8.63e-14	3.49	
	rh702725n00.2+	50258	11.3	7.2h	32.1	2.49	0.88	189.0	4.80	1.11e-12	1.73	0.55
NGC4438-X2	rh600608n00.2+	49703	21.5	3.8d	16.6	2.92	0.91	136.3	8.18	4.84e-13	16.4	0.81
	rh701657n00.1	49907	5.8	2.4h	5.6	3.48	0.97	24.7	22.99	3.24e-13	11	
NGC4472-X2	rh600216n00.u	48967	7.0	3.5d	<3			<10.6		<1.04e-13	<3.31	
	rh600216a01.1+	49522	27.1	19.8d	4.5	5.57	0.99	36.2	26.40	9.13e-14	2.91	
NGC4472-X3	rh600216n00.2	48967	7.0	3.5d	9.3	6.70	0.97	41.8	13.63	4.08e-13	13	
	rh600216a01.4+	49522	27.1	19.8d	18.0	6.63	0.92	161.2	7.65	4.07e-13	13	0.85
NGC4472-X4	rh600216n00.u	48967	7.0	3.5d	<3			<11.1		<1.08e-13	<3.44	

Table 3—Continued

Name	Obs.Src <sup>a</sup>	Date <sup>b</sup> (MJD)	T <sup>c</sup> ksec	$\Delta D$ <sup>d</sup>	$\sigma$ <sup>e</sup>	$\theta$ <sup>f</sup> ( $'$ )	$C(\theta, \sigma)$ <sup>g</sup>	CorCnt <sup>h</sup> (count)	pErr <sup>i</sup> (%)	Flux <sup>j</sup> (cgs)	$L_X$ <sup>k</sup> ( $10^{39}$ erg/s)	$P_{KS}^{-1}$
NGC4472-X5	rh600216a01.6+	49522	27.1	19.8d	7.4	8.01	1.00	60.9	16.91	1.54e-13	4.9	0.99 0.056
	rh600216n00.4	48967	7.0	3.5d	8.6	8.13	0.99	42.7	14.56	4.18e-13	13.3	
	rh600216a01.7+	49522	27.1	19.8d	15.4	8.08	0.94	133.1	8.61	3.36e-13	10.7	
NGC4472-X6	rh600216n00.3	48967	7.0	3.5d	4.0	9.98	1.01	15.7	26.41	1.54e-13	4.9	0.99 0.056
	rh600216a01.5+	49522	27.1	19.8d	4.9	9.99	1.01	36.3	25.82	9.16e-14	2.92	
NGC4476-X1	rh700214n00.u	48780	14.0	13.1h	<3			<40.0		<2.15e-13	<7.65	0.99 0.056
	rh701712n00.u+	49877	44.3	1.9d	<3			<62.3		<1.06e-13	<3.77	
	rh701713n00.u	50064	40.4	6.8d	<3			<62.8		<1.17e-13	<4.16	
	rh702081n00.u	50267	34.2	5.8d	<3			<62.3		<1.37e-13	<4.87	
	rh702774n00.u	50438	38.2	3.2d	<3			<63.0		<1.24e-13	<4.41	
	rh702775n00.6	50606	30.8	3.2d	4.6	12.97	0.80	49.6	26.39	1.21e-13	4.31	
	rh704000n00.u	50796	8.0	24.1h	<3			<30.5		<2.87e-13	<10.2	
	rh704000a01.u	50818	20.6	1.2d	<3			<46.4		<1.70e-13	<6.05	
NGC4486-X2	rh700214n00.u	48780	14.0	13.1h	<3			<21.7		<1.17e-13	<3.63	0.99 0.056
	rh701712n00.u+	49877	44.3	1.9d	<3			<32.8		<5.58e-14	<1.73	
	rh701713n00.13	50064	40.4	6.8d	3.1	5.89	0.98	45.8	25.63	8.53e-14	2.64	
	rh702081n00.u	50267	34.2	5.8d	<3			<32.8		<7.22e-14	<2.24	
	rh702774n00.u	50438	38.2	3.2d	<3			<33.2		<6.54e-14	<2.03	
	rh702775n00.u	50606	30.8	3.2d	<3			<30.2		<7.37e-14	<2.28	
	rh704000n00.u	50796	8.0	24.1h	<3			<17.0		<1.60e-13	<4.96	
	rh704000a01.8	50818	20.6	1.2d	2.9	5.71	0.98	27.7	25.30	1.01e-13	3.13	
NGC4485-ULX1	rh600697n00.3	49857	6.6	23.4h	6.5	2.70	0.96	35.3	19.51	3.73e-13	3.87	0.99 0.056
	rh600855n00.7+	50253	26.7	1.7d	9.2	2.75	0.95	85.5	13.77	2.23e-13	2.31	
	rh600855a01.7	50414	24.6	1.2d	7.2	2.67	0.96	49.9	17.43	1.41e-13	1.46	
NGC4490-ULX1	rh600697n00.u	49857	6.6	23.4h	<3			<11.6		<1.22e-13	<0.891	0.99 0.056
	rh600855n00.5+	50253	26.7	1.7d	7.6	0.48	0.96	72.7	16.46	1.89e-13	1.38	
	rh600855a01.5	50414	24.6	1.2d	9.3	0.31	0.95	67.4	13.63	1.91e-13	1.39	
NGC4490-ULX2	rh600697n00.2	49857	6.6	23.4h	4.0	2.56	0.95	20.4	26.41	2.15e-13	1.57	0.99 0.056
	rh600855n00.3+	50253	26.7	1.7d	6.3	2.31	0.96	57.6	20.46	1.50e-13	1.1	
	rh600855a01.3	50414	24.6	1.2d	7.6	2.40	0.96	54.3	16.55	1.54e-13	1.12	
NGC4490-ULX3	rh600697n00.u	49857	6.6	23.4h	<3			<11.6		<1.22e-13	<0.891	0.99 0.056
	rh600855n00.6+	50253	26.7	1.7d	7.2	0.29	0.97	69.4	17.54	1.81e-13	1.32	
	rh600855a01.6	50414	24.6	1.2d	6.6	0.12	0.97	42.2	19.09	1.19e-13	0.869	
NGC4501-ULX1	rh601003n00.3	50638	4.3	2.3h	5.9	5.76	0.99	24.9	21.84	4.33e-13	14.7	0.99 0.056
	rh601003a01.5+	50815	6.0	4.7d	4.5	5.83	1.00	19.2	26.40	2.40e-13	8.13	
NGC4523-X1	rh800879n00.12+	50620	44.9	17.8d	5.2	14.02	0.71	87.5	24.53	1.43e-13	0.99 0.056	
	rh800879a01.u	50800	21.3	15.4d	<3			<43.2		<1.50e-13	<5.08	
PGC41763-X1	rh800879n00.3+	50620	44.9	17.8d	8.4	4.01	0.96	100.8	14.86	1.65e-13	19.2	0.99 0.056
	rh800879a01.3	50800	21.3	15.4d	5.0	4.15	0.97	45.1	25.45	1.56e-13	18.1	
NGC4536-X2	rh601117n00.1+	50825	3.8	2.2h	7.2	2.54	0.96	23.2	17.52	4.28e-13	10.5	0.99 0.056
	rh600491n00.3	49543	18.0	1.5d	3.9	3.71	0.95	22.4	26.42	9.43e-14	2.67	
NGC4559-ULX1	rh600861n00.8+	50245	53.3	18.9d	43.3	0.25	0.88	624.0	3.42	7.83e-13	3.16	0.99 0.056
	rh600861n00.12+	50245	53.3	18.9d	66.9	2.03	0.87	992.8	1.81	1.25e-12	5.05	
NGC4565-ULX1	rh600691n00.3+	49903	5.3	1.5d	12.6	1.06	0.93	55.8	10.20	6.90e-13	25.2	0.99 0.056
	rh600691n00.1+	49903	5.3	1.5d	3.5	2.19	0.94	11.8	26.13	1.46e-13	5.34	
NGC4569-X2	rh600603n00.u	49544	2.1	0.8h	<3			<8.3		<2.97e-13	<10.1	0.99 0.056
	rh600603a01.3+	49887	21.7	2.9d	9.6	7.66	0.98	54.2	13.28	1.88e-13	6.37	
NGC4594-ULX1	rh600044n00.u	48633	1.7	0.5h	<3			<7.2		<3.61e-13	<4.14	0.99 0.056
	rh600044a01.u	49352	3.6	8.0d	<3			<9.8		<2.22e-13	<2.54	
	rh600044a02.3+	49542	15.7	7.8d	10.8	0.40	0.94	96.4	11.53	5.09e-13	5.83	
NGC4594-ULX2	rh600044n00.u	48633	1.7	0.5h	<3			<7.2		<3.57e-13	<4.09	0.99 0.056
	rh600044a01.u	49352	3.6	8.0d	<3			<9.6		<2.18e-13	<2.5	
	rh600044a02.5+	49542	15.7	7.8d	3.6	2.82	0.94	20.6	26.22	1.09e-13	1.25	
NGC4594-X4	rh600044n00.u	48633	1.7	0.5h	<3			<7.1		<3.56e-13	<4.08	0.99 0.056
	rh600044a01.u	49352	3.6	8.0d	<3			<9.5		<2.17e-13	<2.49	
	rh600044a02.6+	49542	15.7	7.8d	14.2	4.00	0.92	96.7	9.20	5.10e-13	5.84	
NGC4594-X5	rh600044n00.u	48633	1.7	0.5h	<3			<7.2		<3.59e-13	<4.11	0.99 0.056
	rh600044a01.u	49352	3.6	8.0d	<3			<9.7		<2.19e-13	<2.51	
	rh600044a02.1+	49542	15.7	7.8d	3.7	5.93	0.99	17.2	26.40	9.08e-14	1.04	
NGC4631-ULX1	rh600193a00.1	48597	7.0	3.1d	5.4	2.43	0.96	24.1	23.70	2.23e-13	1.27	0.99 0.056
	rh600193a01.4	48779	14.2	3.0d	10.0	2.52	0.95	57.6	12.75	2.63e-13	1.5	
	rh600193a02.3	48969	11.9	1.1d	13.2	2.43	0.93	78.1	9.76	4.24e-13	2.42	
	rh600934n00.4+	50626	23.9	6.9d	13.2	2.48	0.93	109.2	9.82	2.96e-13	1.69	
NGC4649-X2	rh600480n00.2	49545	2.2	0.8h	2.5	3.13	0.92	7.4	24.74	2.45e-13	8.33	

Table 3—Continued

Name	Obs.Src <sup>a</sup>	Date <sup>b</sup> (MJD)	T <sup>c</sup> ksec	$\Delta D^d$	$\sigma^e$	$\theta^f$ ( $'$ )	$C(\theta, \sigma)^g$	CorCnt <sup>h</sup> (count)	pErr <sup>i</sup> (%)	Flux <sup>j</sup> (cgs)	$L_X^{k}$ ( $10^{39}$ erg/s)	$P_{KS}^{l}$
NGC4649-X3	rh600620n00.3	49546	4.8	2.3h	5.0	3.04	0.96	19.8	25.33	3.02e-13	10.3	0.56
	rh600480a01.4	49886	11.8	17.7h	6.9	3.10	0.96	41.1	18.14	2.54e-13	8.63	
	rh600620a01.4+	49889	19.7	4.2d	7.3	3.06	0.96	52.6	17.24	1.94e-13	6.59	
NGC4656-ULX1	rh600480n00.u	49545	2.2	0.8h	<3			<8.1		<2.70e-13	<9.18	0.47
	rh600620n00.1	49546	4.8	2.3h	3.8	6.96	1.00	13.4	26.42	2.05e-13	6.97	
	rh600480a01.1	49886	11.8	17.7h	7.1	6.96	0.99	30.5	17.66	1.88e-13	6.39	
	rh600620a01.1+	49889	19.7	4.2d	13.1	6.96	0.94	96.0	9.84	3.55e-13	12.1	
NGC4697-ULX1	rh600605n00.3+	49502	27.4	1.0d	10.5	9.72	0.99	95.4	11.93	2.24e-13	1.39	0.71
	rh600825n00.1	50284	3.7	5.4h	3.1	2.86	0.93	10.2	25.60	2.01e-13	3.33	
NGC4697-X7	rh600825a01.u+	50619	77.9	30.0d	<3			<29.4		<2.72e-14	<0.451	0.061
	rh600825m00.u	50284	3.7	5.4h	<3			<9.2		<1.81e-13	<3	
NGC4861-ULX1	rh600273n00.3+	48799	11.2	2.4d	7.1	0.39	0.97	33.7	17.69	1.94e-13	7.38	0.9
	rh600273a01.4	48967	10.1	2.2d	25.1	0.43	0.89	130.0	6.09	8.26e-13	31.4	
NGC4861-ULX2	rh600273n00.4+	48799	11.2	2.4d	7.2	1.05	0.97	38.6	17.35	2.21e-13	8.4	0.9
	rh600273a01.5	48967	10.1	2.2d	6.8	0.97	0.97	33.1	18.33	2.10e-13	7.98	
NGC5055-ULX1	rh600742n00.4+	49691	12.2	7.4h	7.5	0.68	0.96	42.2	16.63	2.26e-13	1.96	0.61
	rh601110n00.2	50813	11.0	1.6d	5.5	0.67	0.98	30.8	23.65	1.83e-13	1.59	
NGC5055-ULX2	rh600742n00.5+	49691	12.2	7.4h	4.9	1.79	0.96	25.5	25.91	1.36e-13	1.18	0.777
	rh601110n00.10	50813	11.0	1.6d	3.2	1.77	0.94	15.0	25.72	8.96e-14	0.777	
NGC5055-ULX3	rh600742n00.3+	49691	12.2	7.4h	4.5	1.58	0.96	22.7	26.40	1.21e-13	1.05	0.668
	rh601110n00.u	50813	11.0	1.6d	<3			<12.9		<7.70e-14	<0.668	
NGC5055-X6	rh600742n00.6+	49691	12.2	7.4h	5.5	3.98	0.97	25.6	23.28	1.36e-13	1.18	0.59
	rh601110n00.3	50813	11.0	1.6d	5.9	3.93	0.97	27.8	21.81	1.66e-13	1.44	
NGC5055-ULX4	rh600742n00.7+	49691	12.2	7.4h	28.2	5.86	0.90	201.3	5.45	1.08e-12	9.36	0.49
	rh601110n00.4	50813	11.0	1.6d	16.8	5.84	0.92	94.7	8.14	5.64e-13	4.89	
NGC5055-X9	rh600742n00.9+	49691	12.2	7.4h	4.2	7.80	1.01	22.0	26.41	1.18e-13	1.02	0.687
	rh601110n00.u	50813	11.0	1.6d	<3			<13.3		<7.92e-14	<0.687	
NGC5055-X10	rh600742n00.u+	49691	12.2	7.4h	<3			<16.3		<8.71e-14	<0.755	0.35
	rh601110n00.7	50813	11.0	1.6d	4.8	10.35	1.01	23.1	26.01	1.37e-13	1.19	
NGC5128-ULX1	rh150004n00.u	48099	19.5	19.8h	<3			<15.1		<7.93e-14	<0.169	0.47
	rh701571n00.u+	49571	64.1	3.4d	<3			<27.0		<4.31e-14	<0.0917	
	rh701924n00.6	49911	4.9	3.9h	32.0	2.62	0.88	197.8	4.82	4.13e-12	8.78	
	rh701925n00.7	49912	5.3	3.9h	39.0	2.60	0.88	227.0	3.88	4.36e-12	9.27	
	rh701926n00.6	49916	5.7	3.8h	36.6	2.57	0.88	216.1	4.27	3.87e-12	8.23	
	rh701927n00.5	49920	4.1	2.2h	23.9	2.61	0.89	115.6	6.40	2.89e-12	6.15	
	rh701928n00.3	49921	4.1	2.2h	29.2	2.59	0.89	157.6	5.31	3.97e-12	8.44	
	rh704206n00.u	50850	17.2	1.6d	<3			<16.7		<9.93e-14	<0.211	
NGC5128-X13	rh150004n00.11	48099	19.5	19.8h	17.2	4.85	0.91	126.6	7.96	6.64e-13	1.41	0.0004
	rh701571n00.26+	49571	64.1	3.4d	45.6	4.90	0.88	683.4	3.23	1.09e-12	2.32	
	rh701924n00.7	49911	4.9	3.9h	13.6	4.84	0.93	60.2	9.55	1.26e-12	2.68	
	rh701925n00.8	49912	5.3	3.9h	12.0	4.85	0.94	54.4	10.64	1.04e-12	2.21	
	rh701926n00.7	49916	5.7	3.8h	7.7	4.85	0.97	34.4	16.34	6.16e-13	1.31	
	rh701927n00.6	49920	4.1	2.2h	3.4	4.89	0.96	13.4	25.95	3.36e-13	0.715	
	rh701928n00.4	49921	4.1	2.2h	7.5	4.83	0.97	32.5	16.66	8.19e-13	1.74	
	rh704206n00.9	50850	17.2	1.6d	14.9	4.91	0.92	108.2	8.81	6.43e-13	1.37	
NGC5128-X33	rh150004n00.16	48099	19.5	19.8h	3.2	15.58	0.41	35.9	25.68	1.88e-13	0.4	0.068
	rh701571n00.3+	49571	64.1	3.4d	6.4	15.62	0.54	145.9	19.92	2.33e-13	0.496	
	rh701924n00.u	49911	4.9	3.9h	<3			<28.7		<6.00e-13	<1.28	
	rh701925n00.u	49912	5.3	3.9h	<3			<29.5		<5.67e-13	<1.21	
	rh701926n00.u	49916	5.7	3.8h	<3			<29.9		<5.35e-13	<1.14	
	rh701927n00.u	49920	4.1	2.2h	<3			<26.6		<6.64e-13	<1.41	
	rh701928n00.u	49921	4.1	2.2h	<3			<25.9		<6.52e-13	<1.39	
	rh704206n00.14	50850	17.2	1.6d	6.5	15.51	0.55	79.6	19.58	4.73e-13	1.01	
NGC5128-X37	rh701927n00.8	49920	4.1	2.2h	3.4	19.14	0.26	36.9	26.02	9.20e-13	1.96	
NGC5128-X38	rh701924n00.9	49911	4.9	3.9h	3.7	19.69	0.27	44.4	26.42	9.25e-13	1.97	
NGC5194-ULX1	rh600062a00.u	48597	8.5	33.3d	<3			<11.4		<9.08e-14	<0.646	
	rh600062a01.6	48765	8.7	13.7d	5.8	1.63	0.96	28.8	22.33	2.22e-13	1.58	
	rh600062a03.u	49494	9.3	1.1d	<3			<12.7		<9.24e-14	<0.657	
	rh600601n00.13+	49521	36.0	5.8d	4.9	1.62	0.96	37.7	25.99	7.08e-14	0.504	
	rh601115n00.5	50809	8.0	3.3d	5.8	1.70	0.96	27.5	22.13	2.32e-13	1.65	
NGC5194-ULX2	rh600062a00.u	48597	8.5	33.3d	<3			<11.3		<9.01e-14	<0.641	
	rh600062a01.5	48765	8.7	13.7d	4.7	2.45	0.96	20.4	26.39	1.58e-13	1.12	
	rh600062a03.u	49494	9.3	1.1d	<3			<12.6		<9.16e-14	<0.652	
	rh600601n00.u+	49521	36.0	5.8d	<3			<19.9		<3.74e-14	<0.266	

Table 3—Continued

Name	Obs.Src <sup>a</sup>	Date <sup>b</sup> (MJD)	T <sup>c</sup> ksec	$\Delta D^d$	$\sigma^e$	$\theta^f$ ( $'$ )	$C(\theta, \sigma)^g$	CorCnt <sup>h</sup> (count)	pErr <sup>i</sup> (%)	Flux <sup>j</sup> (cgs)	$L_X^{k}$ ( $10^{39}$ erg/s)	$P_{KS}^{l}$
NGC5194-ULX3	rh601115n00.u	50809	8.0	3.3d	<3			<11.9		<1.00e-13	<0.711	
	rh600062a00.2	48597	8.5	33.3d	10.8	2.16	0.94	57.9	11.60	4.61e-13	3.28	0.043
	rh600062a01.2	48765	8.7	13.7d	12.0	2.29	0.93	71.8	10.65	5.55e-13	3.95	0.14
	rh600062a03.u	49494	9.3	1.1d	<3			<12.6		<9.18e-14	<0.653	
	rh600601n00.7+	49521	36.0	5.8d	18.0	2.22	0.91	193.6	7.65	3.64e-13	2.59	0.021
NGC5194-ULX4	rh601115n00.u	50809	8.0	3.3d	<3			<11.9		<1.00e-13	<0.711	
	rh600062a00.4	48597	8.5	33.3d	3.8	2.34	0.94	16.4	26.42	1.31e-13	0.932	
	rh600062a01.7	48765	8.7	13.7d	6.0	2.21	0.96	32.8	21.61	2.54e-13	1.81	
	rh600062a03.u	49494	9.3	1.1d	<3			<12.6		<9.17e-14	<0.652	
	rh600601n00.14+	49521	36.0	5.8d	10.4	2.27	0.94	92.6	12.06	1.74e-13	1.24	0.76
NGC5194-ULX5	rh601115n00.u	50809	8.0	3.3d	<3			<11.9		<1.00e-13	<0.711	
	rh600062a00.1	48597	8.5	33.3d	8.4	2.64	0.95	40.7	14.91	3.25e-13	2.31	
	rh600062a01.1	48765	8.7	13.7d	10.6	2.74	0.94	50.5	11.90	3.91e-13	2.78	
	rh600062a03.2	49494	9.3	1.1d	7.0	2.70	0.96	34.0	17.82	2.47e-13	1.76	
	rh600601n00.4+	49521	36.0	5.8d	23.4	2.75	0.90	273.2	6.51	5.13e-13	3.65	0.00041
NGC5194-ULX6	rh600062a00.u	48597	8.5	33.3d	<3			<11.3		<8.99e-14	<0.64	
	rh600062a01.3	48765	8.7	13.7d	4.4	2.65	0.95	23.8	26.40	1.84e-13	1.31	
	rh600062a03.u	49494	9.3	1.1d	<3			<12.6		<9.14e-14	<0.65	
	rh600601n00.10+	49521	36.0	5.8d	4.8	2.62	0.96	34.6	26.32	6.50e-14	0.462	
	rh601115n00.u	50809	8.0	3.3d	<3			<11.8		<9.99e-14	<0.711	
NGC5204-ULX1	rh702723n00.1+	50083	14.7	2.8d	50.4	0.41	0.88	428.2	2.77	1.93e-12	4.28	0.45
	rh702723a01.1	50206	13.6	1.0d	54.0	0.37	0.87	476.2	2.55	2.32e-12	5.15	2.3e-13
NGC5236-ULX1	rh600024n00.2	49008	23.3	1.5d	19.1	4.58	0.90	158.7	7.28	5.65e-13	1.5	0.64
	rh600024a01.1+	49564	23.9	3.4d	32.5	4.63	0.89	286.4	4.70	9.94e-13	2.63	0.0026
NGC5457-ULX1	rh600092n00.8	48631	18.5	2.0d	13.4	5.85	0.93	81.0	9.69	2.79e-13	1.57	0.00021
	rh600383n00.11	48967	32.4	3.8d	15.4	5.88	0.92	109.7	8.62	2.16e-13	1.22	0.95
	rh600820n00.11+	50217	107.9	26.0d	26.8	5.84	0.90	439.3	5.76	2.59e-13	1.46	0.031
	rh600820a01.15	50408	68.2	2.7d	17.9	5.91	0.91	220.8	7.68	2.06e-13	1.16	0.57
	rh600092n00.7	48631	18.5	2.0d	6.4	7.24	1.00	30.4	20.09	1.05e-13	0.592	
NGC5457-ULX2	rh600383n00.9	48967	32.4	3.8d	18.2	7.28	0.93	138.6	7.57	2.73e-13	1.54	0.6
	rh600820n00.9+	50217	107.9	26.0d	21.8	7.23	0.92	407.7	6.73	2.41e-13	1.36	0.0001
	rh600820a01.13	50408	68.2	2.7d	14.7	7.20	0.94	159.9	8.87	1.49e-13	0.84	0.51
	rh600092n00.1	48631	18.5	2.0d	9.2	10.70	0.99	63.9	13.71	2.21e-13	1.25	0.0002
NGC5457-X21	rh600383n00.1	48967	32.4	3.8d	6.2	10.68	1.00	48.6	20.58	9.56e-14	0.539	0.13
	rh600820n00.2+	50217	107.9	26.0d	9.9	10.63	0.99	153.6	12.88	9.07e-14	0.511	4e-05
	rh600820a01.2	50408	68.2	2.7d	12.6	10.59	0.98	153.8	10.17	1.44e-13	0.812	0.053
	rh600092n00.2	48631	18.5	2.0d	14.8	11.04	0.97	113.0	8.86	3.90e-13	2.2	0.21
NGC5457-ULX3	rh600383n00.2	48967	32.4	3.8d	24.8	11.00	0.95	285.6	6.09	5.62e-13	3.17	0.2
	rh600820n00.4+	50217	107.9	26.0d	43.7	11.08	0.94	951.1	3.41	5.61e-13	3.16	1.9e-07
	rh600820a01.3	50408	68.2	2.7d	22.8	11.00	0.96	325.7	6.56	3.04e-13	1.71	0.1
	rh600092n00.13	48631	18.5	2.0d	7.4	13.88	0.79	64.8	17.06	2.24e-13	1.26	0.039
NGC5457-X32	rh600383n00.u	48967	32.4	3.8d	<3			<43.8		<8.62e-14	<0.486	
	rh600820n00.u+	50217	107.9	26.0d	<3			<76.9		<4.54e-14	<0.256	
	rh600820a01.u	50408	68.2	2.7d	<3			<65.4		<6.11e-14	<0.345	
	rh600092n00.14	48631	18.5	2.0d	8.0	16.09	0.53	116.0	15.73	4.00e-13	2.26	0.46
NGC5457-X34	rh600383n00.17	48967	32.4	3.8d	9.4	16.13	0.56	155.9	13.55	3.07e-13	1.73	0.55
	rh600820n00.18+	50217	107.9	26.0d	18.7	16.18	0.71	666.2	7.42	3.93e-13	2.22	2.2e-05
	rh600820a01.19	50408	68.2	2.7d	12.7	16.21	0.62	384.2	10.13	3.59e-13	2.02	0.89
	rh600964n00.2+	50646	34.8	8.2d	4.7	3.41	0.96	38.4	26.39	8.96e-14	7.72	
NGC5774-ULX1	rh600964n00.3+	50646	34.8	8.2d	3.8	5.97	0.99	26.5	26.42	6.15e-14	5.3	
NGC6434-X1	rh601018n00.2	50433	20.6	4.7d	15.5	0.88	0.92	149.0	8.58	5.98e-13	78.6	0.39
NGC6654-X1	rh601018a01.4+	50473	23.8	1.0d	16.1	0.89	0.91	123.2	8.37	4.27e-13	56.1	0.24
NGC6654-X2	rh600124a00.18+	48512	36.5	23.0h	4.8	12.79	0.83	51.8	26.00	1.29e-13	13.5	0.11
NGC6654-X2	rh600124a01.u	48731	18.1	1.3d	<3			<26.7		<1.34e-13	<14	
NGC6946-ULX1	rh600124a00.11+	48512	36.5	23.0h	5.8	13.17	0.82	53.2	22.43	1.32e-13	13.8	
NGC6946-ULX1	rh600124a01.u	48731	18.1	1.3d	<3			<28.9		<1.44e-13	<15	
NGC6946-ULX1	rh600501n00.8+	49486	59.9	15.1d	20.5	0.95	0.90	208.4	6.96	4.97e-13	1.8	0.0097
NGC6946-ULX2	rh600501n00.2	49943	21.5	3.0d	5.7	1.29	0.97	44.0	22.67	2.92e-13	1.06	0.64
NGC6946-ULX2	rh500476n00.u	50305	8.4	9.7h	<3			<11.8		<2.02e-13	<0.733	
NGC6946-ULX2	rh600501n00.12+	49486	59.9	15.1d	15.8	2.06	0.92	152.6	8.46	3.64e-13	1.32	0.21
NGC6946-ULX2	rh600718n00.4	49943	21.5	3.0d	9.3	1.78	0.95	66.6	13.57	4.42e-13	1.6	0.4
NGC6946-ULX3	rh600501n00.7+	49486	59.9	15.1d	71.1	2.69	0.87	922.0	1.74	2.20e-12	7.99	0.83
NGC6946-ULX3	rh600718n00.1	49943	21.5	3.0d	47.7	2.36	0.88	455.5	2.97	3.02e-12	11	0.031

Table 3—Continued

Name	Obs.Src <sup>a</sup>	Date <sup>b</sup> (MJD)	T <sup>c</sup> ksec	$\Delta D^d$	$\sigma^e$	$\theta^f$ ( $'$ )	$C(\theta, \sigma)^g$	CorCnt <sup>h</sup> (count)	pErr <sup>i</sup> (%)	Flux <sup>j</sup> (cgs)	$L_X^{k}$ ( $10^{39}$ erg/s)	$P_{KS}^{l}$
	rh500476n00.1	50305	8.4	9.7h	23.7	0.14	0.90	145.8	6.47	2.50e-12	9.07	0.45
NGC7217-X2	rh702933n00.u	50612	4.8	2.0d	<3					<2.06e-13	<6.33	
	rh702933a01.1+	50773	10.7	14.7h	3.3	2.94	0.94	14.9	25.80	1.52e-13	4.67	
PGC68618-X1	rh500493n00.7+	50582	34.0	1.4d	5.8	6.02	0.99	42.5	22.37	8.69e-14	1.28	
NGC7314-ULX1	rh701300n00.4+	49665	19.1	14.0d	5.6	1.66	0.96	33.5	23.11	1.17e-13	2.34	
NGC7314-X4	rh701300n00.8+	49665	19.1	14.0d	4.4	2.68	0.95	26.0	26.40	9.07e-14	1.81	
NGC7314-X5	rh701300n00.5+	49665	19.1	14.0d	11.3	4.50	0.94	74.8	11.20	2.61e-13	5.21	
NGC7582-X2	rh800189n00.u	48780	7.5	3.1d	<3					<32.8	<3.12e-13	<11.6
	rh800189a01.u	49124	4.2	23.9d	<3					<24.5	<4.15e-13	<15.4
	rh701710n00.3+	49860	17.3	18.0h	7.9	1.93	0.96	51.4	15.81	2.10e-13	7.81	0.39
	rh702055n00.u	50418	11.2	8.6h	<3					<13.4	<8.48e-14	<3.15
	rh702055a01.u	50758	12.2	2.9d	<3					<13.8	<8.02e-14	<2.98
NGC7590-ULX1	rh800189n00.u	48780	7.5	3.1d	<3					<11.9	<1.14e-13	<4.09
	rh800189a01.u	49124	4.2	23.9d	<3					<9.7	<1.64e-13	<5.89
	rh701710n00.u+	49860	17.3	18.0h	<3					<17.0	<6.97e-14	<2.5
	rh702055n00.4	50418	11.2	8.6h	5.0	10.21	1.01	28.7	25.31	1.82e-13	6.54	
	rh702055a01.5	50758	12.2	2.9d	3.5	10.09	1.01	16.2	26.14	9.45e-14	3.39	
NGC7714-ULX1	rh600738n00.4+	49713	45.5	2.9d	13.7	0.82	0.92	132.6	9.51	2.56e-13	41.8	
NGC7742-ULX1	rh500386n00.1+	49713	9.6	2.0d	3.4	0.43	0.98	13.5	25.91	1.25e-13	7.39	0.92

<sup>a</sup>Individual observation. Suffix fixed is the sequence number in the source list from wavdetect. 'U' is suffixed when the source is below  $3\sigma$  detection in the observation. '+' is suffixed if the observation has the deepest sensitivity for the host galaxy.

<sup>b</sup>Observation date in MJD.

<sup>c</sup>Exposure time in kilo-seconds.

<sup>d</sup>Duration of the observation.

<sup>e</sup>Detection significance.

<sup>f</sup>Off-axis angle in arcminutes.

<sup>g</sup>The correction factor  $C(\theta, \sigma)$  computed based on the simulations.

<sup>h</sup>The source count corrected by applying  $C(\theta, \sigma)$ .

<sup>i</sup>The fractional error for the corrected count.

<sup>j</sup>The flux in erg/s/cm<sup>2</sup> computed with the corrected source count, by assuming a power-law spectrum between 0.3–8 KeV with a photon index of 1.7.

<sup>k</sup>The luminosity computed from the flux by assuming a distance to the host galaxy.

<sup>l</sup>The probability for the Kolmogorov-Smirnov test null hypothesis that the source is constant during the observation.

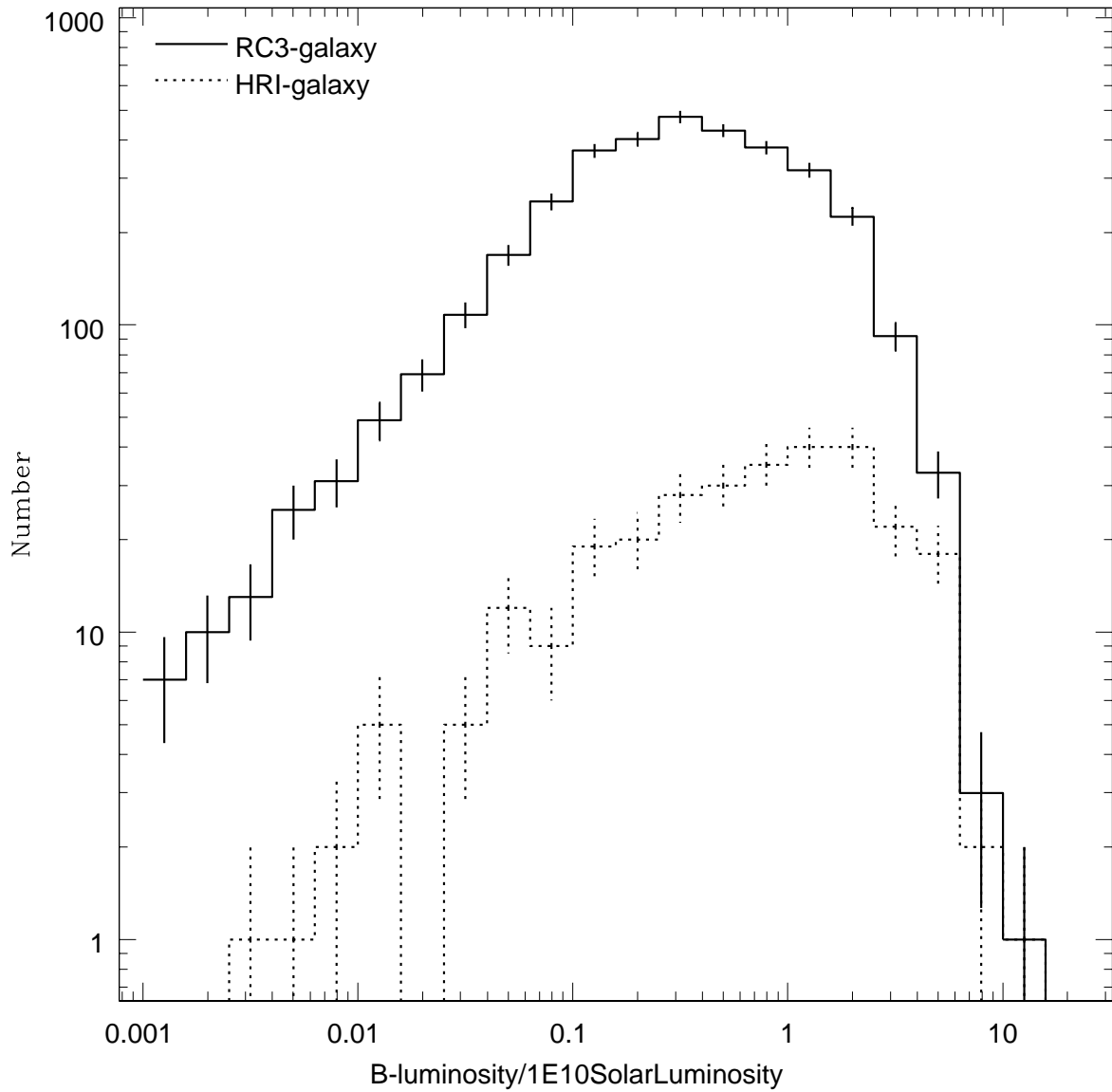


Fig. 1.— The distribution of blue luminosities for the HRI survey galaxy sample in comparison with the RC3 galaxy sample. More bright galaxies, presumably larger in size and closer in distance, were surveyed by the HRI than faint galaxies.

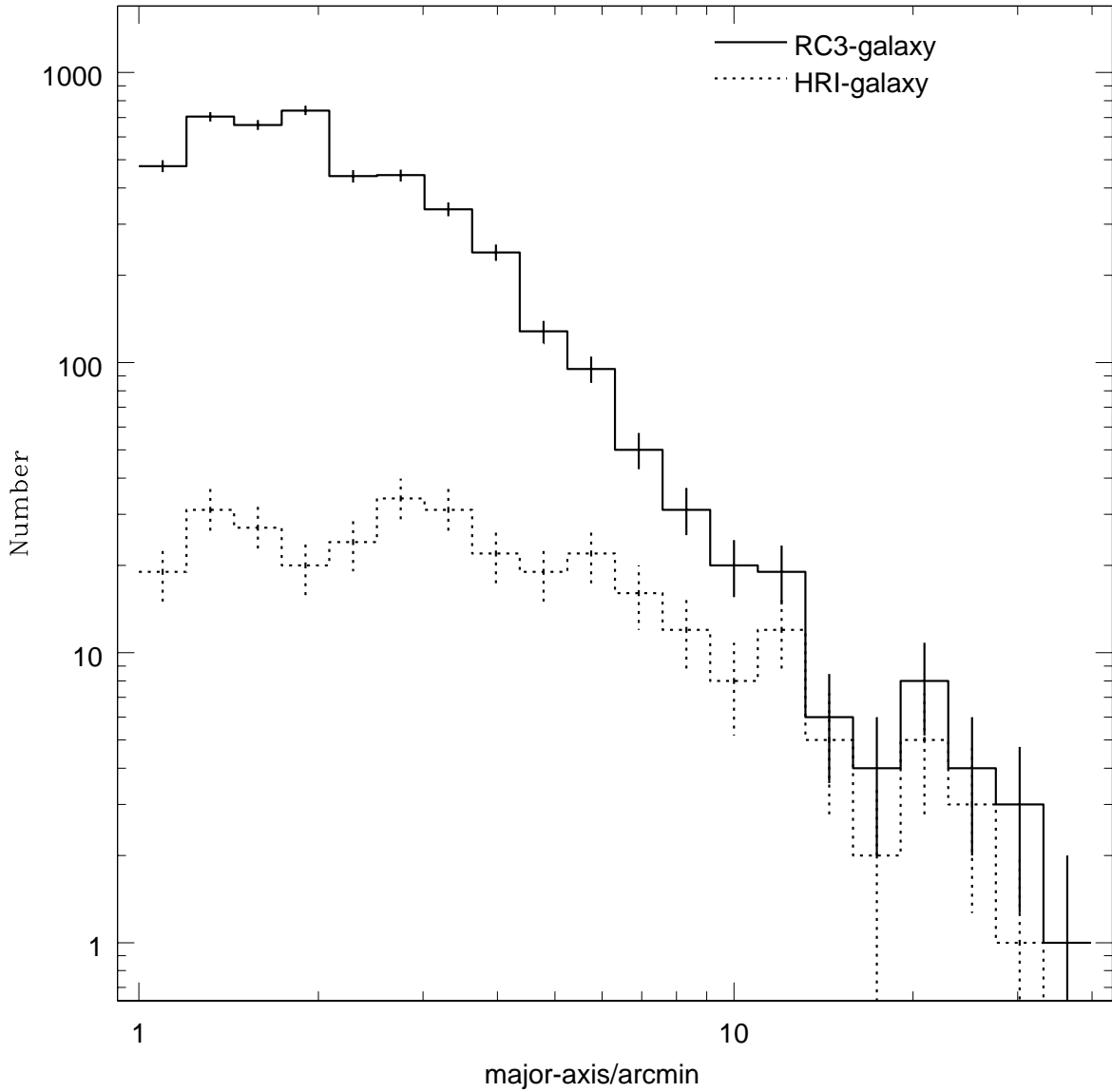


Fig. 2.— Galaxy size distribution of the HRI survey galaxy sample in comparison with the RC3 galaxy sample. Slightly more large galaxies were surveyed by the HRI than small galaxies.

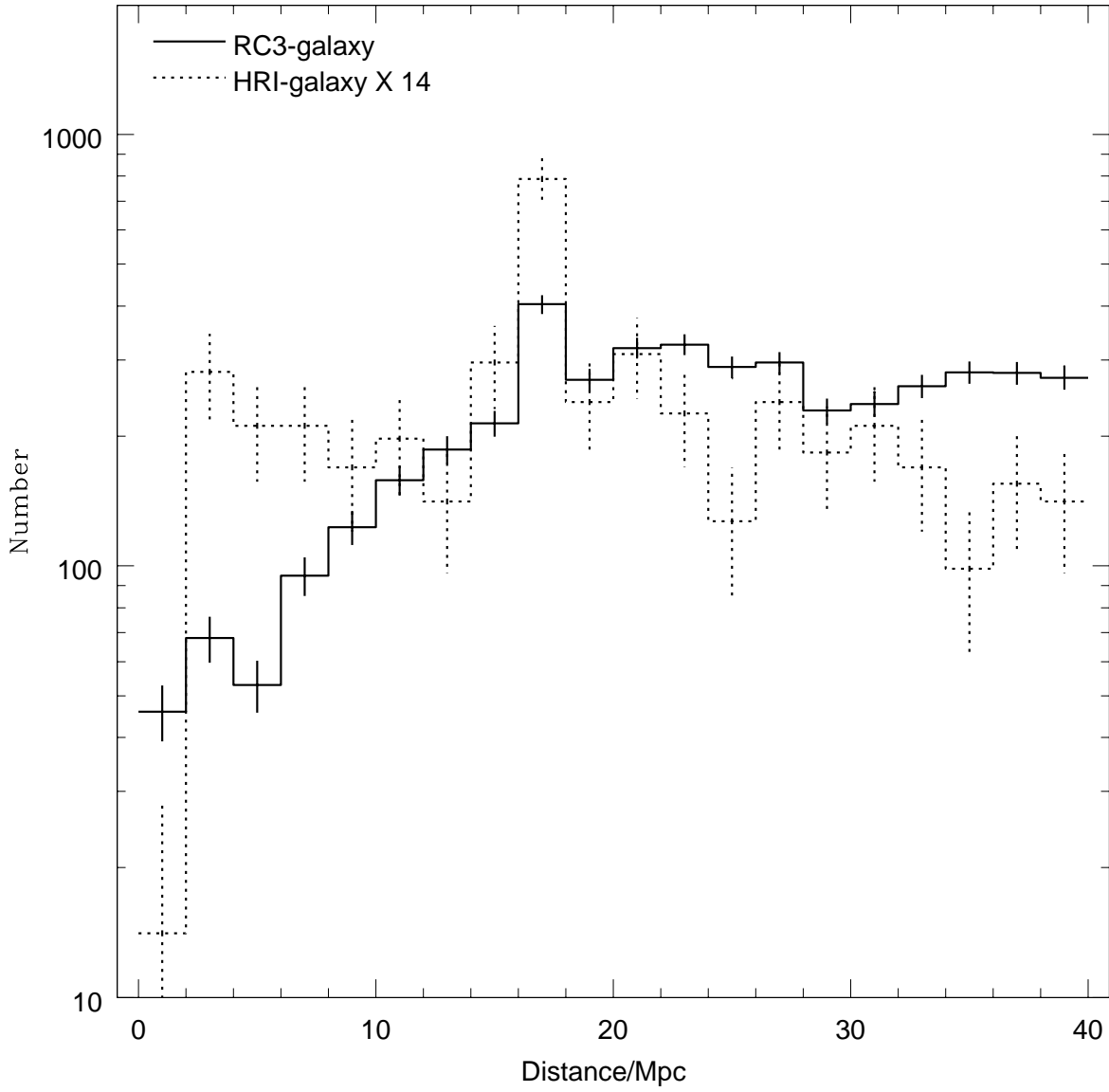


Fig. 3.— Galaxy distance distribution of the HRI galaxy sample in comparison with the RC3 galaxy sample. More nearby galaxies ( $< 15\text{Mpc}$ ) were surveyed than those distant galaxies ( $> 15 \text{ Mpc}$ ).

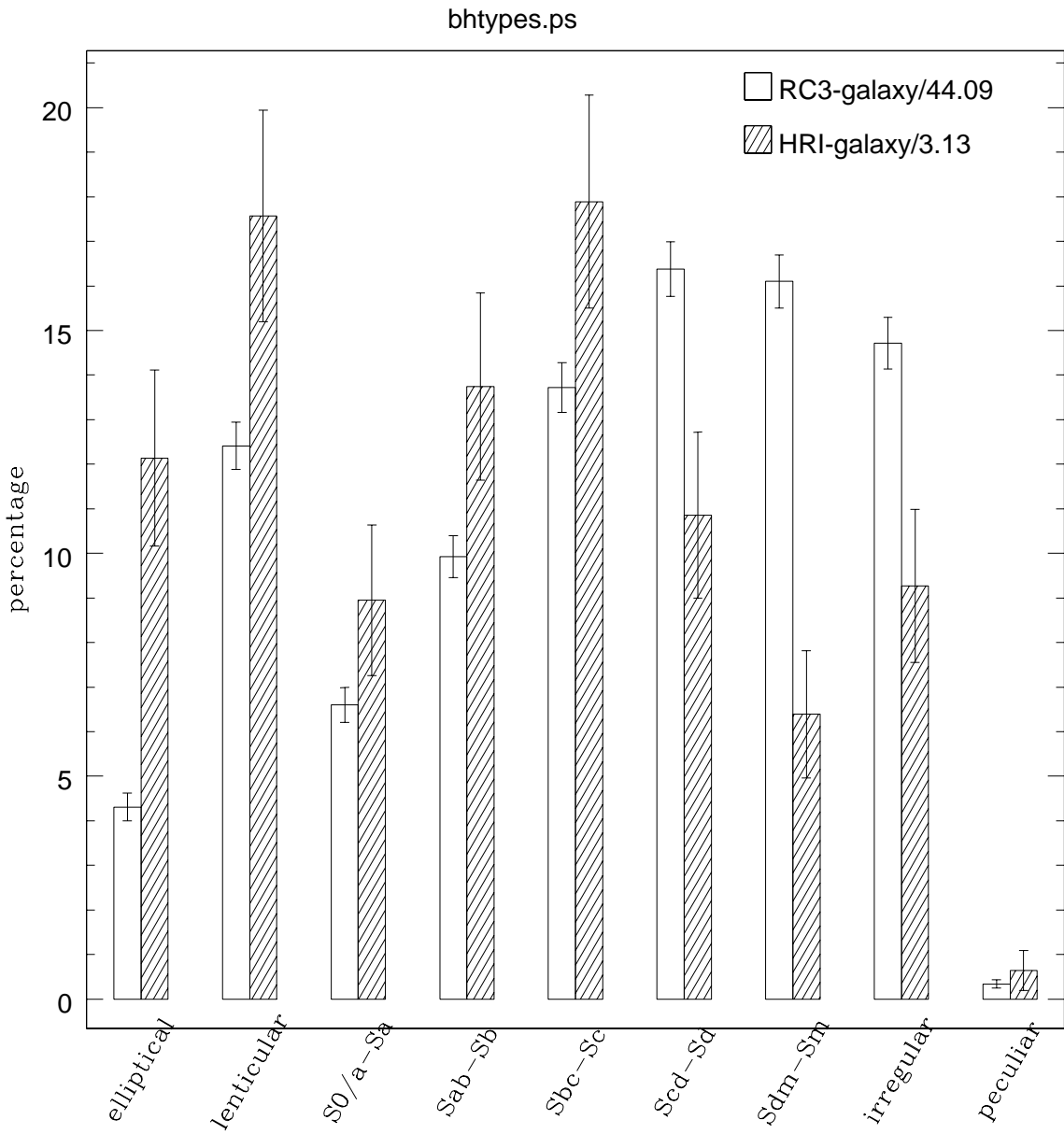


Fig. 4.— The distribution of morphological types of the HRI galaxy sample in comparison with the RC3 galaxy sample. More early-types galaxies and Sa-Sc spiral galaxies were surveyed than other types.

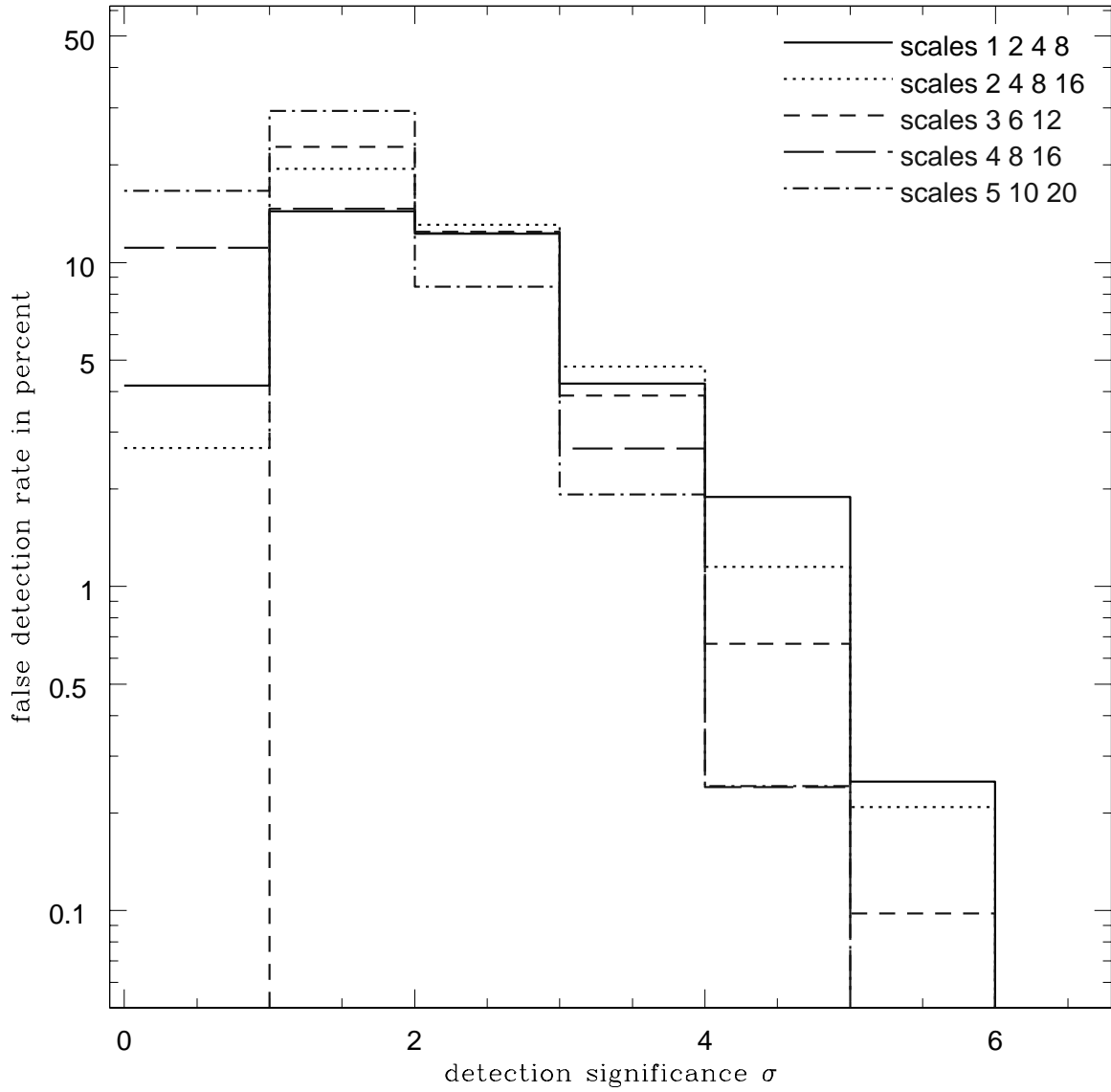


Fig. 5.— False detections in simulations on HRI images with different scale sets. The first three scale sets have larger false detection rates than the latter two. The detections below  $3\sigma$  have a false detection rate  $>10\%$  and are discarded in our data analysis.

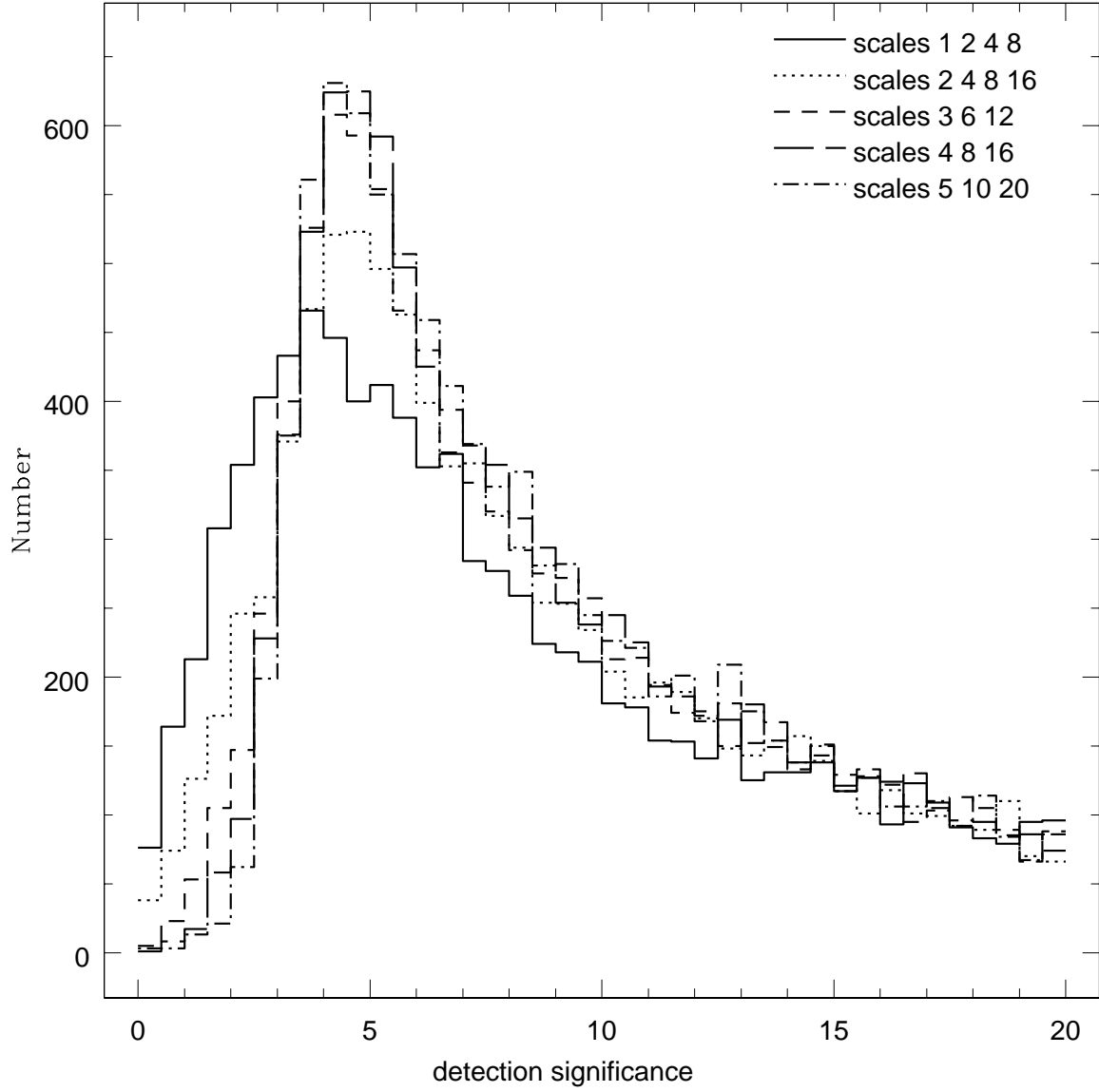


Fig. 6.— Detections in simulations on HRI images with different scale sets. There are more detections for the last two scale sets than the first three, and there are more detections with large  $\sigma$  for the last two scale sets than for the first three.

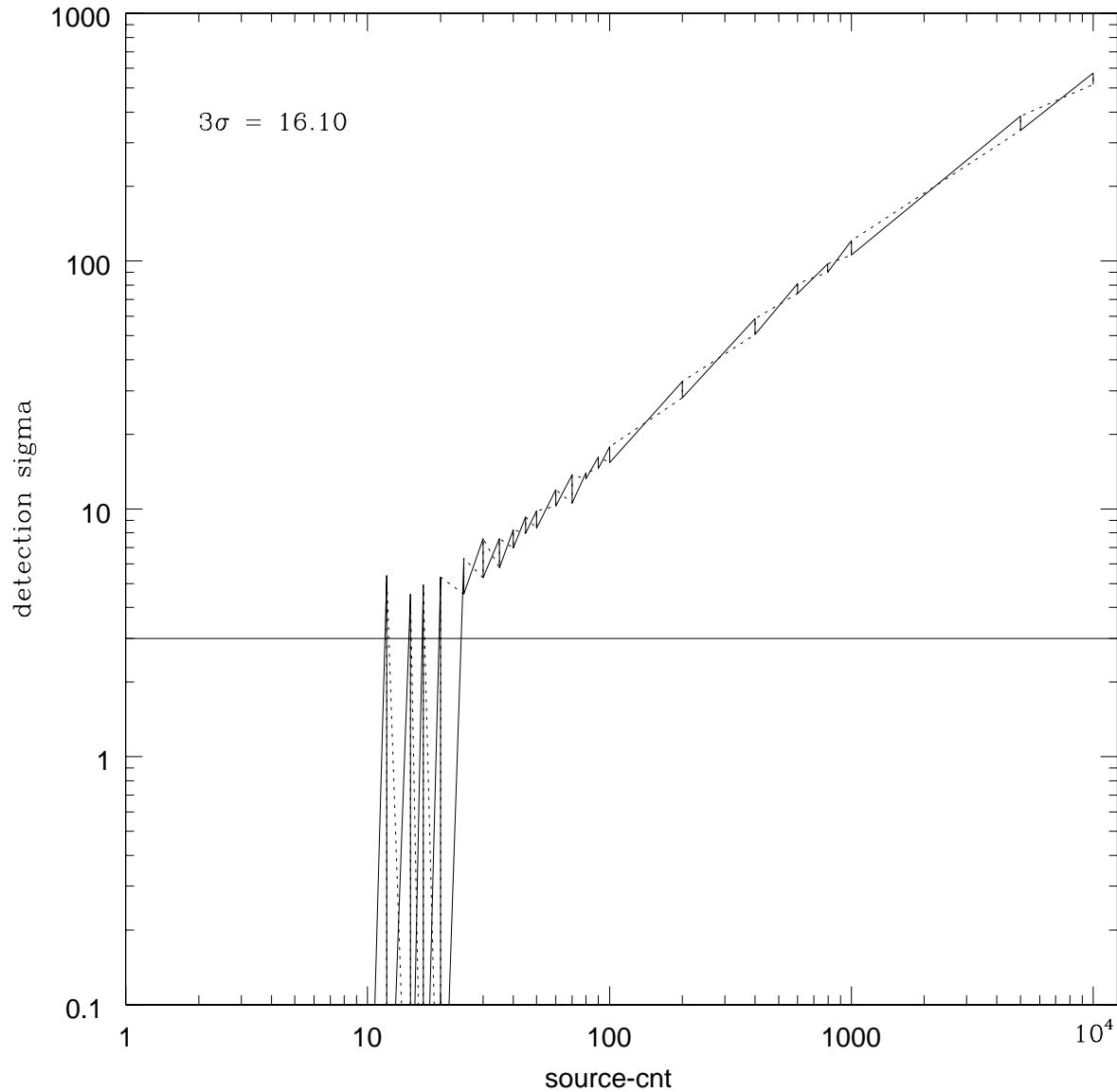


Fig. 7.— Determination of the count threshold for  $3\sigma$  detection from simulations. The example is for an off-axis angle of  $10'$  and an exposure time of 10 kiloseconds. The solid and dashed connecting lines show two ways to sort sources of same counts, one in ascending order of detection  $\sigma$  and another in descending order. The average of counts from the two gives a method-independent count threshold.

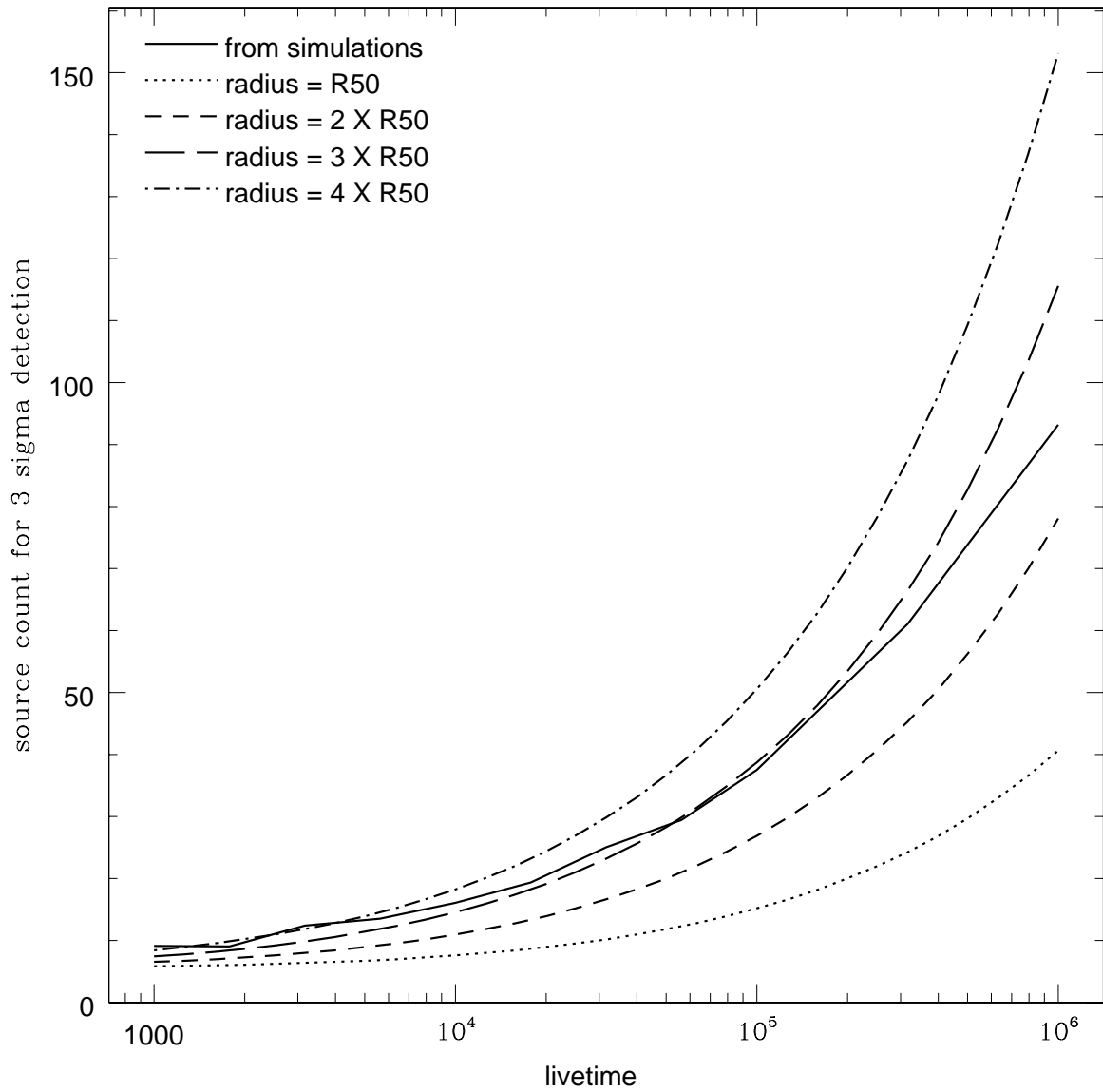


Fig. 8.— The source count thresholds for  $3\sigma$  detection with changes in the background levels. The solid line is for thresholds derived from the simulations, and the other lines for thresholds computed from source regions of various sizes. The simulated thresholds follow closely the computed thresholds for a source region with a radius of  $3 \times R_{50}$  at an off-axis angle of  $10'$  in this example.

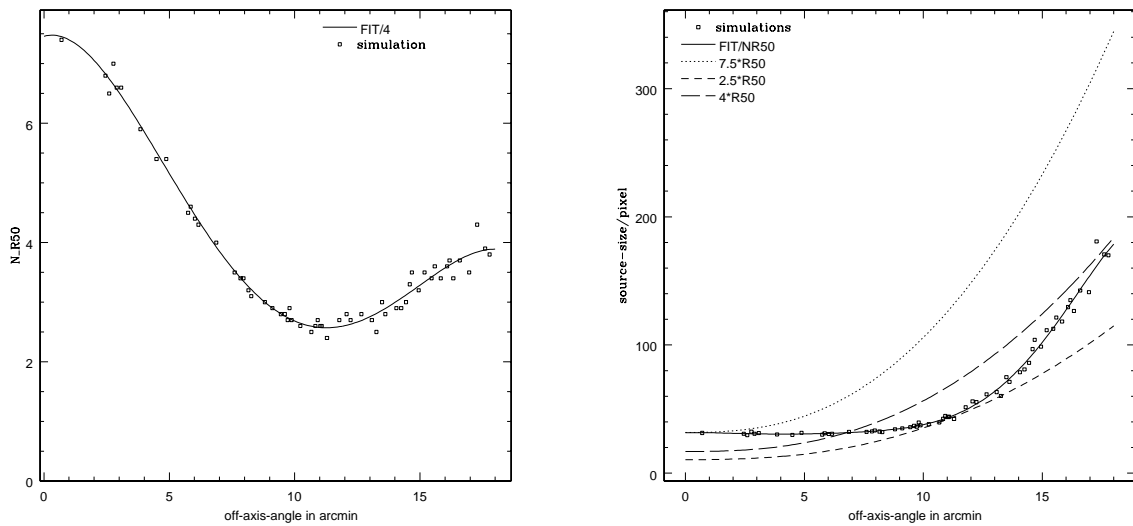


Fig. 9.— The equivalent source region for computing count thresholds as a function of off-axis angles. The left panel shows the best fit source size in unit of  $R_{50}$ . The right panel shows the source size in pixels. The points are source sizes derived from the simulations, and the solid line is a 4-th polynomial fit to the simulations.

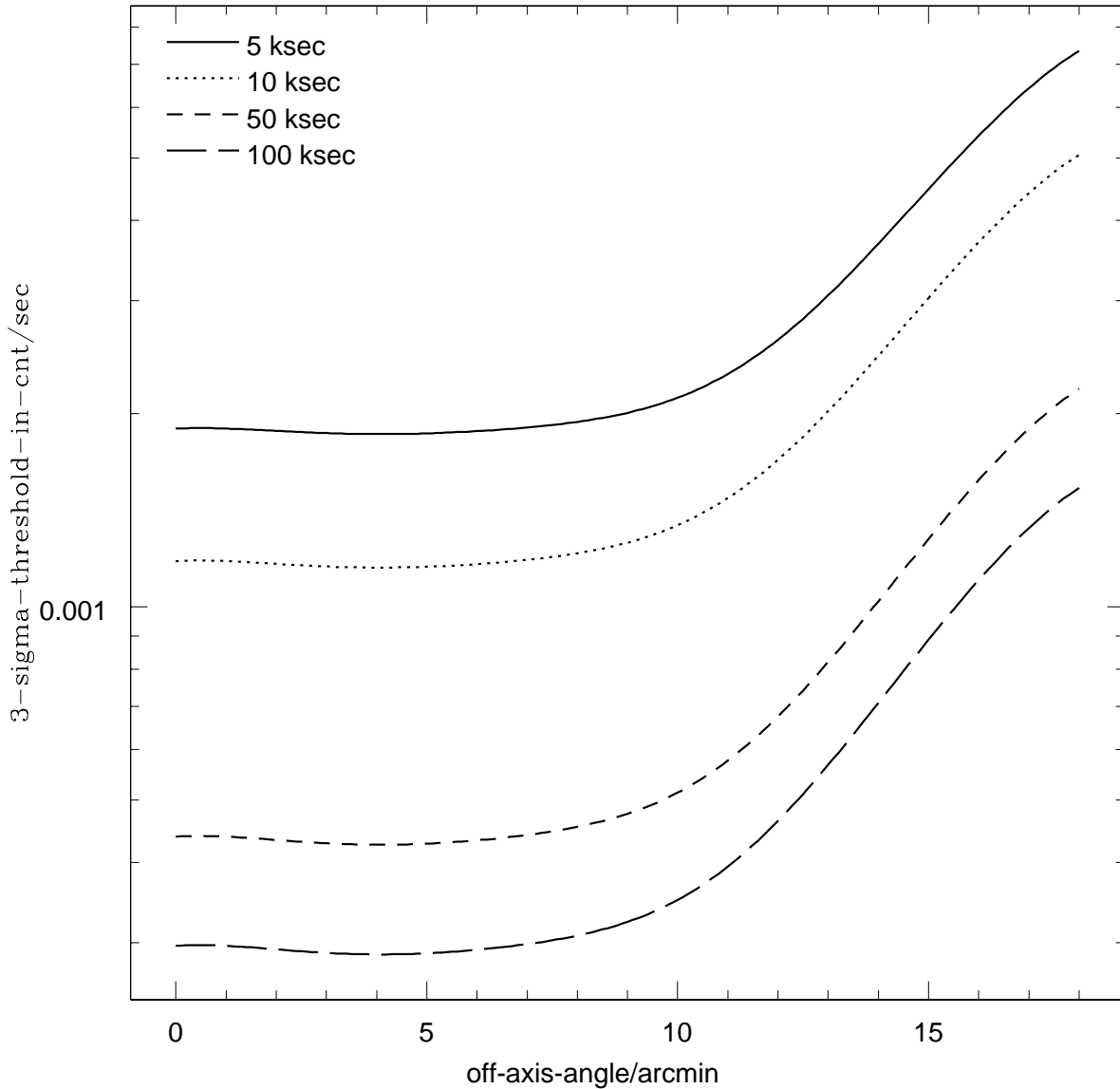


Fig. 10.— The count rate thresholds for  $3\sigma$  detection computed for different exposure times based on the best fit source size derived from the simulations. For an exposure, the sensitivity is approximately the same within  $10'$ , and degrades outwards. At  $\sim 17'$  it decreases by a factor  $\sim 3.5$  for all the shown exposures.

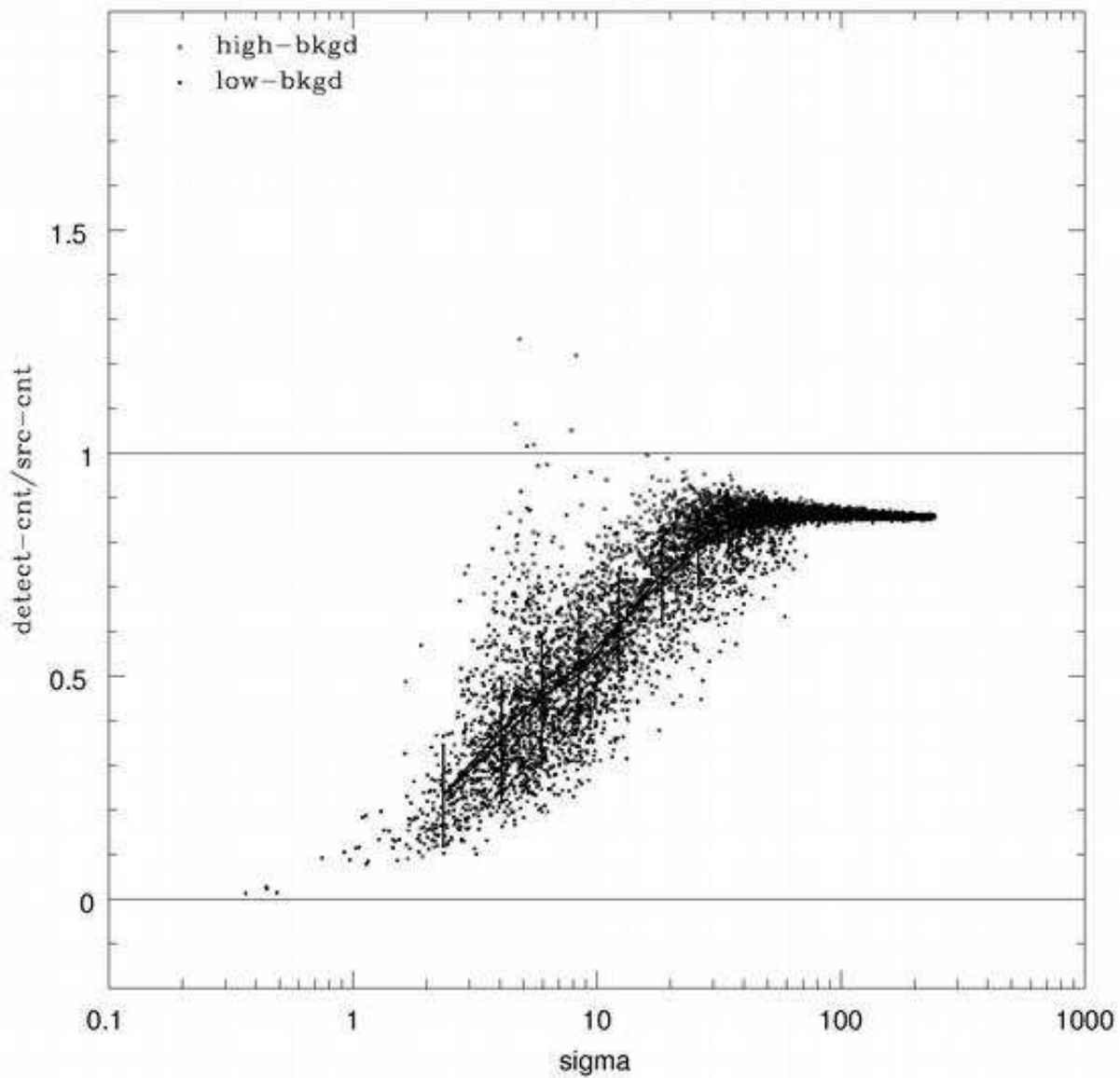


Fig. 11.— Change in the correction factors with detection significance for off-axis angles of  $16.08' \pm 0.1'$ . No significant dependence of correction factors on the background levels is shown.

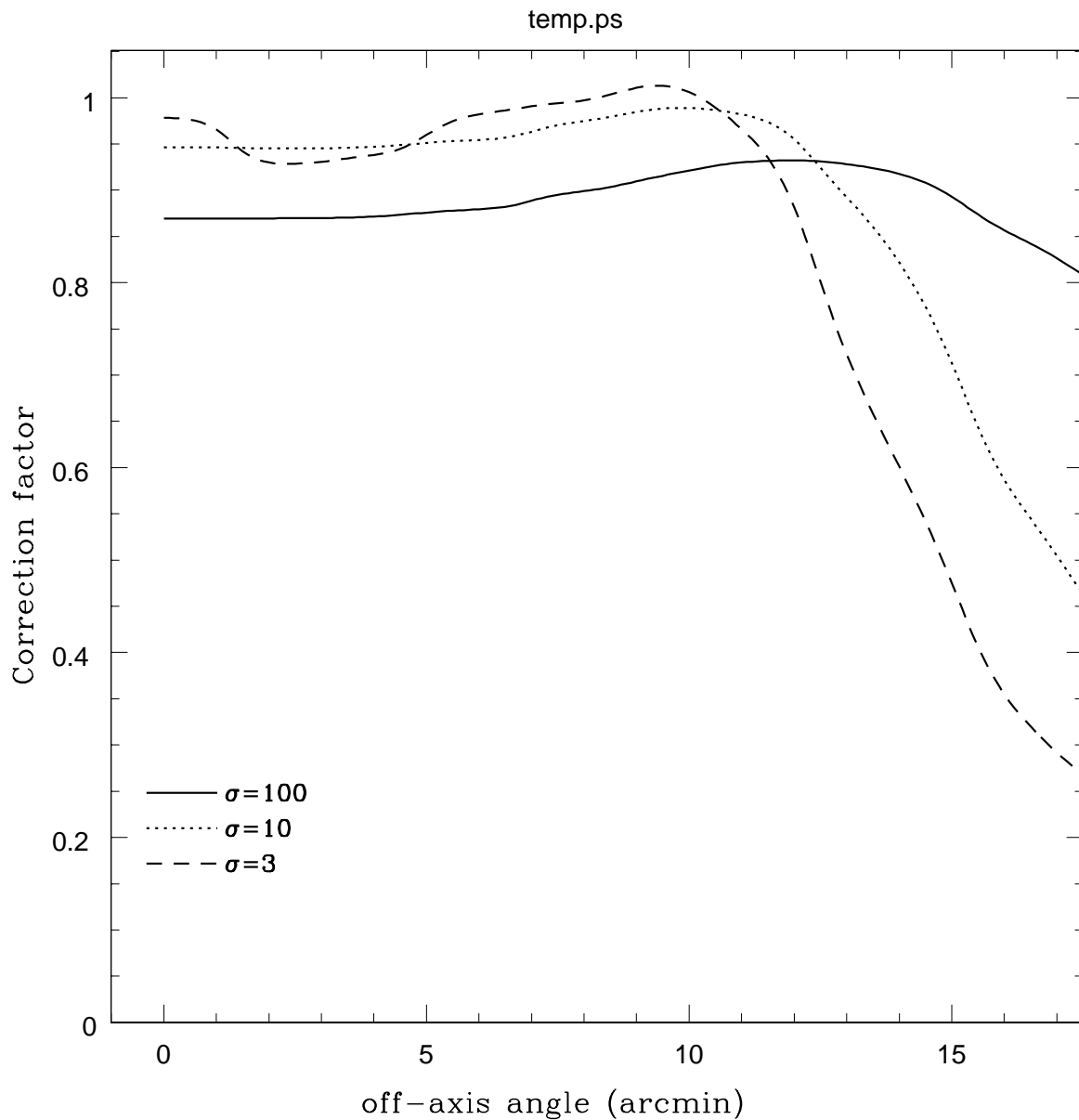


Fig. 12.— The correction factors as a function of off-axis angles for different detection significance. The decrease beyond  $10'$  can be attributed to the increase in the point source sizes and the vignetting function with the off-axis angle.

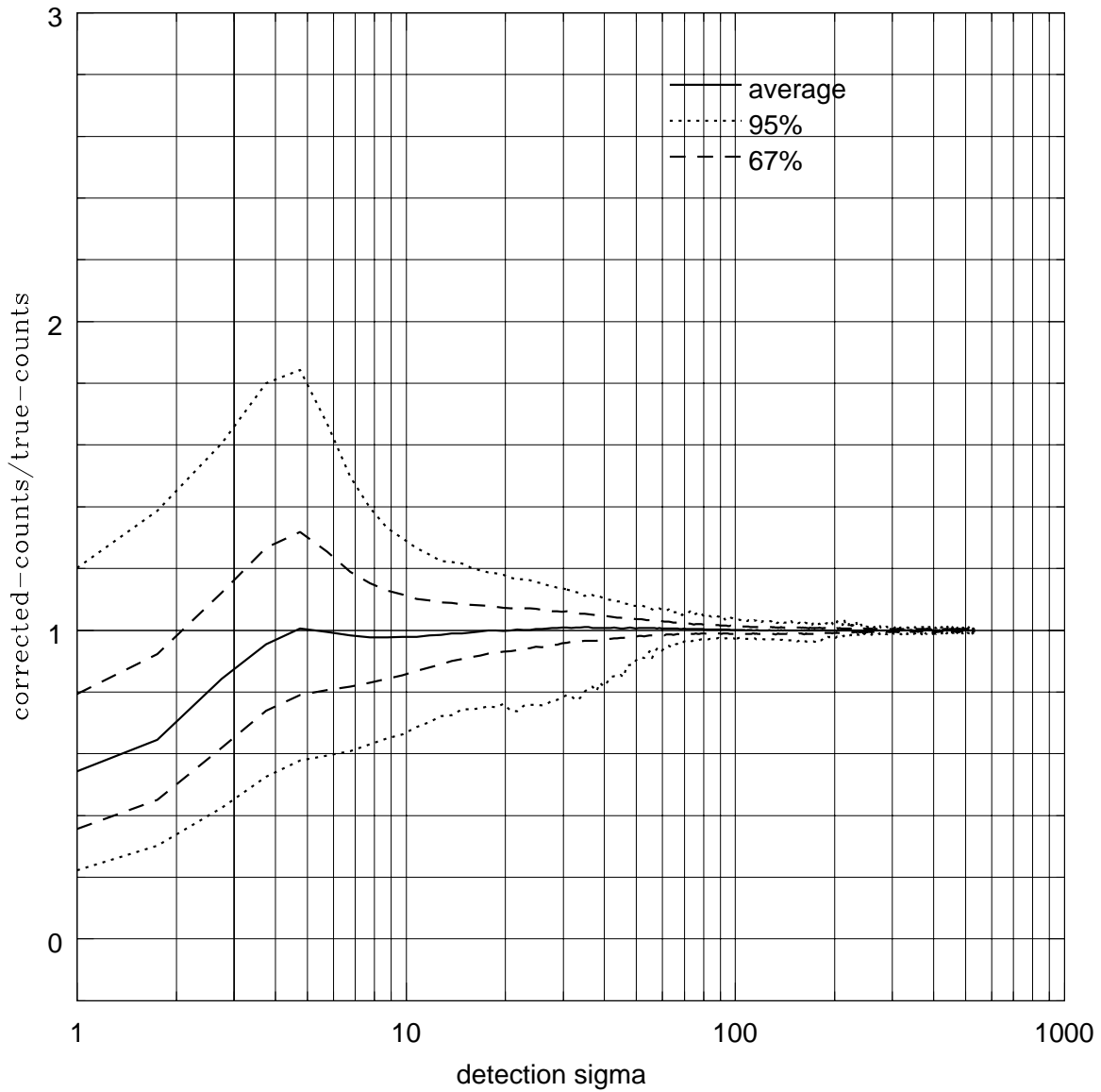


Fig. 13.— The detection count correction factors from the simulations. The solid line shows the mean ratio of corrected counts to true counts, and the dashed/dotted lines show the limits between which are 67%/95% of the simulated sources.

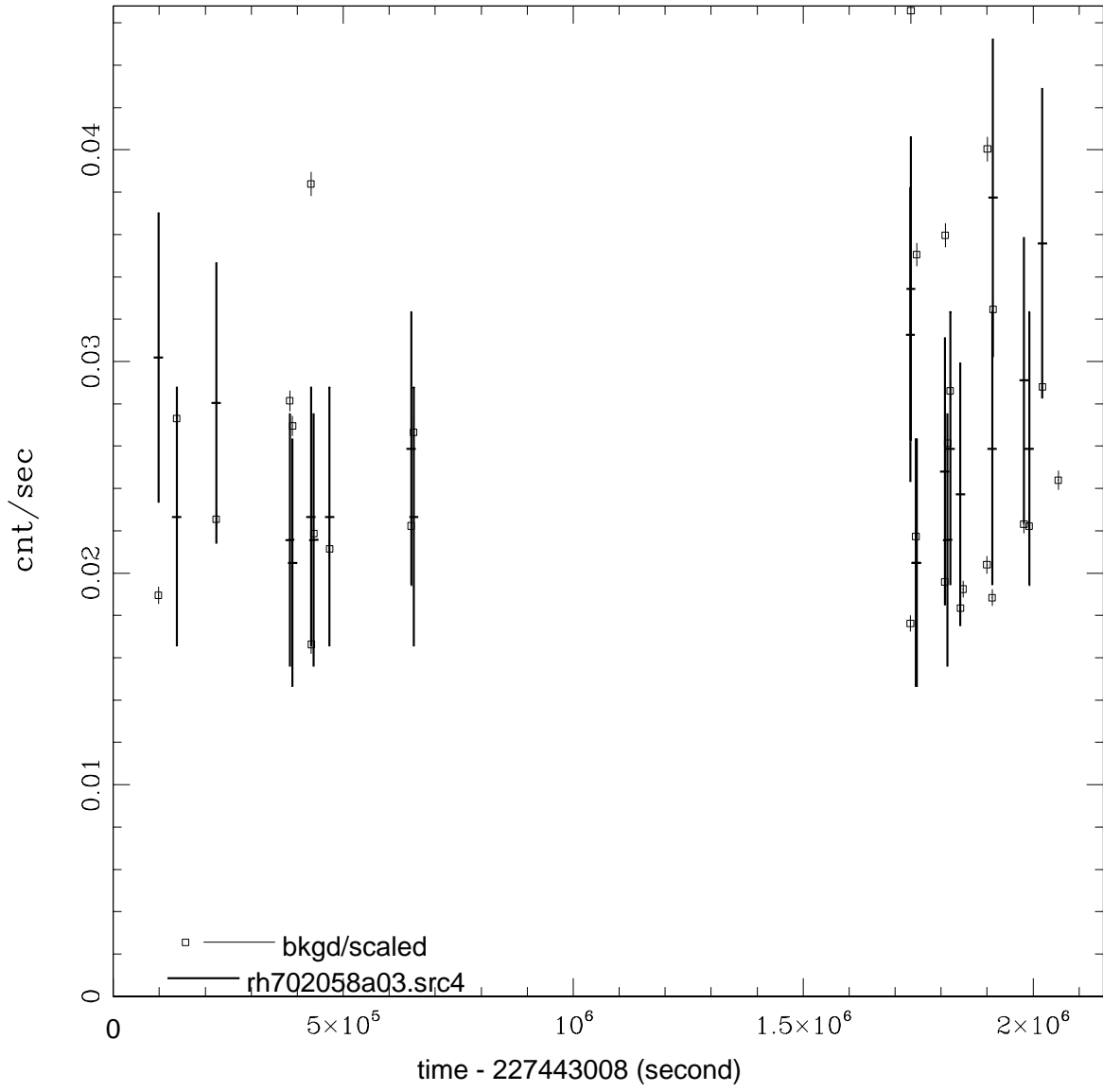


Fig. 14.— The HRI light curve for a ULX in Circinus galaxy which shows X-ray eclipses with a 7.5 hour period in a Chandra observation. The light curve shows clear temporal variations. However, the periodicity is not obvious due to the wide separations between OBIs.

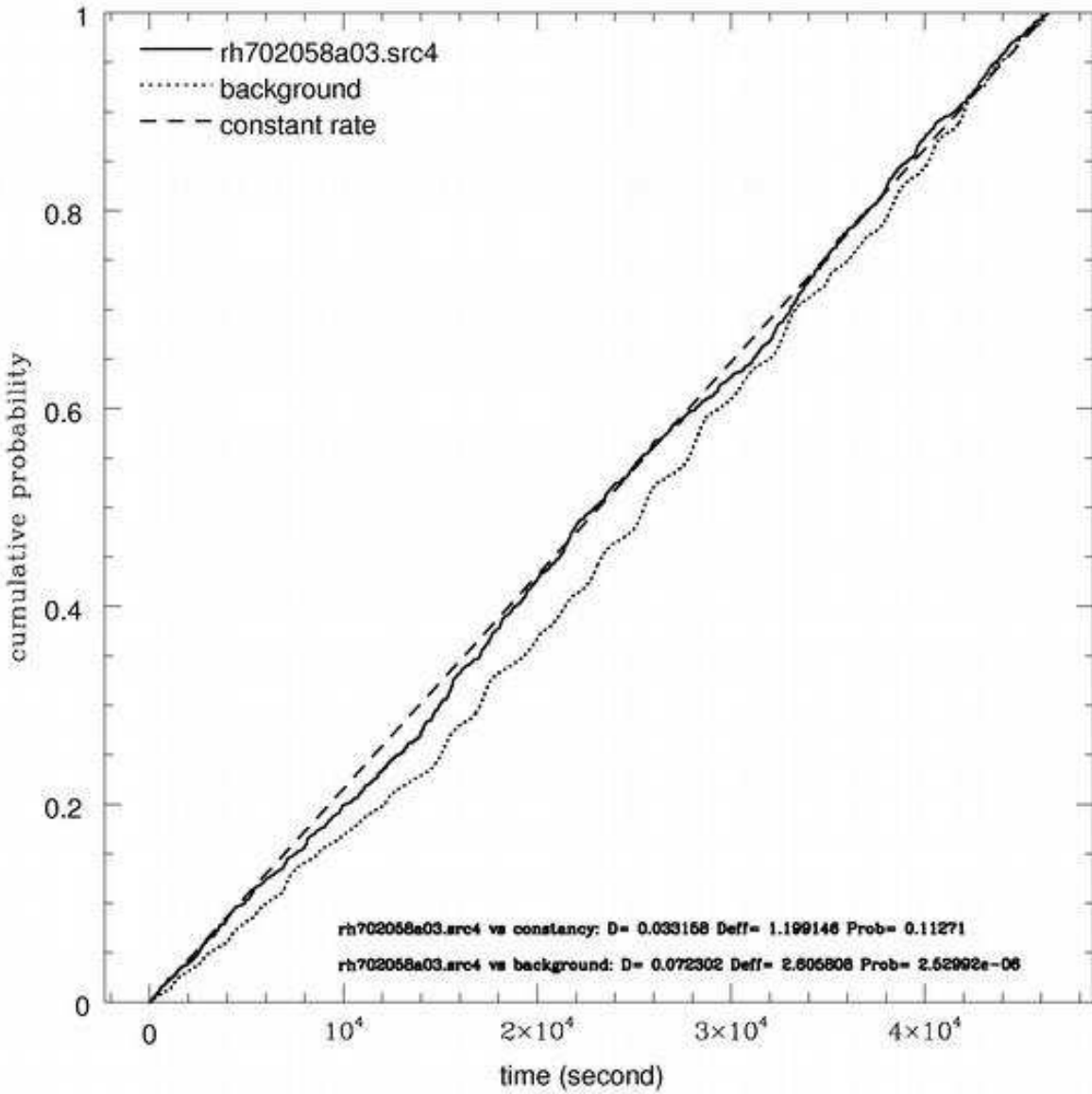


Fig. 15.— The cumulative probability curves for the Kolmogorov-Smirnov tests of the ULX in Circinus galaxy. The tests show that the source was variable with a (insignificant) probability of 89% during the HRI observation.

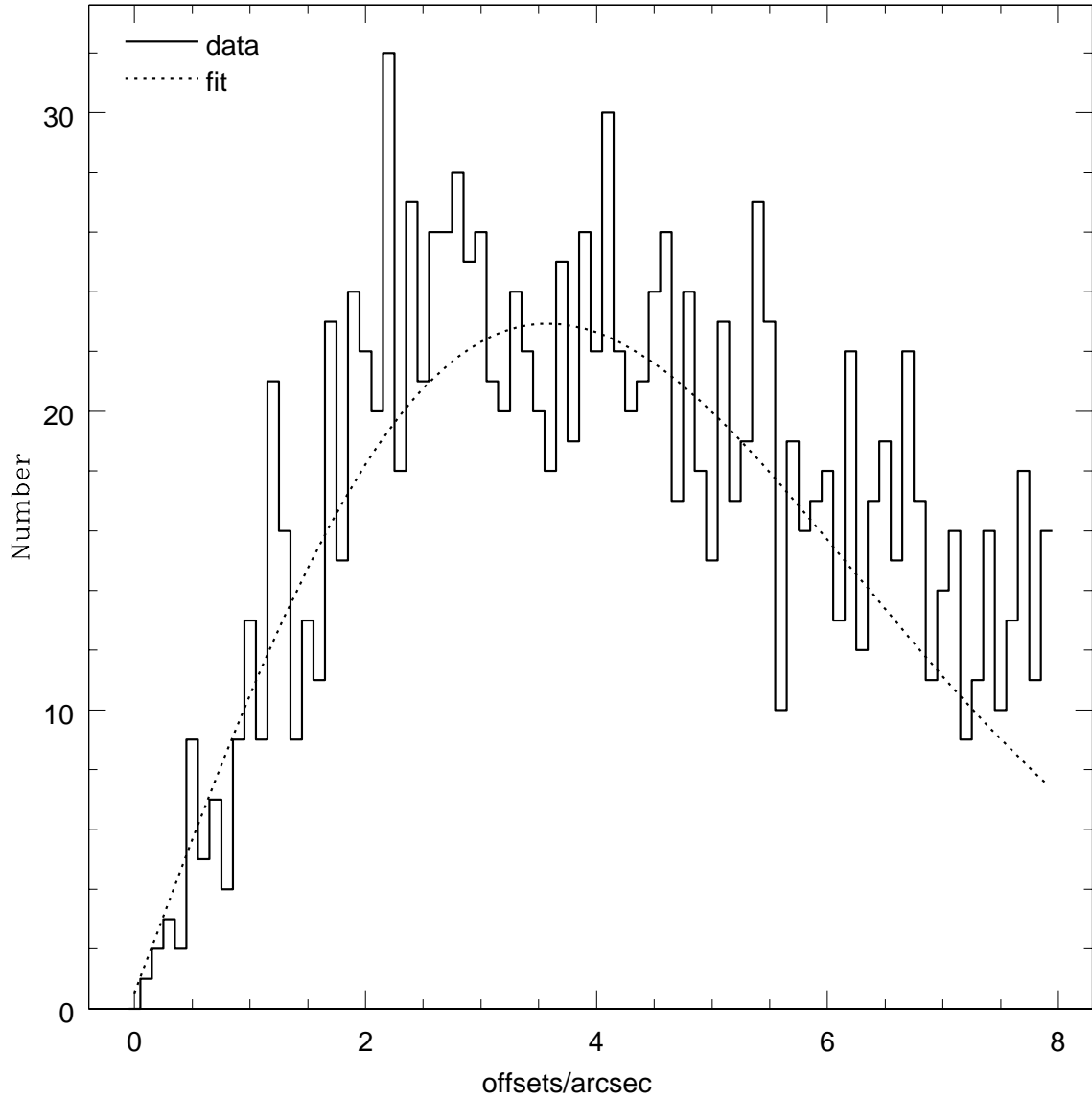


Fig. 16.— Distribution of offsets between the HRI and catalogued positions for 1372 sources detected in HRI observations. This distribution can be fitted by a 2-D normal distribution with  $\sigma = 3\text{''}.62 \pm 0\text{''}.02$ .

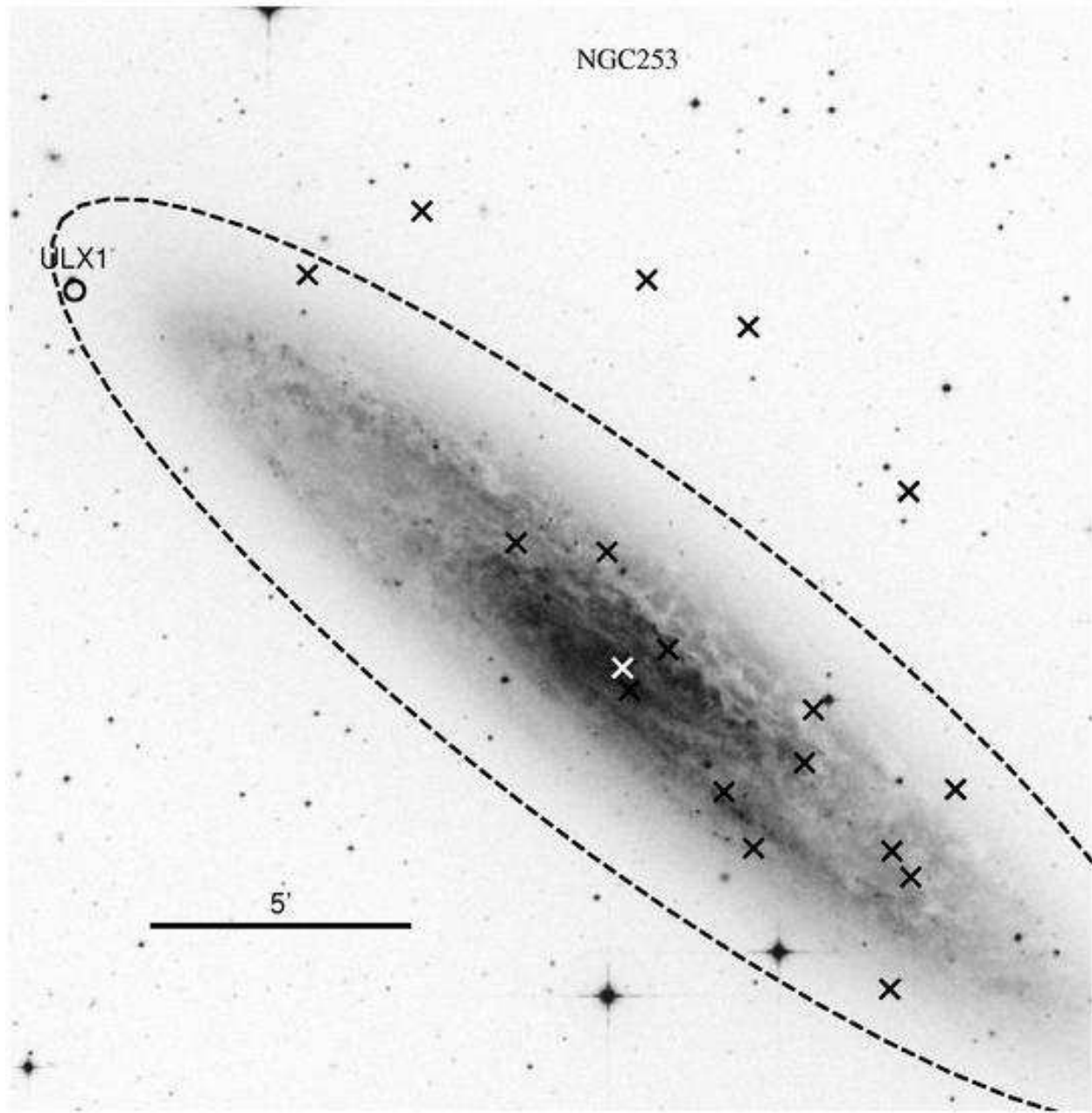


Fig. 17.— The finding chart for the ULXs in NGC253. The ellipse is the  $D_{25}$  isophote, and the galactic nucleus is marked by "+". ULXs in the clean sample or ULX candidates are labelled as circles, and other X-ray sources are labelled by "X". The DSS image is positioned with up as north and left as east.

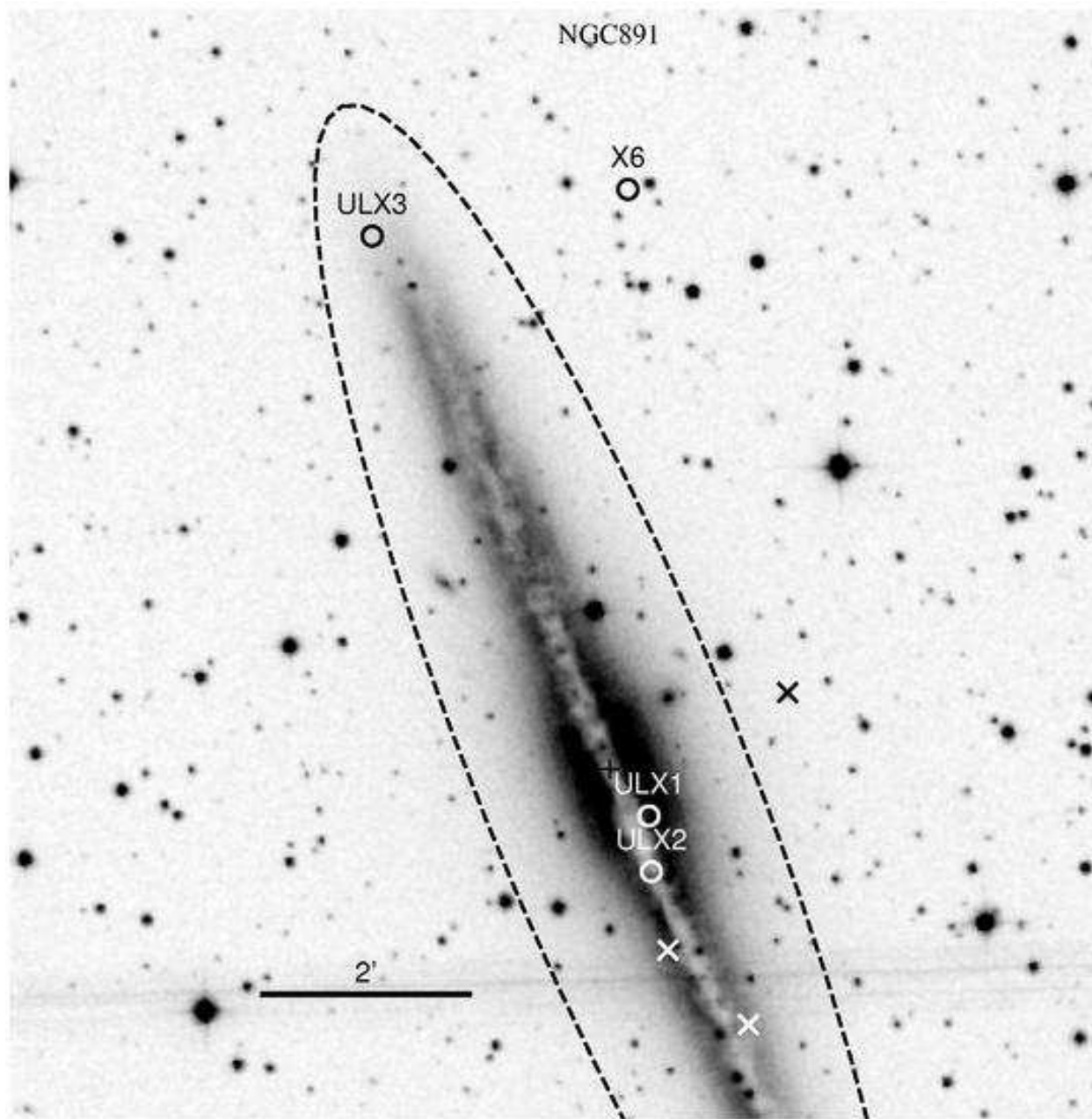


Fig. 18.— The finding chart for the ULXs in NGC891.

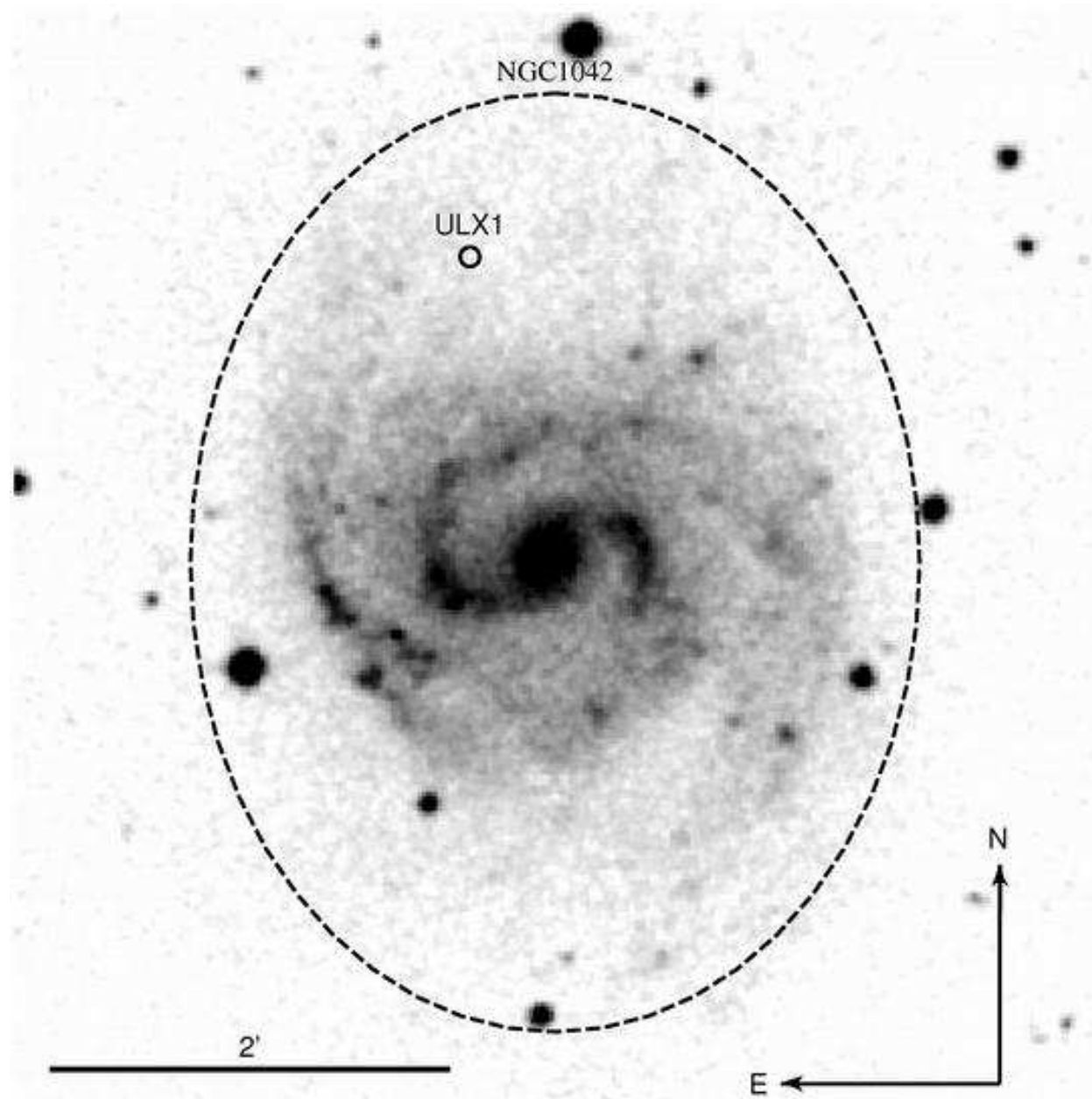


Fig. 19.— The finding chart for the ULXs in NGC1042.

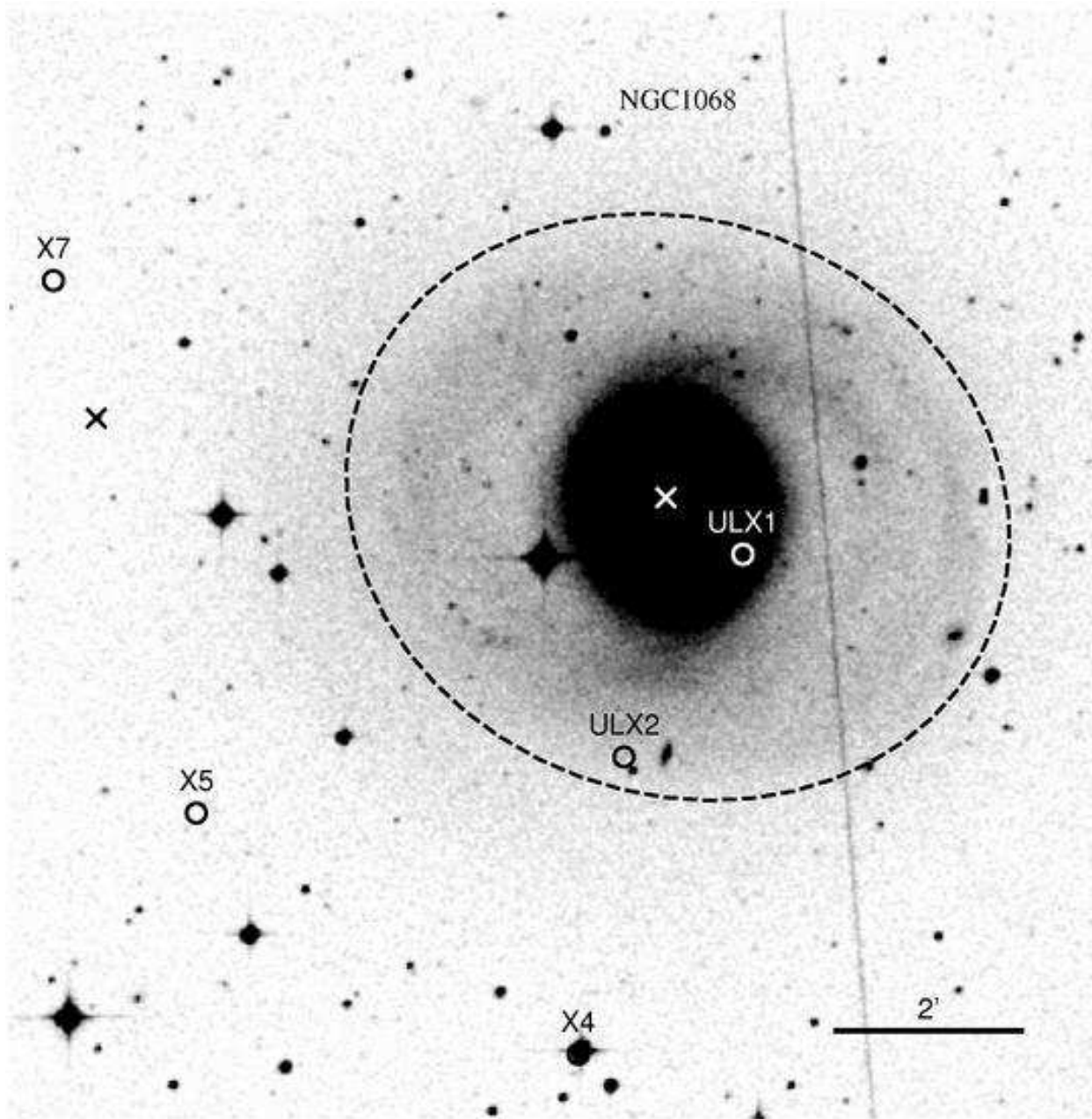


Fig. 20.— The finding chart for the ULXs in NGC1068.

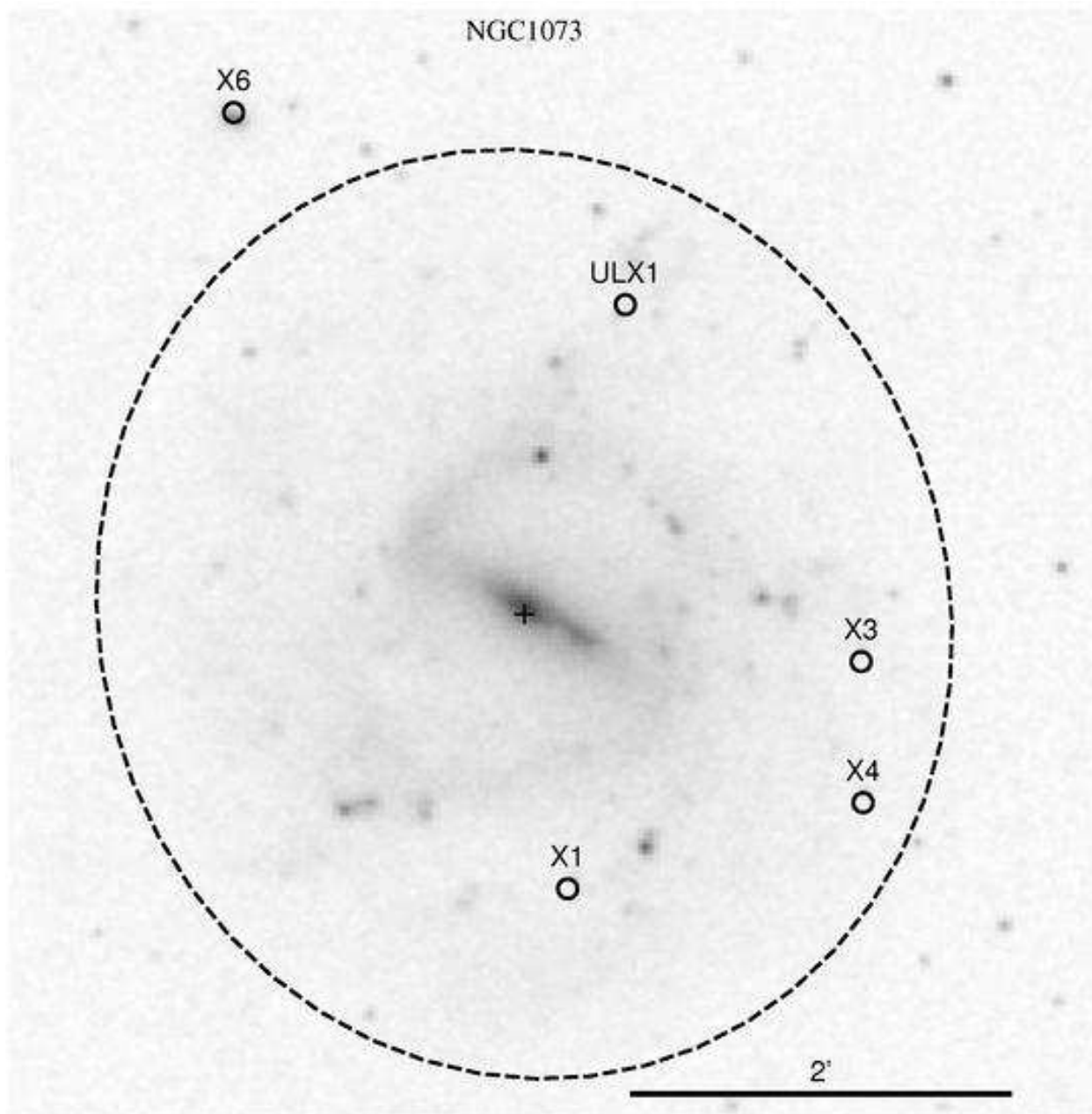


Fig. 21.— The finding chart for the ULXs in NGC1073.

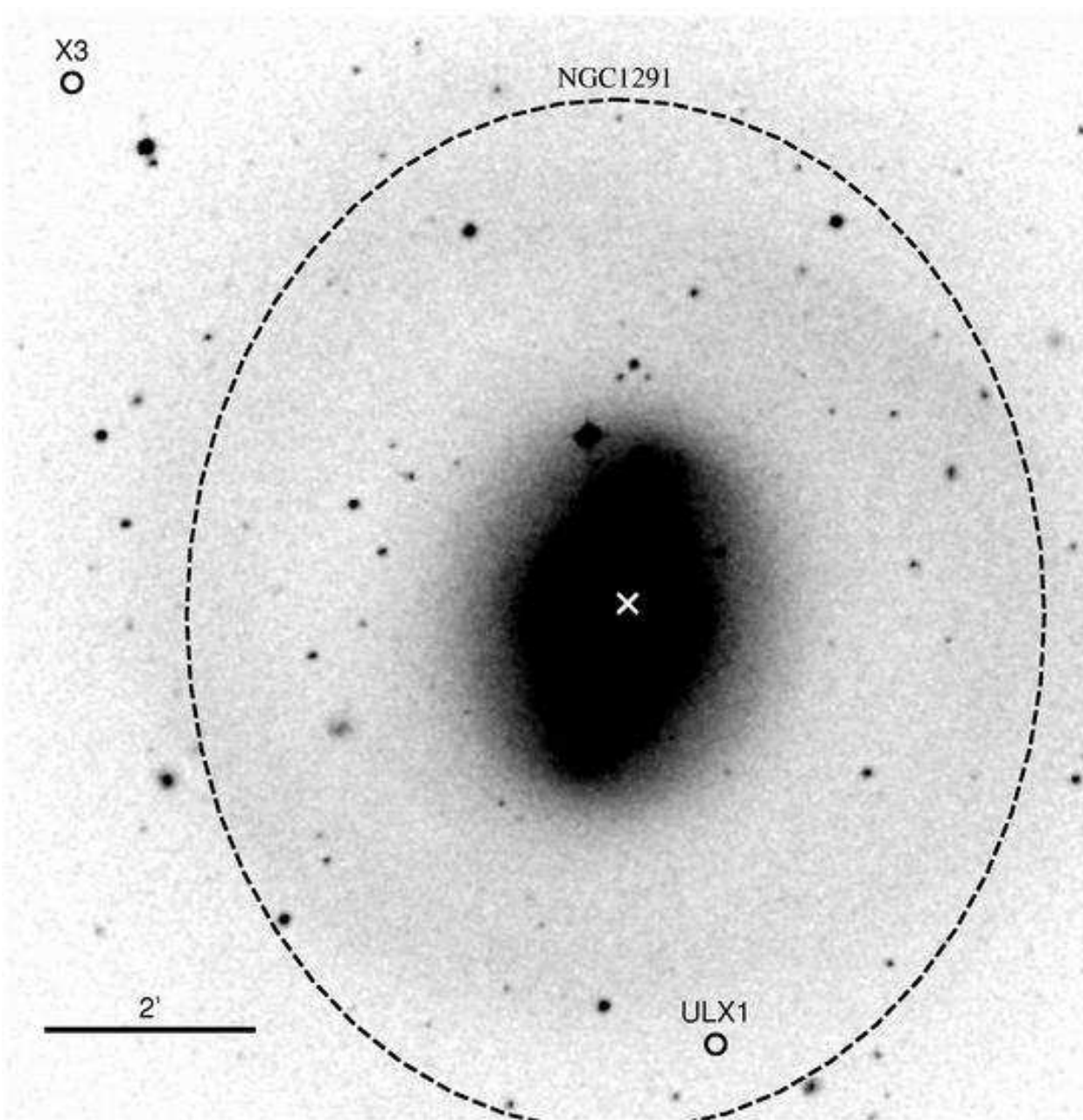


Fig. 22.— The finding chart for the ULXs in NGC1291.

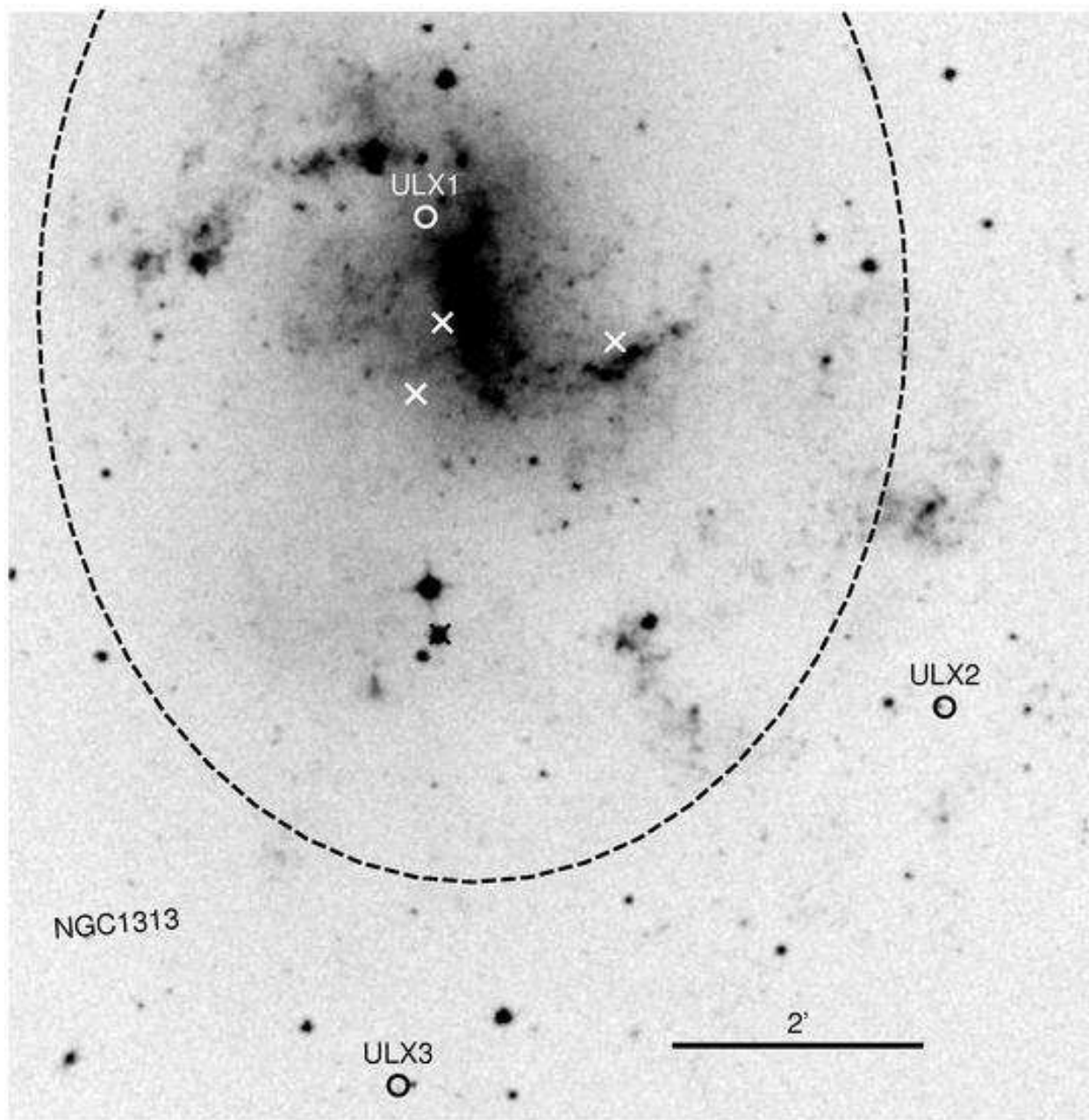


Fig. 23.— The finding chart for the ULXs in NGC1313.

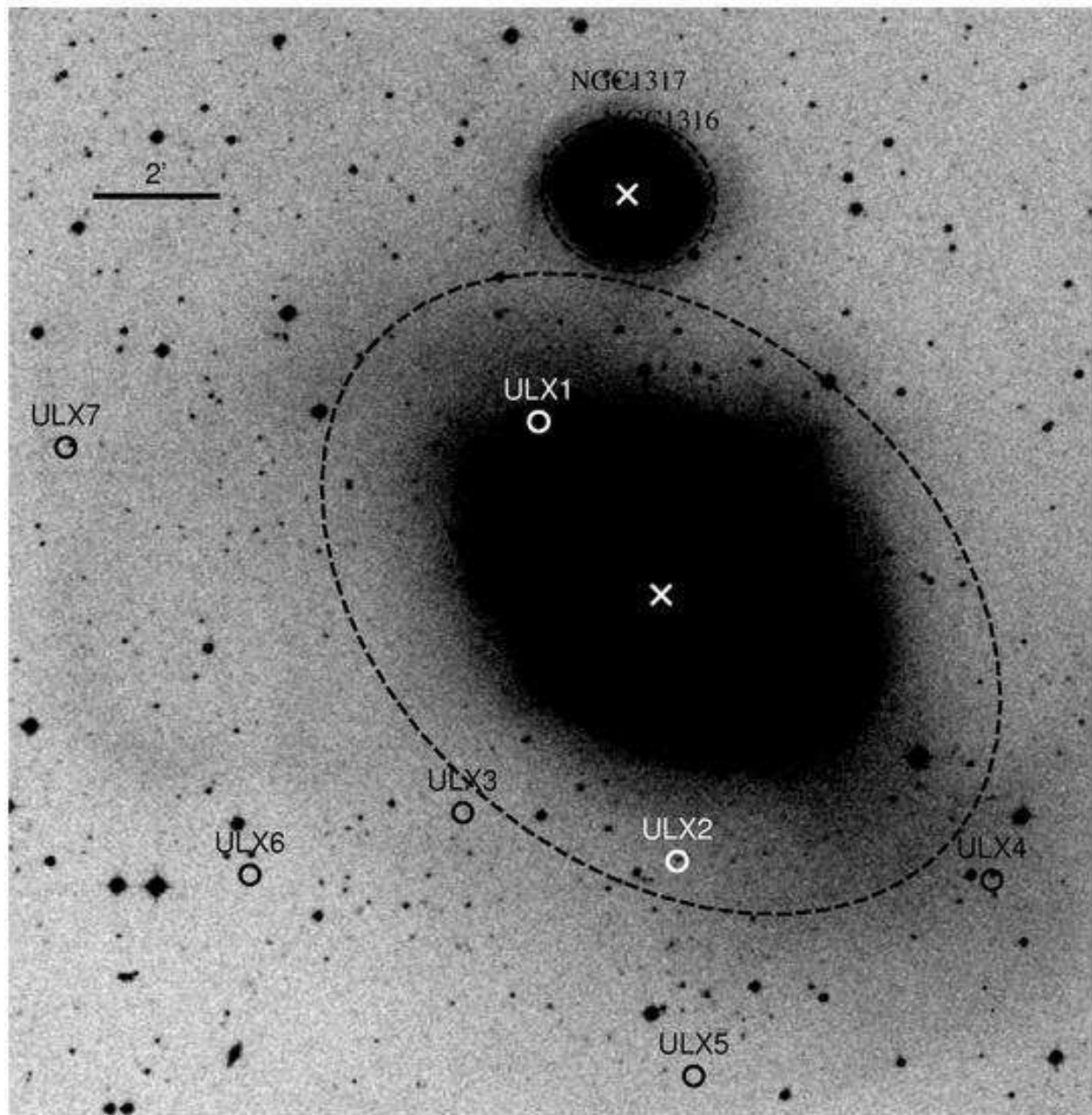


Fig. 24.— The finding chart for the ULXs in NGC1316.

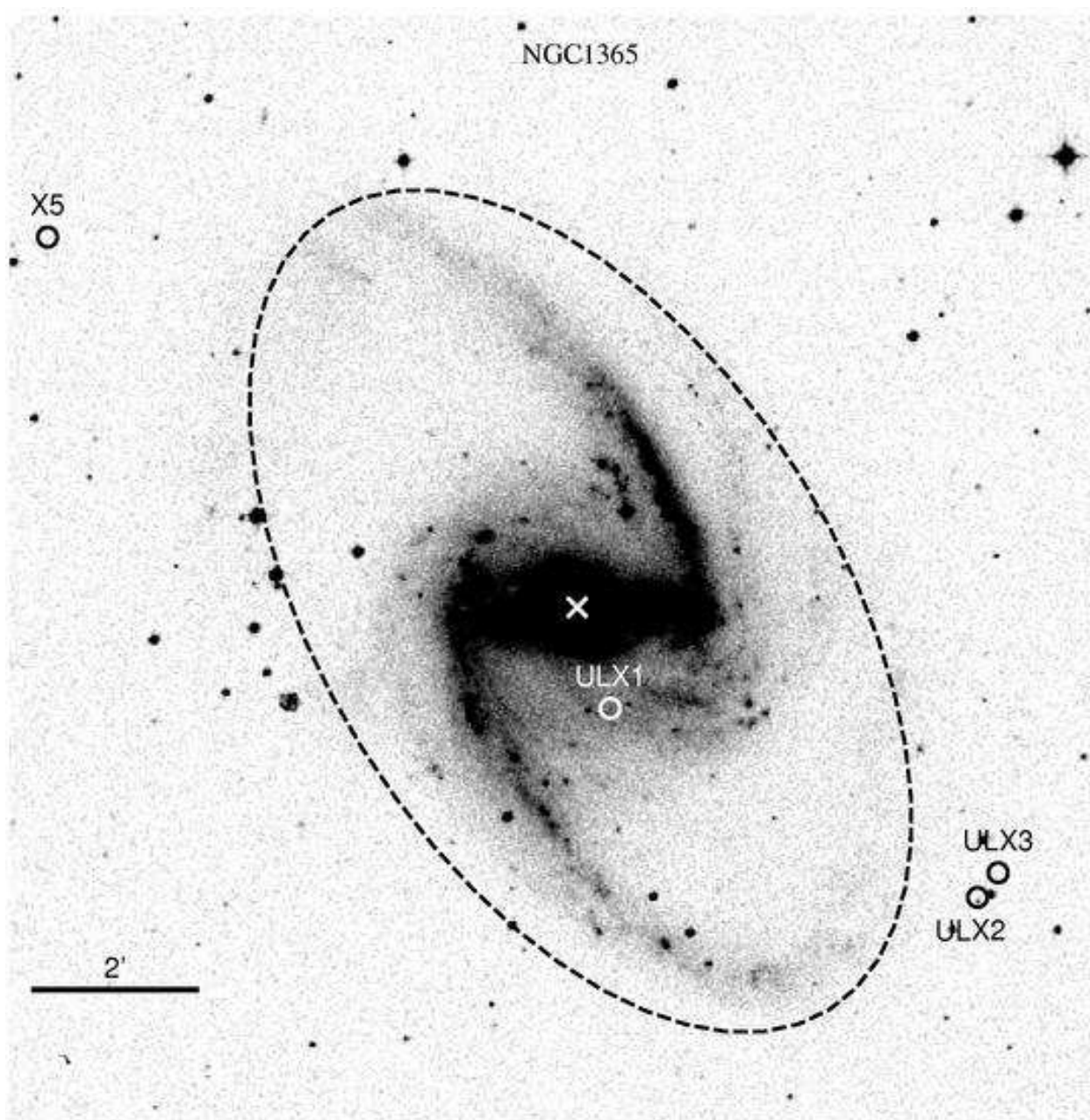


Fig. 25.— The finding chart for the ULXs in NGC1365.

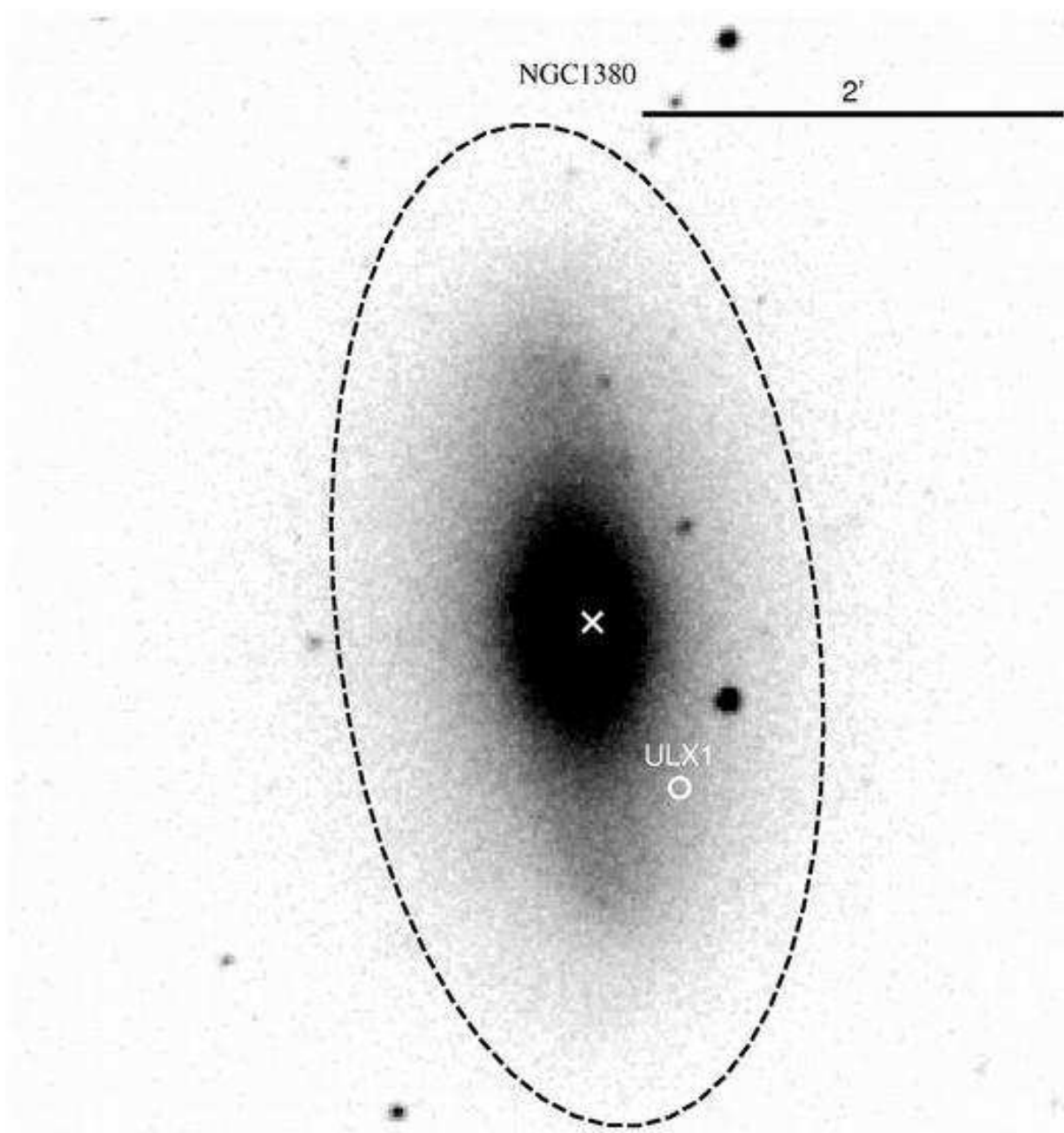


Fig. 26.— The finding chart for the ULXs in NGC1380.

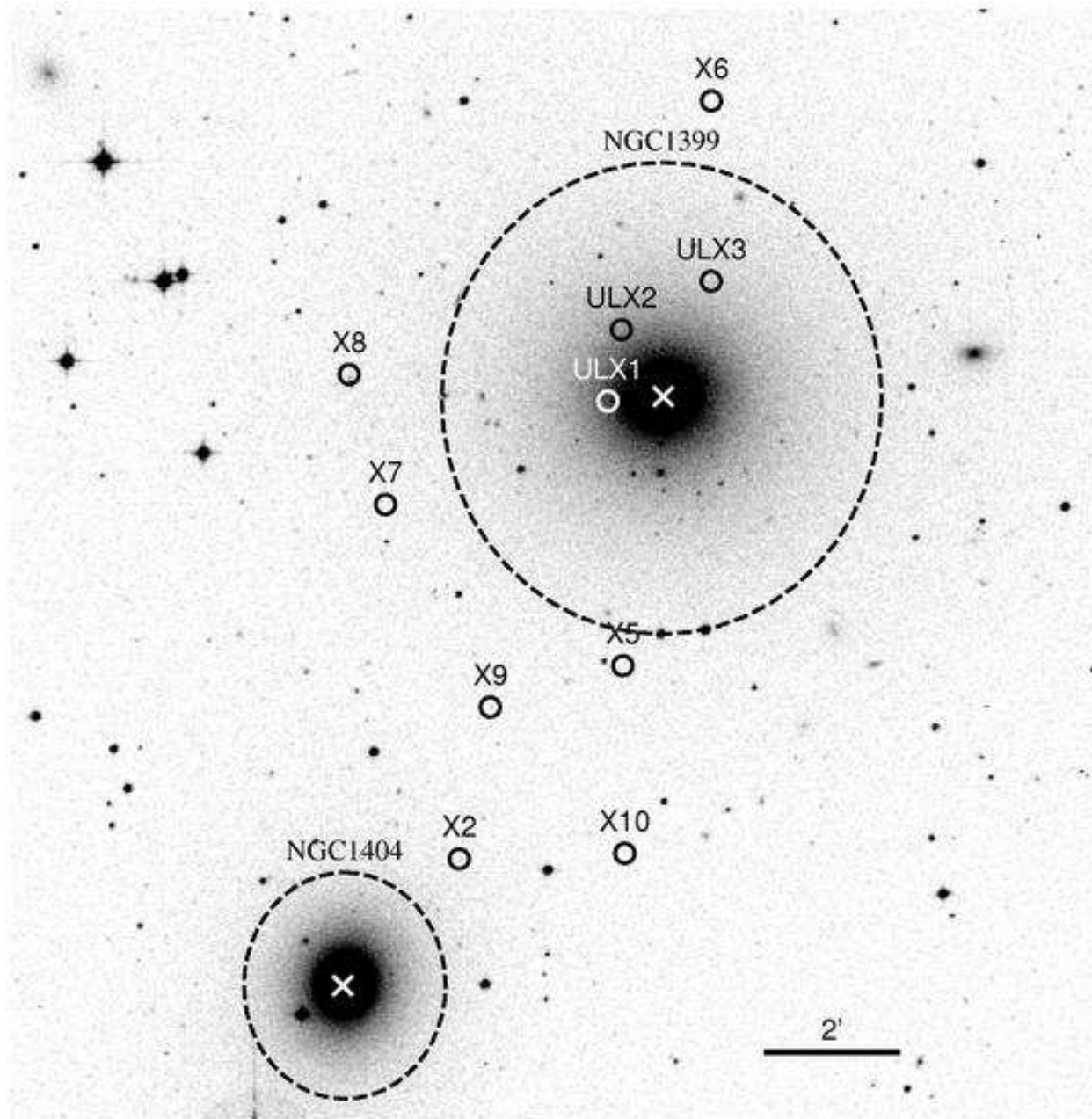


Fig. 27.— The finding chart for the ULXs in NGC1399.

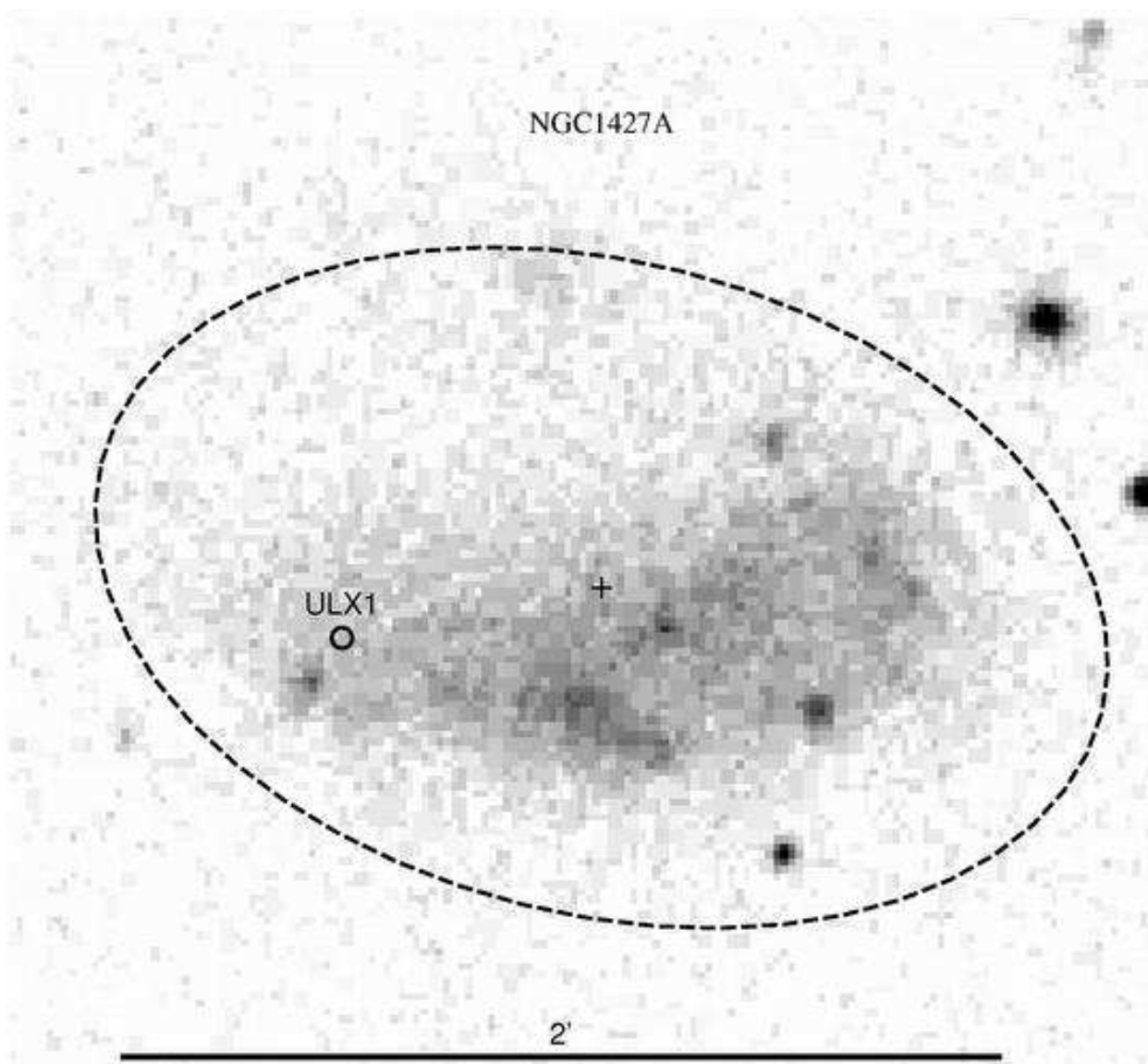


Fig. 28.— The finding chart for the ULXs in NGC1427A.

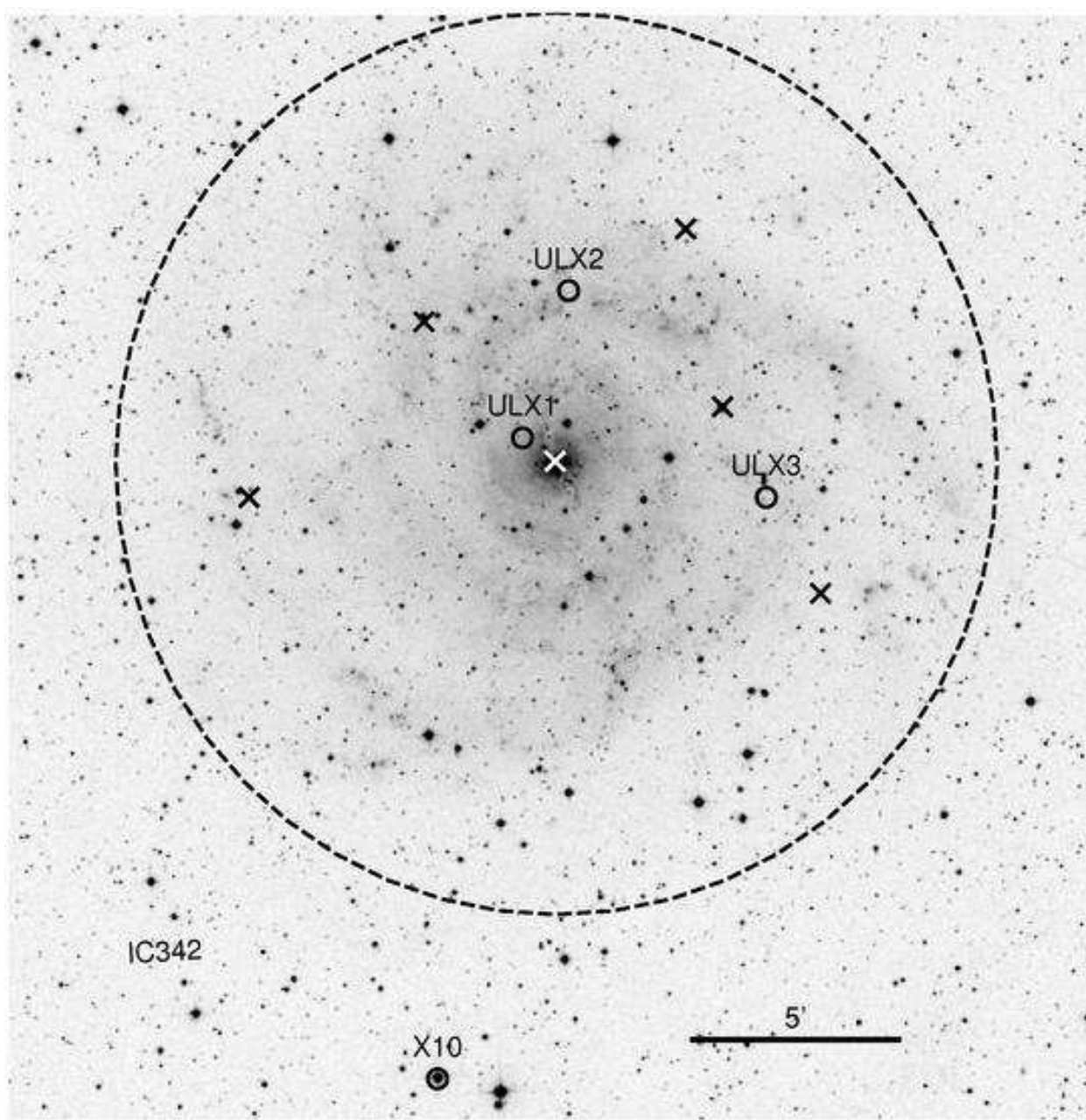


Fig. 29.— The finding chart for the ULXs in PGC13826 (IC342).

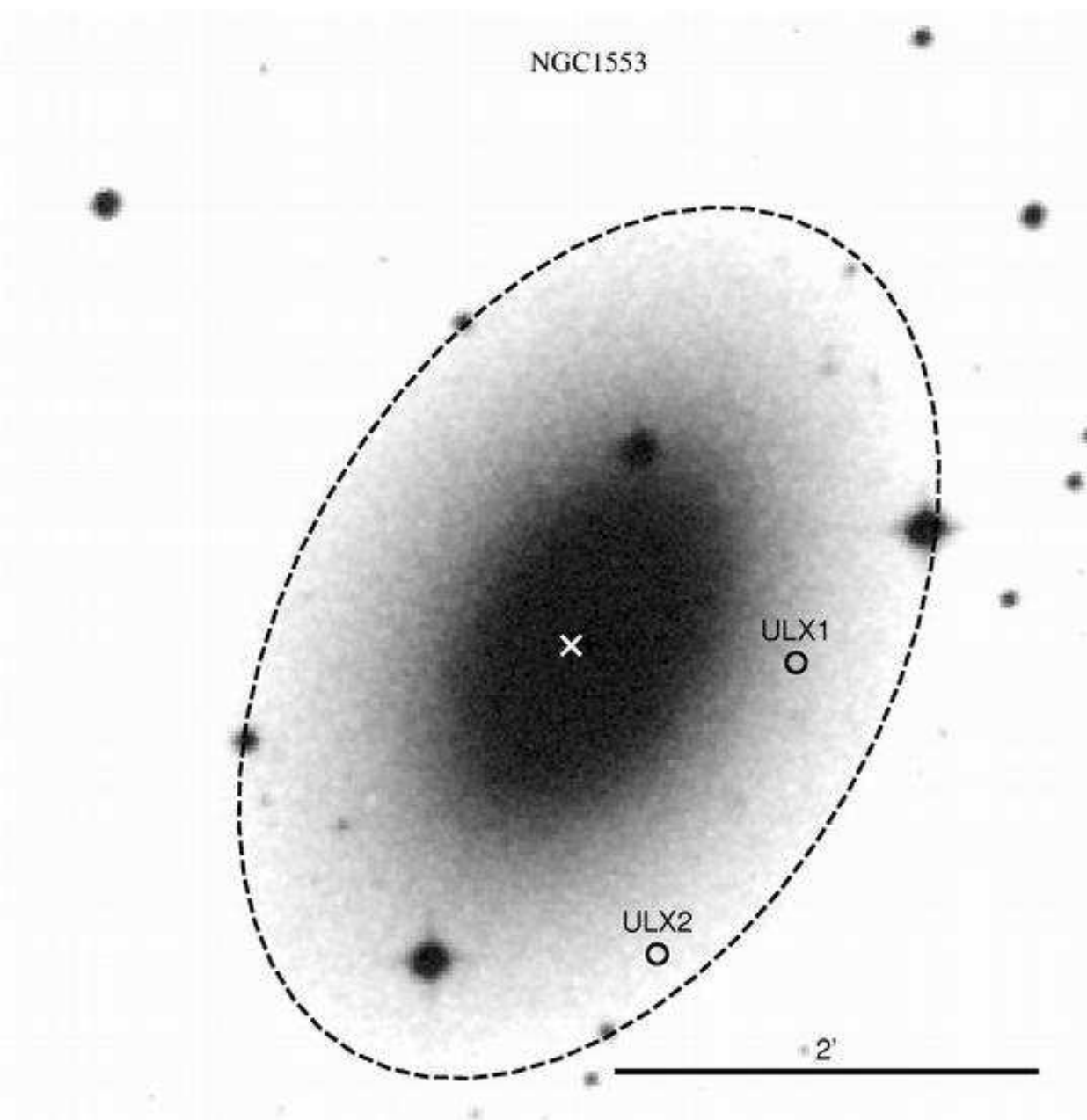


Fig. 30.— The finding chart for the ULXs in NGC1553.

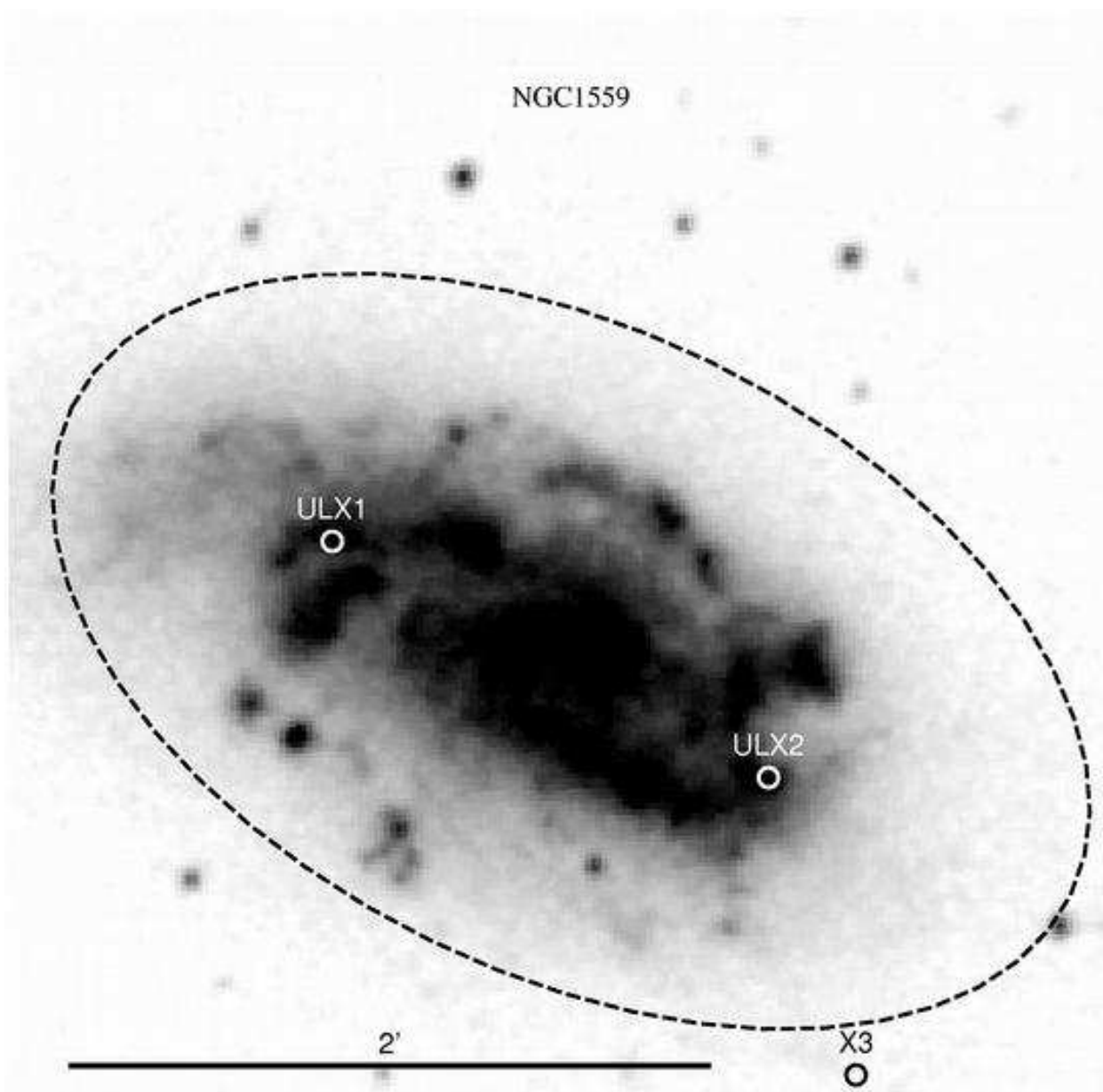


Fig. 31.— The finding chart for the ULXs in NGC1559.

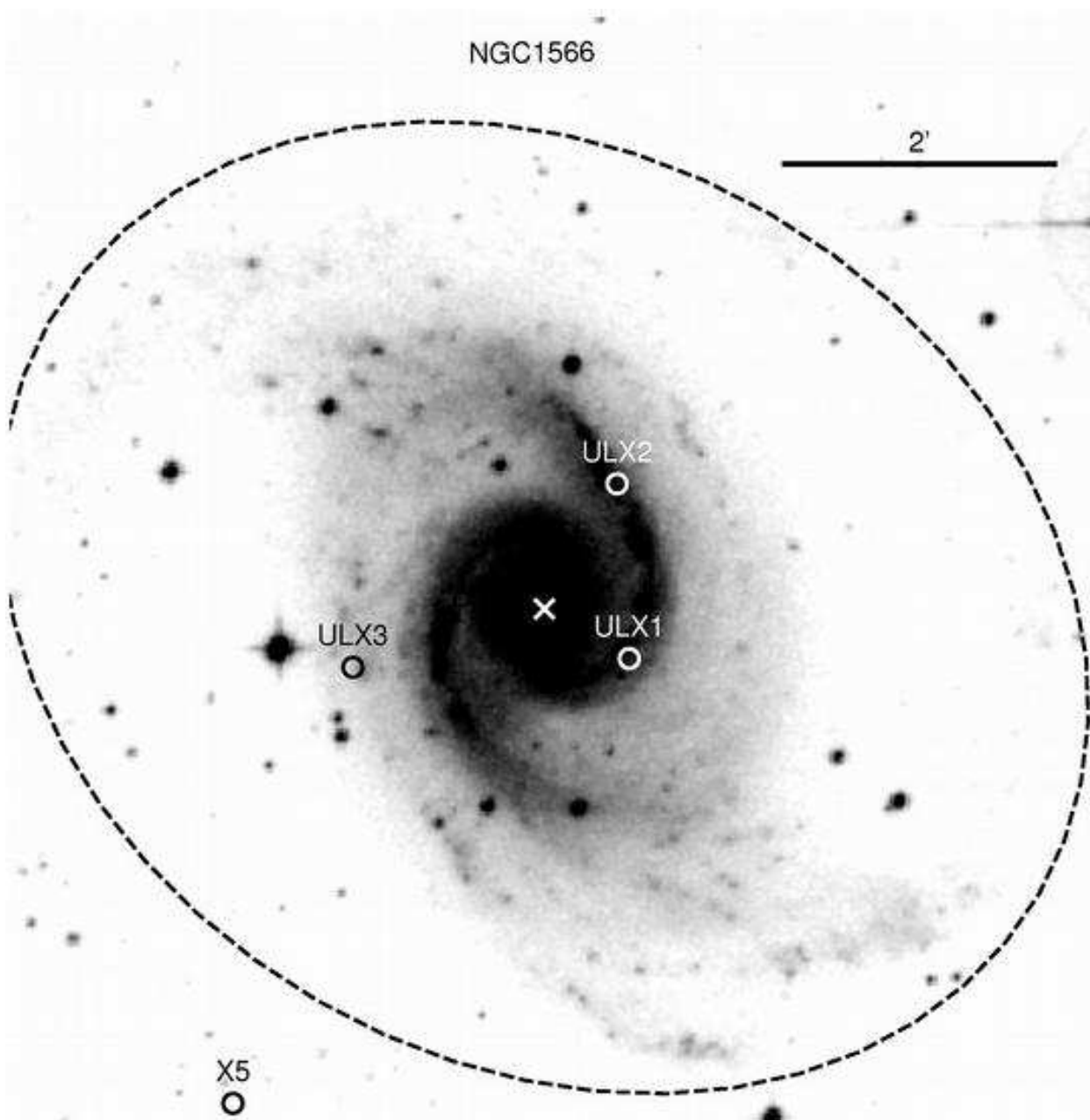


Fig. 32.— The finding chart for the ULXs in NGC1566.

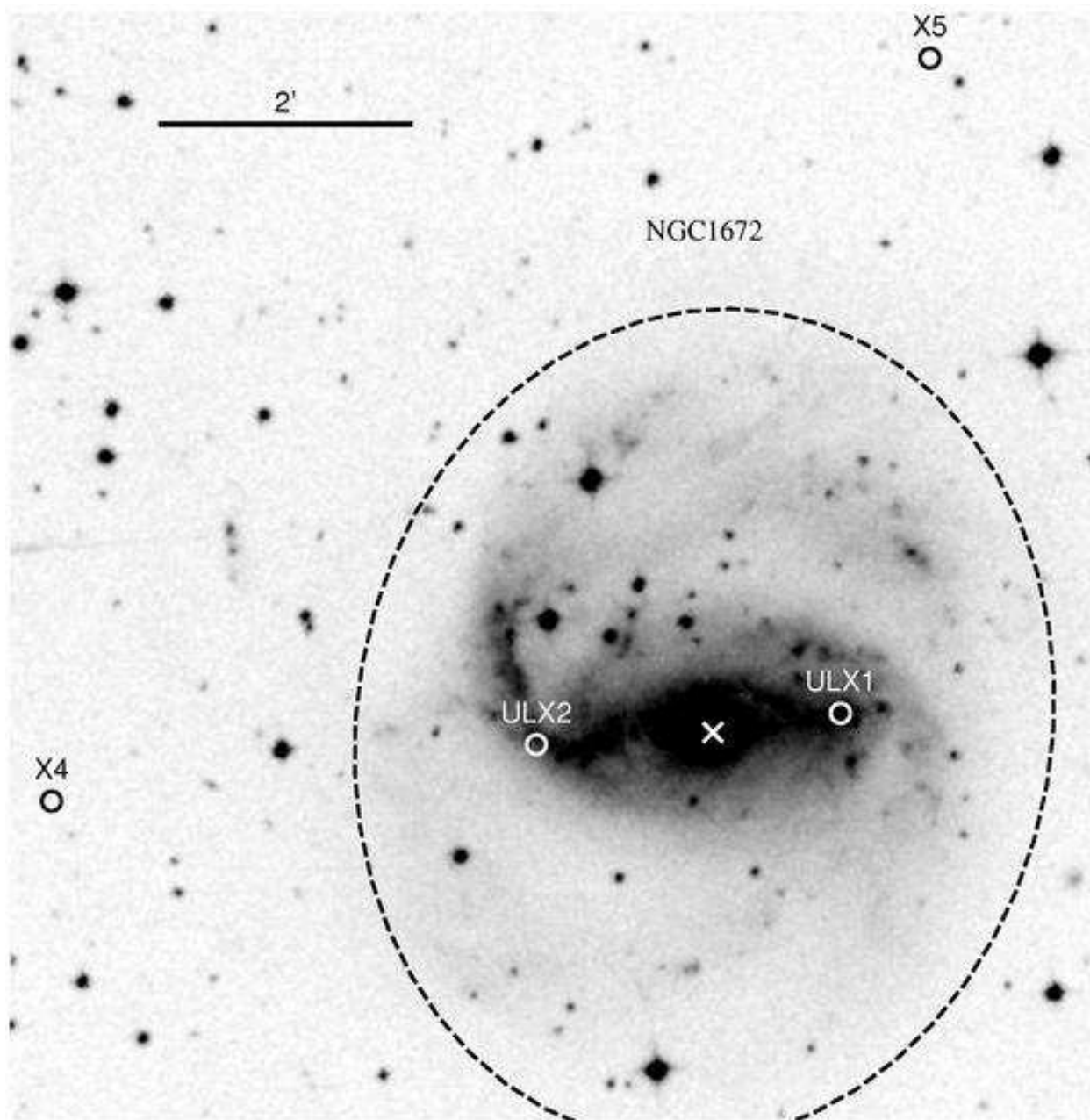


Fig. 33.— The finding chart for the ULXs in NGC1672.

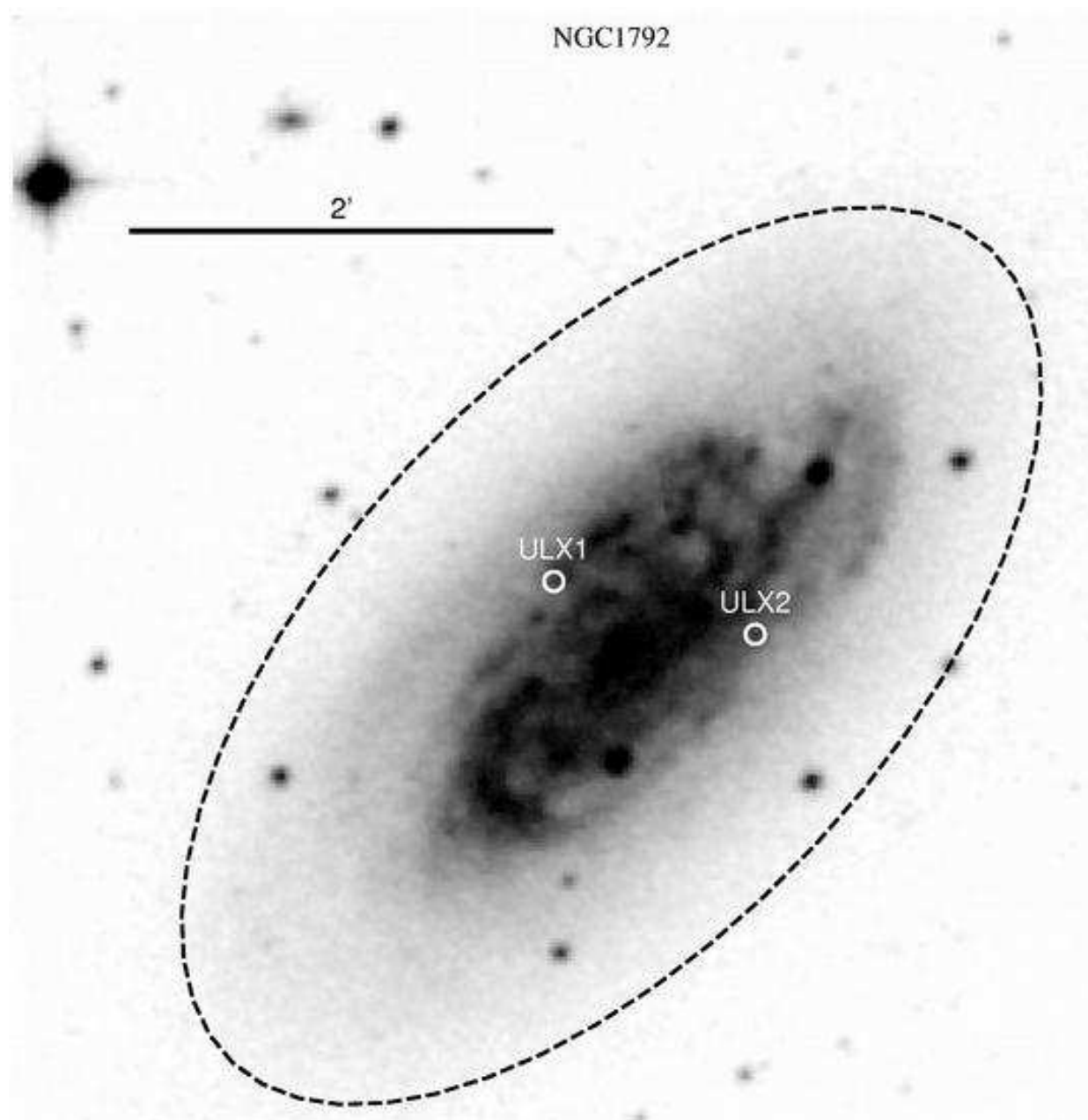


Fig. 34.— The finding chart for the ULXs in NGC1792.

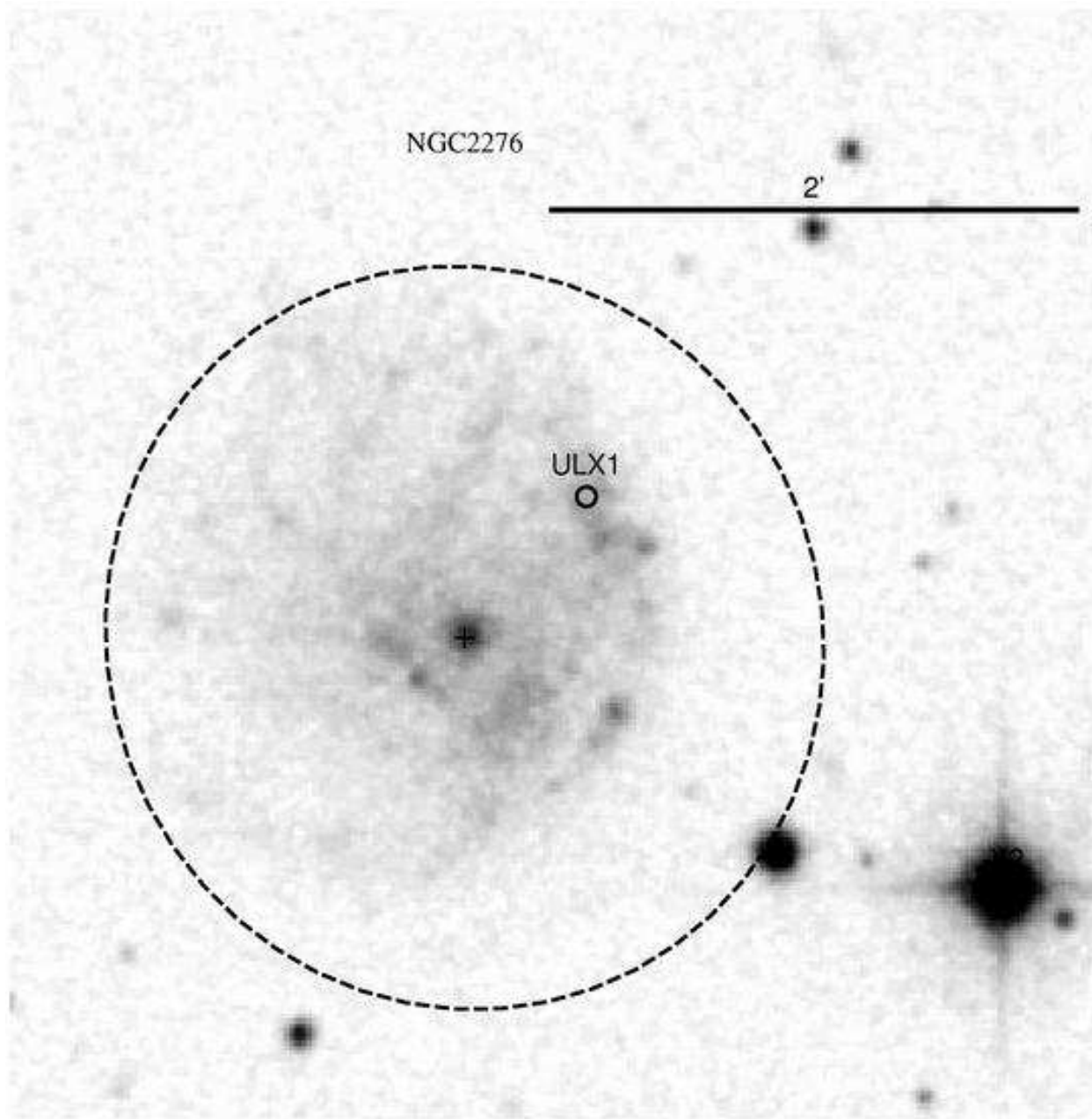


Fig. 35.— The finding chart for the ULXs in NGC2276.

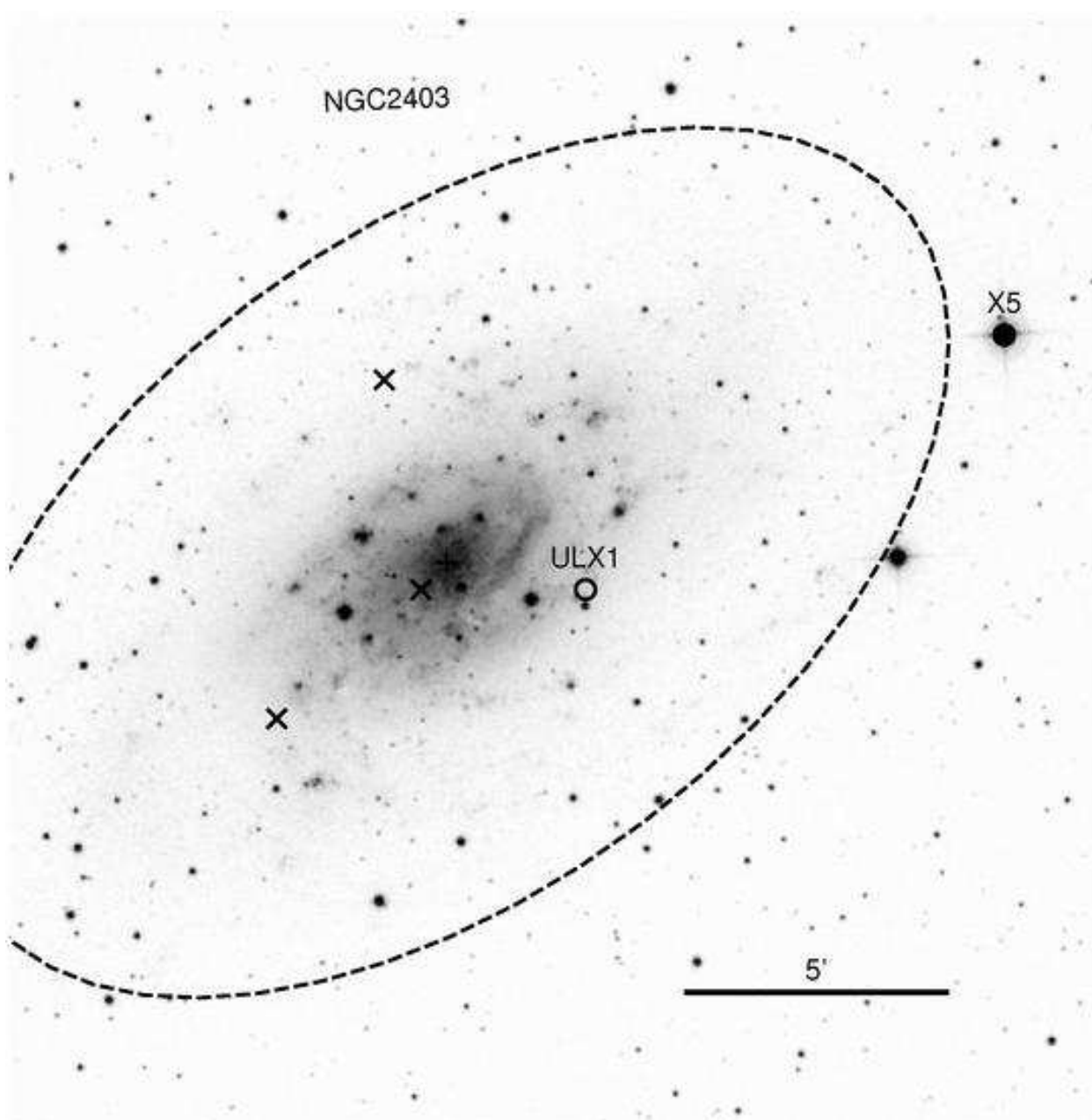


Fig. 36.— The finding chart for the ULXs in NGC2403.

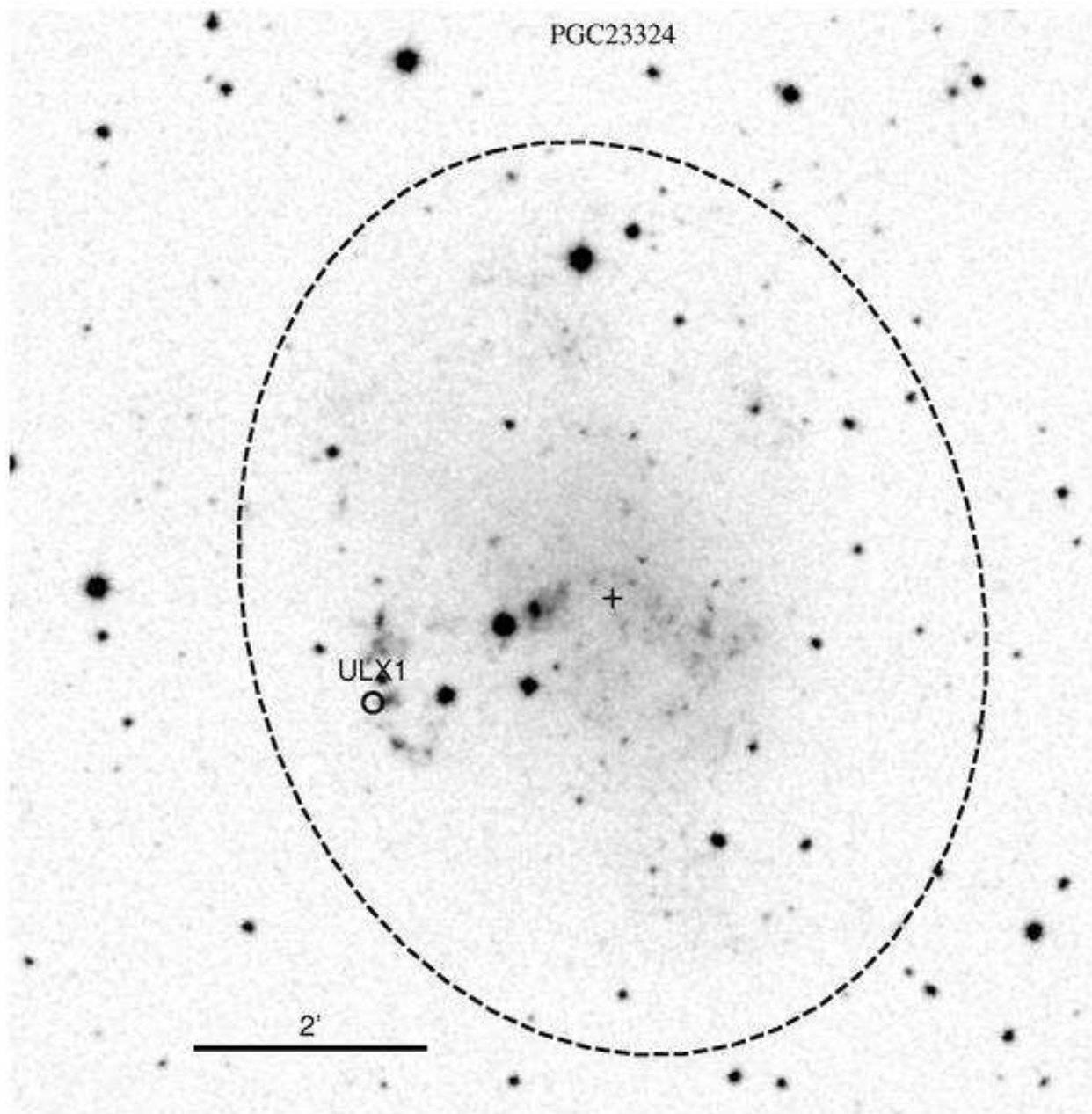


Fig. 37.— The finding chart for the ULXs in PGC23324 (Holmberg II).

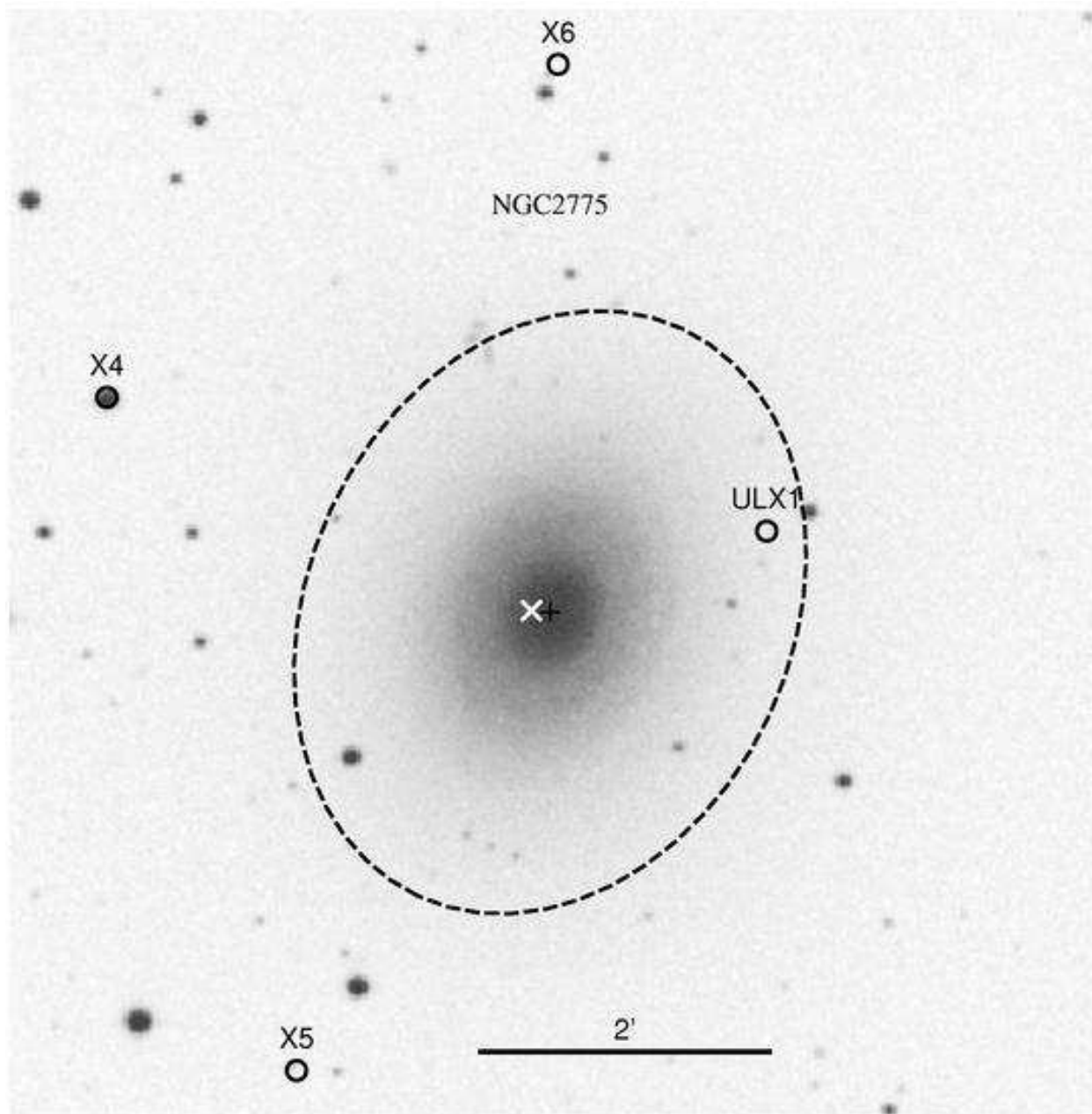


Fig. 38.— The finding chart for the ULXs in NGC2775.

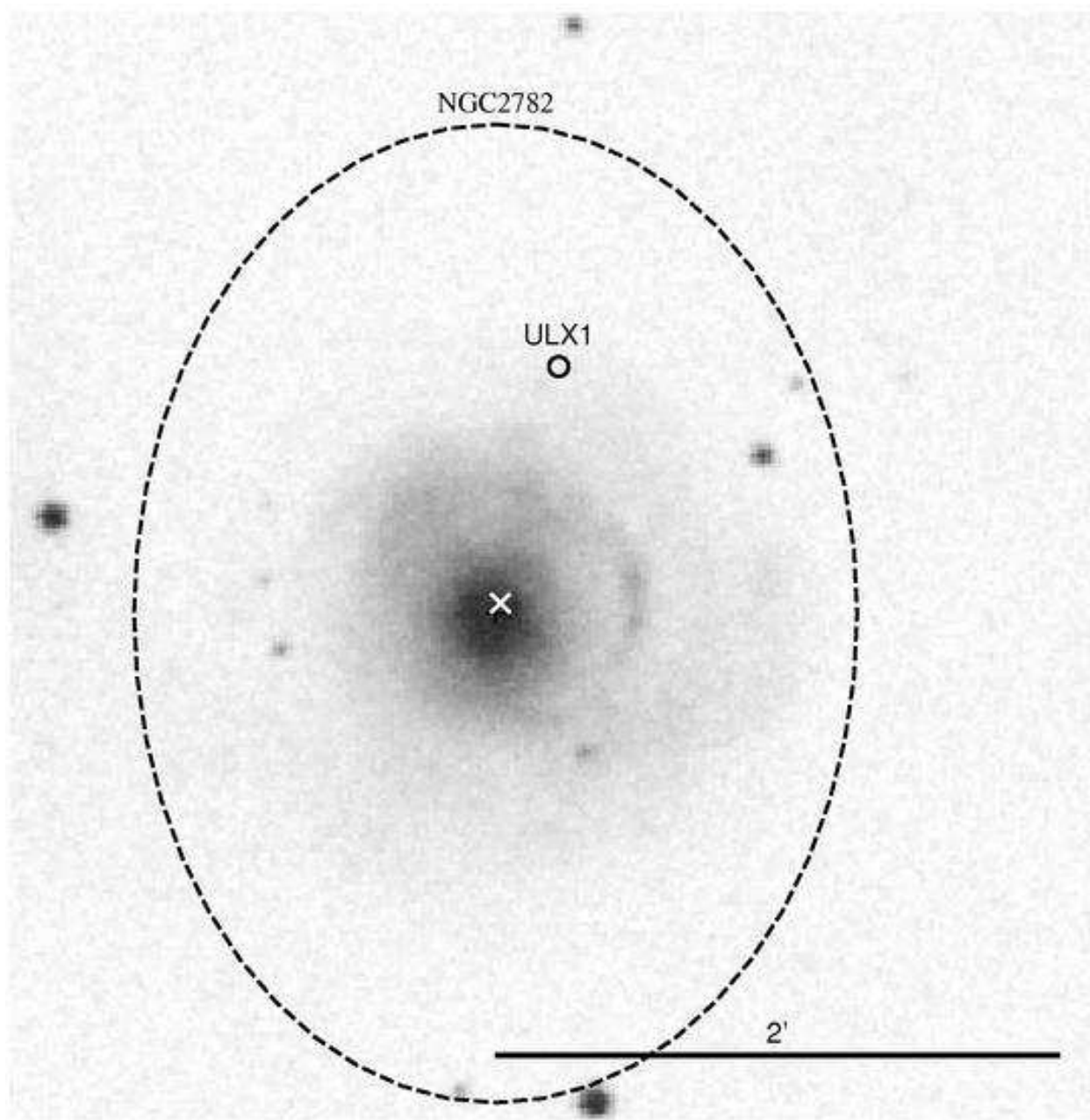


Fig. 39.— The finding chart for the ULXs in NGC2782.

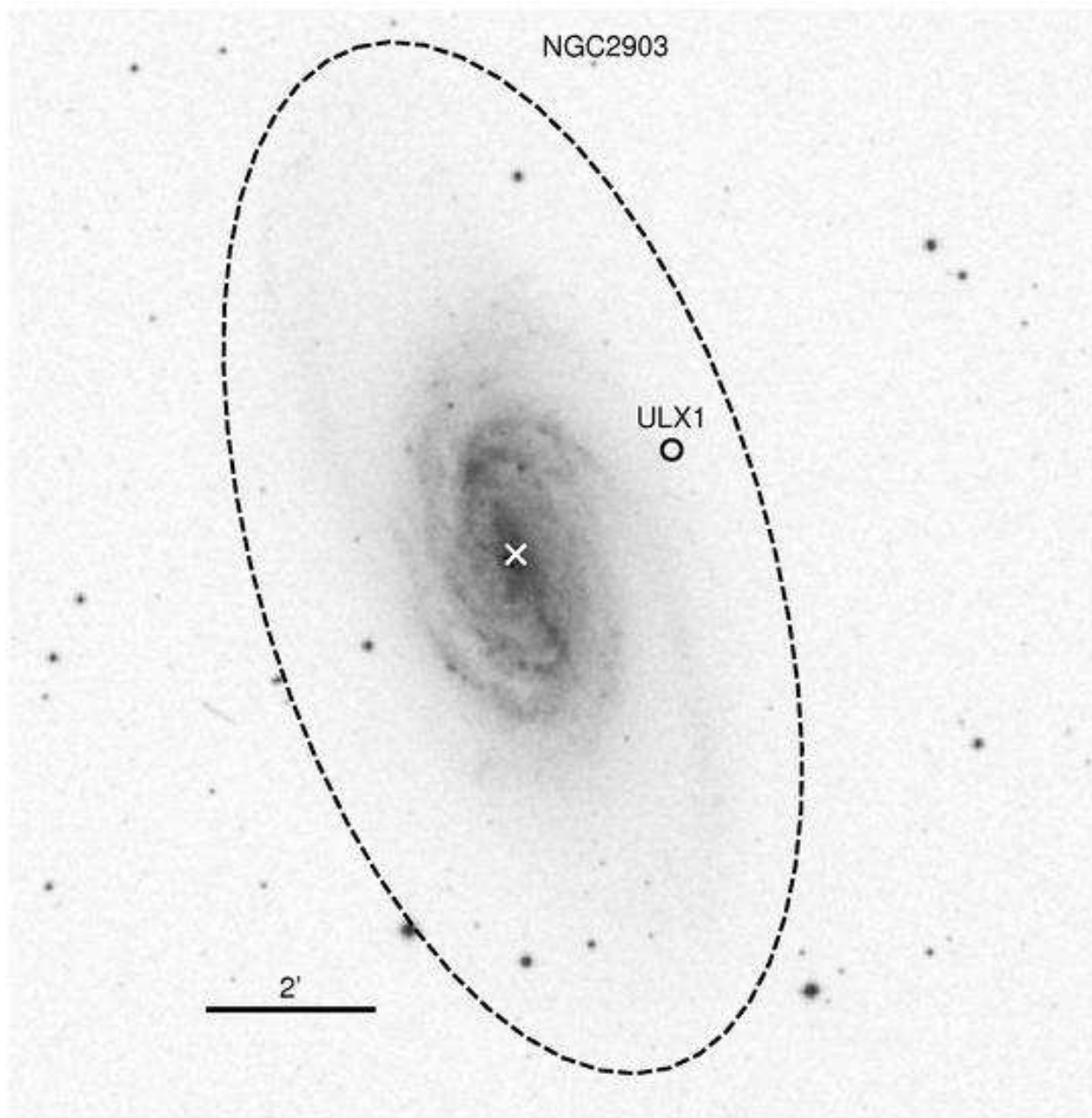


Fig. 40.— The finding chart for the ULXs in NGC2903.

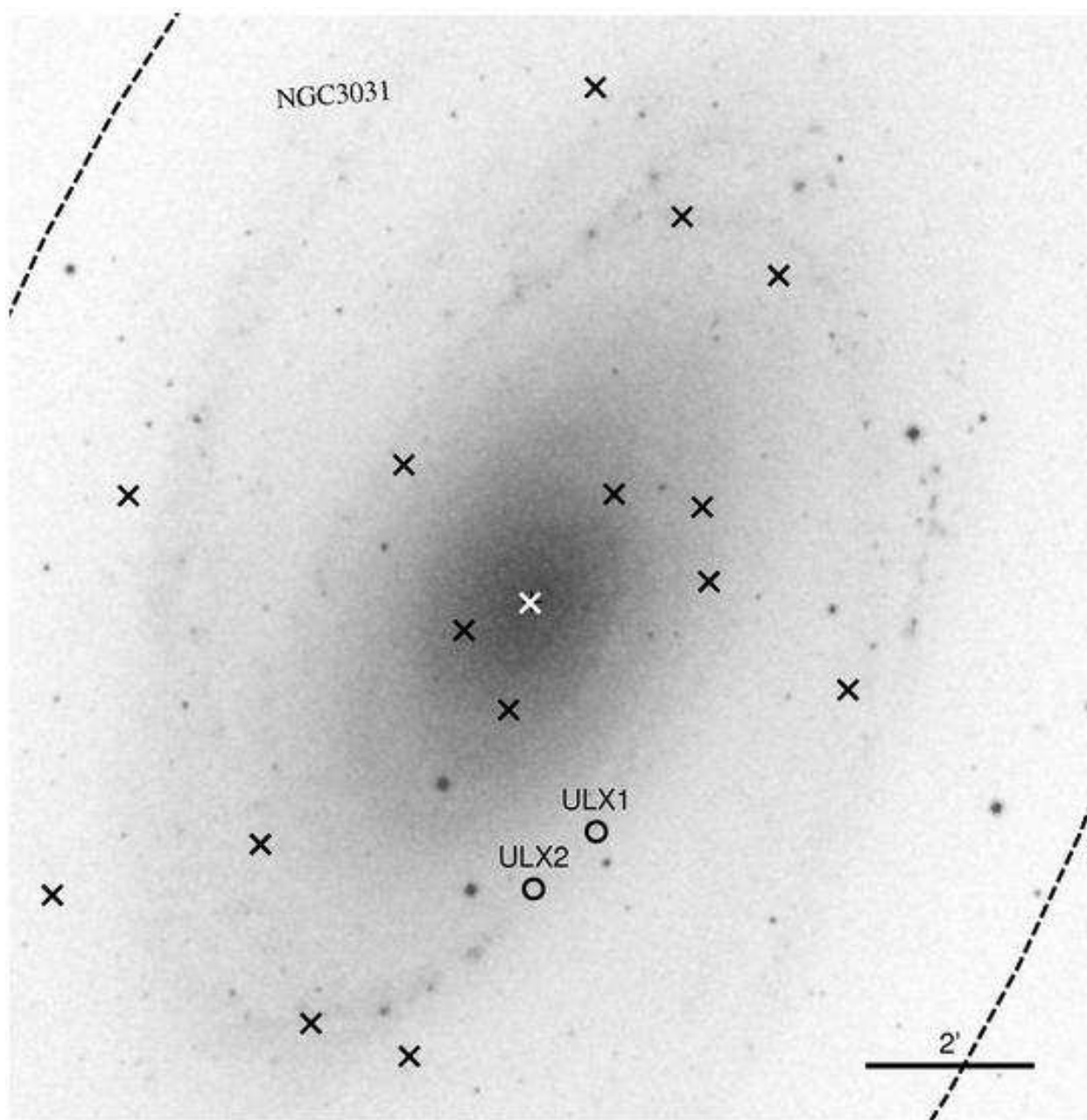


Fig. 41.— The finding chart for the ULXs in NGC3031.

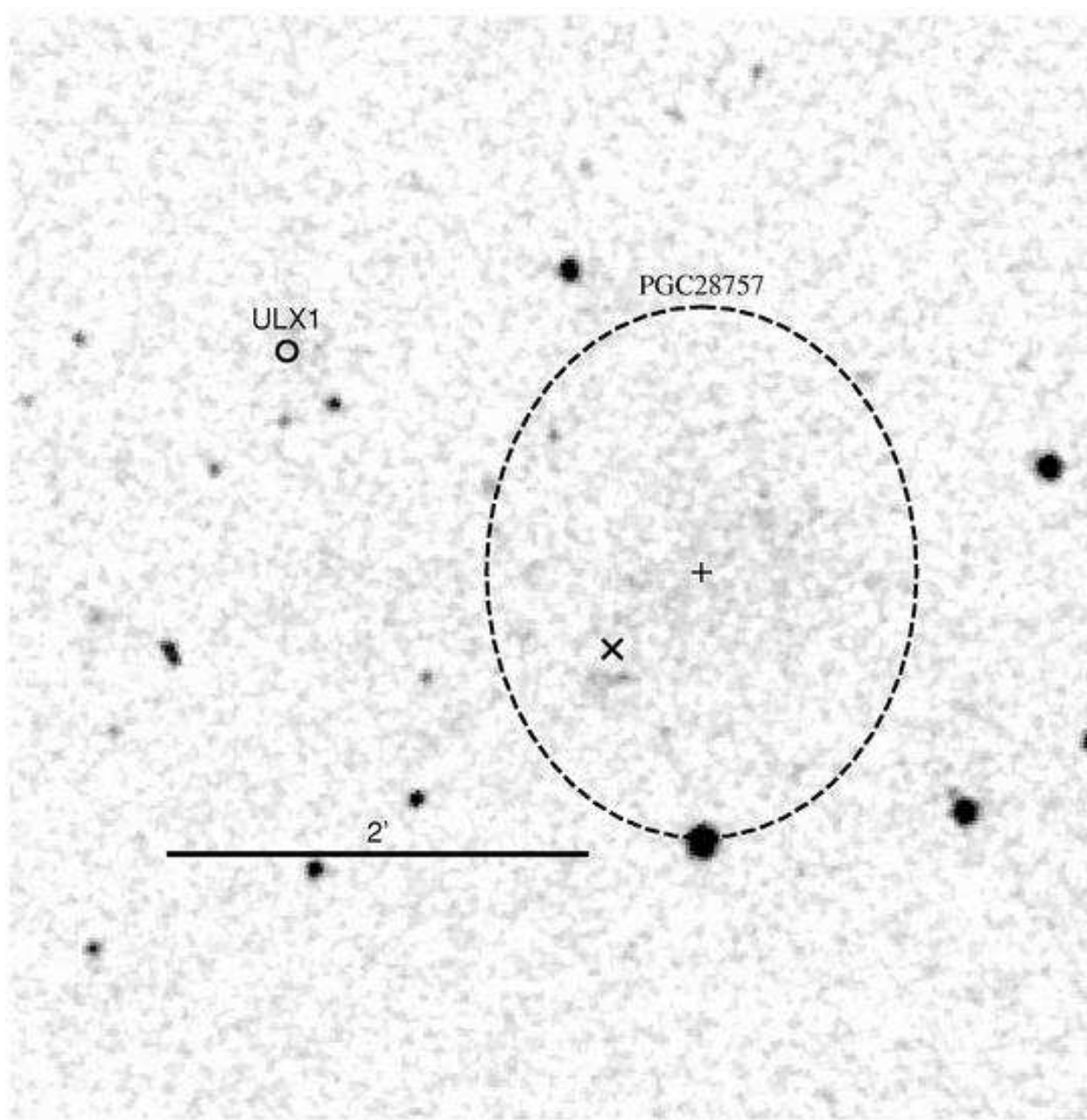


Fig. 42.— The finding chart for the ULXs in PGC28757 (Holmberg IX).

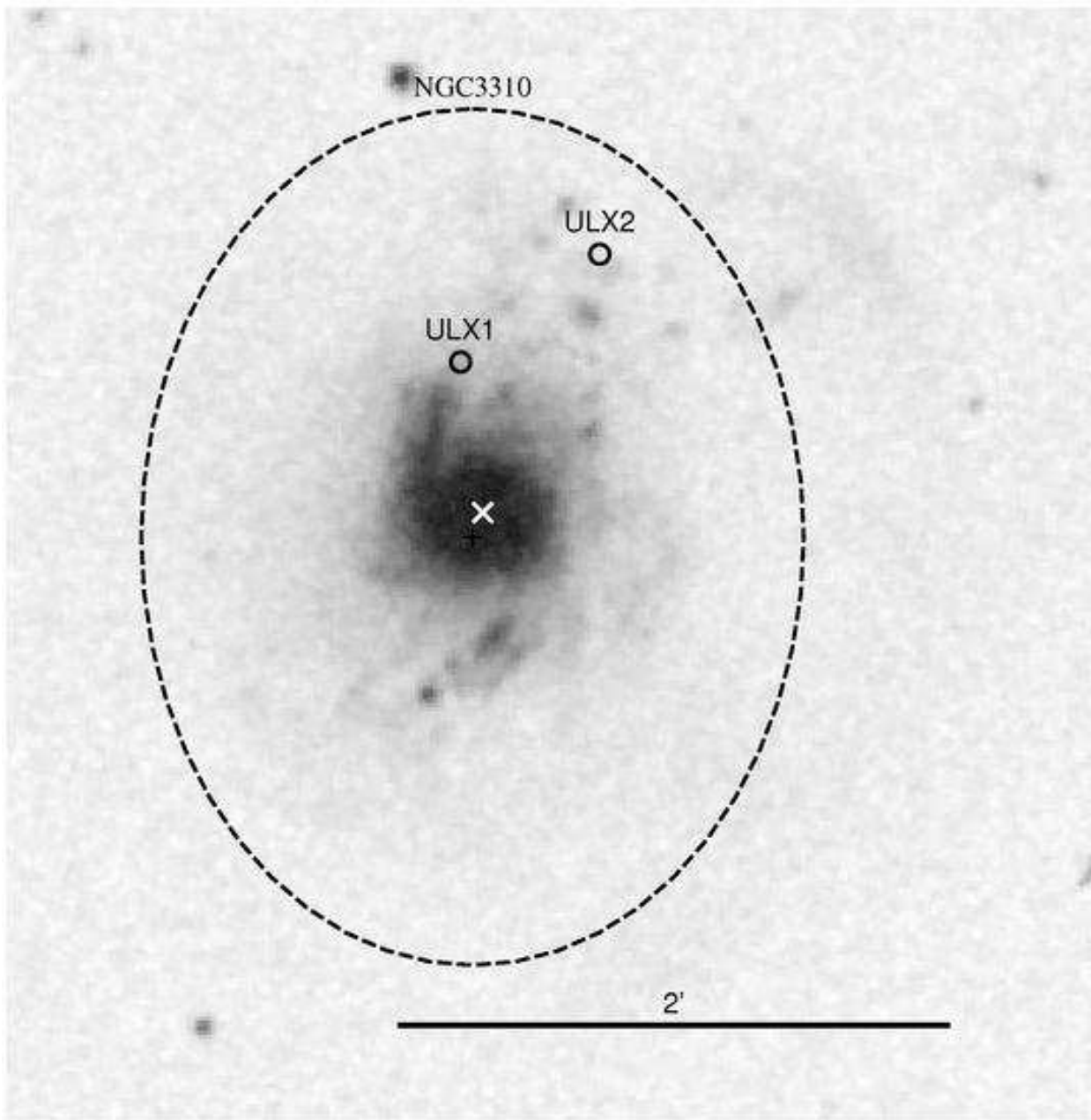


Fig. 43.— The finding chart for the ULXs in NGC3310.

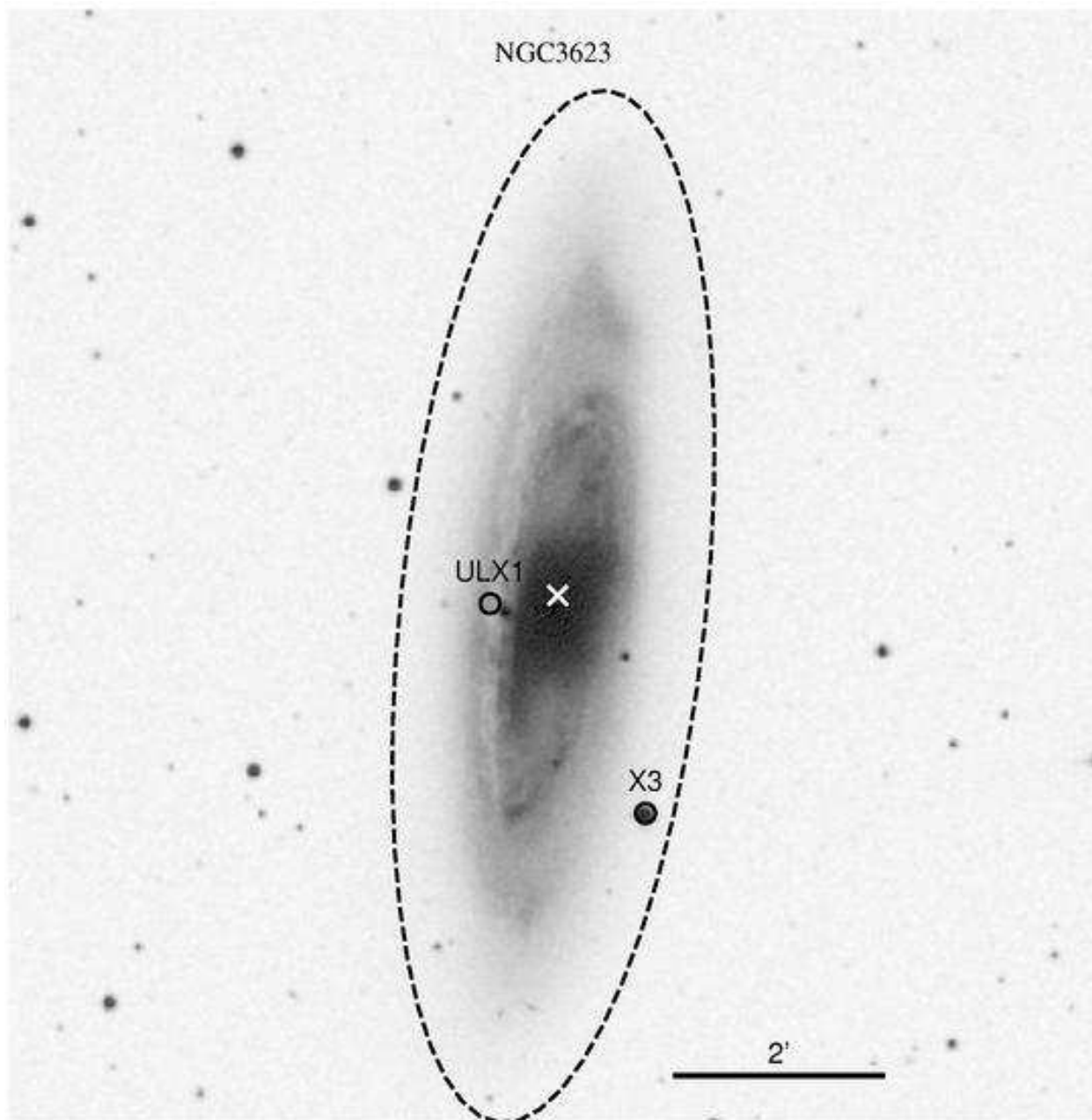


Fig. 44.— The finding chart for the ULXs in NGC3623.

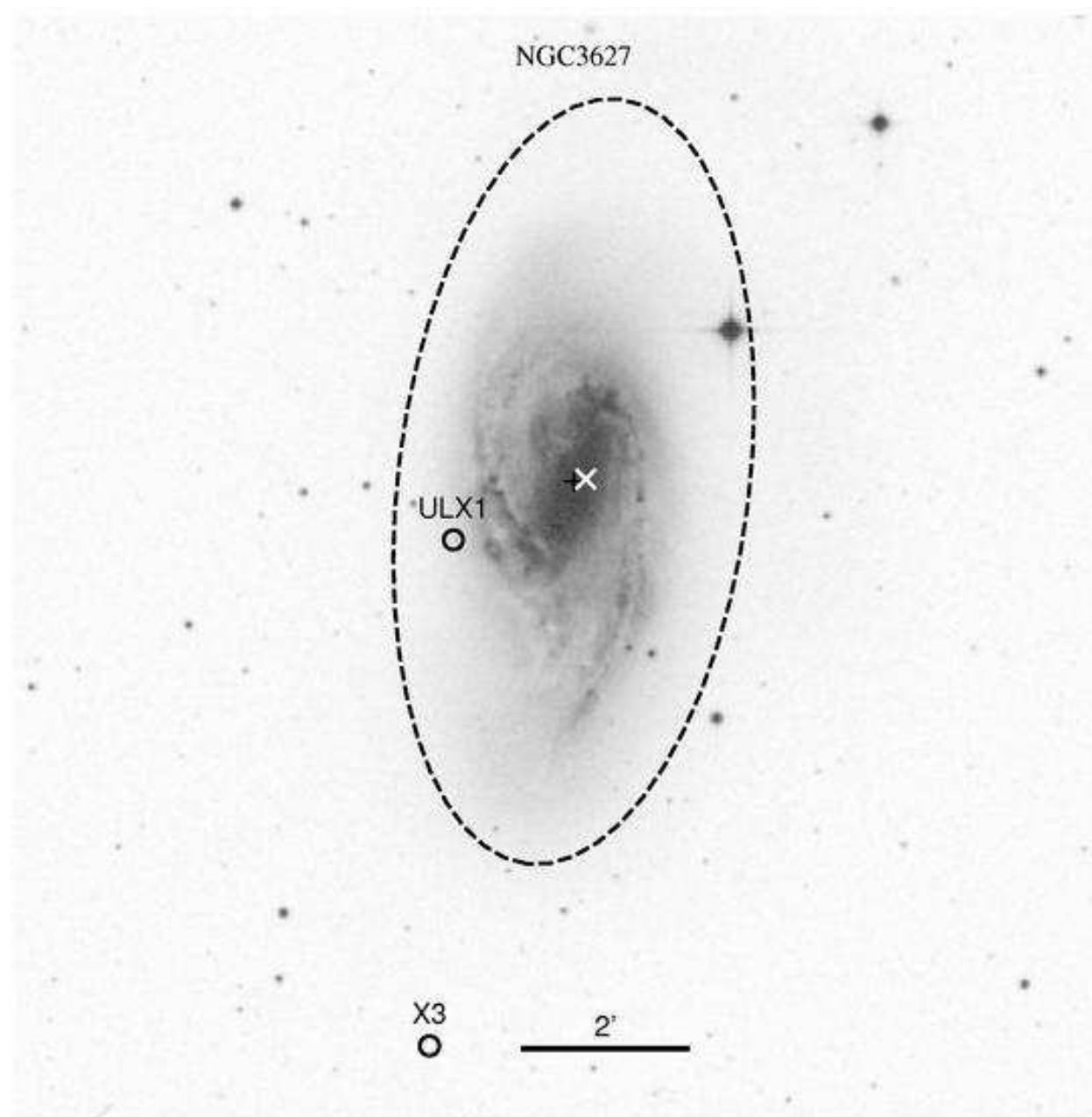


Fig. 45.— The finding chart for the ULXs in NGC3627.

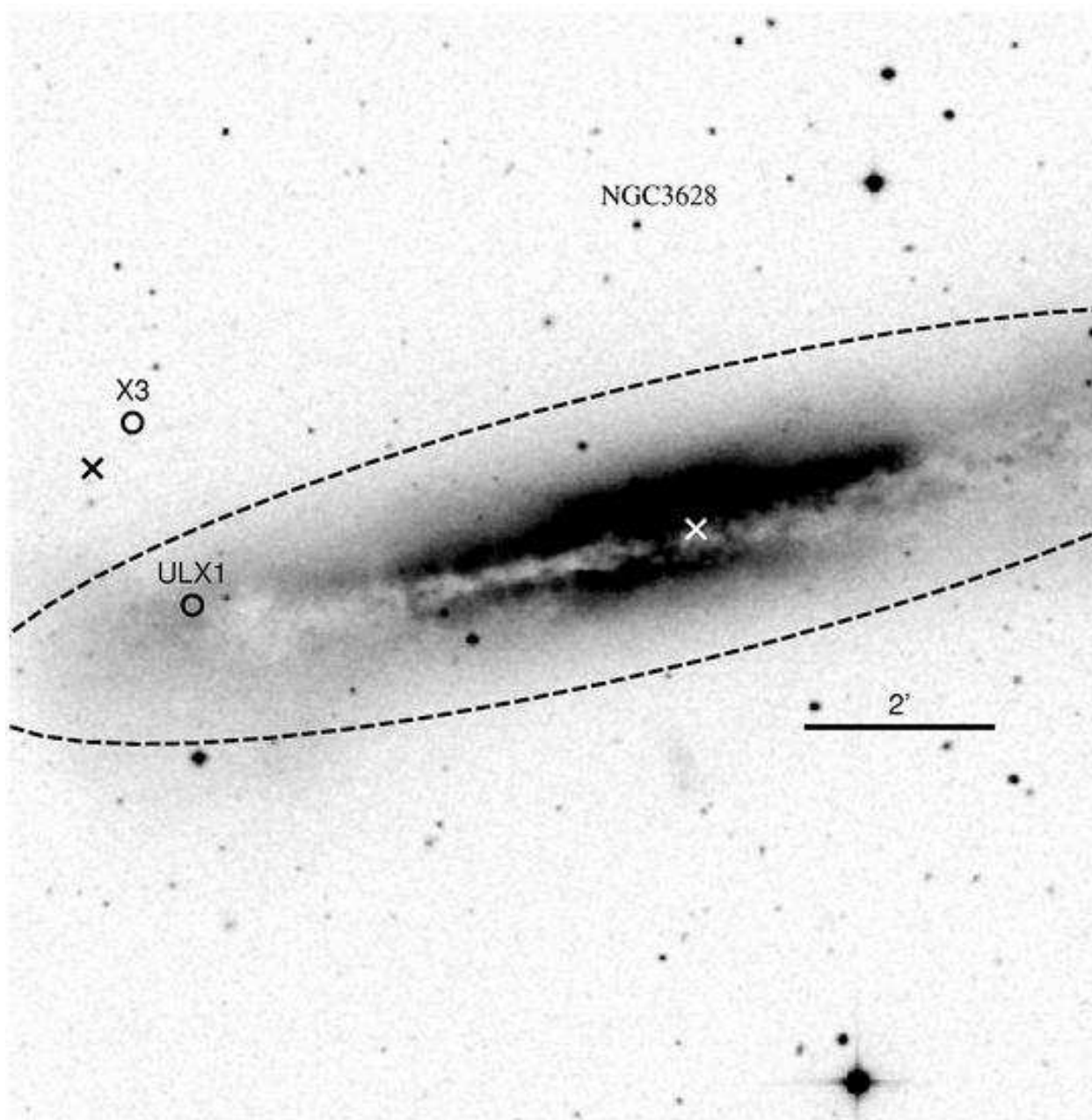


Fig. 46.— The finding chart for the ULXs in NGC3628.

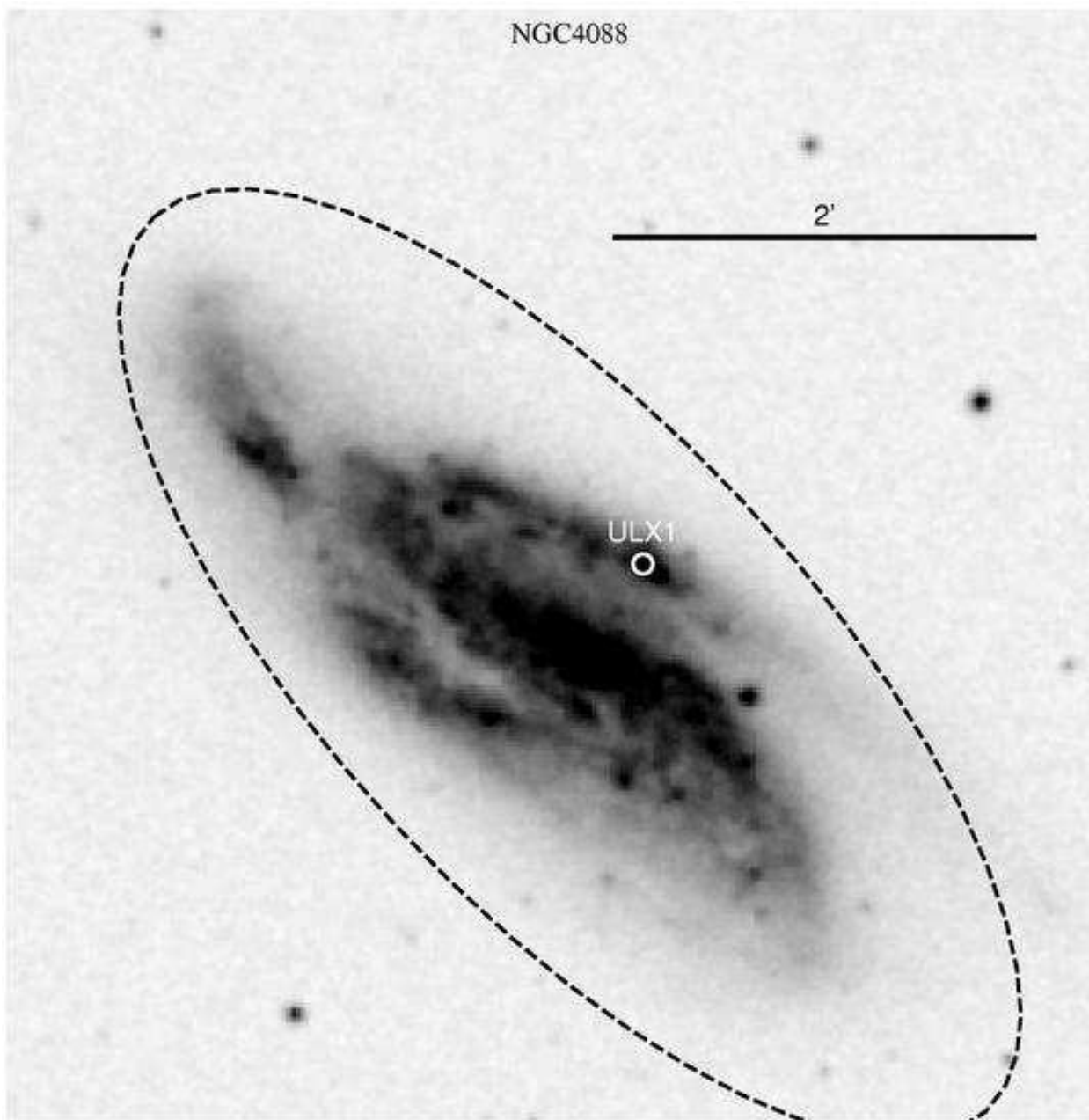


Fig. 47.— The finding chart for the ULXs in NGC4088.

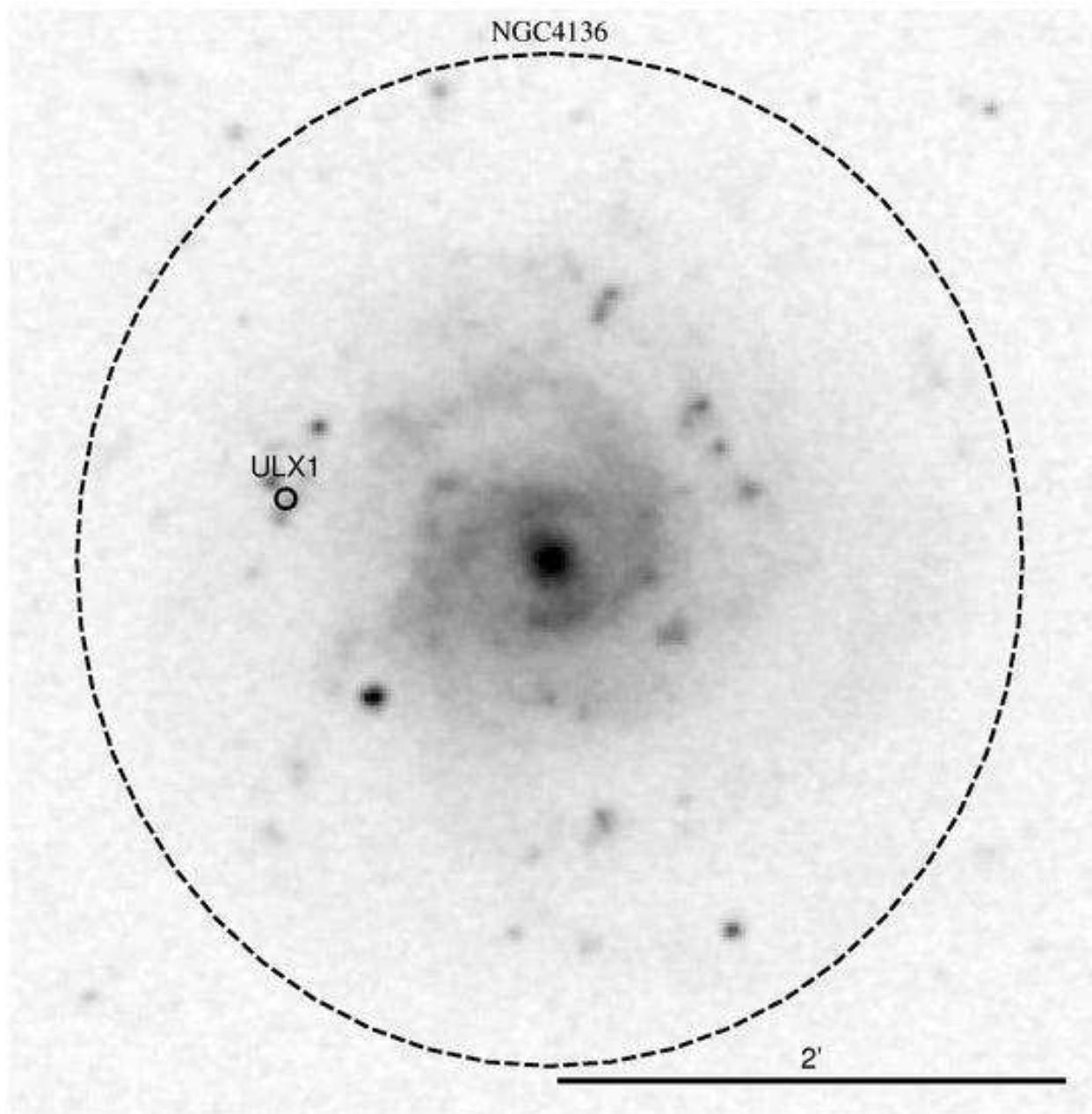


Fig. 48.— The finding chart for the ULXs in NGC4136.

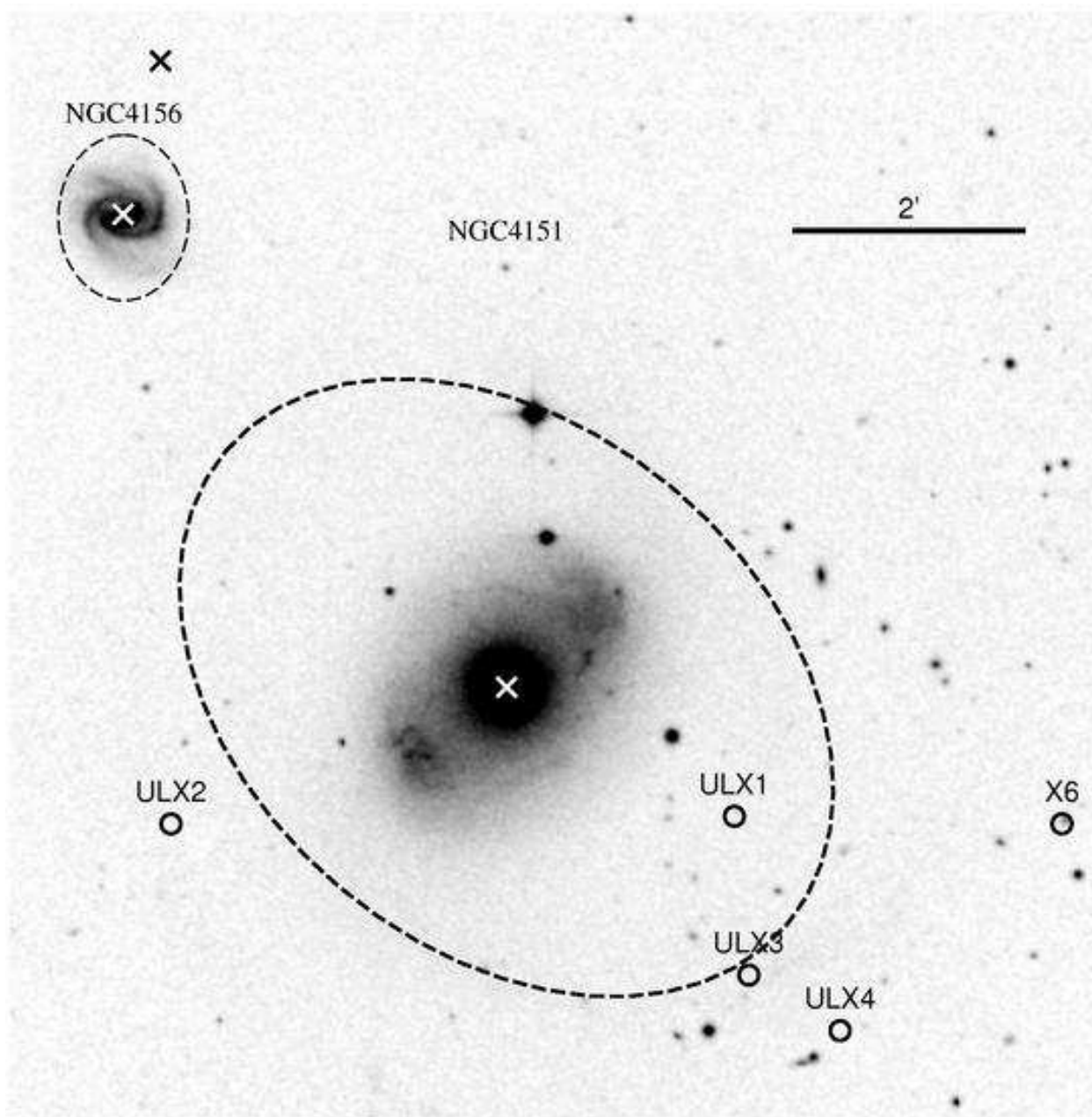


Fig. 49.— The finding chart for the ULXs in NGC4151.

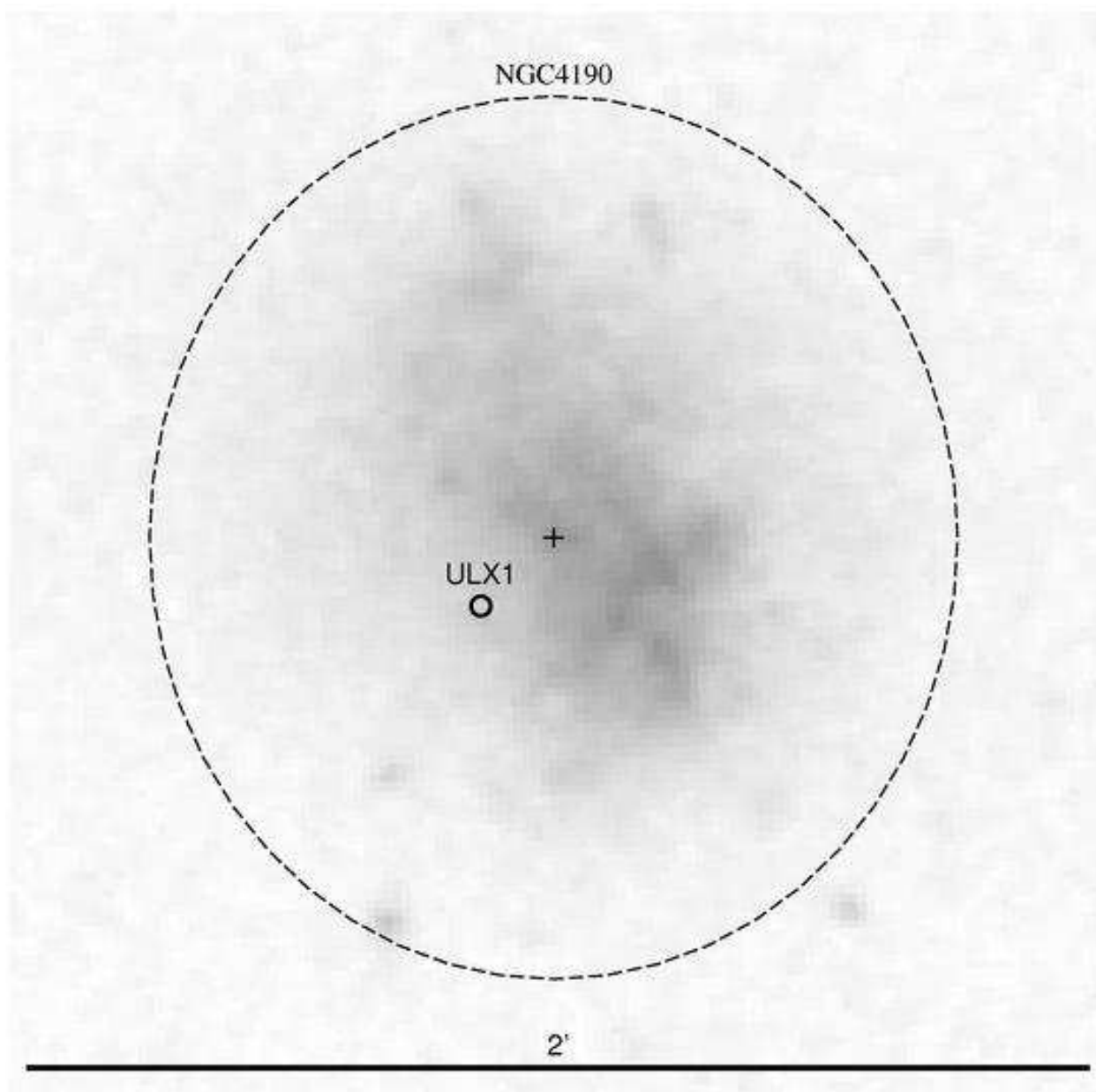


Fig. 50.— The finding chart for the ULXs in NGC4190.

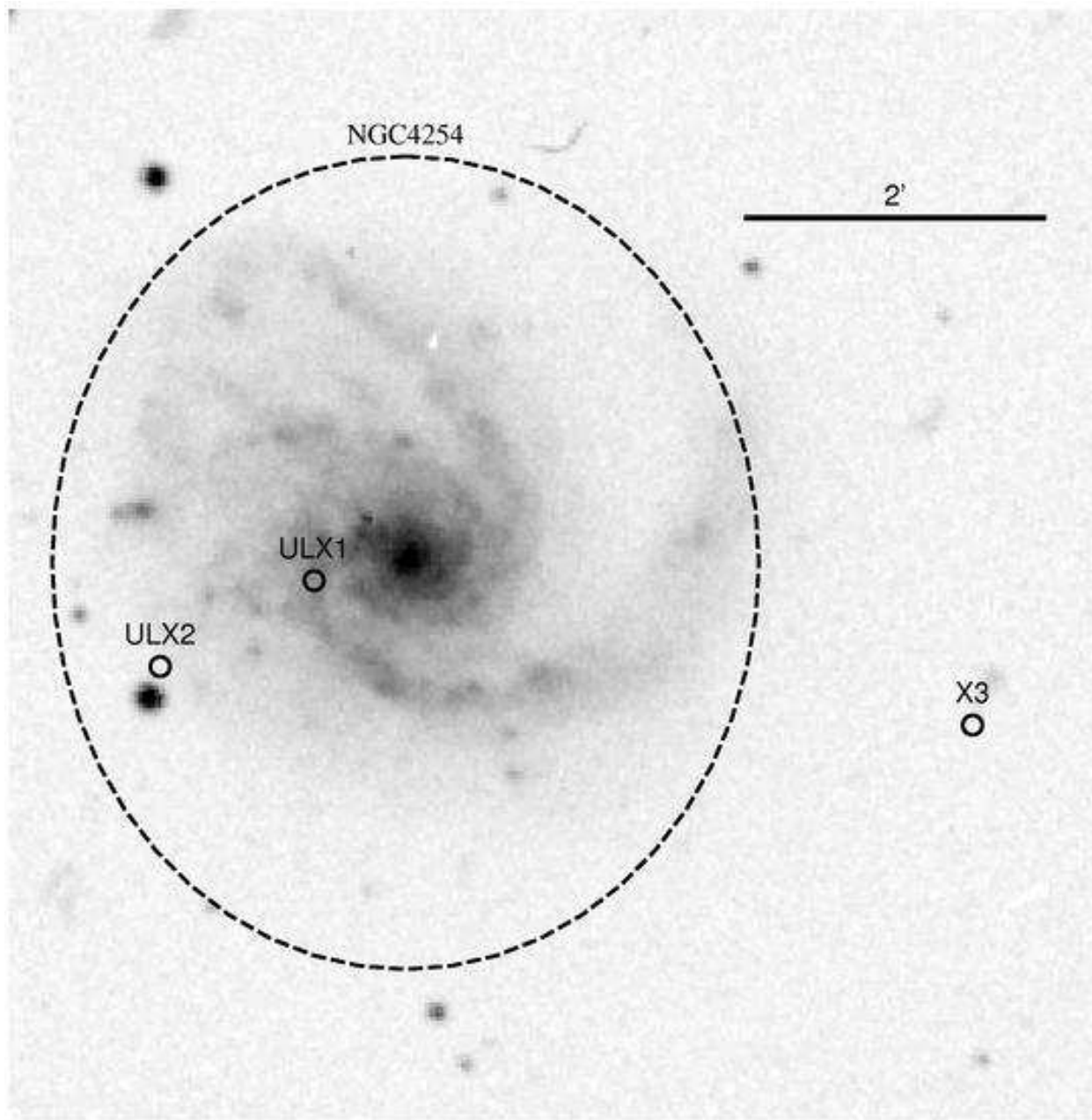


Fig. 51.— The finding chart for the ULXs in NGC4254.

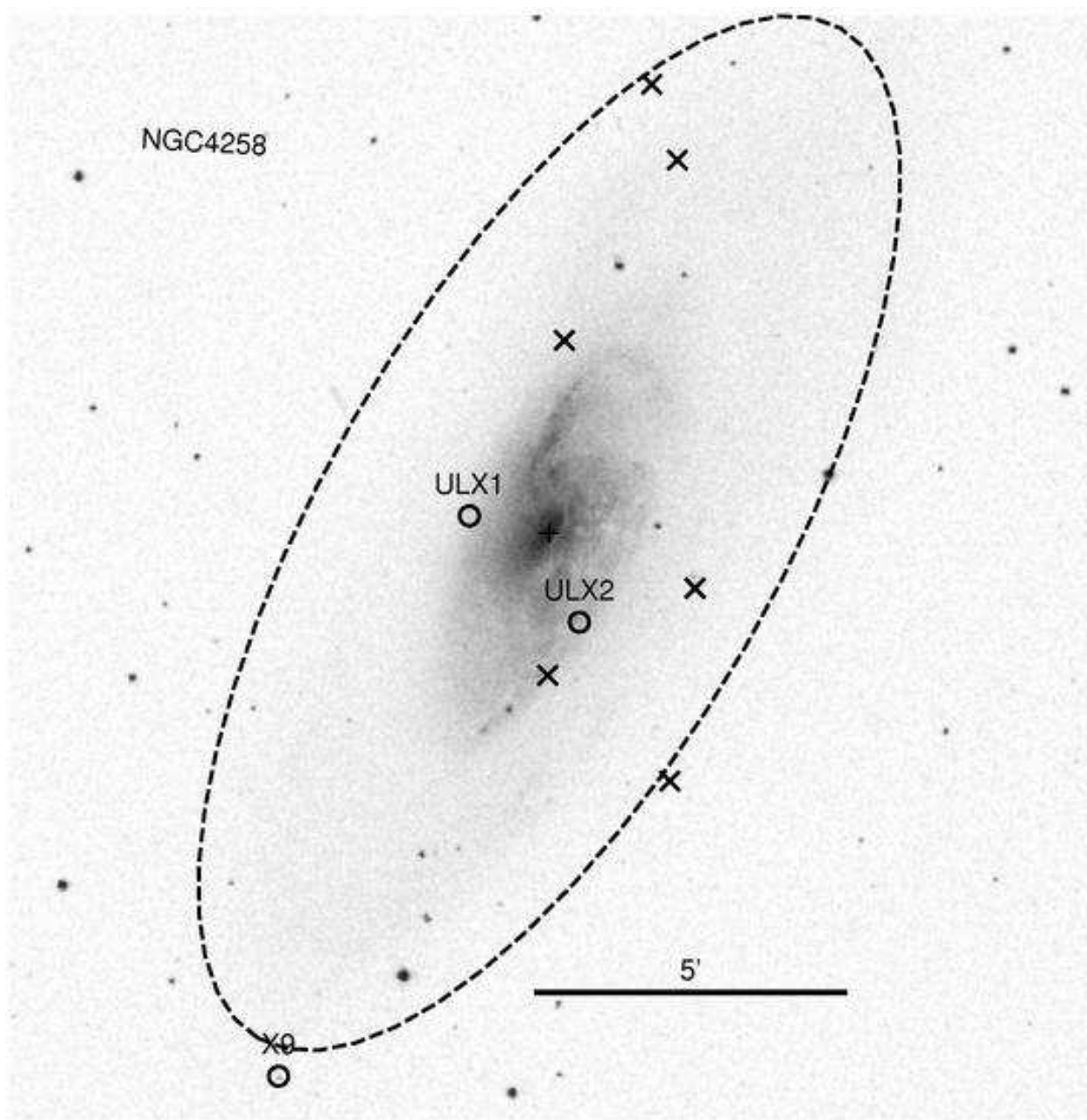


Fig. 52.— The finding chart for the ULXs in NGC4258.

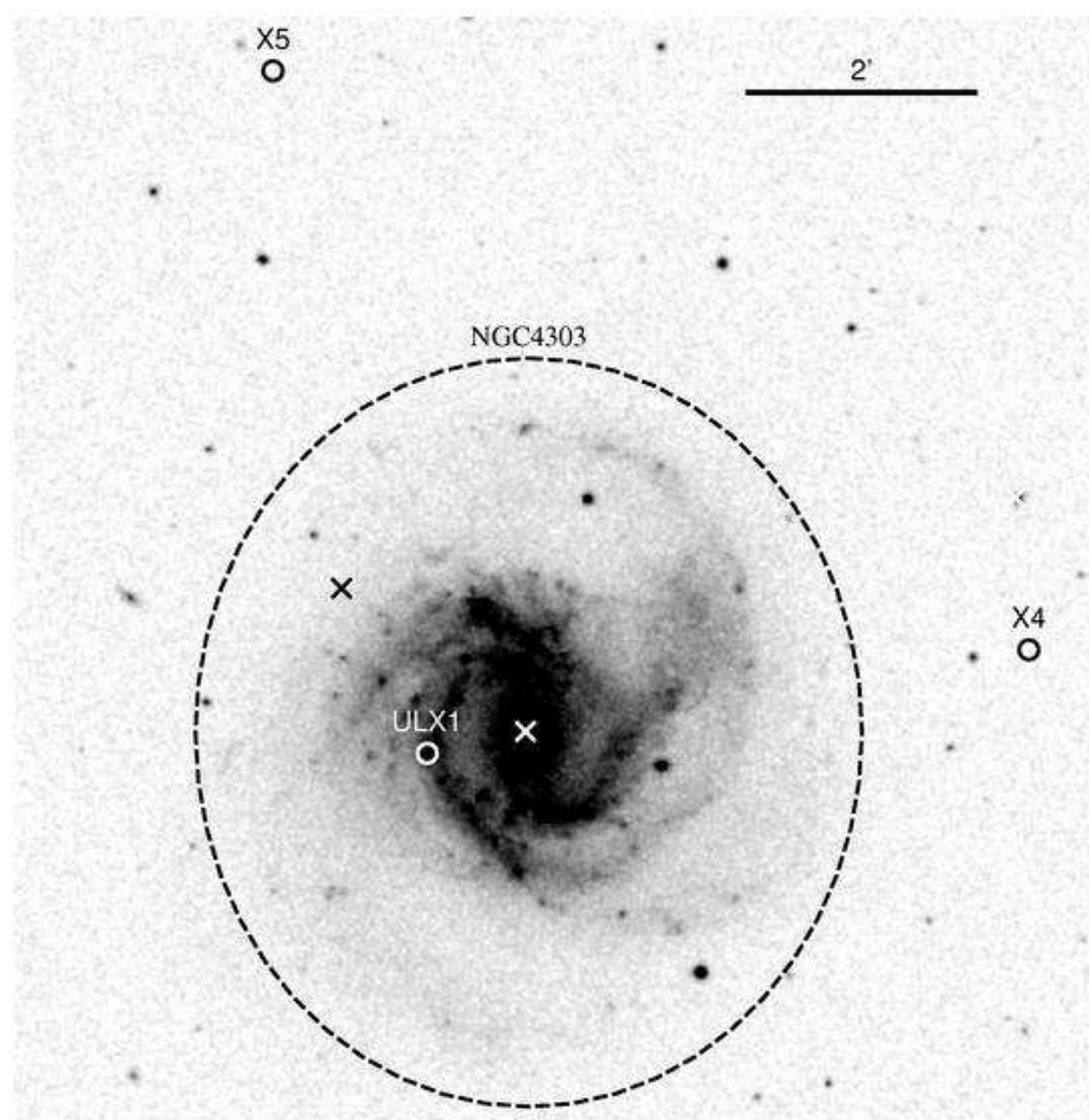


Fig. 53.— The finding chart for the ULXs in NGC4303.

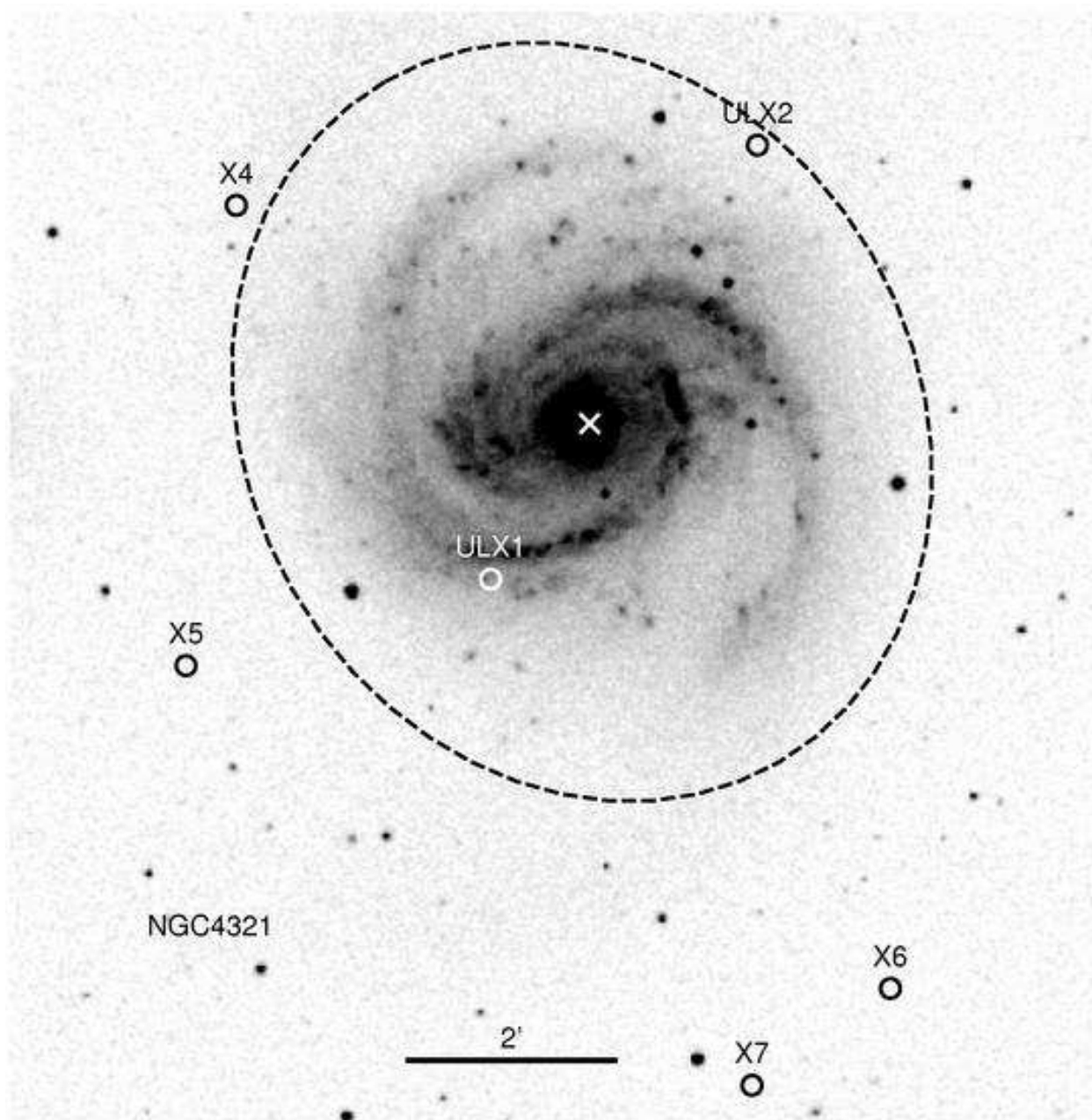


Fig. 54.— The finding chart for the ULXs in NGC4321.

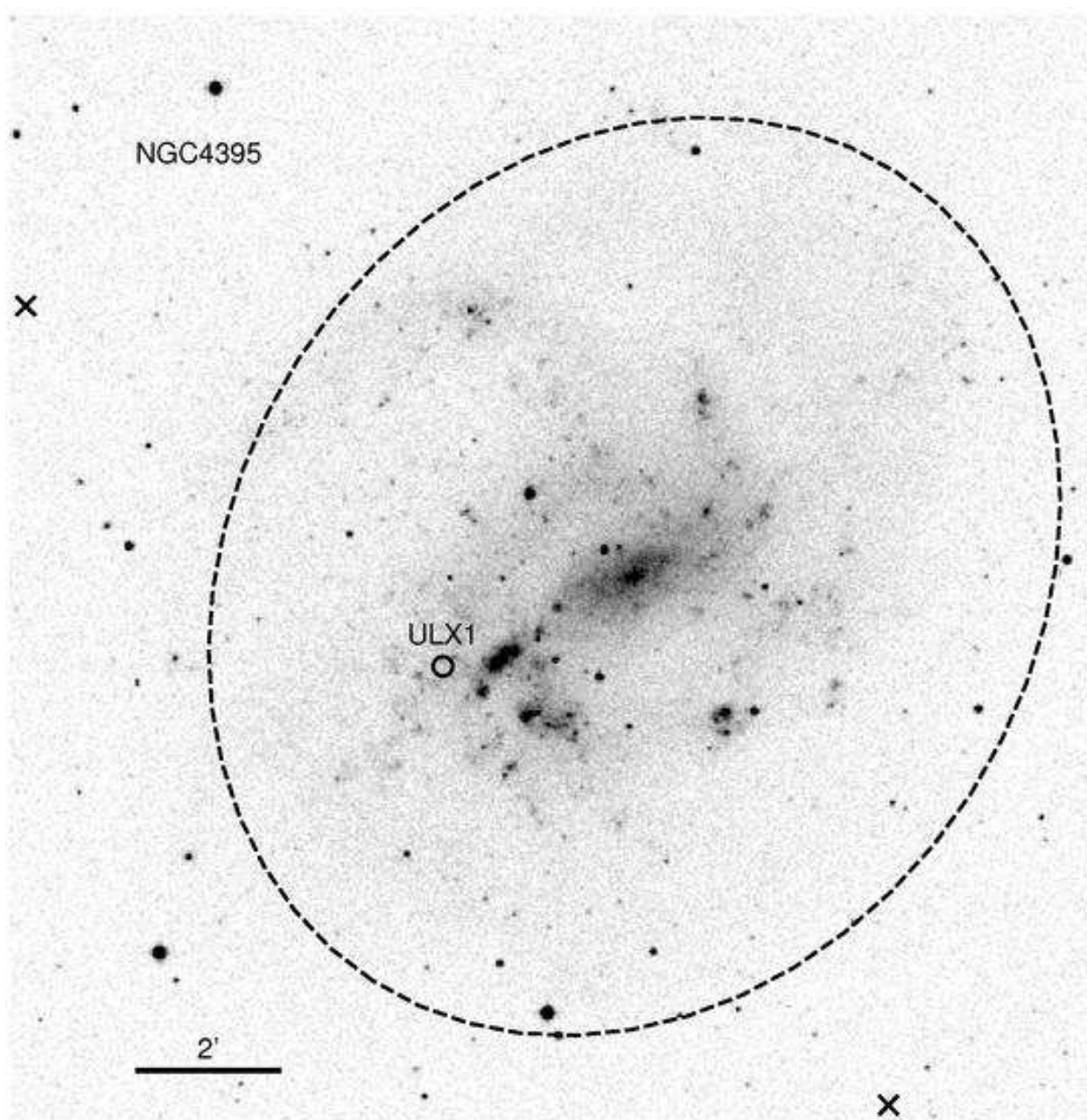


Fig. 55.— The finding chart for the ULXs in NGC4395.

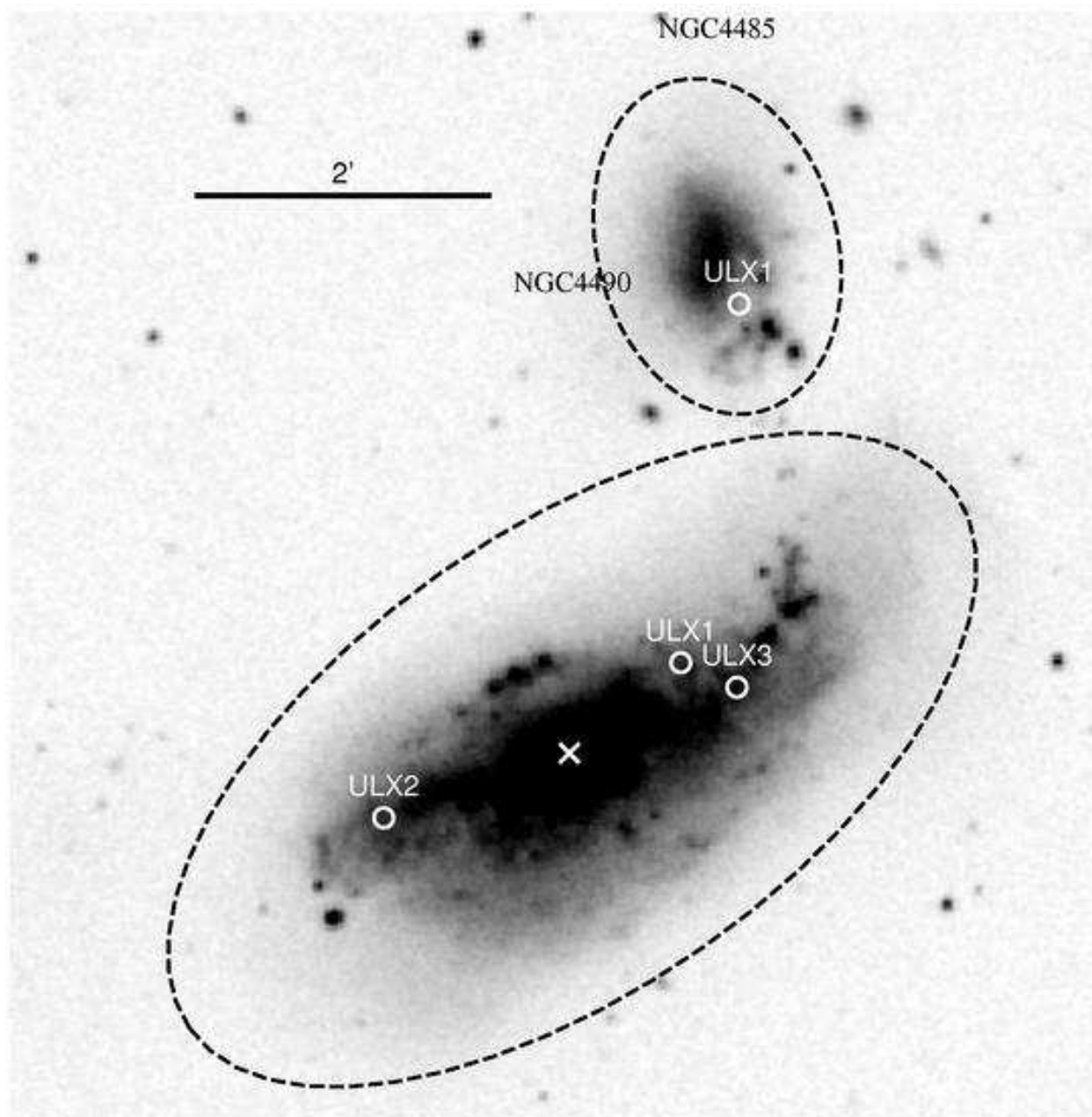


Fig. 56.— The finding chart for the ULXs in NGC4490 and NGC4485.

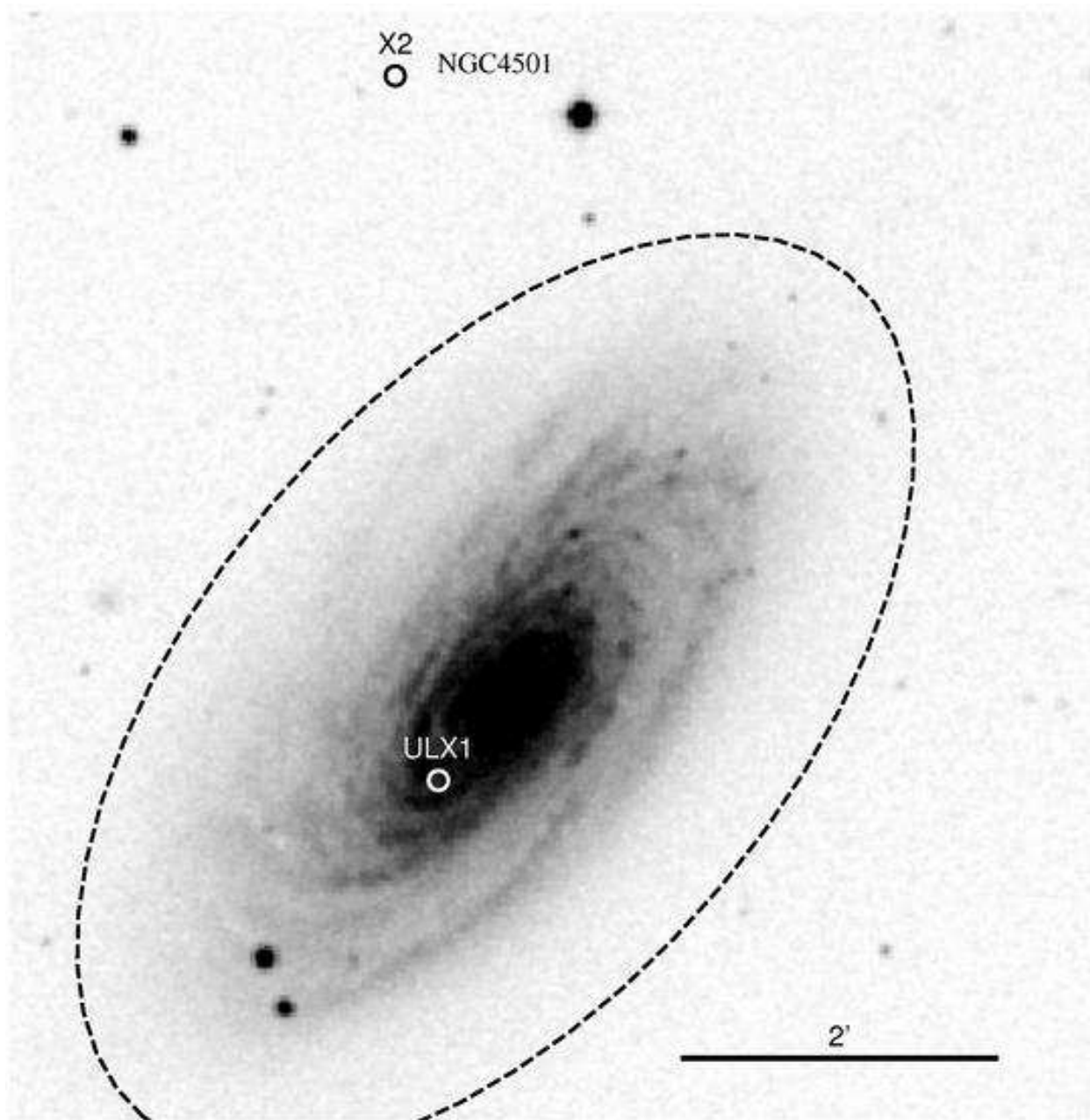


Fig. 57.— The finding chart for the ULXs in NGC4501.

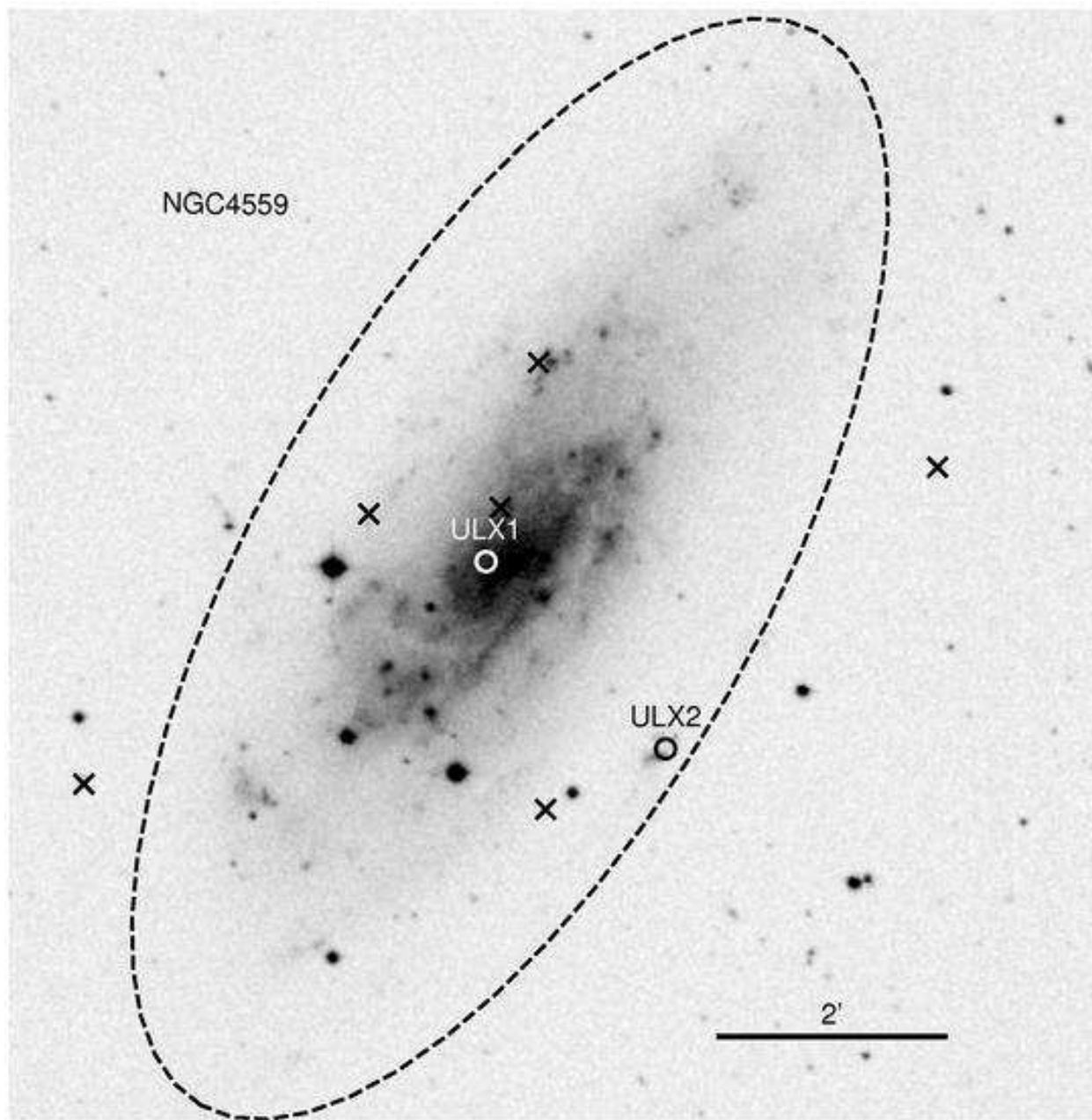


Fig. 58.— The finding chart for the ULXs in NGC4559.

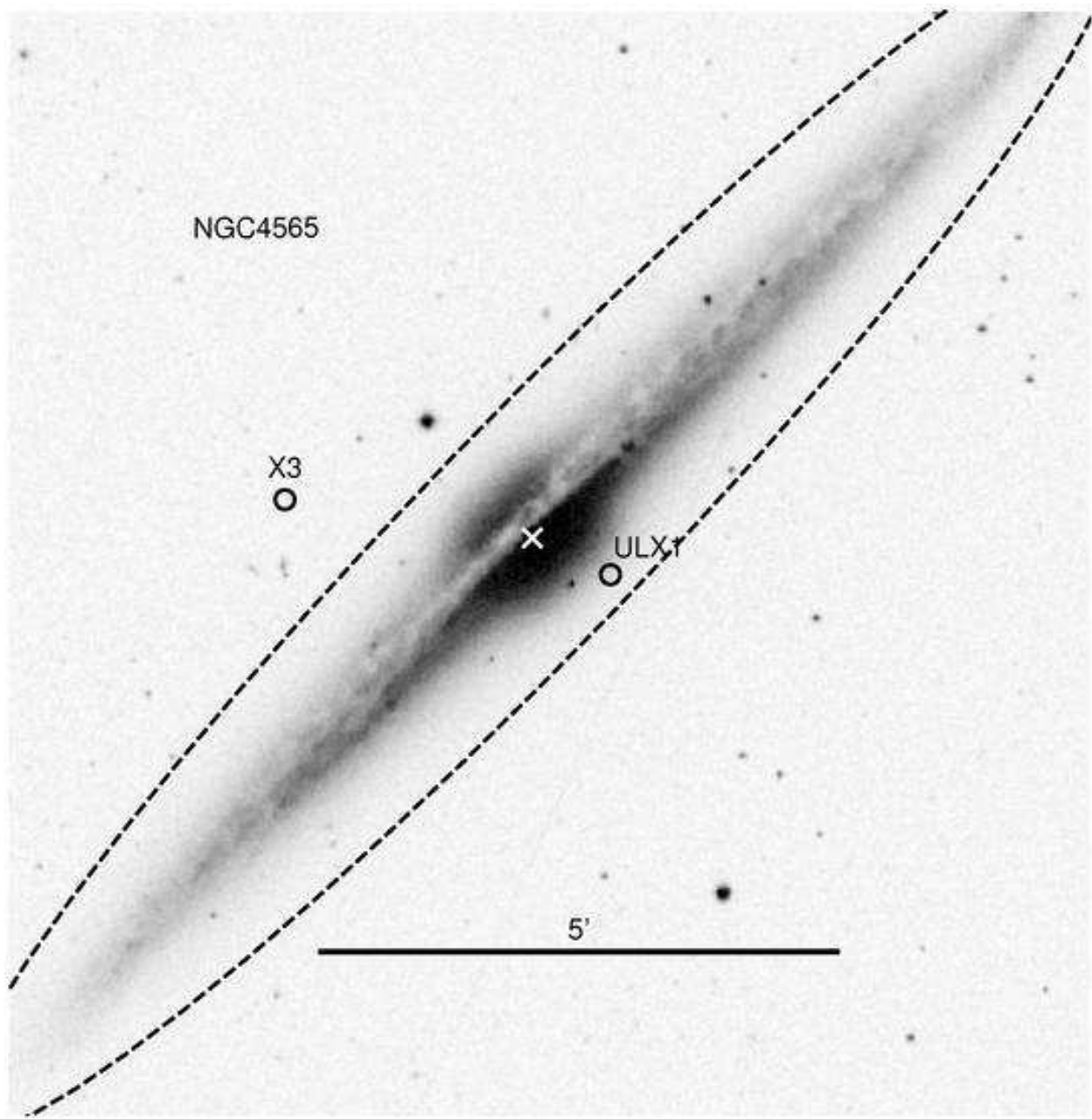


Fig. 59.— The finding chart for the ULXs in NGC4565.

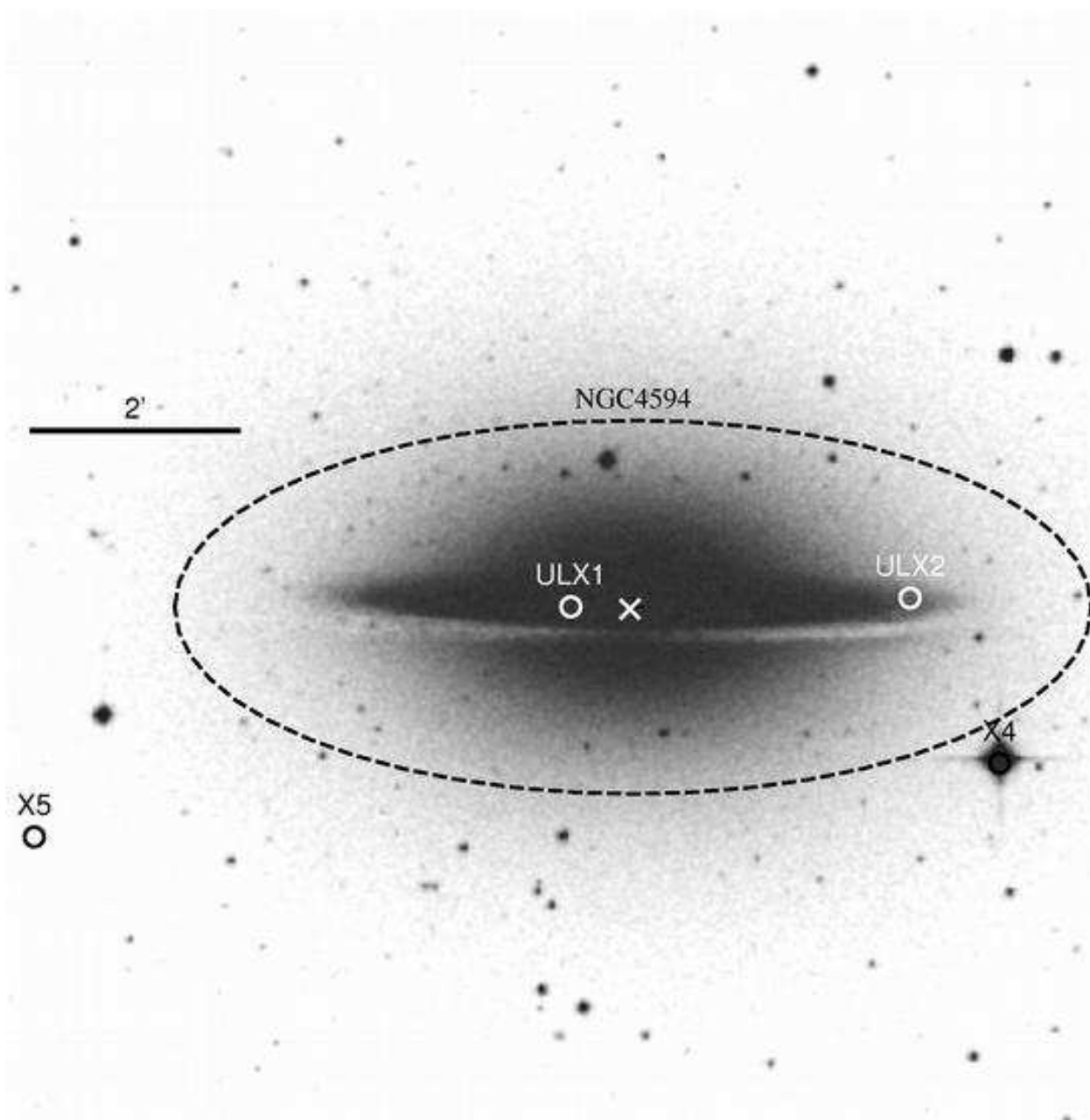


Fig. 60.— The finding chart for the ULXs in NGC4594.

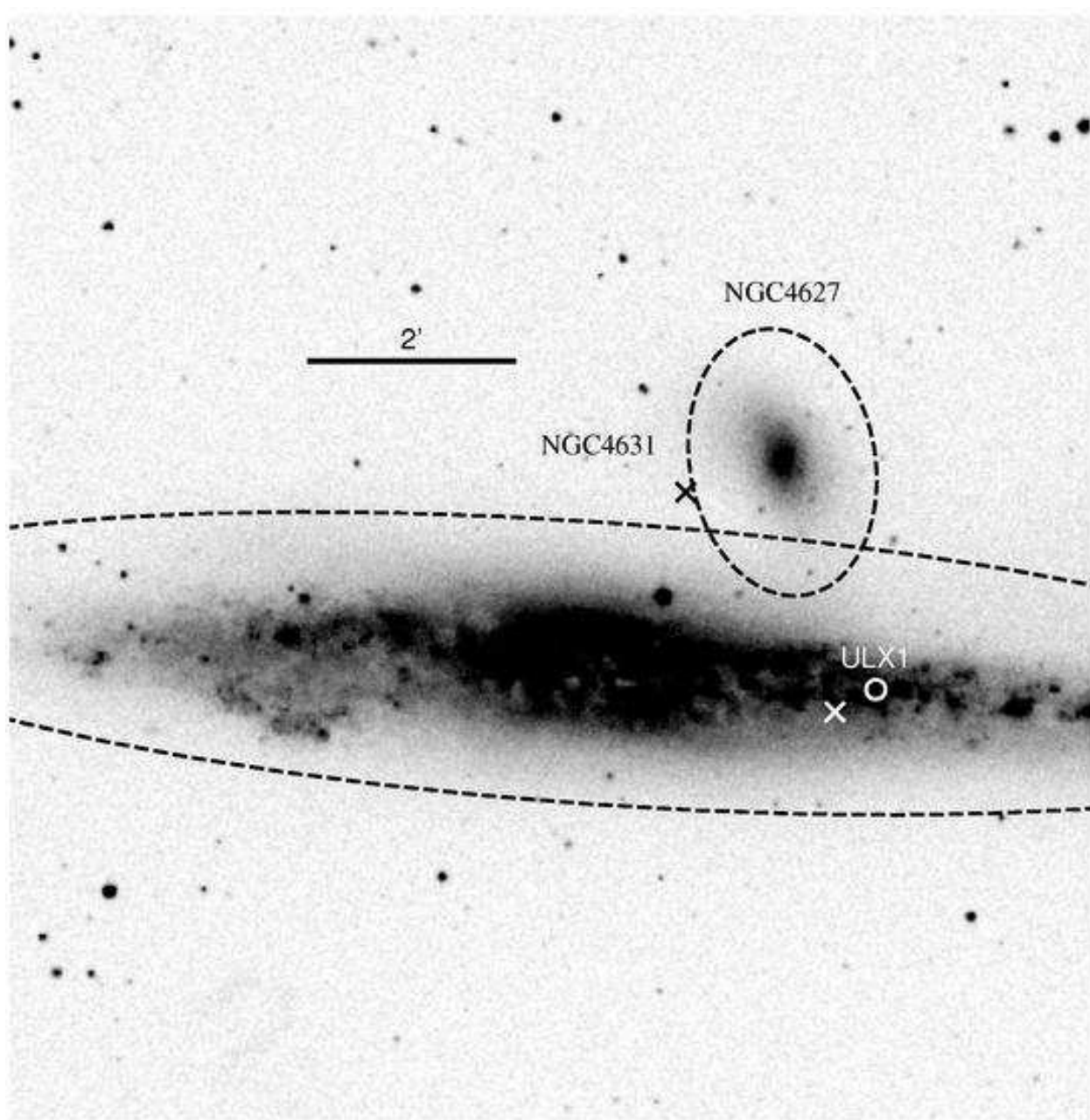


Fig. 61.— The finding chart for the ULXs in NGC4631.

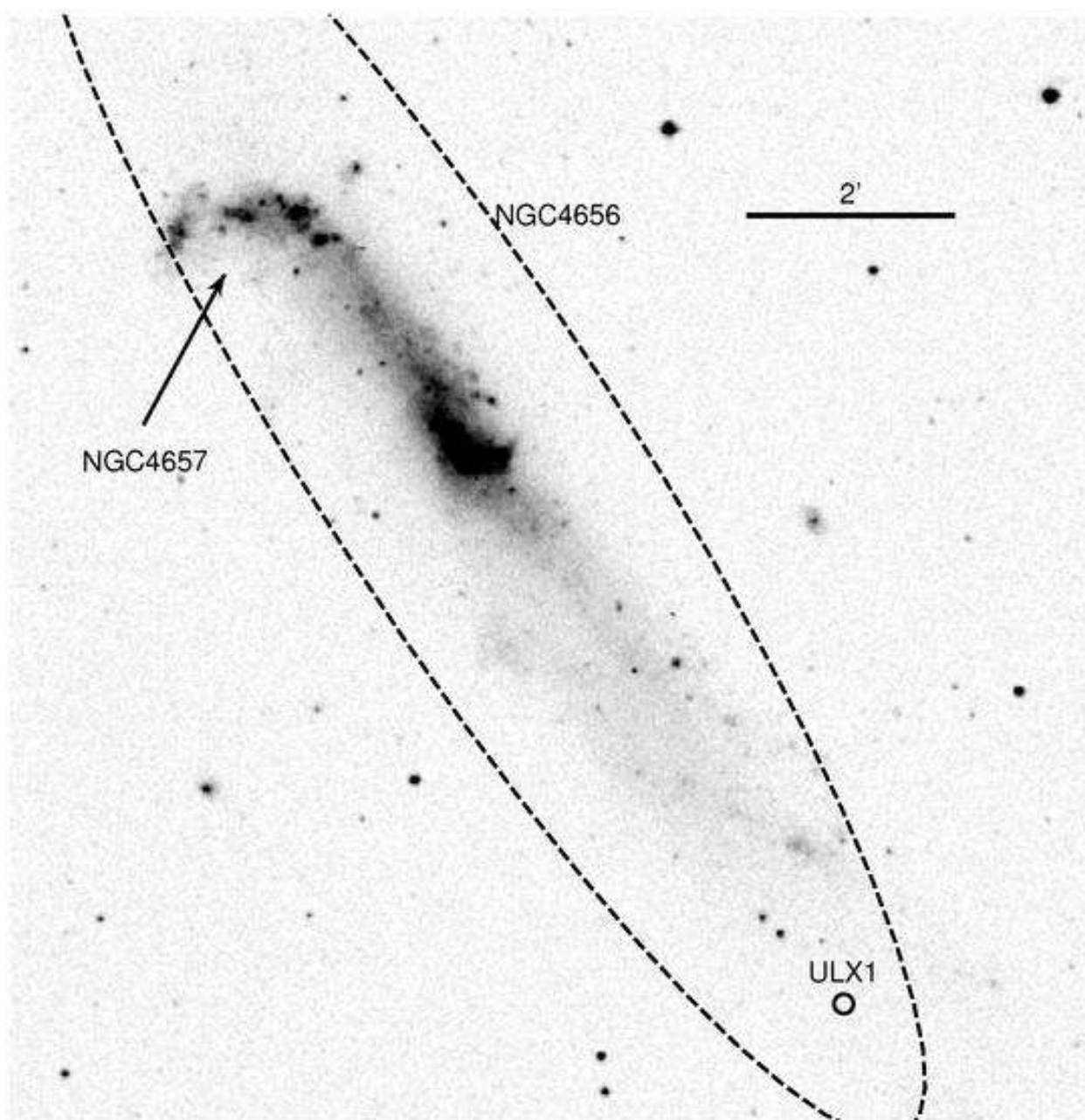


Fig. 62.— The finding chart for the ULXs in NGC4656.

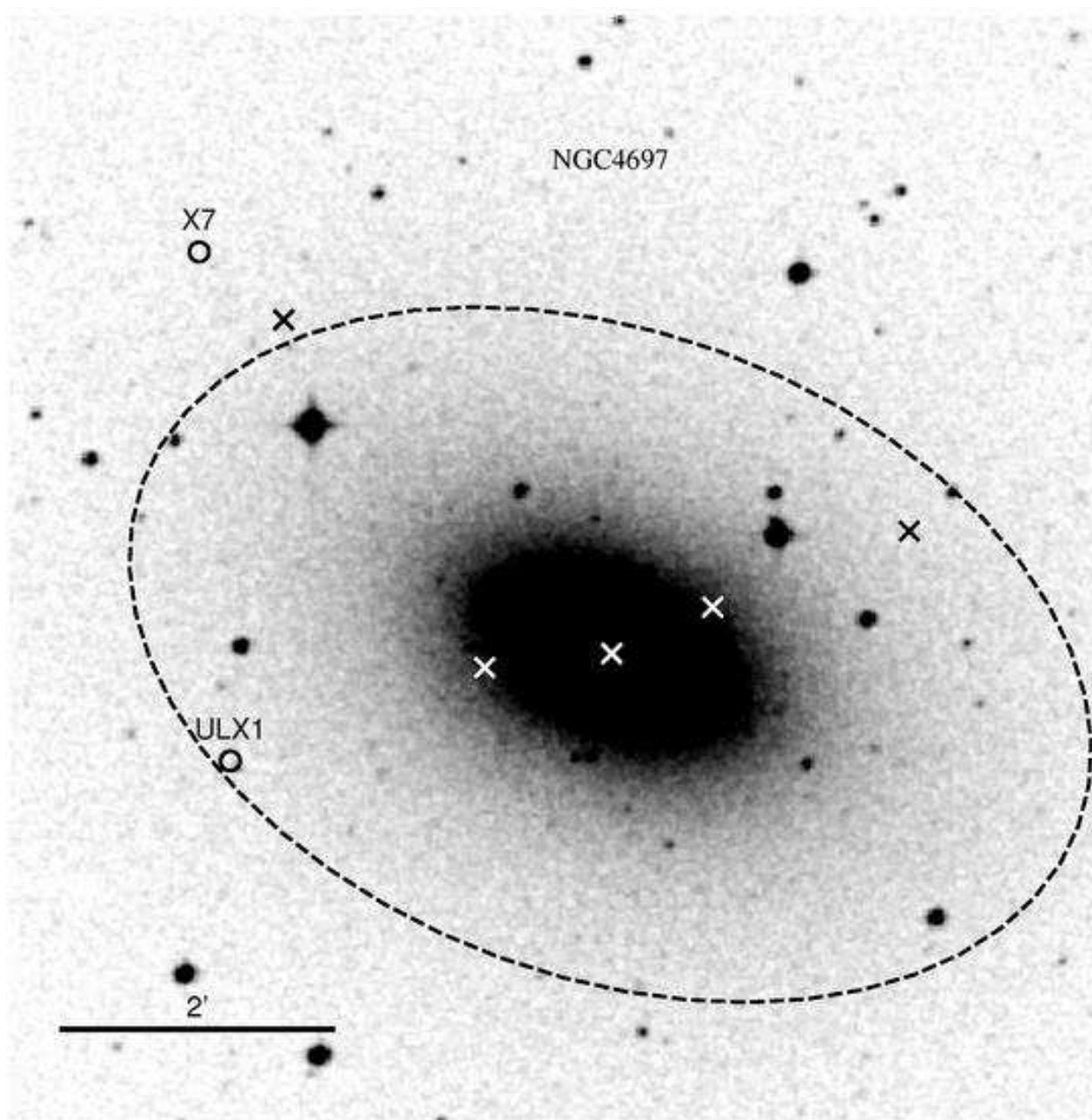


Fig. 63.— The finding chart for the ULXs in NGC4697.

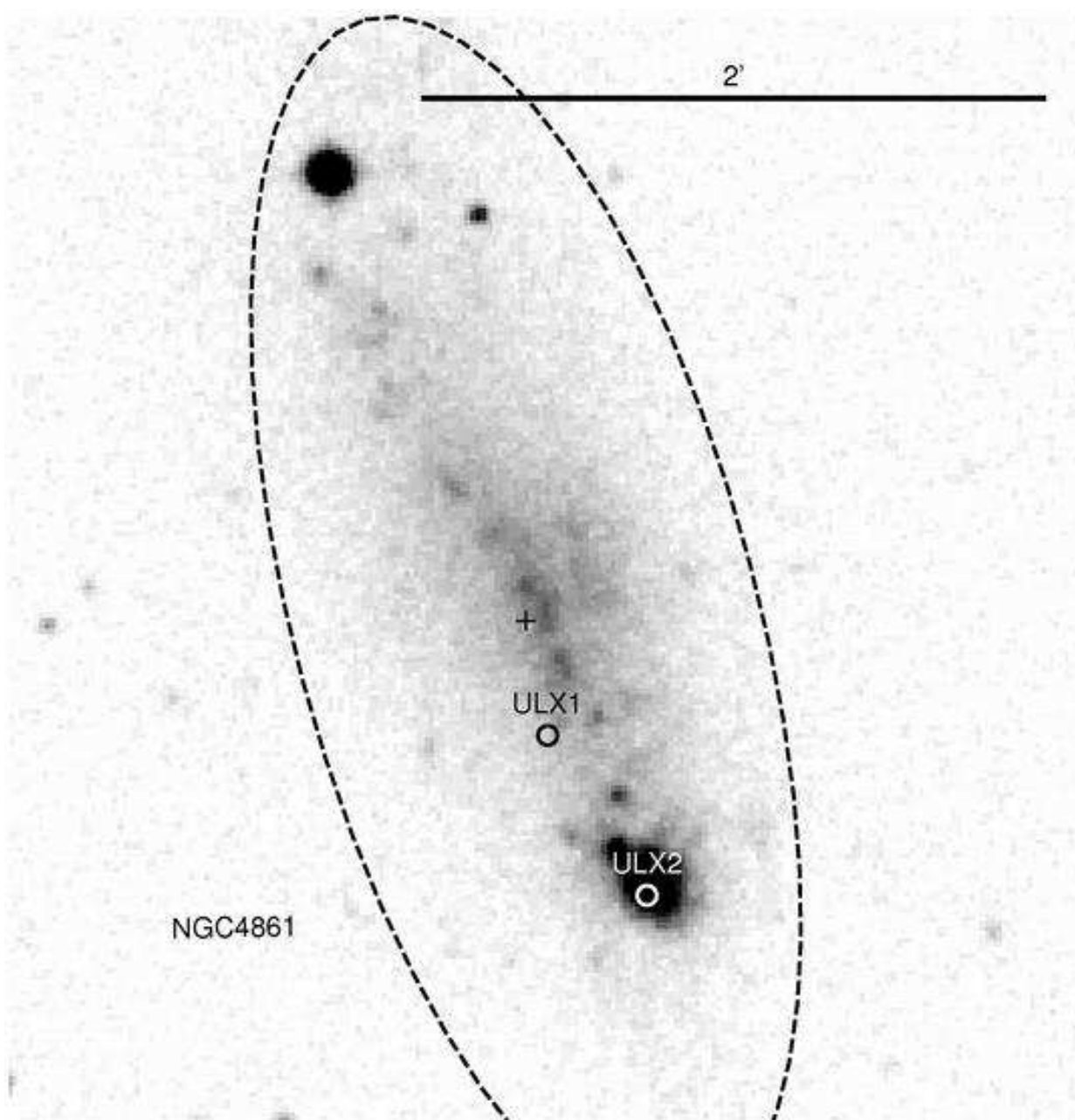


Fig. 64.— The finding chart for the ULXs in NGC4861.

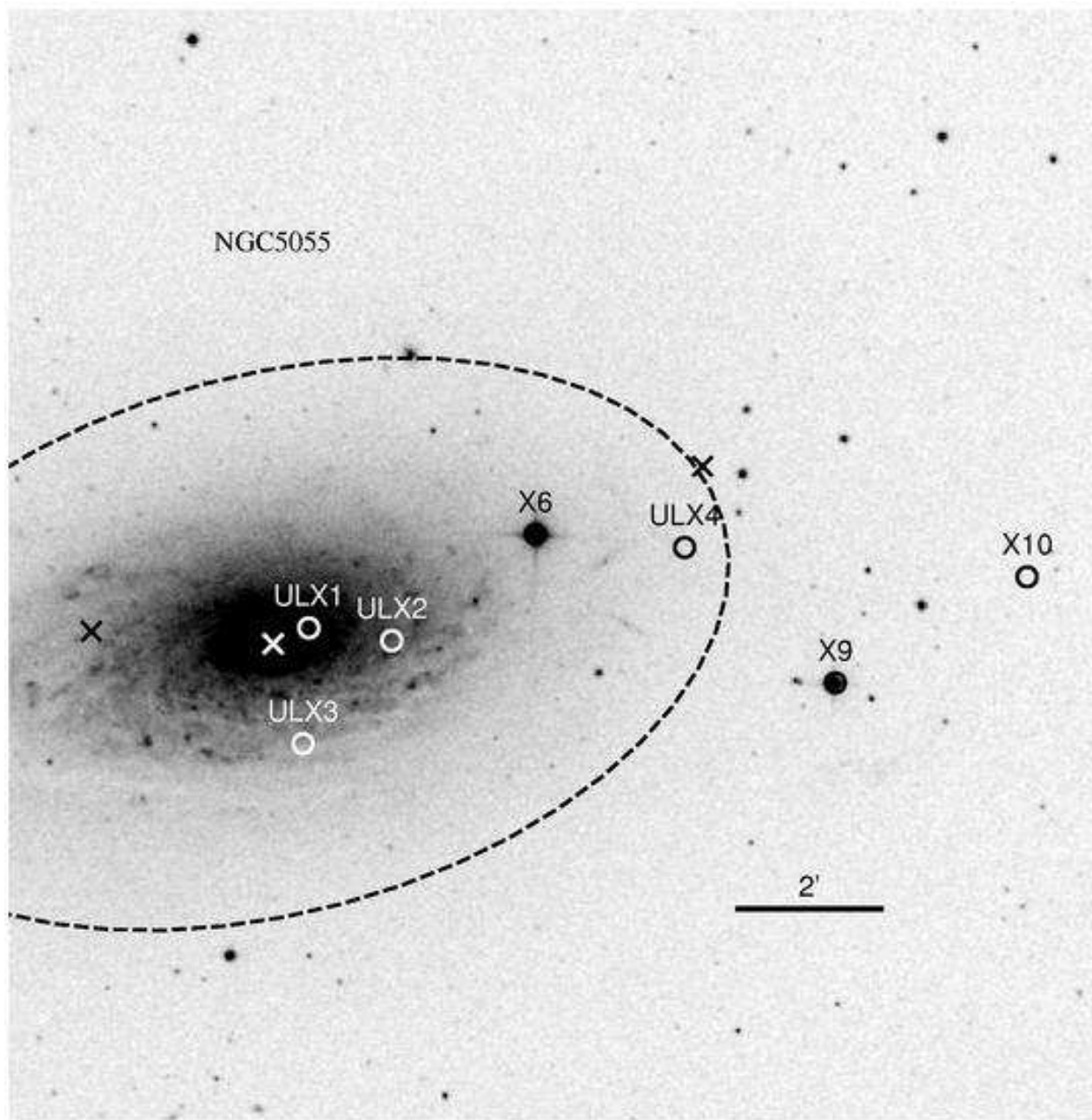


Fig. 65.— The finding chart for the ULXs in NGC5055.

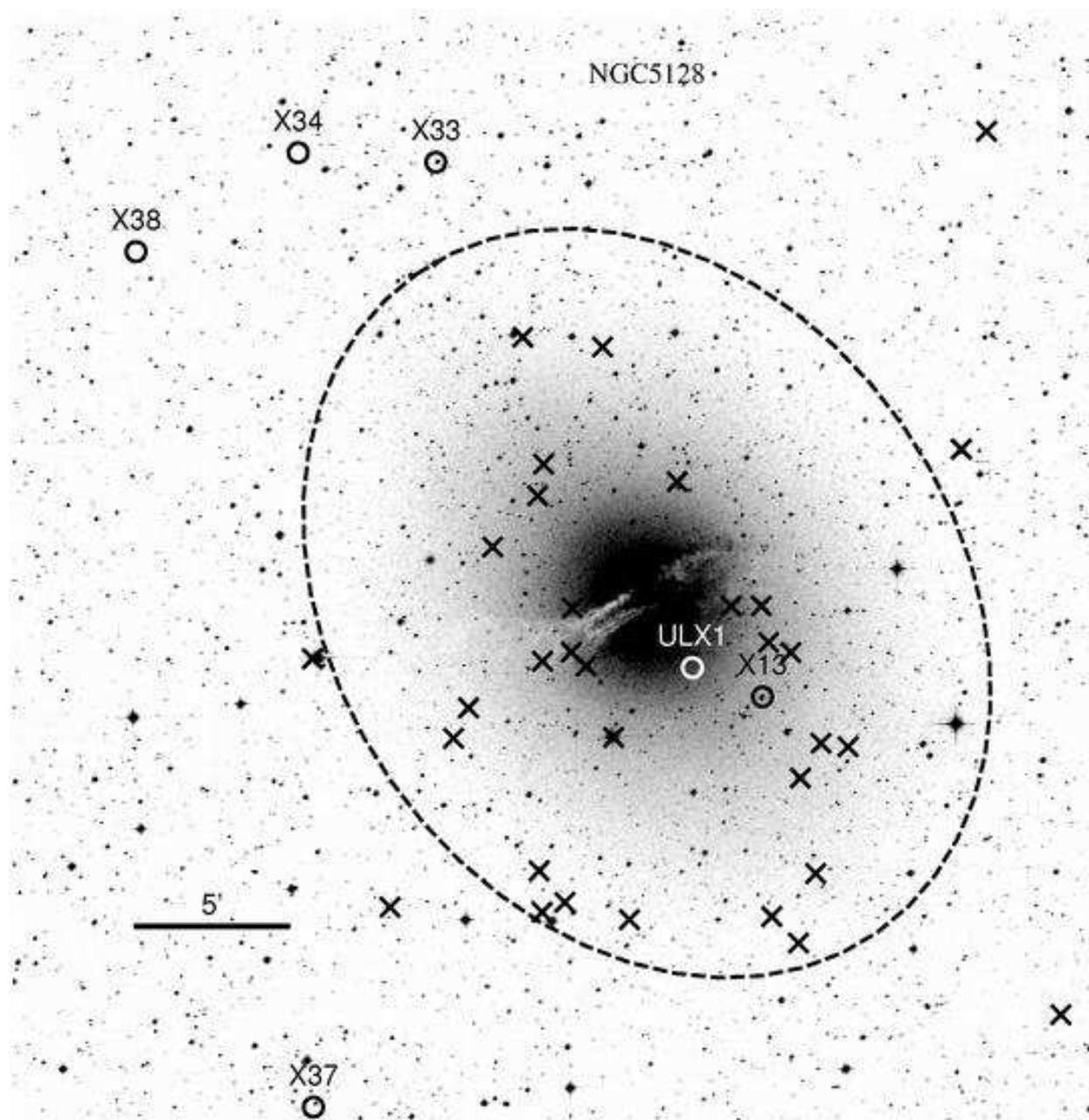


Fig. 66.— The finding chart for the ULXs in NGC5128.

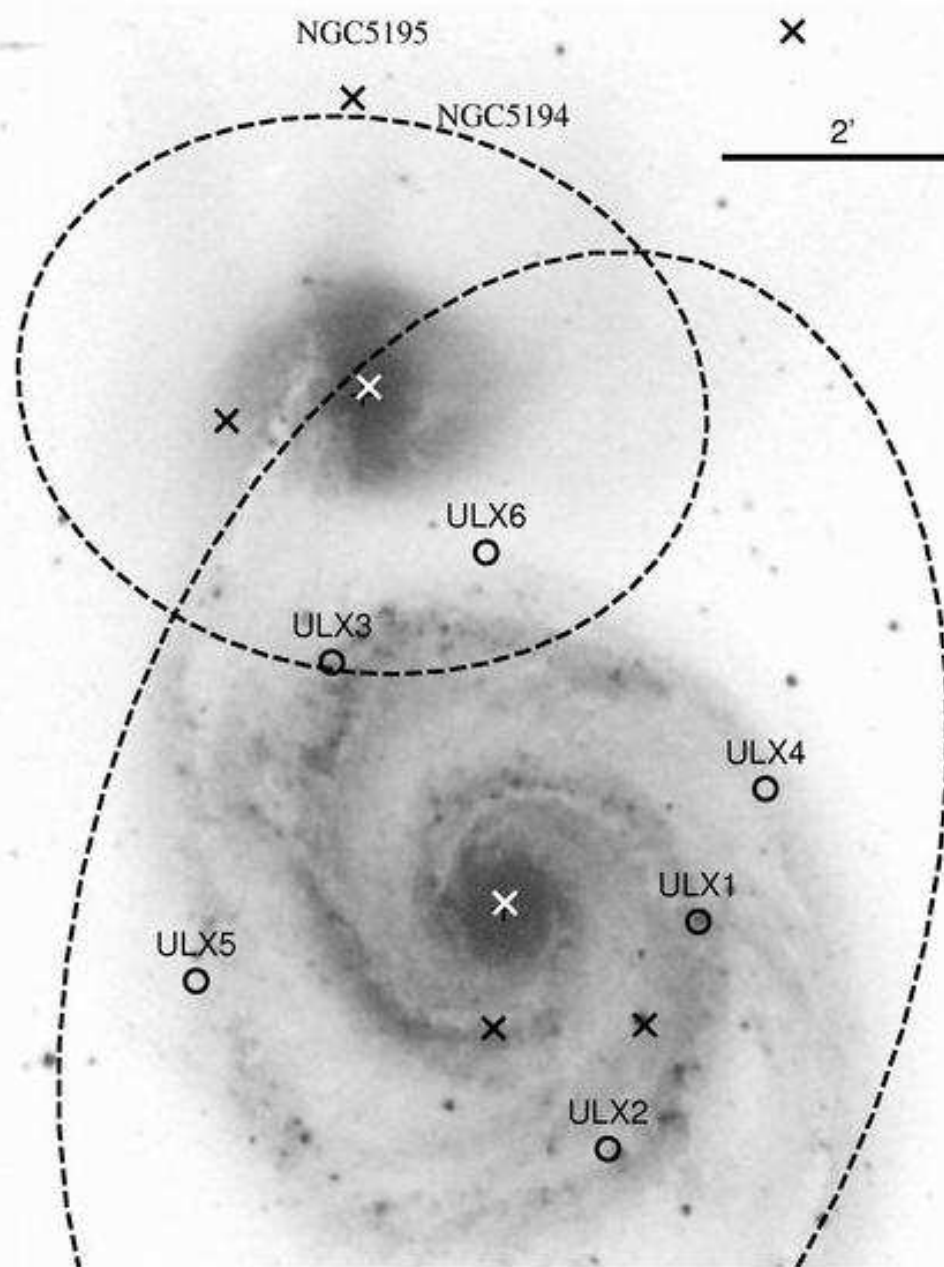


Fig. 67.— The finding chart for the ULXs in NGC5194.

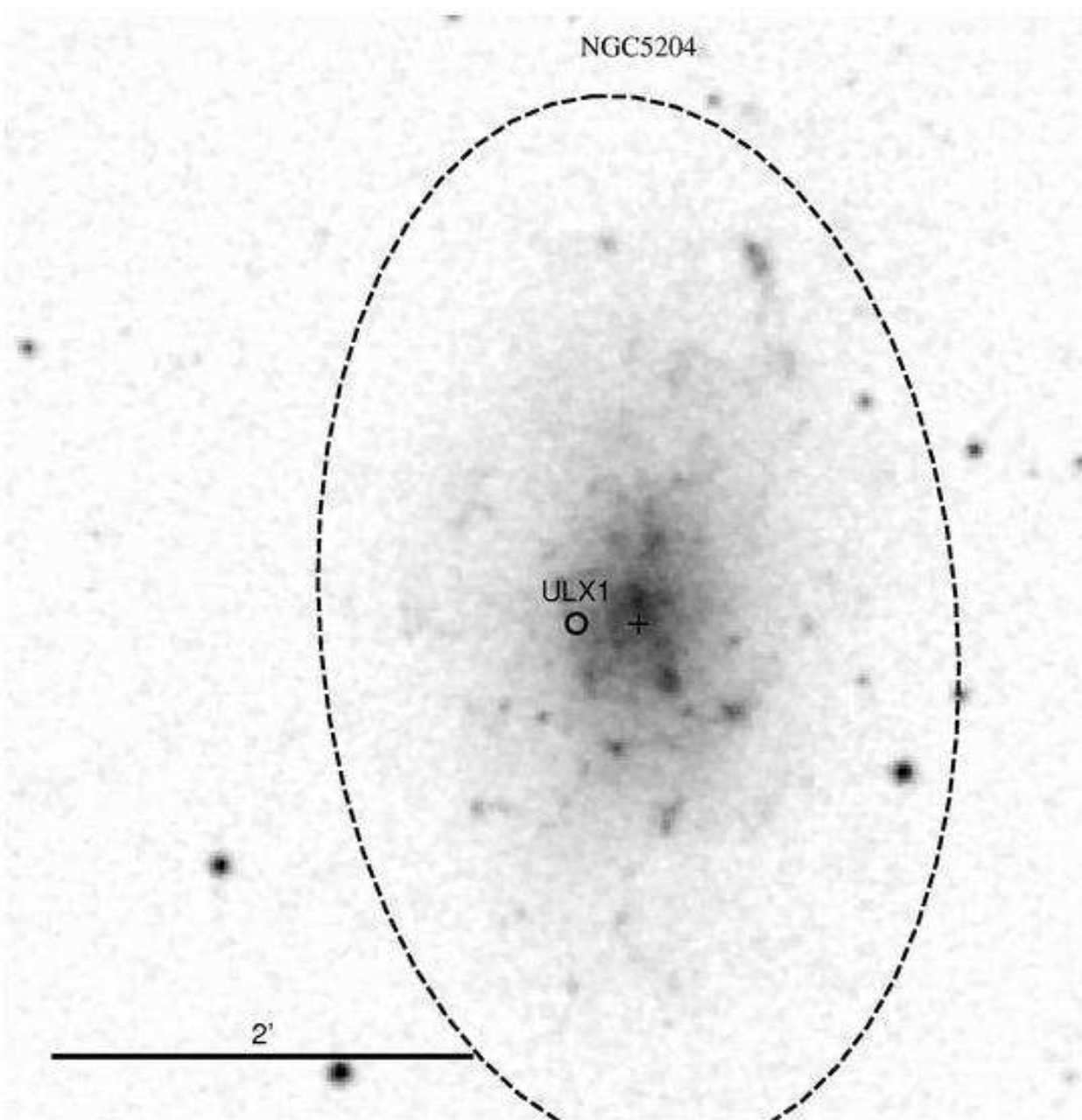


Fig. 68.— The finding chart for the ULXs in NGC5204.

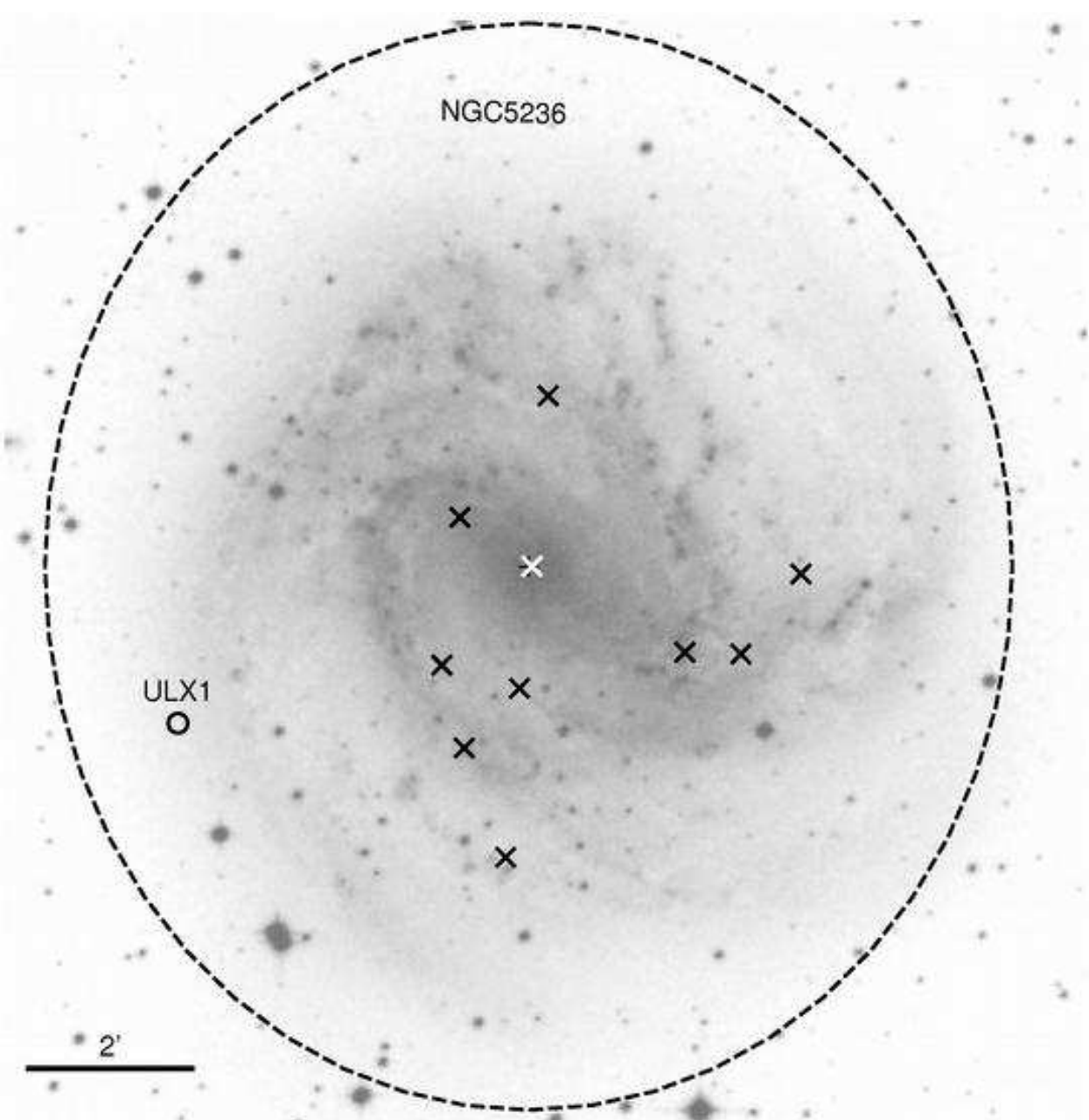


Fig. 69.— The finding chart for the ULXs in NGC5236.

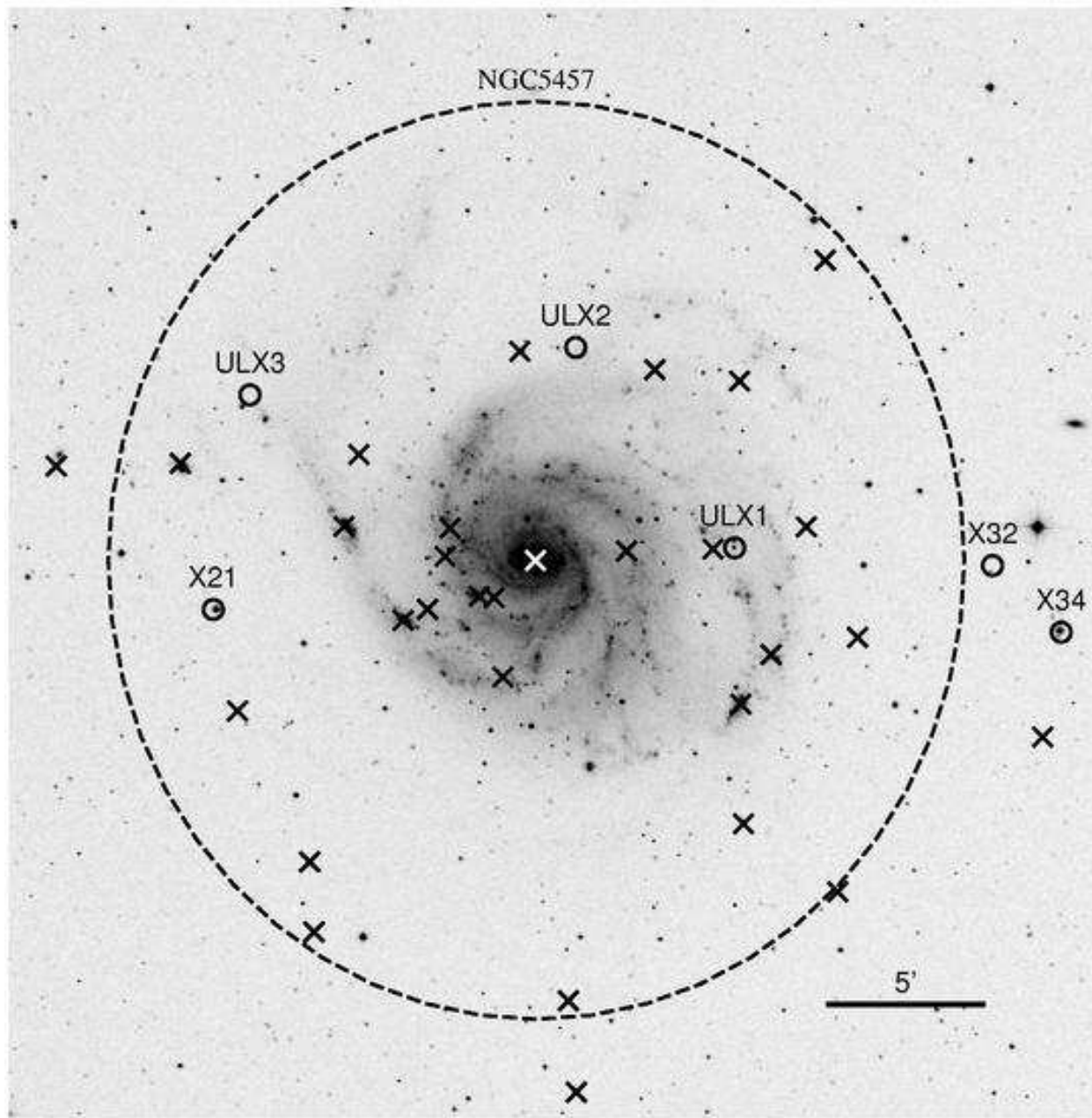


Fig. 70.— The finding chart for the ULXs in NGC5457.

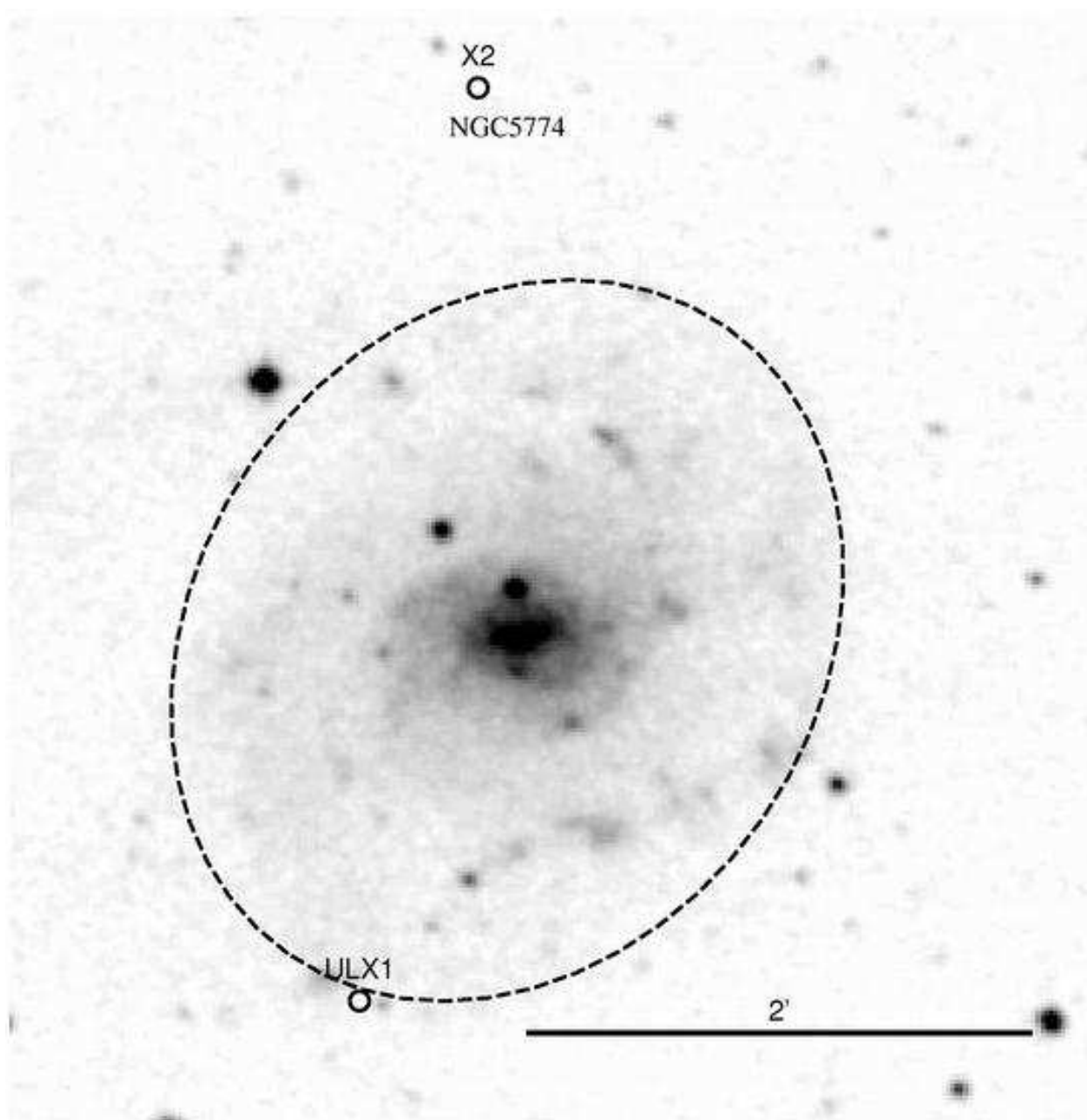


Fig. 71.— The finding chart for the ULXs in NGC5774.

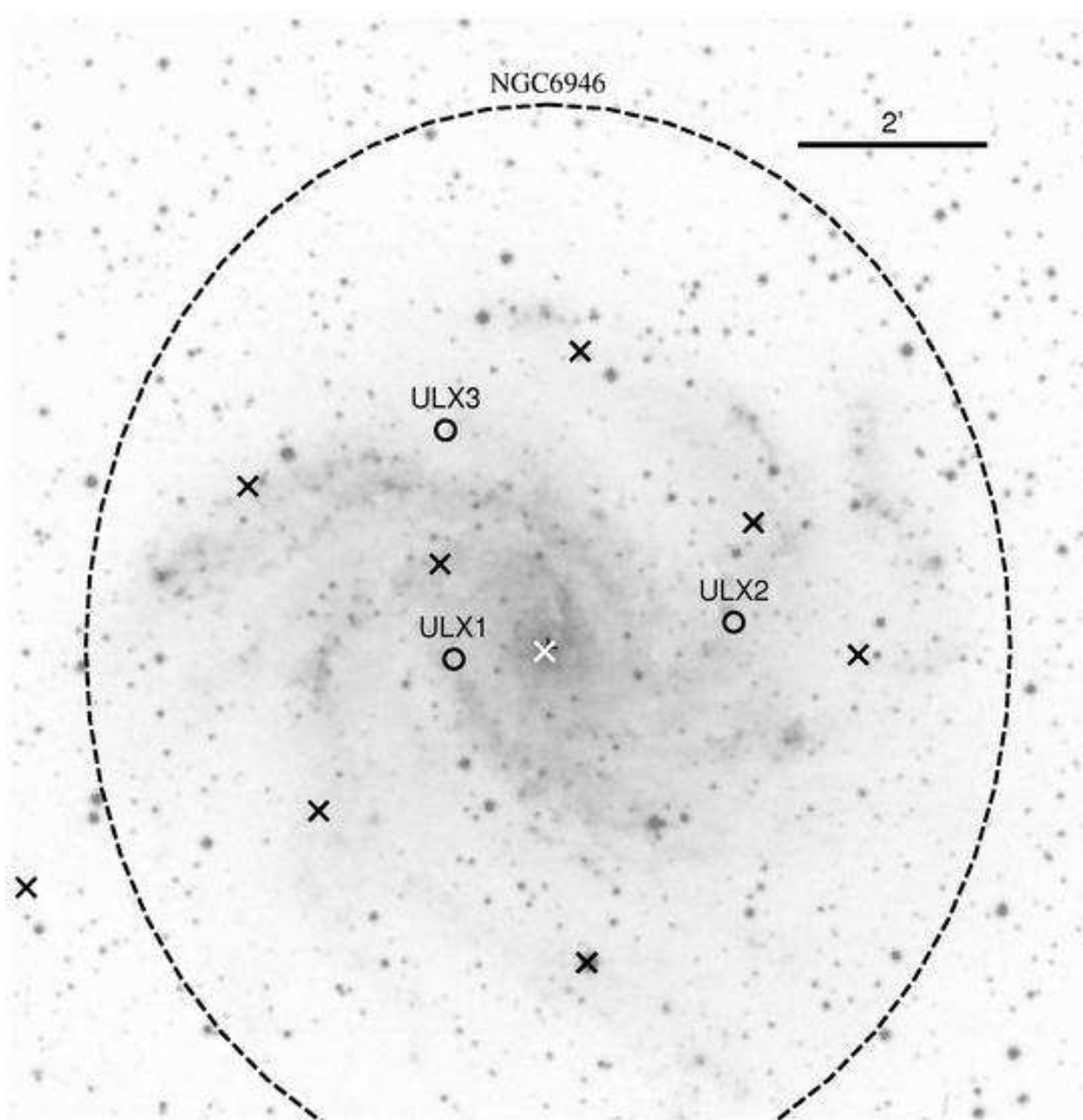


Fig. 72.— The finding chart for the ULXs in NGC6946.

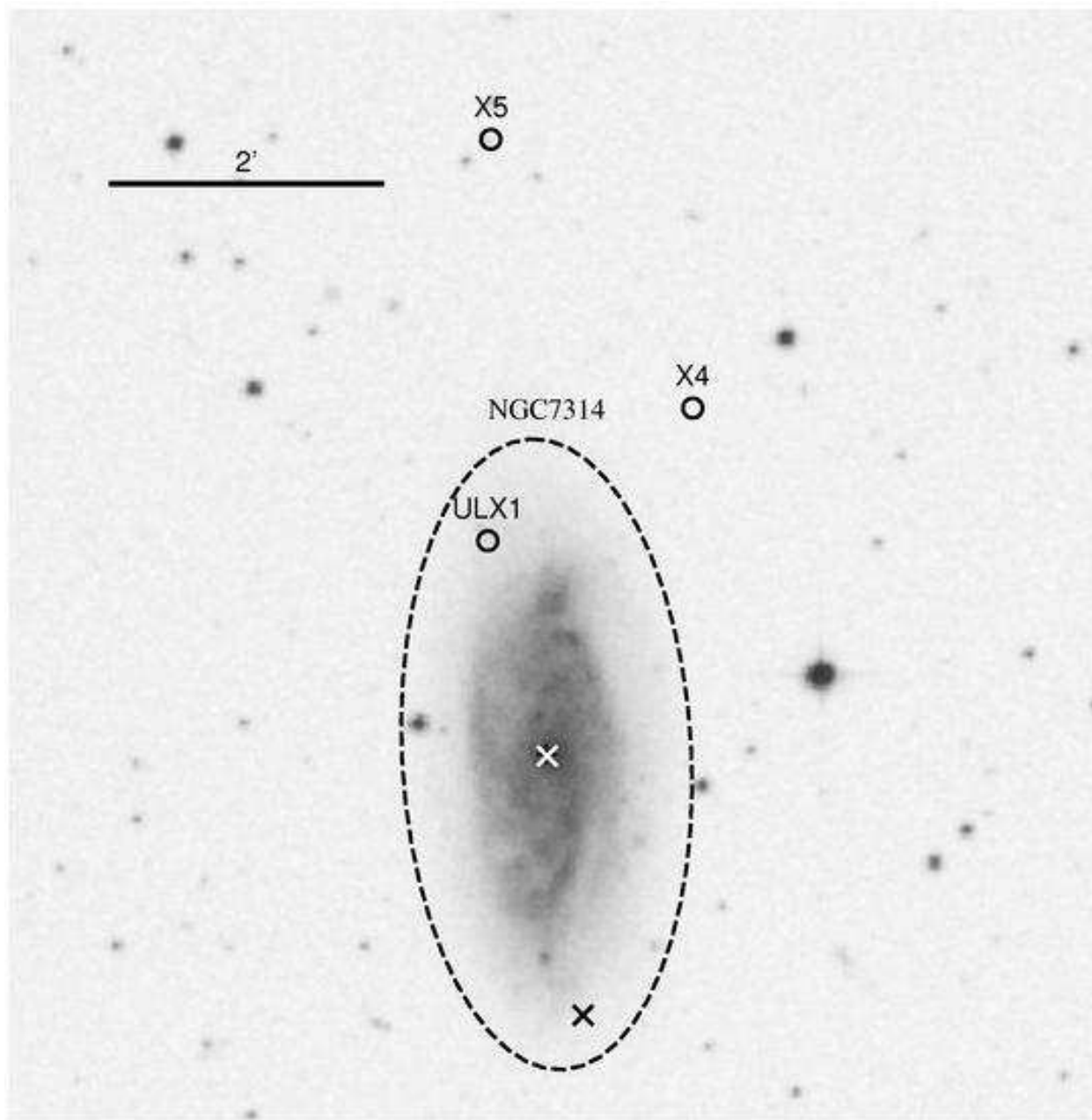


Fig. 73.— The finding chart for the ULXs in NGC7314.

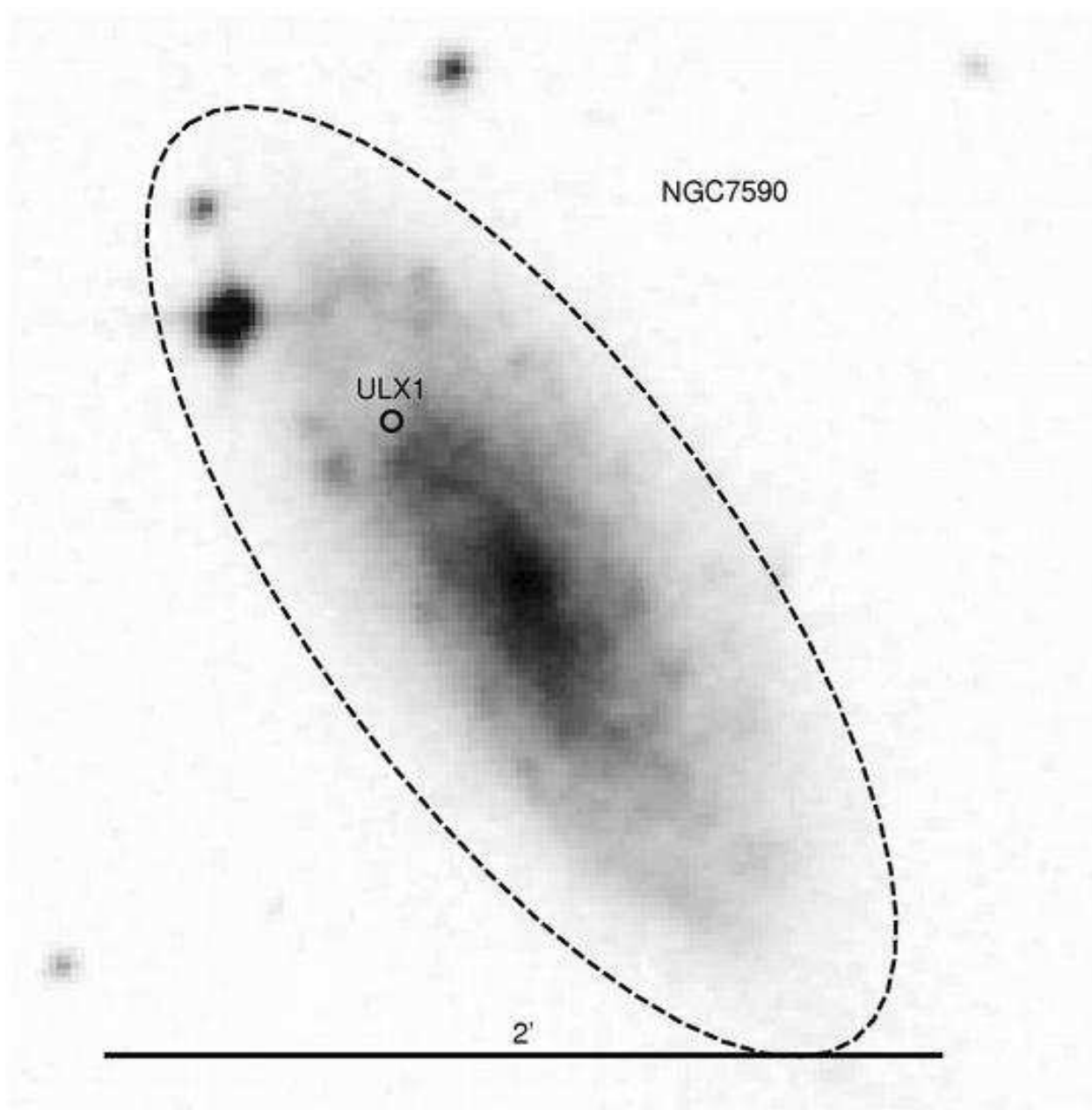


Fig. 74.— The finding chart for the ULXs in NGC7590.

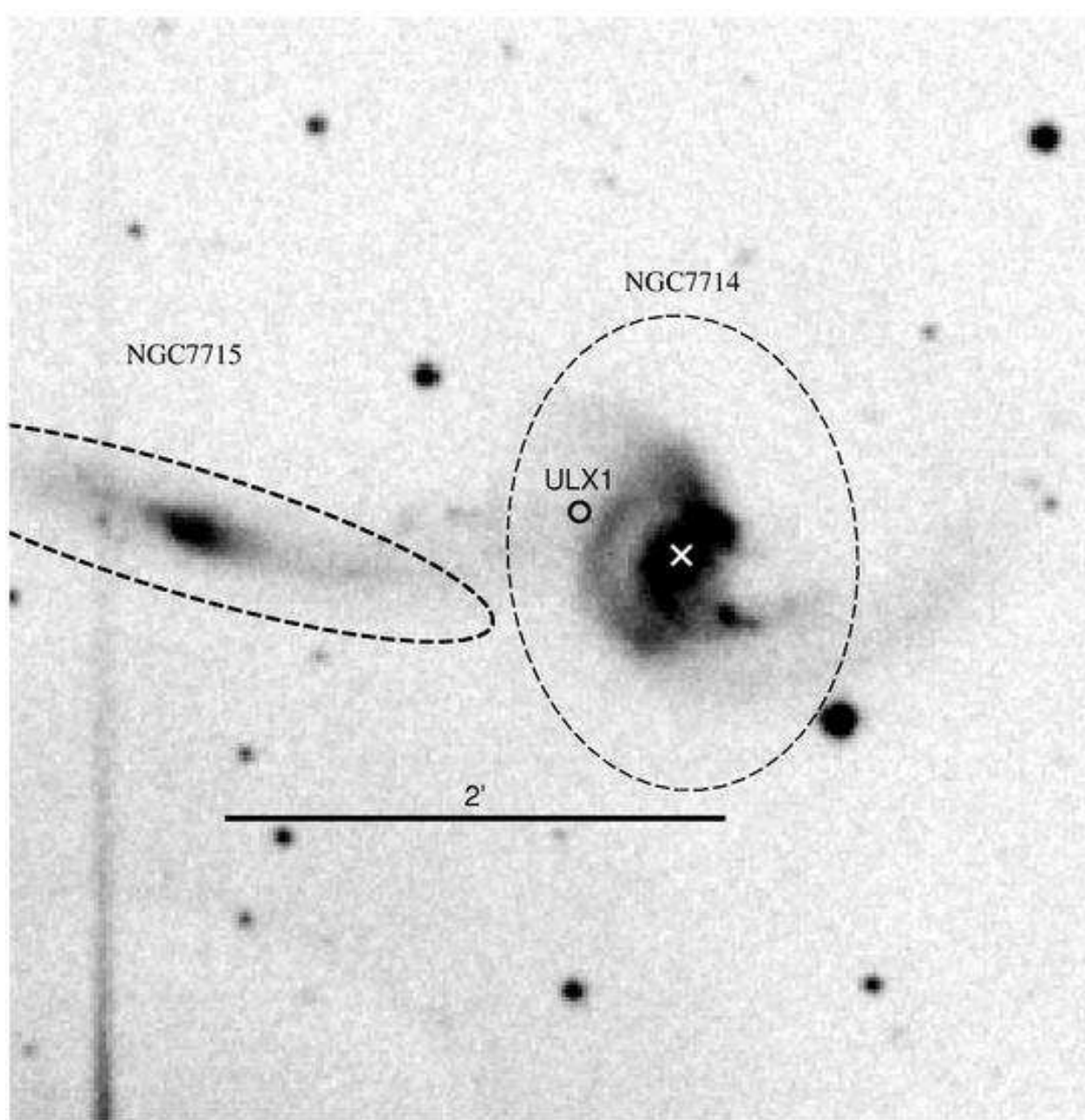


Fig. 75.— The finding chart for the ULXs in NGC7714.

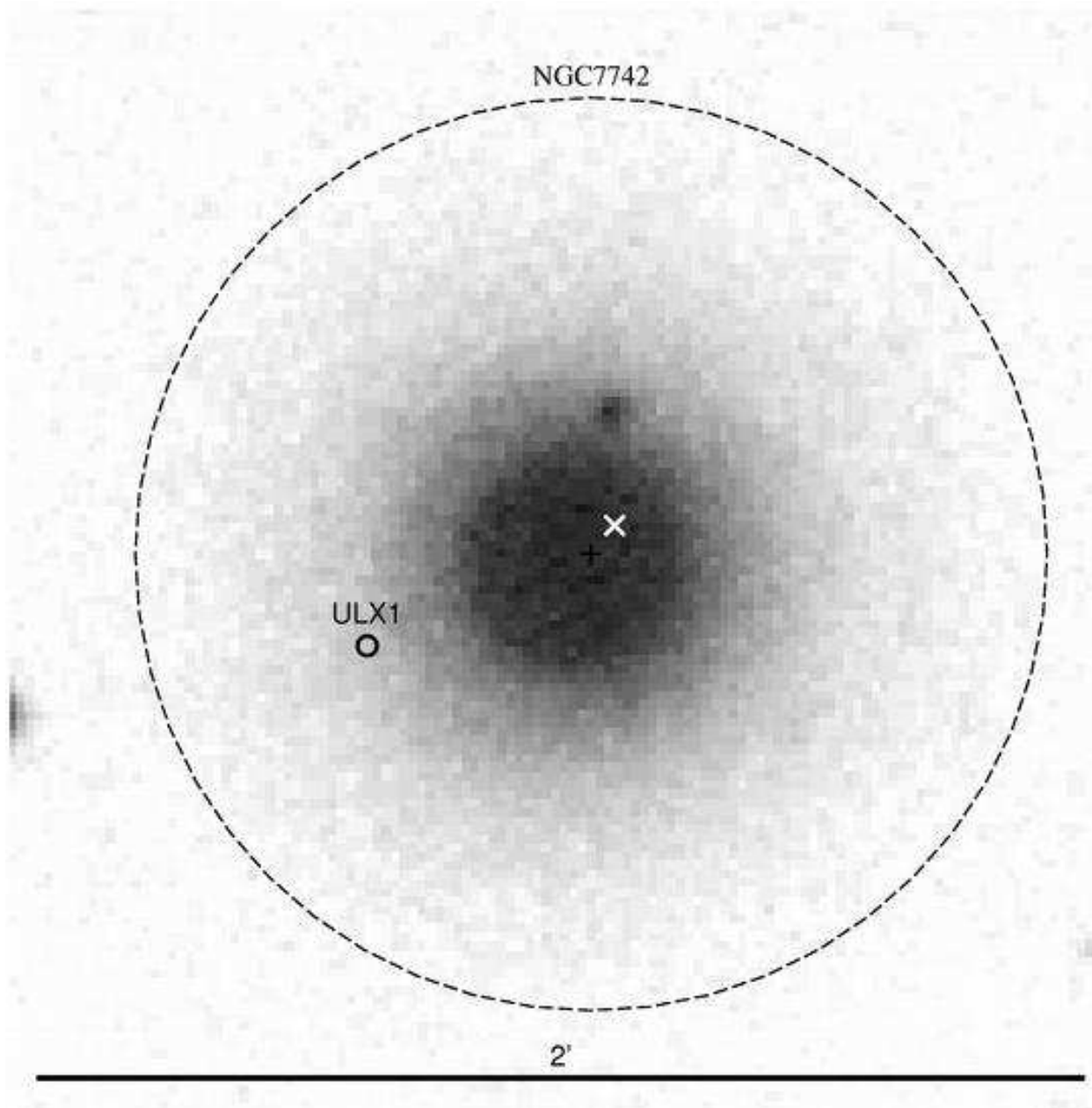


Fig. 76.— The finding chart for the ULXs in NGC7742.